Pure

Bangor University

DOCTOR OF PHILOSOPHY

Organic polymers and solid state fabrication

Jones, Geraint Wyn

Award date:
1999

Awarding institution:
Bangor University

Link to publication

General rights
Copyright and moral rights for the publications made accessible in the public portal are retained by the authors and/or other copyright owners and it is a condition of accessing publications that users recognise and abide by the legal requirements associated with these rights.

- Users may download and print one copy of any publication from the public portal for the purpose of private study or research.
- You may not further distribute the material or use it for any profit-making activity or commercial gain
- You may freely distribute the URL identifying the publication in the public portal ?

Take down policy
If you believe that this document breaches copyright please contact us providing details, and we will remove access to the work immediately and investigate your claim.

Download date: 17. Apr. 2024

Organic Polymers and Solid State Fabrication

Thesis submitted in candidature for the degree of Doctor of Philosophy

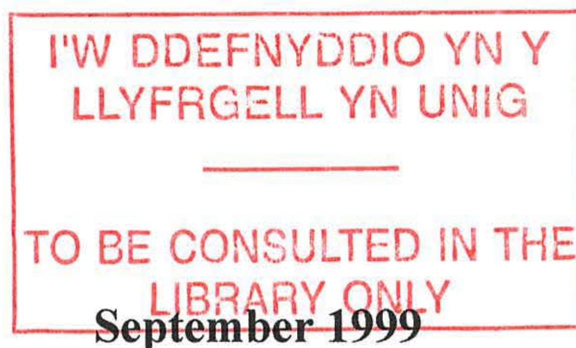
I'W DDEFNYDDIO YN Y LLYFRGELL YN UNIG

TO BE CONSULTED IN THE LIBRARY ONLY

September 1999

Geraint Wyn Jones

School of Electronic Engineering and Computer Systems
University of Wales
Bangor
Gwynedd
United Kingdom

Caf lawenydd y cyflwyno – heddiw
Wrth roddi o'm dwylo
Gynnyrch a fu'n egino
Drwy waith i'w gyflawnder o.

Ieuan Wyn (1999)

Acknowledgements

I wish to express my sincere thanks to Professor D.M. Taylor for his continued support and guidance throughout the duration of this research project and in particular during the detailed preparation of this thesis.

Further thanks are due to Professor Henrique Gomes and Dr Peter Stallinga at the University of Algarve, Faro, for allowing me to use facilities at their laboratories and for useful discussions; Dr Andy Alderson* and Dr Steve Vinton, Company Research Laboratories, BNFL, for their industrial support and supervision; and to Albert Rees and John Tame of the School of Electronic Engineering and Computer Systems, University of Wales, Bangor for their kind assistance and advice.

I would also wish to thank everyone at the School of Electronic Engineering and Computer Systems, for making my seven year stay at the School so enjoyable, and last but not least to all my family and friends for their continued support.

Financial support for this project was provided by BNFL, Springfields, Preston, and EPSRC for which the author is extremely grateful. In addition an industrial CASE studentship was also personally awarded to the author by BNFL.

* Presently Senior Research Fellow (Engineering Materials) in the Faculty of Technology at Bolton Institute.

Summary

This thesis details the fabrication and characterisation techniques used to improve our knowledge and understanding of the electrical and optical properties of conducting polymer devices. This particular study is based upon the continued characterisation of Schottky barrier diode structures prepared from electropolymerised film of poly(3-methylthiophene) (P3MeT) and concentrates on four main areas, (i) the nature and origin of acceptor states in partially dedoped poly(3-methylthiophene), (ii) the nature of the aluminium / polymer interface, (iii) the electrical and optical properties of P3MeT and (iv) improved understanding of the doping / dedoping processes.

Films were electropolymerised onto various substrates depending on the type of measurement and technique used. Gold-coated glass substrates were used as a basis for the formation of most Schottky barrier diodes used in electrical characterisation measurements, whilst ITO coated glass was used for all optical characterisation and gold-coated silicon for all Raman measurements. However, in all cases, constant improvements to the adopted growing procedure resulted in repeatable, high quality, uniform films.

DC, current-voltage (I-V) plots, and ac, frequency dependent, capacitance and loss measurements were used to characterise the electrical and optical properties of conducting polymer based diodes. Anomalies observed in these characteristics were studied and investigated, in particular with respect to the metal / polymer interface and the doping / dedoping processes.

During this study, a number of new analytical techniques have been applied for the first time to conducting polymers. These include, Deep Level Transient Spectroscopy (DLTS), a technique commonly used to analyse acceptor states in inorganic semiconducting devices, in-situ Raman characterisation of the effects of film doping and dedoping and Atomic Force Microscopy (AFM) techniques which has been successfully used to characterise sample structure, roughness and thickness for assessing the quality and uniformity of film samples.

Contents

1. Introduction **1**

1.1 Introduction 1

1.2 Aims 5

2. The Schottky Barrier **8**

2.1 Introduction 8

2.2 Rectifying Metal-Semiconductor Contacts 8

2.3 Depletion Layer 11

2.4 Charge Transport in Ideal Schottky Barrier Diodes 13

2.5 Deviations from Ideal Behaviour 15

2.5.1 Interfacial Layers and Surface States 15

2.5.2 Image Force Lowering of the Barrier 16

2.5.3 Tunnelling 17

2.6 DC Characteristics 19

2.6.1 Space Charge Limited Currents (SCLC) 19

2.6.2 Photocurrents, Photoconductivity and Trapping Effects 22

2.7 AC Characteristics of a Schottky Diode 25

2.7.1 Effects of Bulk Conductivity 29

2.7.2 Interface States 33

2.7.3 Photocapacitance 34

2.8 Deep Level Transient Spectroscopy (DLTS) 35

3. Conducting Polymers **42**

3.1 Introduction 42

3.2 Chemical Structure 46

3.3 Electronic Structure 50

3.3.1 Introduction 50

3.3.2 Doping of Conjugated Polymers: Solitons, Polarons, Bipolarons 54

3.4 Electrical/Optical Properties of Thiophene Polymers and Oligomers 59

3.4.1 Introduction 59

3.4.2 Electrical Properties 60

3.4.3 Optical Properties 66

3.5 Preparation Methods 75

3.5.1 Introduction 75

3.5.2 Electropolymerisation 77

3.5.3 Spin Coating 83

3.5.4 Precursor Polymerisation 84

3.5.5 Langmuir-Blodgett Technique 85

3.5.6 Self-Assembly Technique 86

3.5.7 Plasma Polymerisation 87

3.5.8 Vacuum Evaporation 90

3.6 Concluding Remarks 90

4. Experimental 93

4.1 Introduction 93

4.2 Sample Preparation 93

4.2.1 Substrate Cleaning Procedures 93

4.2.2 Thin Film Evaporation 94

4.2.3 Electropolymerisation 95

4.2.4 Device Formation 98

4.3 Electrical Measurements 99

4.3.1 DC Measurements 100

4.3.2 AC Measurements 101

4.3.3 Deep Level Transient Spectroscopy (DLTS) and Capacitance..... 101

4.4 Spectral Characterisation 102

4.4.1 Raman Spectroscopy 102

4.4.2 In-situ Raman Measurements 102

4.5 Morphology 104

4.5.1 Scanning Probe Microscopy (SPM) and the Atomic Force...... 104

4.5.2 Electric Force Microscopy (EFM) 104

4.5.3 Scanning Electron Microscopy (SEM) 106

4.6 Optical Characterisation 106

4.6.1 UV-Visible Spectroscopy 106

4.6.2 In-situ UV-Vis 107

4.6.3 Photocurrent Measurements 107

4.6.4 Photocapacitance Measurements 108

4.7 Concluding Summary 109

5. Results and Discussion **110**

5.1 Introduction 110

5.2 Morphology and Dedoping 111

5.2.1 SEM and AFM 111

5.2.2 UV-Vis and Raman Spectroscopy 117

5.3 DC Behaviour 131

5.3.1 Typical Device Behaviour 131

5.3.2 Effect of Light 134

5.4 AC Behaviour 136

5.4.1 Capacitance and Loss Curves 136

5.4.2 Mott-Schottky (Capacitance-Voltage) Plots 138

5.5 Capacitance Transients and DLTS 140

5.5.1 Majority Carrier Transients 140

5.5.2 Minority Carrier Transients 145

5.6 Photoconduction and Photocapacitance Measurements 147

5.6.1 Photoconduction 147

5.6.2 Photocapacitance 150

5.7 Electric Force Microscopy (EFM) and Kelvin Probe Microscopy...... 151

6. Low Bandgap Polymers **156**

6.1 Introduction 156

6.2 Experimental 157

6.3 Results and Discussion 159

6.3.1 Sample Characterisation 159

6.3.2 Electrical Characterisation 160

6.3.3 Theoretical Modelling 162

6.4 Conclusion 170

7. Conclusions and Further Work **171**

7.1 Contributions of this Work 171

7.2 Questions Arising from this Work 173

7.3 Further Work 175

References **180**

1. Introduction

1.1 Introduction

In 1956, Bardeen, Brattain, and Shockley were awarded the Nobel Prize in Physics for their invention of the transistor and contributions to the understanding of semiconductors. Two years later, after joining Texas Instruments, Kilby (and separately Noyce) conceived between them the concept of fabricating monolithic-circuits, that is, using germanium or silicon to build entire circuits. No one imagined at that time that silicon would become so important, and eventually, the material of choice in today's Very Large-Scale Integration (VLSI) and Ultra Large-Scale Integration (ULSI) transistor circuits. Today these circuits are still based on the planar technology developed in 1958 by Hoerni, at Fairchild Semiconductor.

Since then, other solid state semiconductor materials such as gallium arsenide (GaAs) and indium phosphide (InP), materials with higher charge mobility, have managed to infiltrate only very small, niche markets of specialised semiconducting devices, such as high-speed and microwave circuits. But in the early seventies a new class of synthetic materials, known as intrinsically conductive or electroactive polymers emerged, and were proclaimed as the materials that would eventually lead to the next major revolution in electronic and optoelectronic devices.

Today the realisation of that vision is imminent with simple transistor and light-emitting structures based on various conducting polymer films having already been fabricated and characterised. By now this new class of semiconducting devices, which forms part of the ever-expanding field of molecular electronics, is becoming highly competitive in specialised areas such as Light-Emitting Diodes (LEDs), previously dominated by alloys based on Ga, As, In and P.

It was in 1974 that Shirakawa and co-workers prepared the first semiconducting polymer films based on polyacetylene (PA) (Ito *et al.*, 1974). Some three years later, it was demonstrated that doping could increase the electrical conductivity of PA (Chiang *et al.*, 1977). These early findings paved the way for what was to become a very exciting and successful field of research. Even though the use of conducting polymers

as electronic materials in molecular based electronics is a relatively new concept (Duke, 1987), the idea of using synthetic materials, such as polymers, for their electrically conducting properties dates back to the 1960's.

Between 1974 and 1990 major advances in the research on conducting polymers led to a better understanding of conducting polymer synthesis, and subsequently, the control of film conductivity and charge transport. The majority of this work used Schottky barrier diodes and field-effect transistor structures to probe the electronic properties of various materials, including poly(3-alkylthiophenes) (P3ATs) (Tomozawa *et al.*, 1987), polyacetylene (Grant *et al.*, 1992), and polypyrrole (Koezuka and Tsumura, 1989) . More recently though, the behaviour of these simple structures has contributed to a better understanding of the electronic properties in polymers such as poly(p-phenylene vinylene) (PPV), PA and polythiophenes (Burroughes *et al.*, 1990; Grant *et al.*, 1992; Burroughes *et al.*, 1988; Taylor and Gomes, 1995; Stubb *et al.*, 1993 (and references within); Garnier *et al.*, 1990; Musa *et al.*, 1997). As a result, these conducting polymers have become more competitive with inorganic devices in some specialised markets (Marks *et al.*, 1993; Gomes, 1993; Bredas *et al.*, 1983). The improved understanding of charge transport mechanisms during this period led to important applications such as anti-static coatings (Ohtani *et al.*, 1992), batteries (Schoch and Saunders, 1992), and capacitors (Kalaji *et al.*, 1999).

Polymeric materials generally possess remarkable properties such as long-term stability, resistance to chemical attack, high strength-to-weight ratio, ease of fabrication and good processability (Salaneck and Brédas, 1994). In addition to the above properties one of the major potential advantages of conducting polymers is their low cost of production when compared with current, silicon-based technology.

Of all the fields of research in conducting polymers by far the most exploited, which also has the greatest envisaged potential in terms of application, is that of Light Emitting Diodes (LEDs). Commercially available flat screen displays of today, for use in notebooks, laptops, mobile phones and generally any piece of portable, electronic equipment currently use liquid crystal displays, gas plasma displays or (inorganic) electroluminescent displays. This market is currently dominated by liquid crystal displays with current sales estimated at $30 billion per annum and having an

exponential growth. The problems with today's LCDs are rooted in the manufacturing complexity, size limitations and restricted viewing angles. In addition LCDs need to become thinner, lighter and more efficient in terms of electrical power consumption - requirements which are general to all portable equipment. Displays based on organic thin films would satisfy the first two requirements but currently not the third i.e. improved electrical efficiency. For example, the typical quantum efficiency (photons emitted per electron injected) for a PPV LED is 0.05 % (Burroughes *et al.*, 1990), compared with 7 % (Sze, 1981) for a GaAs LED. However, an improved derivative of PPV, poly(2-methoxy,5-(2'-ethyl-hexoxy)-1,4-phenylene-vinylene) (MEH-PPV) has been reported to show quantum efficiencies in the range 0.7 % - 4 % (Braun and Heeger, 1991; Wudl *et al.*, 1991). The approach of using thin film technology based on organic materials is promising because (i) manufacturing simplicity (films can be prepared by spin coating) and (ii) polymer LEDs are electroluminescent structures. Unlike traditional LCDs therefore, they do not need backlighting or reflected light in which to operate.

In 1990, Burroughes and co-workers reported the first ever realisation of an LED based on a conjugated polymer film (Burroughes *et al.*, 1990). Since then the field of organic-LEDs (OLEDs) has mushroomed with a number of international research groups involved in developing efficient devices (Braun and Heeger, 1991; Andersson *et al.*, 1995; Campbell *et al.*, 1998; Ohmori *et al.*, 1991; Parker, 1994; Greenham *et al.*, 1993). The two main groups who have already managed to capture a market for conducting polymer LEDs are (i) the optolectronics group of Professor R.H Friend at Cambridge University and (ii) the group of Professor A J Heeger at University of Santa Barbara. Both groups have invested heavily in the future of these materials by establishing companies to further exploit new applications; CDT (Cambridge Display Technology), Cambridge, which has industrial links with Philips and Seiko-Epson and UNIAX Corp, in California.

The work of the companies is progressing at such a rate that by now it is possible to easily fabricate monolithically the complete pixels including the OLED, drive circuits such as thin film transistors (TFTs) and capacitors. Two groups have recently reported such packages, the Cambridge group based their OLED on MEH-PPV and their TFT on Poly(3-hexylthiophene) (P3HT) (Sirringhaus *et al.*, 1998) whilst the Bell Laboratory

group at Murray Hill, based their OLED on a combination of triphenyl diamine (TPD), and 8-hydroxyquinolinato aluminium (Alq), and their TFT similarly prepared using P3HT (Dodabalapur *et al.*, 1998).

The driver for pursuing research in OLEDs was the potential for manufacturing large screen displays based on multi-coloured organic LEDs. Today these can realistically be achieved using a combination of new fabrication techniques and chemically modified materials, a number of them based on various thiophene derivatives (Berggren *et al.*, 1995; Hamaguchi *et al.*, 1997; Berggren *et al.*, 1994; Inganäs *et al.*, 1995). In many cases OLEDs are now so efficient that they can be as much as 100 times as bright as the ordinary CRTs currently used in TV screens. Polymer film structures can now be spin-coated successfully onto large area substrates, with virtually no defects, at low cost and with all the advantageous properties of polymeric materials.

Even though much of the research into conducting polymers is currently concentrated on OLEDs and display technology, a number of other interesting investigations should not be overlooked. These include studies into fundamental conducting polymer properties (Musa *et al.*, 1997; Assadi *et al.*, 1992; Bantikassegn and Inganäs, 1997), solar cell technology (Videlot and Fichou, 1999), fabrication of organic polymer based lasers (Tessler *et al.*, 1996; Berggren *et al.*, 1997), and sensor applications (Ohmori *et al.*,1990).

Over the last year or two it has become increasingly apparent that a number of researchers are now working on the characterisation of a wide range of both new and known thiophene derivatives, in particular thin films which are electropolymerised onto a working substrate (Gomes, 1993; Roncali *et al.*, 1986; Tourillon and Garnier, 1983). New compounds such as poly(3,4-ethylenedioxythiophene) (PEDOT) show partial crystallinity, with short inter-chain distances leading to highly anisotropic films. This gives PEDOT remarkable properties, in particular very high mobility (Inganäs *et al.*, 1999). Similar compounds that have the potential for interesting optical applications include a range of low bandgap materials, such as poly-4-dicyanomethylene-4H-cyclopenta[2,1-b:3,4b']dithiophene PCDM (Ferraris and Lambert, 1991; Gunatunga *et al.*, 1997). Other groups use various oligothiophene FET structures to investigate the

conductivity and mobility of varying lengths of short chain molecules. Some of this work has led to various applications including solar cells (Videlot and Fichou, 1999).

1.2 Aims

The material studied in the context of the present work is a remarkably stable poly(3-alkylthiophene) which has previously been used within this research group for fabricating MISFETs and Schottky barrier diodes (Gomes, 1993; Gomes *et al.*, 1993; Gomes and Taylor, 1993; Gomes and Taylor, 1997; Gomes *et al.*, 1997; Taylor *et al.*, 1991; Taylor and Gomes, 1995). In particular, poly(3-methylthiophene) (P3MeT), the molecular structure of which is given in figure 1.1, has been used to fabricate Schottky barrier diode structures using an electropolymerisation technique for deposition of the films onto various substrates.

Polythiophene (PT) attracted much attention when it was discovered that the polymer was remarkably stable in air, to water, and temperature. However one of the drawbacks of using PT based films, as for many other early conducting polymers (such as polyparaphenylene, polyaniline and polyacetylene), was that they possessed extremely poor processability. In many cases these polymers were initially prepared, as intractable, insoluble films or powders, which once formed could not be easily manipulated further.

It was soon discovered that by modifying the monomer structure of some polymers, and in particular polythiophene, that this limitation could be overcome thus yielding more soluble polymeric material. One modification of the polythiophene monomer, which proved highly successful, involved the substitution of flexible alkyl chains into the 3-position of the thiophene ring (figure 1.1) and led to highly processable polymers (Bryce *et al.*, 1988). However there exists a major drawback to this technique, in that the improved processability is always accompanied by an increased probability of thermal instability (Gustafsson *et al.*, 1988 and 1989; Inganäs *et al.*, 1995).

In this, and previous studies within this group, the justification for using P3MeT is that the well studied electrical and optical properties of PT are combined with the improved processability at a minimum cost to stability, an important property when considering

device lifetimes. However, this trade-off between stability and processability limits the choice of preparation techniques, in that the solubility of P3MeT compared to PT is only marginally enhanced and is not sufficient to allow spin-coating deposition techniques to be adopted. (Modified monomers with butyl or longer alkyl chains at the 3-position of the ring are all known to be highly soluble). Instead anodic electropolymerisation, which is another common technique for depositing high quality polymer films, is the only real option for P3MeT.

As will be shown later, a Schottky barrier which forms at a metal / semiconductor interface has been widely used in the study of inorganic semiconductors to better understand charge transport and trapping, the formation and role of the metal / semiconductor interface, material doping and general processing conditions. These issues are also highly relevant to polymeric semiconductors if devices based on these materials are to be optimised for commercial applications.

The work presented in this thesis sets out to explore and exploit the Schottky barrier formed at the P3MeT / Al interface for improving our knowledge and understanding of the chemical, electrical and optical properties of the polymer.

To achieve this end, a range of experimental and analytical techniques most of which have been widely used for investigating inorganic semiconductors are here applied to a polymeric semiconductor, in some instances for the very first time.

Of particular interest are:

- the nature and origin of acceptor states in partially dedoped poly(3-methylthiophene)
- the nature of the aluminium/polymer interface
- electrical and optical properties of P3MeT
- doping/dedoping process

The relevant background theory is given in Chapters 2 and 3, details of the experimental techniques employed in Chapter 4. Chapters 5 and 6 present the results of the investigation and a detailed discussion of the results. Chapter 7 brings together the main findings of the work and suggests possible further work based on these findings.

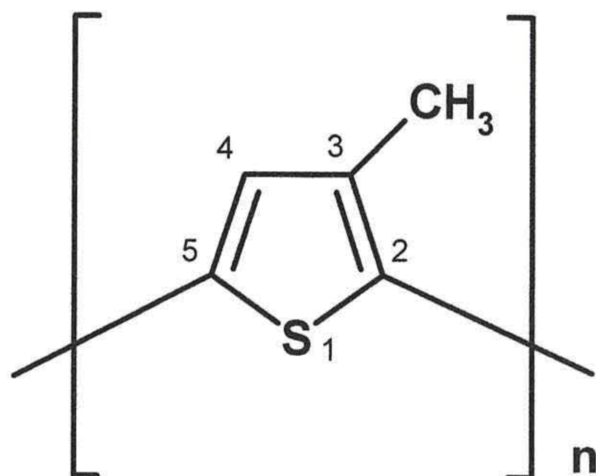

Figure 1.1 *Chemical structure of Poly(3-methylthiophene) (P3MeT)*

2. The Schottky Barrier

2.1 Introduction

The study of metal-semiconductor contacts dates back to 1874 when Braun (Braun, 1874) observed the asymmetrical conduction between metal points and crystals such as lead sulphide. Since this early work, much effort has been expended to understand the nature of metal-semiconductor junctions (Rhoderick, 1978; Henisch, 1984). For interconnects in VLSI circuits and for connecting discrete devices to external circuits, the contacts to the device should be ohmic i.e. allowing facile electron and hole transport across the junction with little potential drop. This is not a trivial problem and requires careful choice of metal or, strictly, metal work-function. In many instances, metal–semiconducting junctions are rectifying in nature, for example, the so-called Schottky barrier diode. Such junctions are widely used in solar cells and fast diodes for microwave applications (Bar-Lev, 1984). Such structures can also be used diagnostically to investigate the fundamental properties of the semiconductor forming the junction.

In this chapter will be presented the fundamental concepts necessary to understand the behaviour of the metal / polymer Schottky diodes fabricated in this work. It will be shown how the current-voltage (I-V) and capacitance-voltage (C-V) characteristics of the devices may be used to extract parameters such as semiconductor doping density and the height of the interfacial potential barrier. It will be further shown how the structure may be used for probing localised trapping states in the semiconductor using deep level transient spectroscopy (DLTS) (Lang, 1974). Indeed, this work (Jones *et al.*, 1997) represents the first application of this technique to semiconducting polymers. Finally, the electro-optical properties of Schottky diodes will be discussed, in particular, concentrating on photocurrent generation in the depletion region of the device.

2.2 Rectifying Metal-Semiconductor Contacts

The origin of rectification in a metal-semiconductor junction is best understood by considering the electron energy band diagrams of the two components forming the junction. Fig 2.1 (a) shows that in a metal all energy states up to the Fermi level, E_F, are

filled while the states above E_F are empty. Strictly this is only true at 0 K. At room temperature the occupancy is governed by Fermi-Dirac statistics i.e. the probability of a state E being occupied is given by the Fermi-Dirac distribution function, F(E)

$$F(E)=\frac{1}{1+\exp\frac{E-E_F}{kT}} \tag{2.1}$$

where E_F is the Fermi energy, k Boltzmann's constant and T the absolute temperature. Clearly, even at room temperature only a small fraction of electrons in states below E_F will be excited to states above E_F. Thus we may define a work function ϕ_M for the metal as the minimum energy required to excite electrons out of the metal i.e. to the vacuum level.

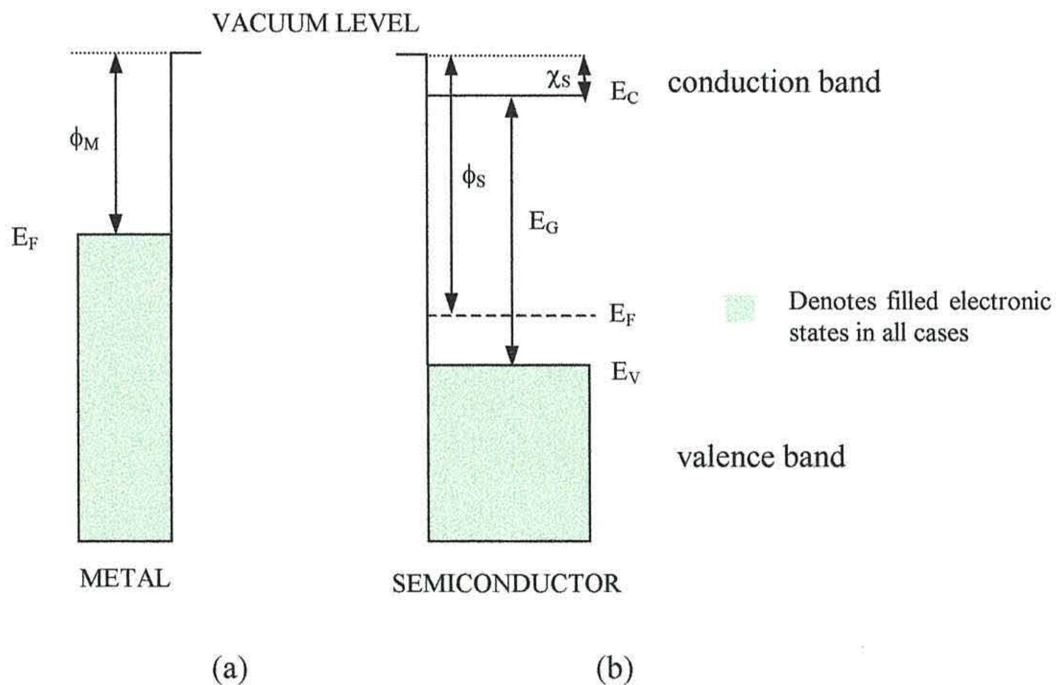

Figure 2.1 *Energy level diagram of (a) a metal and (b) a p-type semiconductor before contact.*

Fig 2.1 (b) shows the energy band diagram for a p-type semiconductor. Here E_C is the conduction band edge while E_V is the valence band edge. The Fermi level, E_F, lies in the energy gap between the filled valence band and the empty conduction band. The

semiconductor work function ϕ_S is now defined as the energy difference between the vacuum level and E_F in the semiconductor. In this case since there are no occupied electronic states at, or near, E_F, a more useful concept for semiconductors is the electron affinity, χ_S, the energy that an electron at E_C must gain in order to be excited out of the semiconductor.

When the metal and the semiconductor come into contact, figure 2.2, holes from the semiconductor diffuse into the metal where they recombine with electrons. Gradually, the metal charges positively relative to the semiconductor building up an internal potential, which acts to reduce the charge transfer. This potential sets up an electric field driving the holes deeper into the bulk of the semiconductor, thus exposing the negatively charged acceptor states. When the junction comes into thermal equilibrium the Fermi energy is continuous across the junction. The positive potential V_{SO} at the semiconductor surface, also known as the junction potential, has a magnitude given by

$$V_{SO} = \frac{\phi_M - \phi_S}{q}. \tag{2.2}$$

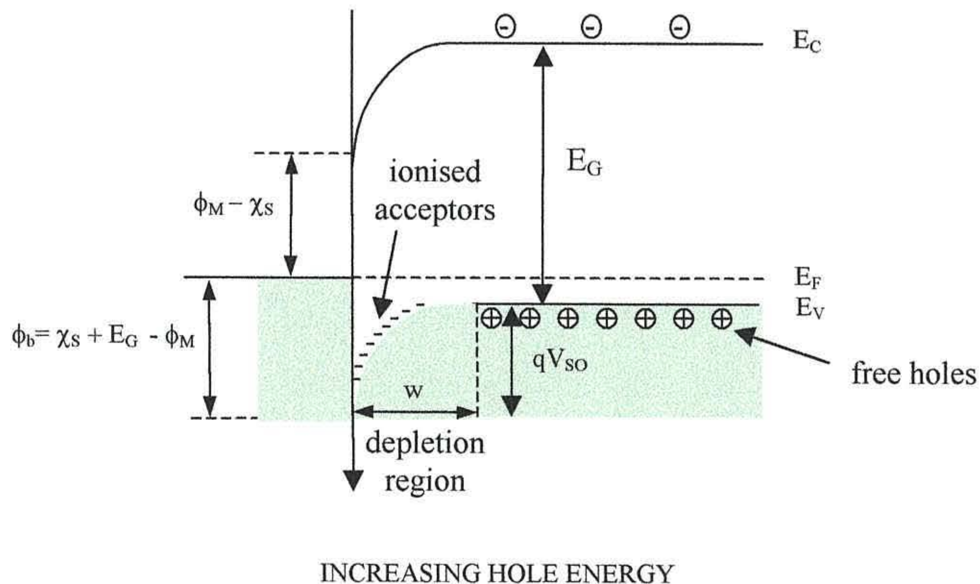

Figure 2.2 *Energy level diagram of Schottky barrier formed when a metal and a p-type semiconductor are brought into contact.*

That this is a rectifying structure is readily demonstrated. With positive bias applied to the semiconductor, the barrier, qV_{SO}, seen by the majority holes diffusing to the metal is reduced resulting in a significant hole current flow into the metal (figure 2.3 (a)).

With negative bias applied to the semiconductor the barrier to hole flow is increased, significantly reducing the hole current, while simultaneously encouraging the flow of minority electrons from the semiconductor to the metal (figure 2.3 (b)). Clearly, this will be a much lower current than observed for positive bias.

This simplistic description will, of course, be complicated by thermal emission of electrons from the metal into the conduction band of the semiconductor, but in most cases this is likely to be a minor component of the junction current.

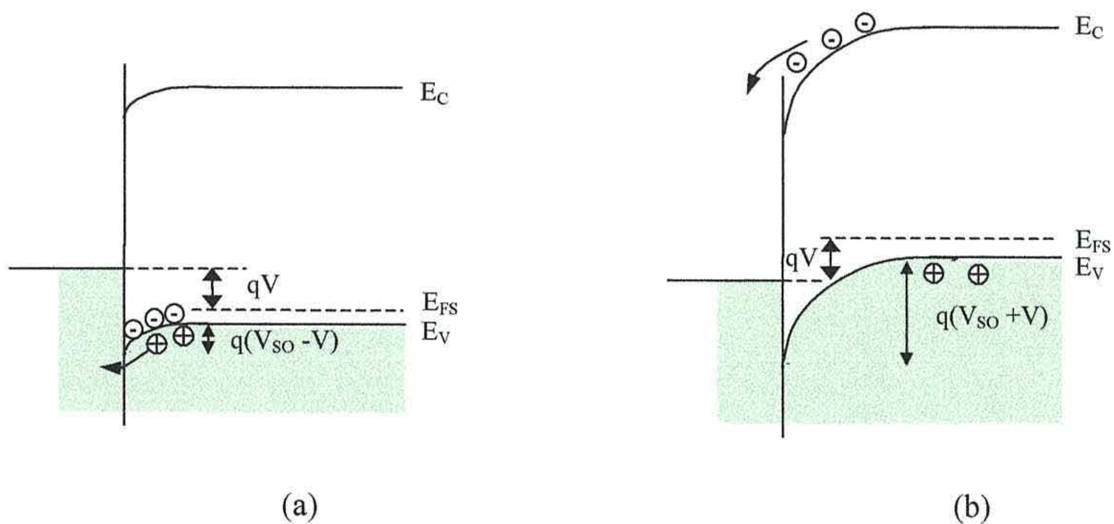

Figure 2.3 *Energy level diagram of a Schottky barrier diode in (a) forward bias and (b) reverse bias*

2.3 Depletion Layer

In the abrupt junction model developed for inorganic semiconductors it is assumed that the depletion region is composed of a space charge layer of uniform charge density, ρ. It is further assumed that the transition from depleted to bulk material occurs at a well-defined plane, say x=0, in the semiconductor. In the depletion region of a p-type

semiconductor ρ=$-qN_a$ where N_a is the acceptor density, so that the one-dimensional Poisson equation may be written as

$$\frac{d^2V(x)}{dx^2} = -\frac{\rho}{\varepsilon\varepsilon_0} = \frac{qN_a}{\varepsilon\varepsilon_0} \tag{2.3}$$

where ε is the relative permittivity of the semiconductor and ε_0 the absolute permittivity of free space (=8.85×10^{-12} F m^{-1}). Integrating equation (2.3) subject to the boundary conditions that both the electric field and potential in the bulk semiconductor are zero, (figure 2.4), yields for the field E(x) and potential V(x) at some point x in the depletion region

$$E(x) = -\frac{dV(x)}{dx} = -\frac{qN_a x}{\varepsilon\varepsilon_0} \tag{2.4}$$

$$V(x) = \frac{qN_a x^2}{2\varepsilon\varepsilon_0}. \tag{2.5}$$

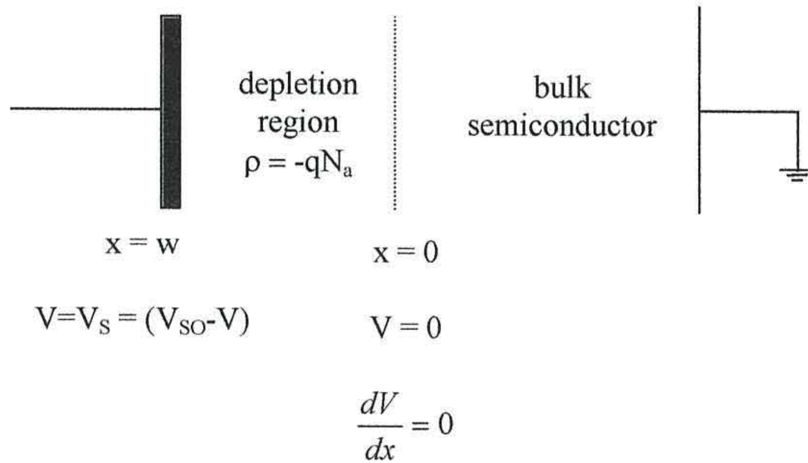

Figure 2.4 *A schematic of the boundary conditions in a typical Schottky diode.*

The change in potential V(x) through the depletion region causes the band bending shown in figure 2.2. At the metal-semiconductor interface x=w and V(x)=V_S yielding

$$V_S = \frac{qN_a w^2}{2\varepsilon\varepsilon_0}$$

which upon rearranging gives

$$w = \left(\frac{2\varepsilon\varepsilon_0}{qN_a}V_S\right)^{\frac{1}{2}} = \left(\frac{2\varepsilon\varepsilon_0}{qN_a}\right)^{\frac{1}{2}}\left(V_{SO} - V\right)^{\frac{1}{2}} \tag{2.6}$$

where V is a potential applied to the metal electrode.

2.4 Charge Transport in Ideal Schottky Barrier Diodes

Figure 2.3 shows that charge transport through a metal / p-type semiconductor junction is controlled mainly by the potential barrier to hole transport from the semiconductor into the metal. In forward bias the barrier is reduced increasing the hole current while reverse bias increases the barrier reducing the hole current. The thermal emission of holes over the barrier into the metal is well-described by the thermionic emission theory (Bethe, 1942). However, this model assumes that holes are already present at the interface. In reality, holes must be transported to the interface from the bulk polymer through a depletion region whose width depends on the applied voltage (equation (2.6)).

The transport of holes to the junction is well-described by the diffusion theory developed by Wagner (1931). Both the thermionic and diffusion theories predict current-voltage relations of the same general form i.e.

$$J = J_0\left[\exp\left(\frac{qV}{kT}\right) - 1\right] \tag{2.7}$$

where J is the current density and V is the voltage applied to the device. The variable, J_0 is known as the reverse saturation current density and is quite different in the two cases. For thermionic emission J_0 takes the form

$$J_0 = A^* T^2 \exp\left[\frac{(-q\phi_b)}{kT}\right] \tag{2.8}$$

where A* is the effective Richardson constant for thermionic emission, neglecting the effects of optical phonon scattering, and is further described as

$$A^* = \frac{4\pi m^* q k^2}{h^3} \tag{2.9}$$

where h is Planck's constant and m* the effective mass of the hole. (For free electrons the Richardson constant A is 120 $Acm^{-2}K^{-1}$). For electron emission from a metal into a semiconductor A* has a value typically in the range 132 to 144 $Acm^{-2}K^{-1}$ whereas values quoted for holes into semiconductors are typically in the range 41 to 75 $Acm^{-2}K^{-1}$ (Sze, 1981).

From diffusion theory J_0 has the form

$$J_0 = qN_v\mu E_{max}\exp\left[\frac{-q\phi_b}{kT}\right] \tag{2.10}$$

where N_V is the effective density of states in the valence band, μ the charge carrier mobility and E_{max} is the maximum field strength at the interface (equation 2.11). From equation 2.4 and figure 2.6 the maximum field occurs at the interface and is given by

$$E_{max} = \frac{2kTa^2wV^{1/2}}{q} \tag{2.11}$$

where

$$a = \left[\frac{q^2N_a}{2\varepsilon\varepsilon_0 kT}\right]^{1/2} F \tag{2.12}$$

and F is a constant known as Dawson's integral which is approximately equal to $(2aw)^{-1}$ (Rhoderick, 1978).

As demonstrated above, one of the characteristic differences between the two theories originates in the relative sensitivity of the reverse saturation current density to voltage

and temperature. The reverse saturation current density as derived from the diffusion theory varies more rapidly with voltage, but is less sensitive to temperature compared to the value derived from the thermionic emission theory.

In a further development a model has been derived by considering the thermionic recombination velocity near the metal-semiconductor interface, which describes the charge transport mechanism in terms of a combination of the emission and diffusion theories. This combined model was first proposed by Crowell and Sze (Crowell and Sze, 1966).

In most practical metal-semiconductor contacts though the ideal situation shown in figure 2.2 is never attained, because there is usually a very thin oxide layer on the surface of the semiconductor. Such an oxide layer is normally referred to as an interfacial layer. In practice, this layer presents a small barrier since it is so thin, allowing charge carriers to penetrate by quantum-mechanical tunnelling (Sze, 1981).

2.5 Deviations from Ideal Behaviour

A number of factors can cause the behaviour of a real Schottky barrier diode to deviate from the ideal predicted by the above theories. These include interfacial layers and surface states, image force lowering of the interface barrier, and tunnelling. The effects of these additional phenomena will be discussed briefly below.

2.5.1 Interfacial Layers and Surface States

In practice, any metal-semiconductor junction, unless prepared in ultra-high vacuum, will inevitably include a thin insulating layer of oxide between the metal and semiconductor.

Aluminium, a widely used electrode material, readily reacts with oxygen to form such an oxide layer during evaporation. The metal is also sufficiently reactive to form complexes with the materials on which it is deposited. Thin, insulating interfacial layers, usually < 50 Å thick, act as tunnelling barriers to holes and electrons. Part of the

applied voltage appears across the layer, so that the device current increases more slowly with voltage than predicted by equation (2.7)

The presence of the insulating layer also influences the occupation of surface states at the semiconductor surface in addition to being a source of trapping states for carriers crossing the interface. The effect on the current-voltage characteristics depends very much then on whether the Fermi energy in the metal or in the semiconductor determines the state occupancy (Sze, 1981).

Where the interfacial layer is sufficiently thin that the metal Fermi level determines surface state occupancy, Crowell and Sze (1966) have shown that the forward current may be described by

$$\log(J) \propto \frac{qV}{nkT} \tag{2.13}$$

where n is the ideality factor. For Schottky junctions formed on inorganic semiconductors n is close to unity, for example, n=1.02 for a W-Si diode and 1.04 for a W-GaAs diode.

As the interfacial layer thickness increases, the behaviour increasingly approaches that of metal-insulator-semiconductor (MIS) junctions (Green *et al.*, 1974).

2.5.2 Image Force Lowering of the Barrier

A band diagram such as that shown in figure 2.2, neglects the effect of image forces experienced by charge carriers as they move closer to the metal surface. Within a few nanometres of the interface, forces between a carrier and its image are significant so that the total potential energy of a charge carrier close to the metal should include a term to account for this interaction. Thus, the potential energy, $\phi(r)$, of a hole located a distance r from the metal is given by (Sze, 1981)

$$\phi(r) = \frac{q^2}{16\pi\varepsilon_\infty\varepsilon_0 r} + qE_{\max}r \tag{2.14}$$

where ε_{∞} is the high frequency relative permittivity and the field in the depletion region near the metal is assumed uniform and equal to the maximum field E_{max} (see equation 2.11).

It is readily shown that at $r = r_0 = (q/16\pi\varepsilon_{\infty}\varepsilon_0 E_{max})^{1/2}$ the potential energy goes through a minimum value given by

$$\phi(r_0) = q\left(\frac{q^3 N_a (V_{SO} - V)}{8\pi^2 \varepsilon_{\infty}^2 \varepsilon \varepsilon_0^3}\right)^{1/4}. \tag{2.15}$$

In the absence of imaging, the potential energy of a hole at the interface undergoes a step change equal to ϕ_b. Therefore, $\phi(r_0)$ represents the lowering of the potential barrier, $\Delta\phi_b$, resulting from the inclusion of imaging effects.

Since E_{max} increases with increasing reverse bias, the effect of imaging is to increase the sensitivity of J_0 (or J_R) to applied bias. Now ln J_R increases approximately as $V^{1/4}$ (Gomes, 1993).

In real devices where interfacial layers are common, image lowering of the barrier is not generally regarded as an important process (Henisch, 1984).

2.5.3 Tunnelling

The effect of quantum-mechanical tunnelling through a Schottky barrier is important only for very thin barriers, usually < 50 Å. For moderately doped, inorganic semiconductors (up to $N_d \sim 10^{16}$ cm $^{-3}$) normally used in practical devices, tunnelling is significant only in the reverse direction, where, although the width of the depletion region increases with reverse bias, the width of that part of the barrier through which the electrons have to tunnel decreases (figure 2.5). The effect of this is to make the reverse current increase rapidly above a certain voltage, as in a Zener diode (Sze, 1981).

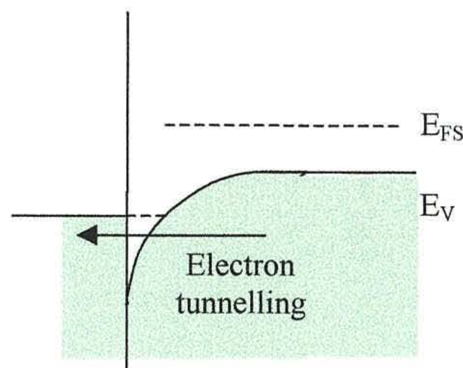

Figure 2.5 *A schematic of the electron tunnelling process through a Schottky barrier under reverse bias conditions.*

However, both image–force lowering (section 2.5.2) and tunnelling may be exaggerated if the surface of the semiconductor is accumulated. In this case the depletion layer is much thinner in a direction parallel to the surface than it is in a direction normal to the surface (Yu and Snow, 1968), with the result that tunnelling and image-force lowering effects are both enhanced.

As a consequence, in forward bias the ideality factor, n, is a function of voltage, however, in reverse bias the current increases very quickly, as shown for a Pt-Si Schottky diode with an accumulated surface in figure 2.6 (Yu and Snow, 1968).

Here the slow increase, up to – 0.3 V is due to image force lowering and the fast increase above – 1.0 V due to tunnelling.

The ideality of the I-V characteristics (i.e. low n, good saturation in reverse direction and high reverse breakdown) is thus very sensitive to the semiconductor surface potential adjacent to the metal (section 2.5.2).

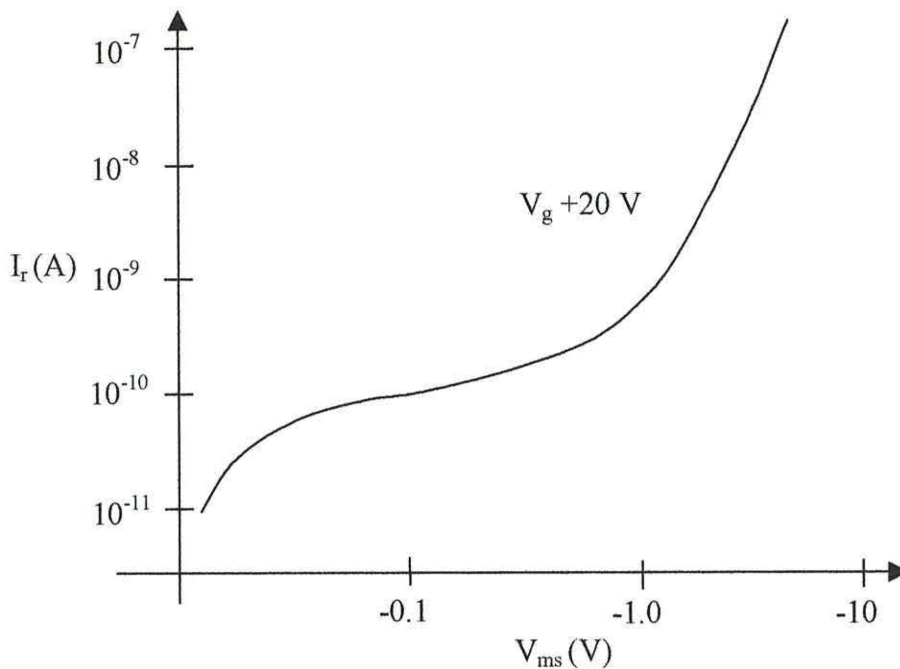

Figure 2.6 *Reverse I-V characteristic for Pt-Si Schottky diode with accumulated surface (Yu and Snow, 1968).*

2.6 DC Characteristics

2.6.1 Space Charge Limited Currents (SCLC)

Trapping of charge carriers plays an important role in devices based on conducting polymeric materials, since I-V curves are influenced by trapped charges. These space charges distort the fields in the charge injection region at low voltages (Meyer *et al.*, 1995)

In inorganic semiconductors it is not uncommon for some materials, such as gallium arsenide, to contain deep-lying traps around the middle of the gap. Evidence has also been presented for the presence in semiconducting polymers of localised trapping states, which can affect both the optical and electrical properties of devices based on these materials (Kaneto *et al.*, 1984; Gomes, 1993; Taylor and Gomes, 1995).

In conducting polymers the density of injected carriers at very low voltages is low so that the conductance of the material is totally due to thermally generated carriers in the

polymer. Below a certain threshold voltage, then the I-V characteristic exhibits ohmic behaviour (where $I \propto V$). As the injected carrier concentration exceeds the thermal concentration a supralinear regime best fitted by $I \propto V^n$, where n >2, is observed at higher voltages.

In the ohmic region the major contribution to conduction will be due to bulk generated "free" carriers. Since most conducting polymers are p-type the expression that describes this relationship is given by

$$J = q\mu_h pE \qquad (2.16)$$

where J is the current density, μ_h the hole mobility, p the concentration of holes and E the applied field. In this case an assumption has been made that the concentration of holes (p) far exceeds that of electrons (n).

Evidence by Taylor and Gomes, 1995 supports the theory that a non-linear Mott-Schottky plot of $1/C^2$ against applied bias (as discussed in section 2.7) for P3MeT diodes may be due to the presence of two acceptor states in the bandgap. It is already known that the shallow state controls conduction through the bulk polymer, but the origin and characteristics of the deep acceptor state is still not fully understood.

In general though, charge transport and electroluminescence in light emitting diodes (LEDs) have been extensively studied but remain rather poorly understood. Simple band models (Brédas, 1995; Vannikov *et al.*, 1994) have been challenged by models based on quasiparticles of all sorts including intrachain, interchain and Coulombic interactions. However, whatever species are proposed as basic excitations, all of them are positively charged (in p-type material).

The motions of both holes and electrons in semiconductors are commonly limited by trapping on for example defect states. In general conjugated polymers exhibit low charge carrier mobilities and are therefore very favourable media for the formation of space charge (Andre *et al.*, 1985). For example, in 1988, Burroughes and co-workers were the first to demonstrate that a space charge limited current was the most likely

mechanism for explaining the supralinear regime observed in Schottky barrier diodes based on PA (Burroughes *et al.*, 1988).

Whether holes contribute to transport directly or in the form of polarons or bipolarons (Gustafsson *et al.*, 1990), their mobility and concentration determine the total current. However, increasing the potential causes the additional injection of charge carriers into the polymer from the hole-injecting electrode. As a result of trapping, only a fraction of all injected holes participate in conductance, the rest being immobilised in the traps. This fraction, θ, is given by

$$\theta = \frac{p}{p + p_t} \tag{2.17}$$

where p is the concentration of mobile holes and p_t the concentration of trapped holes. When the density of the additional, injected charge carriers exceeds the density of thermal carriers, the I-V curve deviates from the observed ohmic relationship. The exact shape of the curve is determined by the distribution of traps in the energy gap. For example the quadratic law reported by Savvate'ev and co-workers (Savvate'ev *et al.*, 1997) and Musa and co-workers (Musa *et al.*, 1997 and 1998) suggests that the SCLC is dominated by a single set of shallow traps. However, Musa went on to report the observation of characteristics in a thiophene-derivative, which suggested up to four trapping states.

In a simple SCLC model with a single shallow trap

$$\theta = \exp\left[\left(\frac{E_F - E_t}{kT}\right)\right] \tag{2.18}$$

where E_t is the trap energy and predicts an I-V characteristic of the form

$$J = \frac{9}{8}\varepsilon\mu\theta\frac{V^2}{d^3} \tag{2.19}$$

which for the case of saturated traps ($\theta = 1$) is known as Child's law (Smith and Rose, 1955).

With further increase in voltage beyond the threshold value, the growth of injection leads to saturation of traps. As a result most of the newly injected charge carriers cannot be trapped and contribute directly to the conductance. This transition, called the trap-filled limit (tfl) appears in the I-V characteristics as an extremely fast current growth.

2.6.2 Photocurrents, Photoconductivity and Trapping Effects

Intrsinsic conductivity arises from the thermal excitation of an electron from the valence band across the energy gap, into the conduction band. The electron and the resulting hole in the valence band are free to carry charge.

By supplying energy quanta equal to or greater than the energy gap, E_G, an electron-hole pair is produced, imparting additional conductivity to the material. If the energy required to initiate this process is supplied by absorption of electromagnetic radiation, then the additional conductivity is known as photoconductivity, and the resulting current known as the photocurrent. In this case the quantum restriction takes the form of the Einstein relation:

$$hf = qE_G \tag{2.20}$$

where h is Planck's constant and f frequency.

The limiting or threshold frequency $f_0 = qE_G/h$ corresponds to a limiting wavelength, λ_0 given by

$$\lambda_0 = hc/E_G' = 1.237/E_G' \tag{2.21}$$

for λ in microns, E_G' in electron volts and c is the velocity of light in vacuum. However E_G' need not be equal to the thermal gap energy, E_G: while light absorption causes a strictly vertical transition across the gap, the presence of phonon interactions may cause

the transitions involved in thermal excitation to be nonvertical and thus E_G to be smaller than $E_G^{'}$. The quantity λ_0 is known as the long wave limit and only radiation of a wavelength shorter than λ_0 can yield electron-hole pairs and produce a photocurrent resulting in an increase in photoconductivity (Ashwell, 1992).

If a semiconducting material is illuminated with light of a wavelength so that equation 2.21 is satisfied a concentration, Δn, of additional electron-hole pairs are generated, above the number, n_{th} of those which are present as the result of thermal excitation, the material being at a non-zero temperature T. If the illumination is suddenly interrupted, the number of charge carriers decays by recombination, following an exponential relationship:

$$n = n_{th} + \Delta n \exp\left(-\frac{t}{\tau}\right) \tag{2.22}$$

where t is time after switching off the illumination and τ the lifetime of the carriers.

Recombination is not so much due to an electron and a hole recombining directly and thus eliminating each other, but to a variety of complex processes which involve an intermediate state or inactivation of the free carrier in the first instance. These intermediate states are usually known as traps. If the electron (or hole) falls into such a trap, it is, for a finite average time interval, no longer free and its probability of recombination with a carrier of opposite sign is greatly increased. However, there is a finite probability that the carrier may escape from the trap. Both of these probabilities depend on the energy of the trap and the mean energy of the carrier. Traps are usually associated with material imperfections, dislocations, grain boundaries and surface material, which allow the excess momentum of the electron-hole pairs to be transferred to the lattice.

The lifetime τ of a carrier may thus be written as

$$\tau = \frac{1}{vsn} \tag{2.23}$$

where v is the velocity of the charge carrier, s is the collision cross section of the trap, determined by its energy and called the capture cross section and n is the concentration of traps.

The photocurrent I_{ph} in a Schottky barrier type structure incorporating a photoconducting material is

$$I_{ph} = \frac{qF\tau}{T_r} \tag{2.24}$$

where F is the number of charge carriers photoelectrically excited into the conduction band per second, in a given specimen which has an electrode spacing d and to which a voltage V is applied. The transit time T_r of the carriers is defined as

$$T_r = \frac{d^2}{V\mu}. \tag{2.25}$$

The number of electronic charges which pass through the photoconductor per second per photon absorbed from the incident radiation defines the gain factor G:

$$G \equiv \frac{\tau}{T_r}. \tag{2.26}$$

G values greatly in excess of unity may be obtained if carriers are injected from at least one electrode and if the field is high enough. This effect is present in inorganic materials but is of special importance in organic photoconductors, which always incorporate injecting contacts.

The photoelectric excitation produces free electron-hole pairs. In inorganic materials, one of these charge carriers (usually the free holes) is rapidly trapped, but the remaining carrier often the electron, moves under the influence of an applied external field. Once one electron leaves the semiconductor at the anode another enters from the external circuit at the cathode so that current still flows until eventually the trapped hole manages to recombine with a free electron. However in organic polymeric materials,

this simplified view is often complicated by the presence of polaronic and bipolaronic species rather than electron-hole pairs, as discussed in section 3.3.2.

Energetically, traps must be regions of localised positive potential for electrons and regions of local negative potential for holes. Traps are usually closely coupled to the lattice of the semiconductor, which means that a number of discrete energy levels must exist within the trap, thus allowing one or more electrons to be accommodated until the positive charge of the trap is exactly balanced by the electrons caught in it. At this point the net charge vanishes and the deformation vanishes at which point the trap is considered full. The time an electron spends, on average, within a trap depends on the depth of the trap and the initial energy of the electron.

Trapping causes the concentrations of free holes and electrons to be no longer equal and results in a non-equilibrium state where the trapping probabilities and lifetimes will be widely different. In the presence of traps, current will be carried mainly by charges of one sign only, usually known as the majority carriers. A shallow trap is usually defined as one where the lowest energy level within an electron (hole) trap and the bottom (top) of the conduction (valence) band is comparable to kT. Similarly a deep trap is defined as one where the depth of the trap is large compared to kT. Shallow (electron) traps are nearly always empty and can be considered to be in thermal equilibrium with the conduction band, and electrons trapped in such a trap are quickly released. However, electrons may spend considerable time in deep traps and once captured the probability of an electron accumulating sufficient energy to escape is not much greater than the probability of an electron being excited across the energy gap in intrinsic conduction.

2.7 AC Characteristics of a Schottky Diode

Based on the abrupt junction model (section 2.2) the total charge per unit area, Q_{SC} contained in the depletion region of a Schottky junction is given by

$$Q_{SC} = -qN_a w = -(2q\varepsilon\varepsilon_0 N_a)^{1/2}(V_{SO} - V)^{1/2}. \qquad (2.27)$$

Application of a small signal, alternating voltage to the junction will modulate this charge through the dependence on V. Thus a depletion region capacitance C_d may be defined by

$$C_d = \frac{\partial Q_{SC}}{\partial V} = \left(\frac{q\varepsilon\varepsilon_0 N_a}{2(V_{SO} - V)} \right)^{1/2}. \qquad (2.28)$$

Upon rearranging, equation (2.28) yields the Mott-Schottky equation

$$\frac{1}{C_d^2} = \frac{2}{q\varepsilon\varepsilon_0 N_a}(V_{SO} - V) \qquad (2.29)$$

which can be used to extract the doping density N_a , and the degree of band bending, V_{SO}, from the experimentally observed dependence of C_d on V, as shown in figure 2.7.

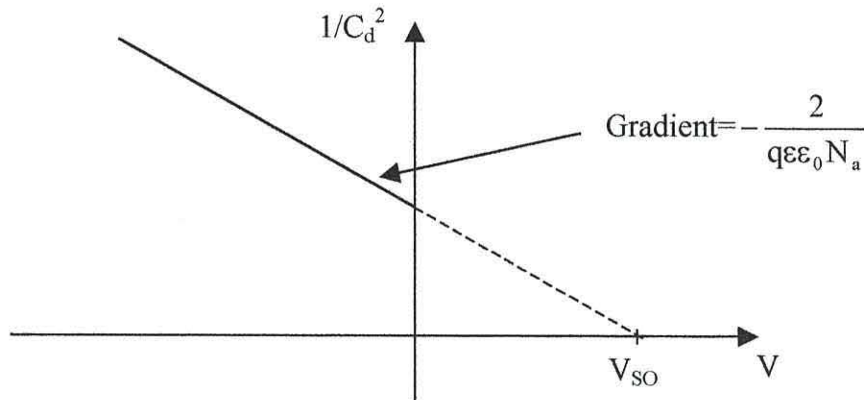

Figure 2.7 *An ideal Mott-Schottky plot for a Schottky barrier diode. The x-axis intercept gives the value of* V_{SO}.

Equation 2.29 can be adequately used to describe the behaviour of devices having an uniform space charge region, however, departures from this relationship will occur when a real Schottky diode with a non-uniform space charge region is considered.

Consider the case of a more realistic device as depicted in figure 2.8 (a). In this case the acceptor density in a layer of width X adjacent to the electrode is N_1, but increases abruptly to ($N_1 + N_2$) beyond this point.

Equation 2.29 will hold until the applied bias is sufficiently high to cause band bending such that the depletion region edge reaches the plane at x = X. By further increasing the reverse bias and applying Poisson's equation to the two regions independently a relation of the form

$$C_d^{-2} = \frac{2}{q\varepsilon\varepsilon_0(N_1 + N_2)}\left(V_{SO} + V + \frac{N_2}{N_1}V_X\right) \tag{2.30}$$

may be obtained (Taylor and Gomes, 1995), where V_X is the potential at the boundary X.

The increase in ionised acceptor density at X abruptly reduces the gradient of a Mott-Schottky plot at V_X. However the corresponding shift in the intercept ensures that no discontinuity occurs in the plot (see curve (i) fig 2.9).

The change in the gradient of a Mott-Schottky plot in the presence of deep-lying localised states was used as strong evidence to support the fact that localised deep states affect both the electrical and optical properties of Schottky barrier diodes (Taylor and Gomes, 1995). Consider fig 2.8 (b) in which two discrete acceptor levels are present in the semiconductor, one at E_1 (which lies below E_F) and another at E_2 (which lies above E_F) when band bending is small.

If V_S is a measure of the degree of band bending (as shown in figure 2.8) and $qV_S < (E_2 - E_F)$ then the probability of occupation , by electrons, of the states at E_2, is low and so equation 2.18 holds with $N_a = N_1$, the density of states at E_1. However, when $qV_S > (E_2 - E_F)$ then the acceptor states at E_2 which fall below E_F will now capture electrons. In this case the space charge layer is composed of two distinct regions (i) $0 \leq x \leq X$ where $N_a = N_1 + N_2$ and (ii) $X \leq x \leq W$ where $N_a = N_1$. The device

capacitance, as a function of potential, in this case depends on the signal frequency (Roberts and Crowell, 1970 and 1973).

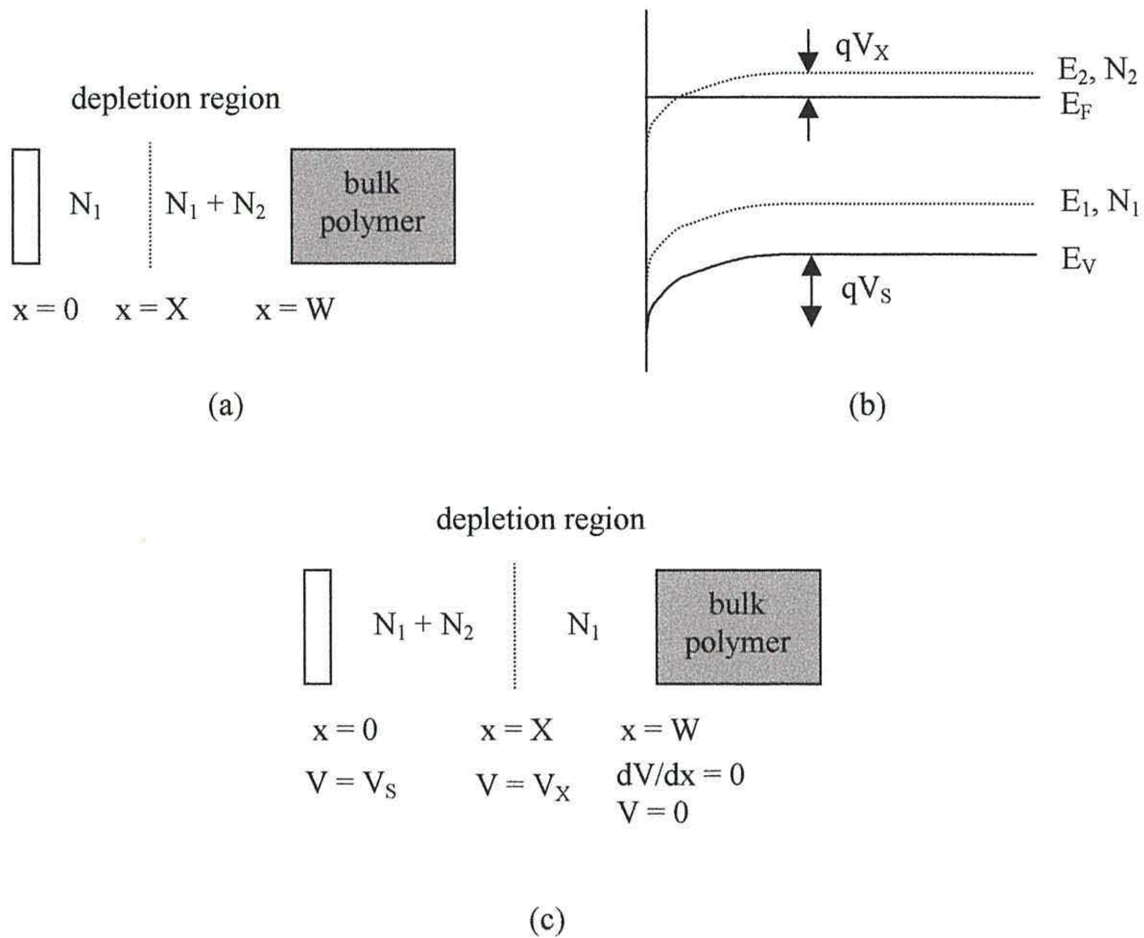

Figure 2.8 *(a) Charge distribution in the depletion region of a classical Schottky diode when an abrupt increase in the density of acceptors occurs at x = X. (b) Band diagram and (c) the resulting charge density when band bending is sufficient to cause the activation of a deep lying acceptor state.*

At high frequencies, the deep acceptor states at x = X are unable to follow the signal so that the capacitance is determined by the modulation of the majority carriers at the edge of the depletion region. The capacitance-voltage relationship in this case is given by

$$C_d^{-2} = \left(\frac{2}{q\varepsilon\varepsilon_0 N_1}\right)\left\{V_S - \frac{N_1 N_2}{(N_1+N_2)^2}V_X\left\{\left[1+\left(\frac{N_1+N_2}{N_1}\right)\left(\frac{V_S}{V_X}-1\right)\right]^{\frac{1}{2}}-1\right\}^2\right\} \tag{2.31}$$

as deduced by Taylor and Gomes, 1995, and is distinguished from the relationship given in equation 2.30 by the curvature in the plot when $V_S > V_X$ (c.f. curves (i) and (ii) fig 2.9).

At sufficiently low frequency the states at x = X lying within a few kT of E_F will charge and discharge in response to the signal voltage. This additional contribution results in a sudden decrease in the Mott-Schottky plot at V_X (see curve (iii) fig 2.9).

As a result measuring the capacitance of the depletion region is often complicated by (i) the influence of the bulk conductivity (high frequency) and (ii) interface states (low frequency).

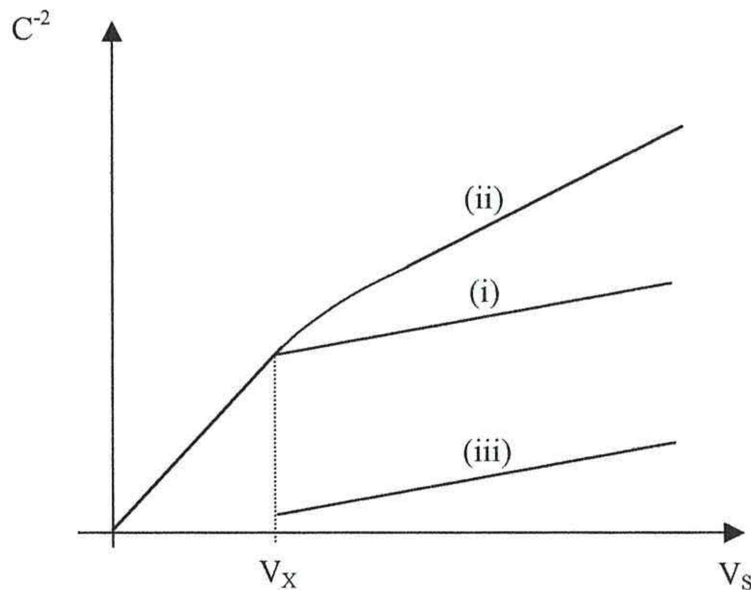

Figure 2.9 *A schematic representation of a Mott-Schottky plot for a Schottky barrier diode showing the effect of band bending V_S on the depletion region capacitance.(i) When an abrupt increase in the shallow acceptor density from N_1 to $N_1 + N_2$ occurs at a depth X below the contact.(ii) the high frequency and (iii) the low frequency behaviour of a device with a density N_1 of shallow states and N_2 of deep lying states.*

2.7.1 Effects of Bulk Conductivity

The equivalent circuit of a Schottky diode is given in figure 2.10. C_d is the depletion region capacitance (equation 2.29) and R_d the associated resistance. The bulk

semiconductor can also be represented by a capacitance C_b in parallel with the bulk resistance R_b. Normally C_d>>C_b and R_d>>R_b.

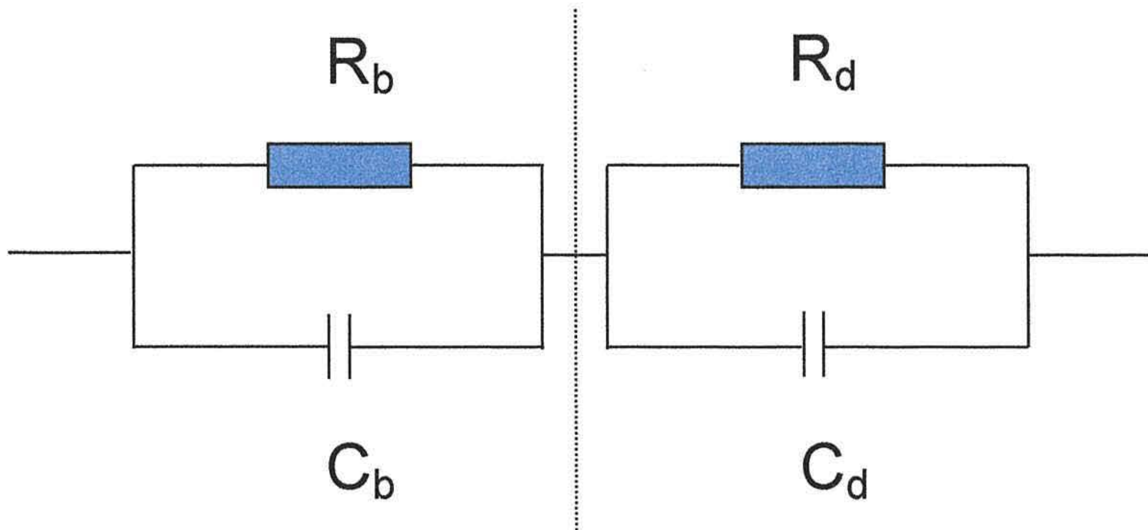

Figure 2.10 *A simple equivalent circuit for a Schottky barrier diode based on an organic polymer.*

The total admittance of a Schottky diode as measured using, for example, an ac bridge will be

$$Y_P = G_P + j\omega C_P \tag{2.32}$$

where

$$G_P = G_{LF} + \frac{G_a}{1+(\omega\tau_R)^2} \tag{2.33}$$

and

$$C_P = C_g + \frac{C_{LF} - C_g}{1+(\omega\tau)^2}\,. \tag{2.34}$$

In this case C_g is the series sum of the barrier and bulk capacitances $C_dC_b/(C_d + C_b)$ and C_{LF} the effective low frequency capacitance of the device given by

$$C_{LF} = \frac{C_d R_d^{\,2} + C_b R_b^2}{(R_d + R_b)^2} \,. \tag{2.35}$$

G_{LF} is the low-frequency (dc) conductance $(R_d + R_b)^{-1}$, G_a the ac conductance given by

$$G_a = \omega^2 \frac{R_d R_b (R_d C_d - R_b C_b)^2}{(R_d + R_b)^3} \tag{2.36}$$

and τ_R the circuit relaxation time given by

$$\tau_R = \frac{R_d R_b}{R_d + R_b}(C_d + C_b) \,. \tag{2.37}$$

From this it can be seen that the system follows a classical Debye-like relationship as suggested by Von Hippel. If $R_d >> R_b$ then

$$\tau_R \cong R_b(C_d + C_b) \tag{2.38}$$

which can be used as a quantitative measure of the doping density in the semiconductor. This finding means that in order to calculate C_d from device capacitance, C_p, measurements need to be performed at frequencies well below τ_R . In general, if the doping density N_a is high, the bulk resistance is reduced thus reducing the circuit relaxation time, τ_R. Equations 2.32 to 2.38 can be used to determine the capacitance and loss vs. frequency plots for a theoretical Schottky diode as shown in figure 2.11.

(a)

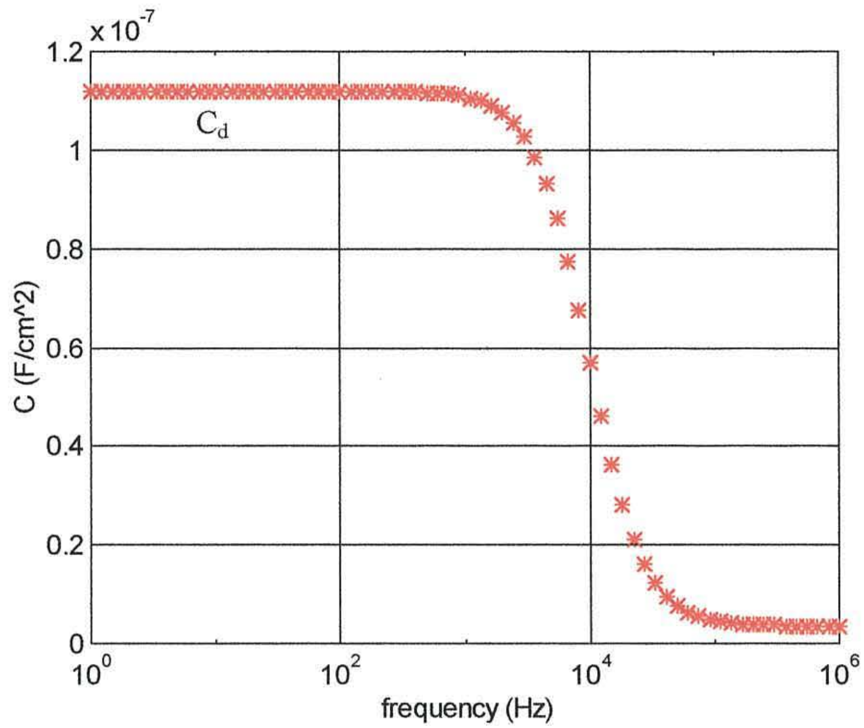

(b)

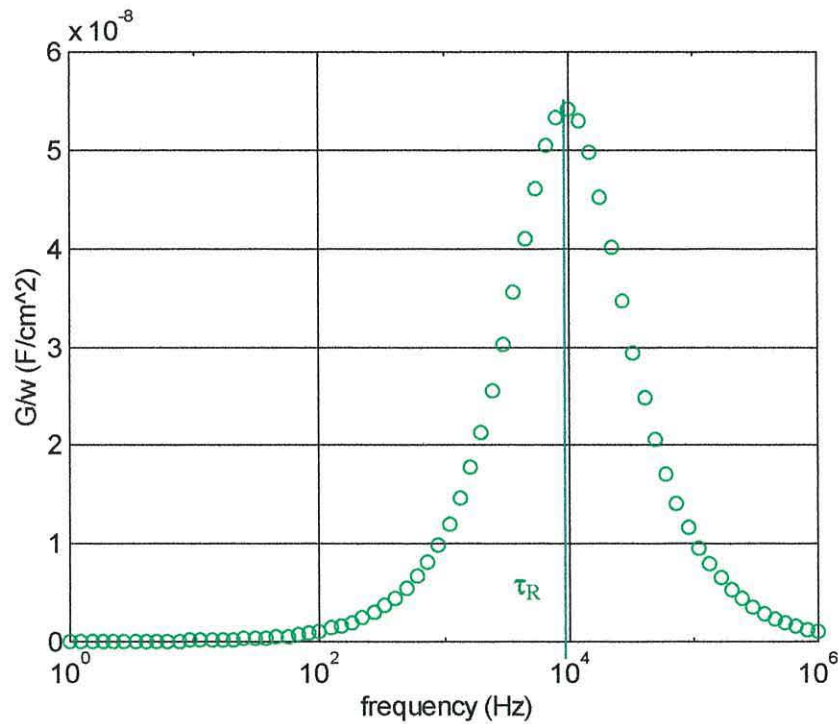

Figure 2.11 *Capacitance (a) and loss (b) versus frequency plots for a theoretical Schottky diode using equations 2.32 to 2.38. Parameters per unit area are* $R_d = 70.4$ $M\Omega, C_d = 112\ nF$, $R_b = 140\ \Omega$, $C_b = 3.77\ nF$.

2.7.2 Interface States

In a practical Schottky barrier diode it is the disruption of the crystal lattice at the interface that produces a large number of energy states called interface or surface states, located within the forbidden gap.

The states are usually continuously distributed in energy and characterised by a neutral level E_0 such that if the interface states are occupied up to E_0 and empty above E_0 , the surface is electrically neutral. That is, the states below E_0 are positively charged when empty acting like donors; the states above E_0 are negatively charged when occupied thus acting like acceptors.

If E_0 is aligned with the Fermi level, the net charge of the surface is zero. However, in a practical Mott-Schottky contact whenever $E_0 > E_F$, the net charge of the interface states is positive (donor like) so that fewer ionised donors are needed in the depletion region to reach equilibrium. As a result the built-in potential is effectively reduced, and similarly the barrier height (ϕ_b) is reduced.

A smaller ϕ_b brings E_F closer to E_0. Similarly if $E_0 < E_F$, there is a negative charge in the interface states and ϕ_b is increased to bring E_F closer to E_0 again.

Thus charge in the interface states has a negative feedback effect which tends to keep E_F close to E_0. In extreme cases where the interface state density is large the Fermi level is effectively pinned at E_0 and ϕ_b becomes independent of the work functions of the metal and the semiconductor.

However, the effect of interface states can be particularly pronounced when low frequency ac measurements are performed on diode structures. The varying ac signal applied to the diode when making capacitance and loss vs. frequency plots leads to a change of occupation of the interface states which result in an increase of the apparent capacitance and loss which deviates from the expected trap-free relationship as shown in figure 2.12.

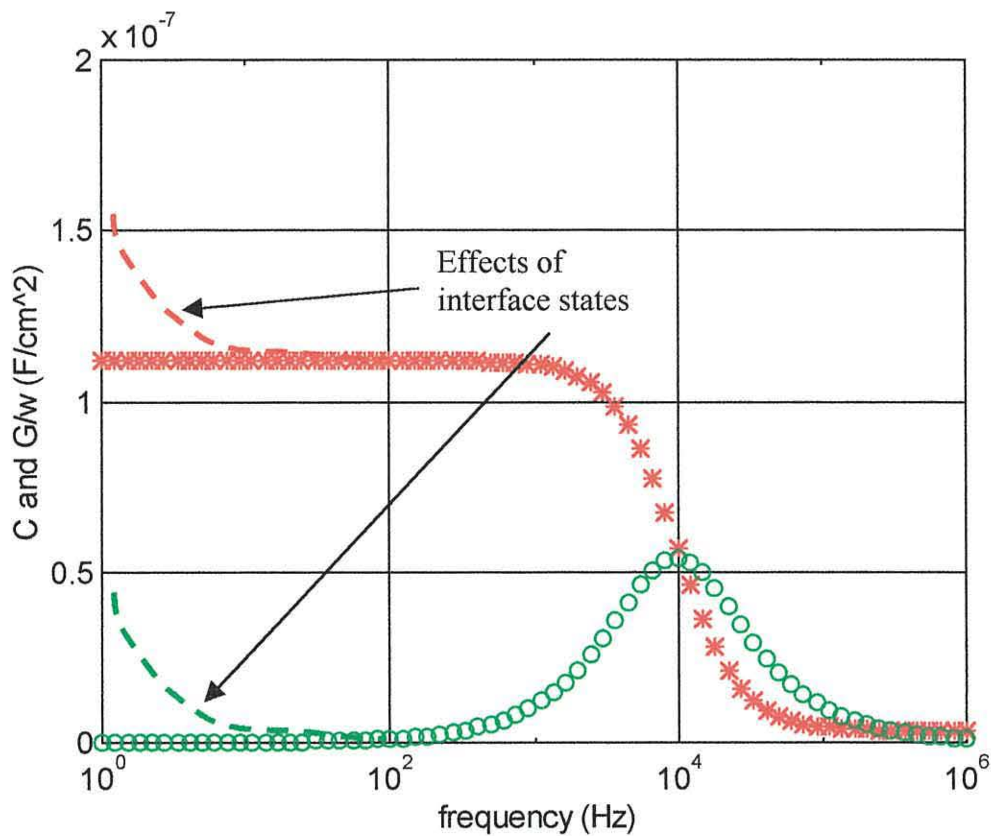

Figure 2.12 *Capacitance and loss versus frequency plots for a theoretical Schottky showing the effect of interface states at low frequency.*

So as to minimise the effects of capacitance dispersion resulting from interface states, device measurements should be performed in excess of the low frequency limit, at which dispersion becomes pronounced.

2.7.3 Photocapacitance

The origins of electron-hole pair generation in the depletion region of a Schottky barrier diode when illuminated has already been discussed in section 2.6.2.

The electron-hole pairs created can diffuse until they recombine with carriers supplied from the external circuit, decay, or are trapped by deep levels in the gap. This last process will result in an increase in the net negative space charge and a corresponding increase in the diode capacitance due to a decrease in the depletion region width.

As a result photocapacitance measurements can improve our understanding of the kinetic mechanisms of trapping processes within both the depletion region and the bulk material. When the optical stimulus is removed electrons (already held in electron traps) detrap and decay or recombine, thus reducing the measured capacitance of the device, which eventually returns to a steady-state value.

As discussed previously, in the trap-free case the charge carrier concentration associated with electron-hole pair generation/recombination follows an exponential relationship (Sze, 1981), which gives rise to an exponential-like transient when the light source is pulsed. In the presence of trapping states, this transient is modified resulting in an exponential relationship having more than one time constant.

A behaviour similar to this is also observed during electrical stimulation of diode structures and is the basis of deep level transient spectroscopy (DLTS) which is described in the following section.

2.8 Deep Level Transient Spectroscopy (DLTS)

In section 2.7 it was shown that the existence of deep states may be inferred from a change in slope of the high frequency C-V characteristic and confirmed by the appearance of a discontinuity in the low frequency characteristic. Often it is not possible to make measurements at a sufficiently low frequency to obtain the necessary corroborative evidence. This will be true particularly for the deepest states. Deep level transient spectroscopy (DLTS, first reported by Lang (1974)), is a technique that allows these deep states to be probed.

In conventional DLTS, as applied to inorganic semiconductors, a reverse biased Schottky barrier diode is momentarily switched into forward bias. This has the effect of swamping the depletion region with charge carriers (majority carriers from the semiconductor and minority carriers from the electrode). During the forward bias pulse, therefore, localised states in the bandgap are filled with the probability of occupation depending on the position of the quasi-Fermi level. The return to steady-state occupancy of these states, after the forward bias pulse, may be followed by measuring the time-dependence of the depletion region capacitance. In the following discussion, it will be

assumed that the localised states are electron traps and that they are electrically neutral when empty.

If the steady-state occupation of an electron trap, of a given energy, is $\bar{n}$ and the total number of states is N, then the emission and capture rates can be given as $e_2\bar{n}$ and $e_1(N-\bar{n})$ respectively, where e_2 is defined as the thermal emission rate constant and e_1 as the capture rate constant.

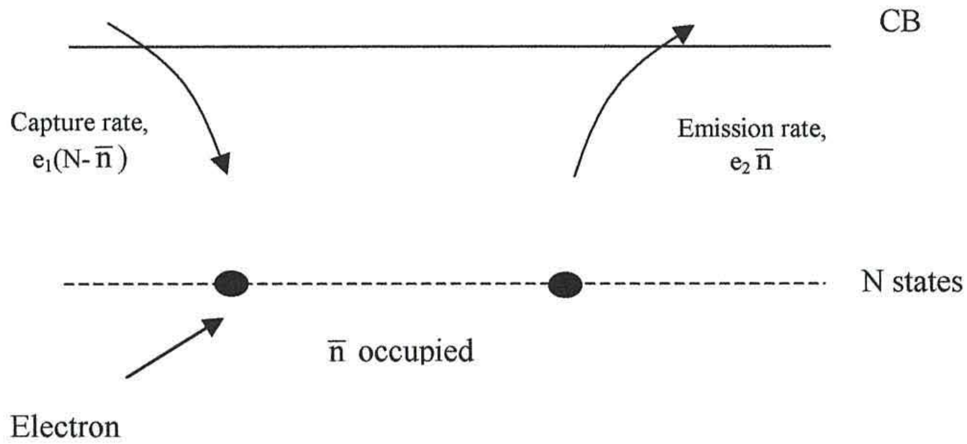

Figure 2.13 *Schematic representation of the emission and capture processes of an electron trap.*

At equilibrium

$$e_2\bar{n} = e_1(N - \bar{n}) \tag{2.39}$$

giving

$$\bar{n} = \left(\frac{e_1}{e_1 + e_2}\right)N. \tag{2.40}$$

During the forward bias pulse it may be assumed that the capture rate constant e_1 greatly exceeds the emission rate constant e_2, so that $\bar{n} = N$, and all traps are filled. Upon returning to reverse bias, the capture rate is initially zero and the state occupancy is governed by the emission rate $e_2\bar{n}$.

Thus the rate of change of the trap occupancy is given by

$$\frac{d\overline{n}}{dt} = -e_2\overline{n} \ . \qquad (2.41)$$

Integrating subject to the boundary conditions that at t = 0, $\overline{n} = N$ then it is readily shown that

$$n(t) = N\exp(-e_2 t) = N\exp\left(-\frac{t}{\tau}\right). \qquad (2.42)$$

Therefore the trap occupancy decreases exponentially with a time constant equal to e_2^{-1}. According to Shockley-Hall-Read statistics (Sze, 1981), the emission rate constant is given by

$$e_2 = \frac{1}{\tau} \cong \upsilon \exp\left[-\left(\frac{E_C - E_T}{kT}\right)\right] \qquad (2.43)$$

where υ is the attempt to escape frequency (~ 10^{12} s^{-1}), and ($E_C - E_T$) the depth of the trap below the conduction band edge.

From equation 2.28, the depletion capacitance, C, in a p-type semiconductor in the presence of a uniform concentration $\overline{n}$ of trapped electrons will be given by

$$C = a(N_a + \overline{n})^{1/2}, \qquad (2.44)$$

where a is a constant. For $\overline{n} << N_a$ then equation 2.44 simplifies to

$$C = aN_a^{1/2}\left(1 + \frac{\overline{n}}{2N_a}\right) = C_d\left(1 + \frac{\overline{n}}{2N_a}\right). \qquad (2.45)$$

Thus, filling and emptying of the electron traps will lead to a change, ΔC, in the measured depletion region capacitance, given by

$$\Delta C = \frac{C_d \overline{n}(t)}{2N_a} = \frac{C_d}{2N_a} N \exp\left(-\frac{t}{\tau}\right). \tag{2.46}$$

Therefore by measuring the temporal evolution of the capacitance following a forward bias pulse it is possible to determine the concentration of traps, N, the emission rate constant e_2 and hence the trap energy E_T.

In the case where both a hole and an electron trap are active, $\overline{n}$ must be replaced by $(\overline{n} - \overline{p})$ where $\overline{p}$ is the occupancy of the hole trap. In the general case where a set of electron and hole traps of different energies are present, then $\overline{n}$ is replaced by $\left(\sum_i \overline{n}_i - \sum_i \overline{p}_i\right)$.

From equation 2.43 it is seen that the emission rate constant e_2 is a strong function of temperature. The essential feature of the DLTS technique is that by varying the sample temperature, the emission rate from the trap can be made to coincide with an emission rate window set by the measuring apparatus.

Figure 2.14 shows a series of capacitance transients obtained at different temperatures following a forward bias pulse. At low temperatures e_2 is small and thermal emission from traps is slow. As the temperature increases, the emission rate increases and the return to equilibrium becomes more and more rapid. Consider now that at each temperature the change in capacitance, $C(t_1) - C(t_2)$, between two fixed time intervals t_1 and t_2 is measured. A plot of $C(t_1) - C(t_2)$ will pass through a maximum (figure 2.14) when e_2^{-1} is approximately equal to $(t_2 - t_1)$.

Then if the normalised DLTS signal, S(T) is defined as

$$S(T) = \frac{C(t_1) - C(t_2)}{\Delta C_0} \tag{2.47}$$

where ΔC_0 corresponds to the initial change in capacitance induced by trap filling. Then substituting from equation 2.46 yields

$$S(T) = \exp\left(-\frac{t_1}{\tau}\right) - \exp\left(-\frac{t_2}{\tau}\right) \quad (2.48)$$

Equation 2.48 may also be written as

$$S(T) = \exp\left(-\frac{t_1}{\tau}\right)\left[1 - \exp-\left(\frac{\Delta t}{\tau}\right)\right] \quad (2.49)$$

where $\Delta t = t_2 - t_1$. It is readily shown that the function passes through a maximum at a temperature T_{max} when the emission time constant τ_{max} is given by

$$\tau_{max} = (t_1 - t_2)\left[\ln\left(\frac{t_1}{t_2}\right)\right]^{-1} \quad (2.50)$$

Thus, by varying systematically the rate window, a series of values may be obtained for τ_{max} corresponding to a series of temperatures T_{max}. An Arrhenius plot of such data leads to an estimate of the trap energy E_T (see equation 2.43). The best method for carrying out this measurement is to keep the ratio t_1/t_2 fixed while varying t_1. This results in a series of peaks that shift more or less rigidly without changing their shape as the rate window is varied (see figure 2.15).

The density of traps can be determined from equation (2.42) by noting the initial capacitance change ΔC_0.

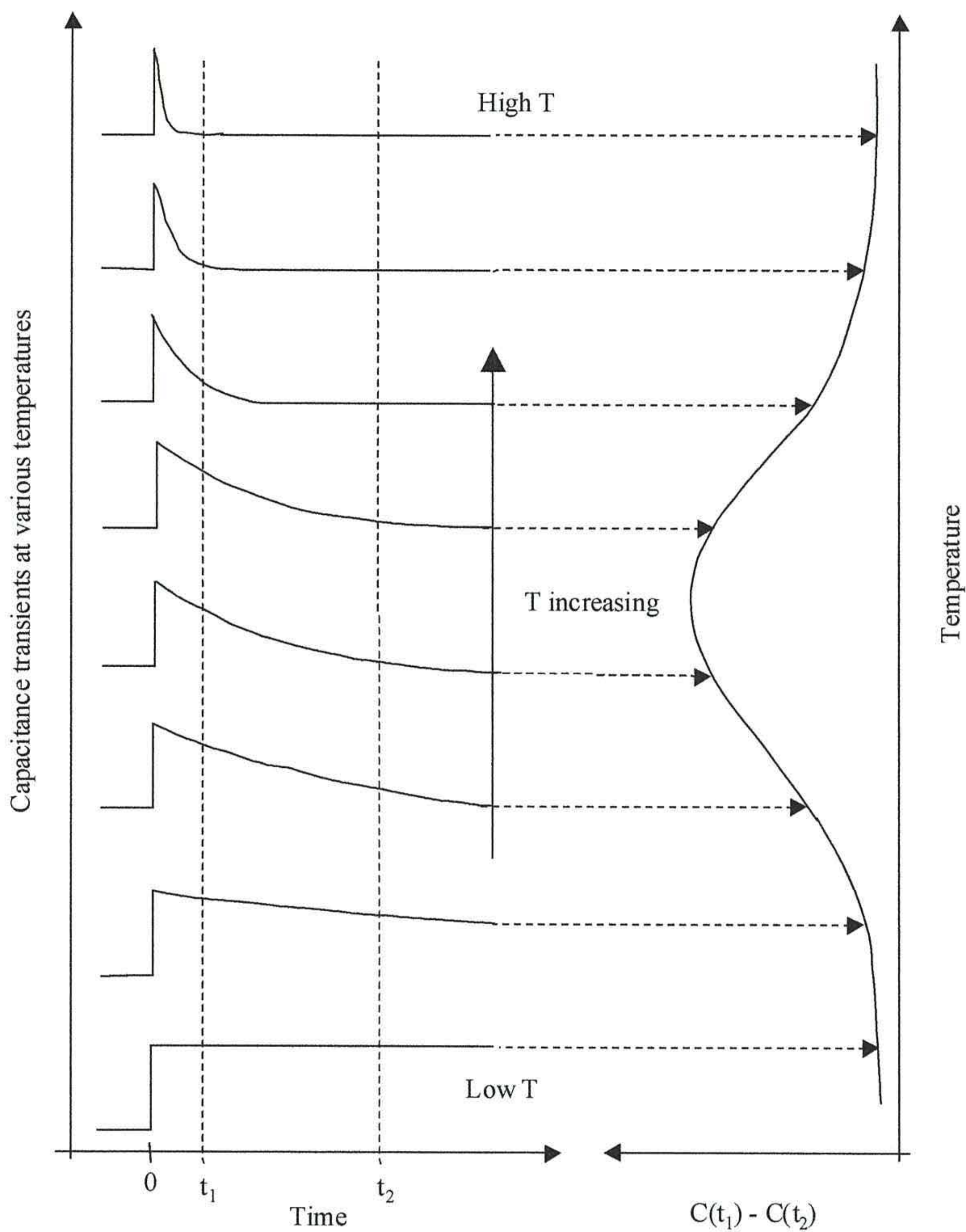

Figure 2.14 *A series of capacitance transients corresponding to trap emptying at different temperatures. Also shown is the corresponding DLTS vs. temperature plot. (from Lang, 1974).*

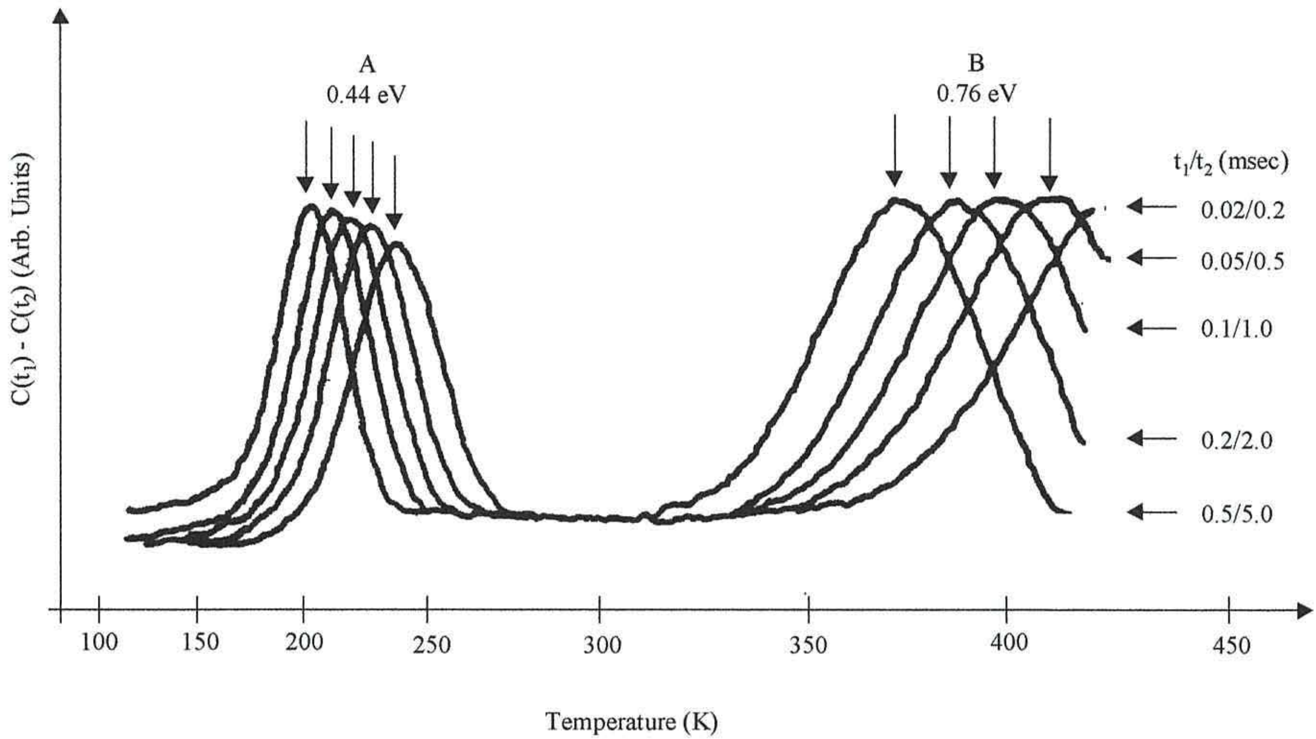

Figure 2.15 *Typical experimental DLTS spectra for hole traps in n-GaAs. The two traps labelled A and B have activation energies as shown. Five different spectra are shown corresponding to the five rate windows determined by the values of t_1 and t_2. (from Lang, 1974).*

In Chapter 4 the techniques and ideas discussed in this Chapter are applied to Schottky diodes formed at the aluminium / P3MeT interface.

3. Conducting Polymers

3.1 Introduction

When considering the relative electrical properties of various materials, one normally associates conducting and semiconducting properties with inorganic materials e.g. metals, silicon, GaAs, and insulating properties with polymeric materials, such as polyethylene. Except for a few specialised transducer applications where polymeric piezoelectric and pyroelectric materials have been used, this has certainly been the traditional view of polymers, especially in the electronic industry, where only their insulating properties have been exploited for isolation of various components in an electrical circuit. As discussed in Chapter 1, this view is rapidly changing since the discovery of a new class of polymeric materials, namely conducting polymers, so-called after their first foreseen application as conducting layers.

Conducting polymers were first discovered by Shirakawa and co-workers in 1974 when the first conducting polymer film, based on PA was prepared (Ito *et al.*, 1974). By 1977 the same group of researchers had identified that this material was extremely susceptible to chemical or electrochemical oxidation (and reduction), which meant that its conductivity could easily be modified (Shirakawa *et al.*, 1977). This fact was subsequently used to modify both the electrical and optical properties of PA.

Between 1977 and the mid 1980s, the emphasis was placed on achieving large variations in the electrical conductivity of films such as PA. This led to the discovery of new conducting polymers and an improved understanding of charge storage mechanisms (MacDiarmid and Heeger, 1979; Wegner and Ruhe, 1989; Baughman *et al.*, 1982). Once the requirements for good quality, highly conductive films had been identified, the research effort moved towards the development of films that had improved stability and simplified preparation methods whilst retaining high electrical conductivity in the oxidised state. In particular, spin-coated poly(p-phenylene vinylene) (PPV) (Murase *et al.*, 1984; Karasz *et al.*, 1985), various electropolymerised poly(3-alkylthiophene) (Diaz, 1981; Tourillon and Garnier, 1982) and Langmuir-Blodgett (LB) deposition of polyaniline films all received considerable attention. These studies proved invaluable at the time, since most previously studied conducting polymers were

unstable in air and rather difficult to process. For example the conductivity of PA films was reported to initially increase on exposure to air, but reversal of this trend was quickly observed as conjugated chains of the polymer underwent irreversible oxidation (Pochan, 1986; Billingham *et al,* 1987). Similar effects were observed for polypyrrole, in particular where sensitivity to ambient oxygen appeared to dope the films in a similar manner to I_2 and PF_6^- (Pfluger *et al,* 1983; Tourillon and Garnier, 1983).

Figure 3.1 shows the range of conductivity that can be achieved in conjugated polymers compared with the values of some conventional solids. Dedoped conjugated polymers are essentially highly insulating in nature but can become highly conducting upon doping by either chemical or electrochemical methods. One of the highest values of conductivity published to date for conducting polymers is approximately 4×10^5 S cm^{-1}, obtained in highly defect-free Naarman-type *trans*-PA (Naarman and Theophilou, 1987), which is close to the conductivity of copper, ~ 6×10^6 S/cm. Electrical conductivities ranging between about 10^3 and 10^4 S cm^{-1} have similarly been identified in stereoregular polythiophene (McCullough and Williams, 1993) and highly stretched polyaniline. It appears though, that only polyacetylenes and polyanilines are currently close to the metal-insulator transition.

Since the late 1980s, the continued improvement in the understanding of the electrical and optical properties of conjugated polymers has allowed the emphasis to be placed on the application of conducting polymers, in particular, light emitting diodes (LEDs) (Burroughes *et al.*, 1990; Parker, 1994; Braun and Heeger, 1991). Considerable interest is being shown at the moment in LED structures for use in display applications where conjugated polymers have the potential for simple and cheap fabrication of large area devices (Cambridge Display Technology). Even, flexible, almost entirely metal-free LEDs have been developed (Gustafsson *et al.*, 1992). It is advances in the chemistry of processable conjugated polymers over the last 20 or so years that have led to this successful achievement. This application area is continually expanding and is already competitive with older GaAs based technology for some niche applications. Recent developments have led to a number of reports of organic smart pixels (Sirringhaus *et al.*, 1998; Dodabalapur *et al.*, 1998), colour tuneable LEDs (Berggren *et al.*, 1994 and 1995), inkjet printing of polymer electroluminescent devices (Bharathan and Yang, 1998) and general low cost, all-polymer integrated circuits.

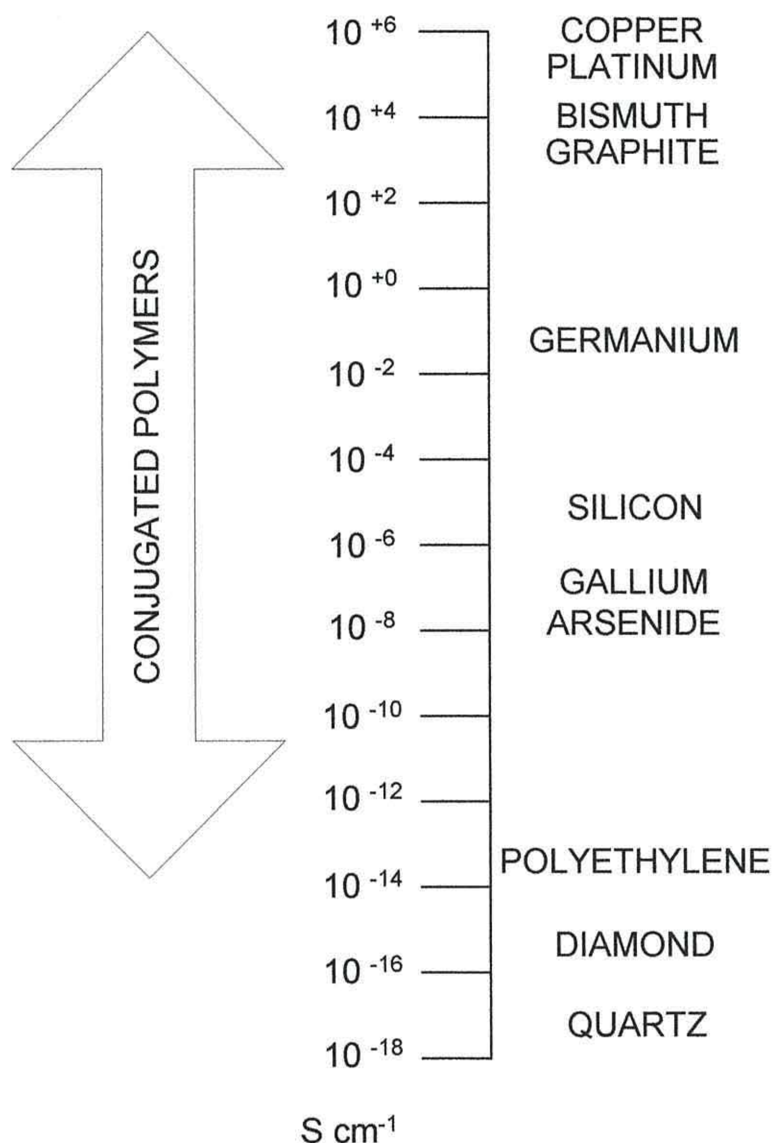

Figure 3.1 *Conductivity of conjugated polymers compared to other conventional solids.*

OLEDs generally have a simple, single layer or 2-layer based polymer structure. Both structures use a metallic base layer, usually indium tin oxide (ITO) coated glass substrate, (an) active layer(s) (each ~ 1000 Å thick), and an evaporated top metal electrode (usually Ca, In or Al) as shown in figure 3.2.

Light emission is achieved when sufficient bias is applied to the respective contacts to achieve injection of positive and negative charge carriers from opposite electrodes, into the active region. Capture of the separate hole and electron entities within the bulk

polymer leads to the formation of excitonic species, which radiatively decay to a lower energy level (Salaneck *et al.*, 1996).

Early designs were based on a single polymer layer structure, which generally had low values of quantum efficiencies (< 0.01 %) (Burroughes *et al.*, 1990 and references within). However for high light output it was soon identified that it was essential to maximise the rates at which electrons and holes were injected into the active conducting polymer. As a result, later designs were based on a 2-polymer layered structure, usually incorporating a hole-transporting layers (HTL) such as N,N′-diphenyl-N,N′-bis(3-methylphenyl)-1,1′-biphenyl-4,4′-diamine (TPD) and 8-hydroxyquinolinato aluminium (Alq), as an electron transporter and emitter (Dodabalapur *et al.*, 1998; Brown *et al.*, 1992) in addition to the active conducting polymer. A number of devices based on the new multi layered structures were more efficient, with typical quantum efficiencies of the order of 3 % (Greenham *et al.*, 1993).

To fully appreciate the major developments in the field of conducting polymers since their first discovery, the reader is referred to a number of review papers and other extensive literature for additional information (Munn, 1984; Bloor, 1983; Stubb *et al.*, 1993; Salaneck and Brédas, 1994).

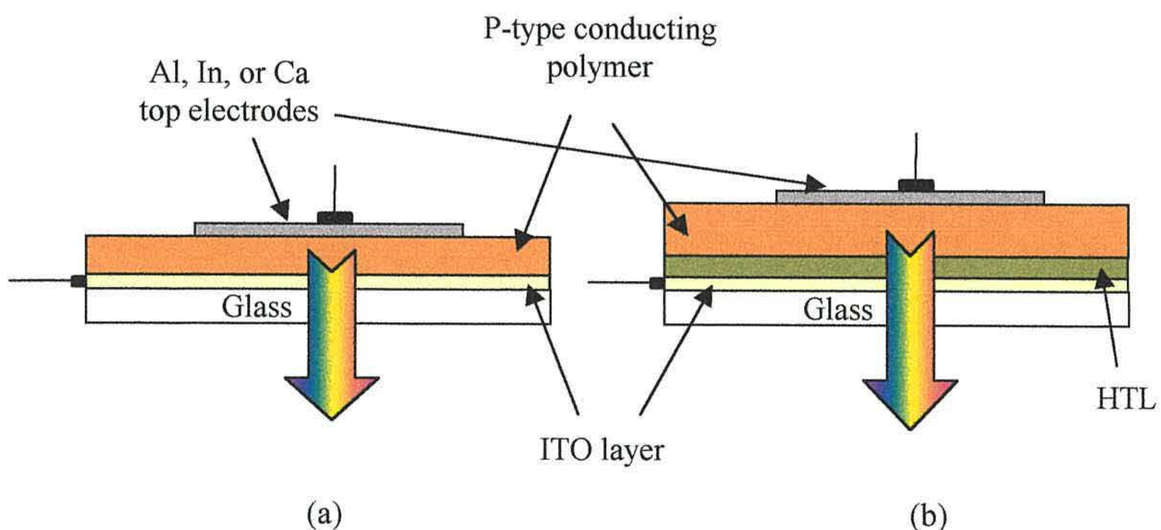

Figure 3.2 *The structure of (a) a single-layer OLED and (b) a 2-layer OLED incorporating a hole transporting layer.*

3.2 Chemical Structure

The remarkable electrical properties of polyacetylene can be attributed to the "backbone" of alternating single and double carbon-carbon bonds, or conjugated bonds forming the molecule. Many different polymers, all possessing this same "backbone", have been synthesised, so that the family of conjugated polymers is now quite extensive.

The structures of some of the more common polymers are shown in fig. 3.3. The conjugation in each molecule (or repeat unit) can readily be observed. In the case of polyacetylene both the *trans* and *cis* forms are given. In this case the two different isomers have different geometrical configurations with respect to the C-C double bonds. These two "similar" structures have been included to complement the fact that the two different isomers of PA can show unique electrical and optical properties. Trans-polyacetylene differs from the other polymers in figure 3.3 in that two, degenerate ground state bonding configurations occur. The second configuration differs from that shown in figure 3.3(a) simply by a reversal of the bond alternation. The degeneracy of the ground state has important consequences for transport and other properties of conjugated polymers (see later) (Rice, 1979; Su *et al.*, 1979). In all the other cases shown in figure 3.3, the ground state is non-degenerate, which means that a reversal of the bond alternation results in a higher energy state.

Apart from PA, all polymers shown in figure 3.3 support excitons (bound electron-hole pairs), in which case the optical absorption edge is smaller than the bandgap by an amount corresponding to the exciton binding energy, as shown in Table 3.1. In polyacetylene, where the lowest excited state has the same symmetry as the ground state, few excitons exist since radiative transitions are not permitted. In this case the bandgap is equal to the absorption edge at 1.4 eV. However, in PPV as in other exciton supporting polymers, there is considerable evidence that the exciton binding energy is of the order of a few tenths of an electron volt (Frankevich *et al.*, 1992; Gomes da Costa and Conwell, 1993). In practice it has proved extremely difficult to precisely quantify the excitonic binding energy but most conducting polymers have values from one electron volt down to a few hundredths of an electron volt. One common problem is that there exists some uncertainty in the absorption edges, because they are not

normally well defined experimentally, possibly due to variations in the conjugation length and other disordering mechanisms.

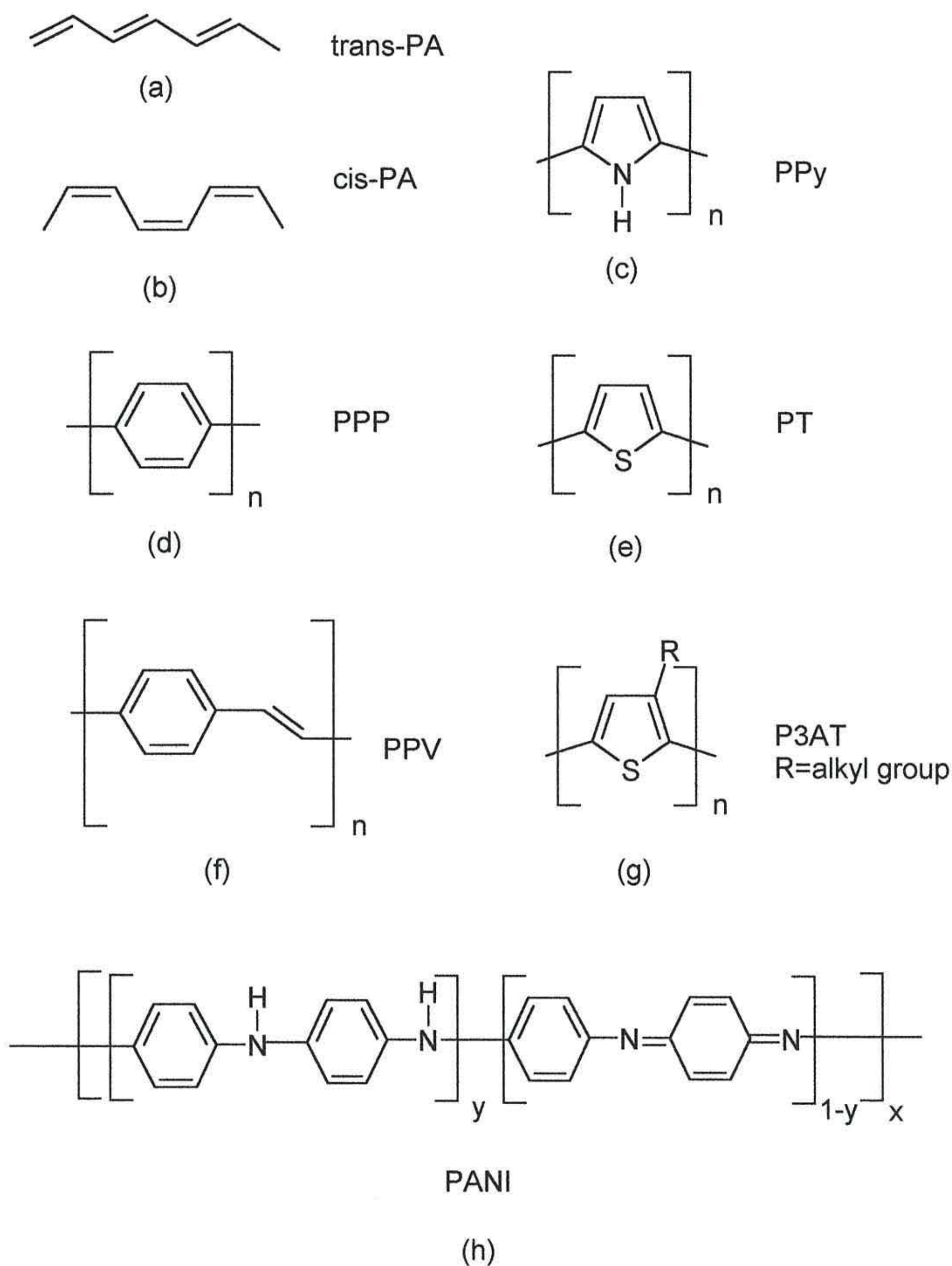

***Figure 3.3** Molecular structure of the most common conjugated polymers.*

	Acronym	Polymer	Optical Absorption Edge (eV)[1]	Bandgap (eV)
(a)	*trans-PA*	*Polyacetylene (trans – orientation)*	*1.4*	*1.4*[1]
(b)	*cis-PA*	*Polyacetylene (cis – orientation)*	*2.0*	*2.0*[1]
(c)	*Ppy*	*Polpyrrole*	*2.5*	*3.2*[2]
(d)	*PPP*	*Poly(p-phenylene)*	*3.0*	*3.4*[3]
(e)	*PT*	*Polythiophene*	*2.0*	*2.1*[4]
(f)	*PPV*	*Poly(p-phenylene vinylene)*	*2.4*	*2.5*[5]
(g)	*P3AT*	*Poly(3-alkylthiophene)*	-	-
(h)	*PANI*	*Polyaniline*	*1.6*	*1.7*[1]

Table 3.1 *Acronyms, optical absorption edges and bandgaps of the most common, neutral polymers. ([1] Handbook of Organic Conductive Molecules and Polymers, [2] Handbook of Conducting Polymers 1986 Vol. 2, [3] Ivory et al., 1979, [4] Kaneto et al., 1984, [5] Friend et al., 1987)*

Polyanilines, (PANI) (as shown in figure 3.3) represent a special class of polymers. They are composed of y and (1-y) reduced and oxidised units, respectively. The y value may vary continuously, from unity for the completely reduced polymer (containing only amine nitrogens), to zero, for the completely oxidised polymer (containing imine nitrogens). The different degrees of oxidation lead to states called lucoemeraldine (y=1), emeraldine (y=0.5) and pernigraniline (y=0).

Polyaniline has attracted much attention because of (a) its unique doping mechanism, which is different to that commonly found in other conducting polymers and (b) its high stability in air.

The electrical conductivity of polyaniline (PANI) increases by over ten orders of magnitude when doping with strong acids (chemical doping) causes a transformation of its emeraldine base form (EB) into the emeraldine salt form (ES). It is in the EB form that PANI reaches its highest conductivity. During the doping which is commonly known as protonation (or primary doping) there is no accompanying change in the number of electrons associated with the polymer backbone (internal redox process).

It was discovered six years ago (Cao *et al.*, 1992) that the conductivity of PANI films doped with camphor sulphonic acid in m-cresol can reach values close to 400 S cm^{-1} as a result of the expanded conformation of the polymer chains. This process is known as secondary doping.

It is interesting to note that the properties acquired by the polymer after secondary doping remain even though the secondary dopant (m-cresol) is removed. This observation is known as the "memory effect" and only occurs in the secondary doping process of polyaniline. In common with most conducting polymers, polyaniline can be both chemically and electrochemically polymerised.

Polypyrrole, (PPy) was first polymerised in 1916 by the oxidation of pyrrole with hydrogen peroxide to give an amorphous powdery product known as pyrrole black. Little further interest was shown in this material, though, until it was electrochemically prepared in the form of a continuous film. In 1979, following the great success of the work by Shirakawa and co-workers on PA, electrochemical techniques to synthesise polypyrroles became a useful way of obtaining highly conductive, free-standing materials. Pyrrole is one of the most easily oxidised monomers and hence a variety of oxidising agents are available for preparing PPy, for example, iodine, bromine, chlorine, iron chloride, iron bromide and potassium chloride (Vandersluijs *et al.*, 1987 - and references within).

Over many years PPP, PPV and PPy have all been the subject of intensive research but following the revolutionary work of the Cambridge group on LEDs, in 1990 (Burroughes *et al.*, 1990), the interest in PPV and its derivatives such as poly(2-methoxy-5-(2'-ethyl-hexoxy)-p-phenylenevinylene) (MEH-PPV) and poly(2,5-hexyloxy-p-phenylene cyanovinylene) CN-PPV has grown from strength to strength, particularly in the field of electroluminescent devices and displays (Halls *et al.*, 1995; Parker, 1994; Friend *et al.*, 1997; Marks *et al.*, 1993, Ioannidis *et al.*, 1998).

Another important class of conjugated polymers, which is currently increasing in popularity, is polythiophene and its derivatives. In particular, poly(3-alkylthiophenes), where alkyl groups of various lengths including methyl, hexyl and octyl have been substituted onto the '3' position of the thiophene ring, are some of the most

environmentally and thermally stable conducting polymer materials. Contrary to the prevailing view at the time, Taylor and co-workers (1991) reported that FET structures formed from poly(3-methylthiophene) were, however, adventitiously doped when exposed to ambient air.

Even though this finding meant that most device measurements on poly(3-alkylthiophenes) had to be performed under vacuum, these materials have continued to attract much interest. For example, polythiophene and its derivatives have been used as electrical conductors, non-linear optical devices (Mazumdar *et al.*, 1993), polymer LEDs (Parker, 1994; Andersson *et al.*, 1995; Burroughes *et al.*, 1990; Romero *et al.*, 1995), electrochromic or smart windows (Kaneto, 1983), photoresists, antistatic coatings, sensors (Ohmori *et al.*, 1990), batteries (Nigrey *et al.*, 1981), electromagnetic shielding materials, artificial noses (Shurmer *et al.*, 1991), solar cells (Glenis *et al*, 1984; Videlot and Fichou, 1999), memory devices (Kaneto *et al.*, 1991), nanoelectronic and optical devices and transistors (Romero *et al.*, 1995; Burroughes *et al.*, 1988 and 1990; Assadi *et al.*, 1988; Tsumura *et al.*, 1991).

The delocalised electronic structure of π-conjugated polymers is responsible for their unusual electronic properties, and as a result, this class of polymers tend to have (but not exclusively) relatively stiff chains and exhibit very little flexibility. In addition, strong, attractive interchain forces result in the insolubility and non-processability of most of these polymers. Neither polythiophene nor poly(3-methylthiophene) is soluble in common organic solvents; but as discussed earlier the addition of long, flexible, hydrocarbon chains to the thiophene ring can increase solubility and processability of the polyheterocycle, without significant variation of the π-electonic structure (Brédas *et al.*, 1983).

3.3 Electronic Structure

3.3.1 Introduction

Most polymers have bonding electrons that are strongly localised between the carbon atoms that they hold together, which means that they cannot easily contribute to the conduction process. In fact any attempt to promote these electrons to higher energy

states where conduction might take place will most probably result in an alteration of the molecular structure.

An essential requirement for the new class of electrically conducting polymers is that the bonding system needs to establish both the molecular structure of the polymer and provide a continuous overlapping system of orbitals. This in turn establishes the required delocalised electronic states that are needed for the electric field assisted movement of electrons/holes. Such a bonding arrangement is present in polymers containing unsaturated conjugated bonds.

Carbon (which has an atomic number 6) is the main building block element in the formation of conducting polymeric materials and in the ground state has an electronic configuration of $1s^2\ 2s^2\ 2p^2$. However in the excited state one of the 2s electrons is promoted into an empty p_z orbital.

As shown in figure 3.4, conjugated materials, in contrast to saturated hydrocarbons where all four valence atomic orbitals form identical sp^3 hybridised orbitals, form three identical sp^2 hybridised orbitals, displaced at 120° to each other, whilst the remaining p_z electron forms an orbital perpendicularly directed to the plane containing the sp^2 orbitals.

A chemical bond can occur between two carbon atoms when the singly occupied sp^2 orbitals overlap forming a bonding σ–orbital and an anti-bonding $\sigma*$–orbital. The two electrons occupy the low energy bonding orbital. Similar bonding arrangements can also occur between carbon and hydrogen atoms. Figure 3.5 shows the formation of bonding orbitals in a sigma-bonded network of a simple molecule. The presence of both σ orbitals in addition to the perpendicularly oriented p_z orbital is normally represented as a C=C double bond

The single electron occupying the perpendicular p_z orbital in each excited carbon atom can also overlap with other p_z orbitals in adjacent atoms to form π–orbitals. Constructive overlap of the orbitals leads to the formation of bonding, molecular π orbitals, whilst destructive overlap leads to the formation of anti-bonding $\pi*$ molecular

orbitals, as shown in figure 3.6. The bonding π–orbital is occupied by the two former p_z electrons whilst the π* orbital is vacant.

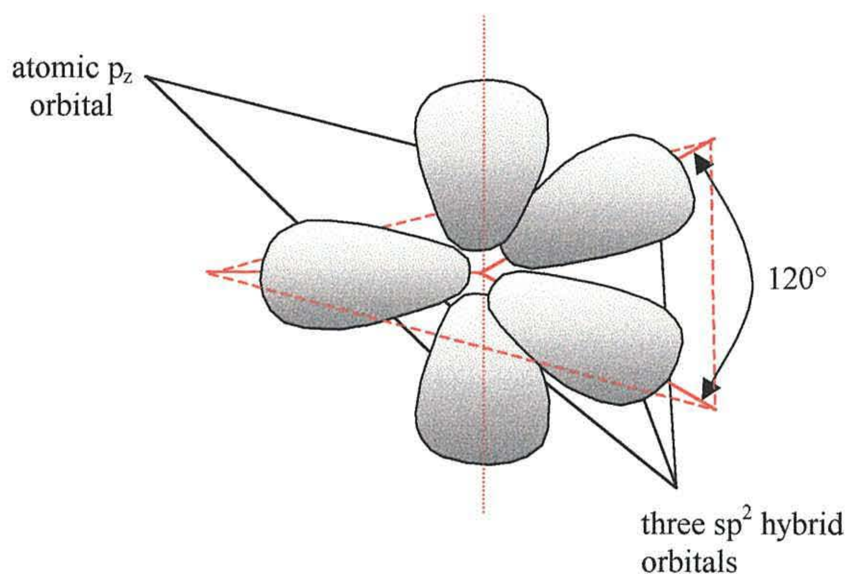

Figure 3.4 *A schematic of the orientation of the p_z and the sp^2 orbitals for carbon in the excited state.*

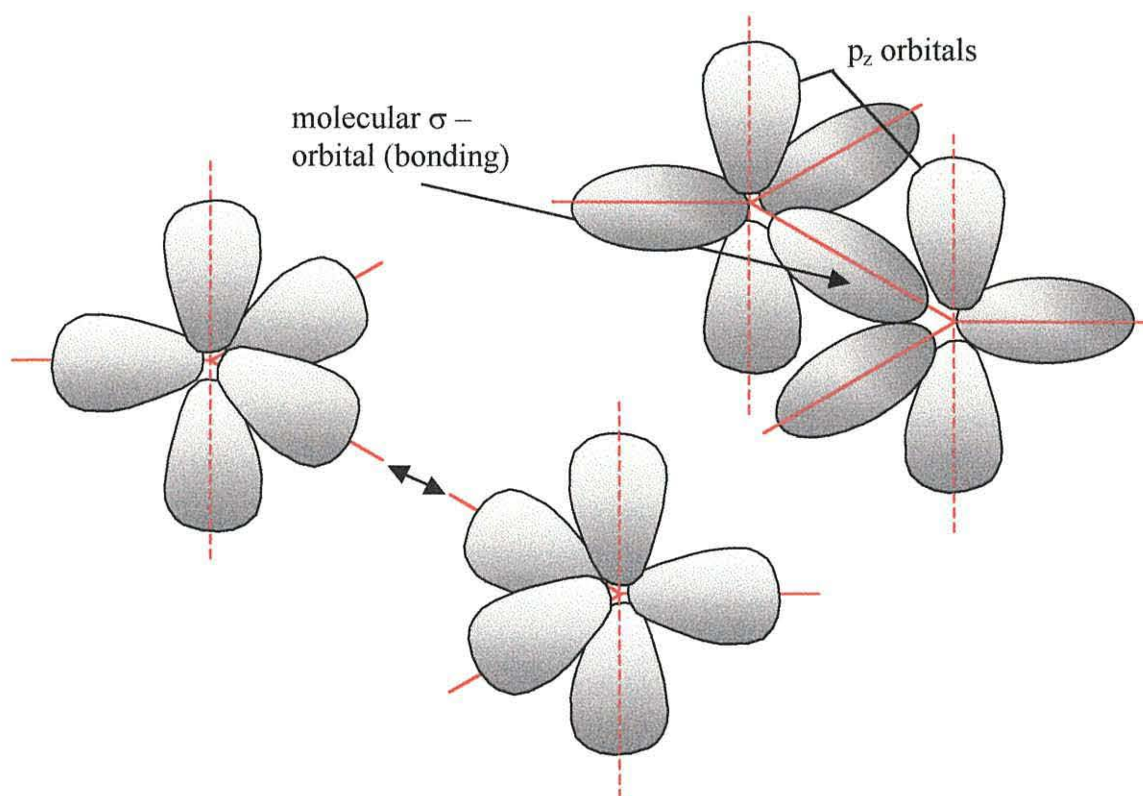

Figure 3.5 *A schematic showing the formation of σ – bonds between two carbon atoms (only the bonding orbitals are shown).*

In simple terms a conjugated polymer is described as having a sequence of alternating single and double bonds along its backbone, known as conjugation. Each carbon atom is linked to the next by a sigma bond but additionally has a π-orbital oriented perpendicularly to the backbone, which is capable of overlapping with its neighbours. The wave functions of the π-orbital system can be delocalised over large portions of the polymer chain and in the ideal case of a planar molecule can occur over the entire chain length. Large torsion angles between, for example, two aromatic groups can lead to a decrease in the extent of delocalisation, which results in variations of the unique electronic properties of conducting polymers, such as the optical bandgap (Kaneto *et al.*, 1984).

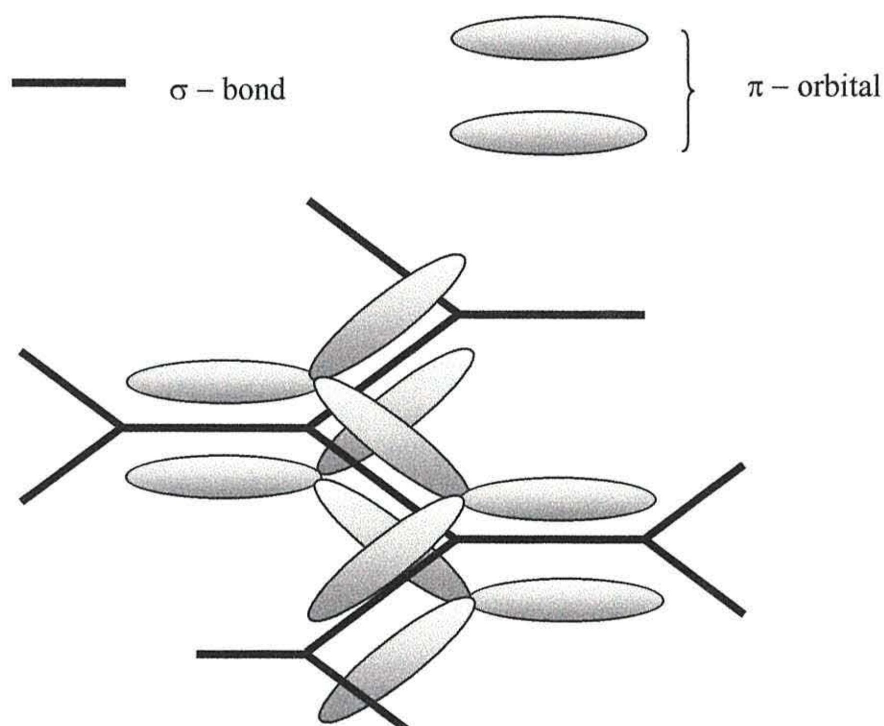

Figure 3.6 *A schematic showing the formation of molecular π orbitals in a simple structure (only the bonding orbitals are shown).*

One might assume that the resulting conducting polymers, with their continuous π-system, would behave as a one-dimensional metal with a half-filled conduction band. In the ideal case this might well occur, but in practice, though, conjugation along the backbone proves to be more energetically favourable and has the effect of limiting the extent of delocalisation.

In addition to describing conjugation in terms of alternation of single and double bonds it can also be defined in terms of a charge density wave, where the electron density of a double bond is greater than that of a single bond. In the latter case the electron density periodically oscillates along the backbone of the chain. The charge density wave of electrons can modify the lattice of the "positive ion" CH groups but in order to maintain charge neutrality the ions move into the regions of high electron density in the double bonds. It is this fact that makes the double bond shorter than the single bond. This phenomenon is known as a Peierls distortion , (Peierls, 1955), but is also called dimerisation, because the ions tend to group in pairs. The process of dimerising, i.e. the formation of alternate double and single bonds – reduces the total configurational energy of the molecule and as a consequence a band gap, E_g, opens up between the occupied (valence) states and the unoccupied (conduction) states. It is the opening of the gap at the Fermi level (in the middle of the band in the case of half-filling) that transforms the material from a metal to a semiconductor. In conducting polymers the magnitude of this gap lies in the range 0.5 – 3 eV, which is small compared to the very large energy gaps in materials such as polyethylene which generally gives rise to good electrically insulating properties. Conducting polymers also have the important advantage of being susceptible to chemical or electrochemical doping which can lead to a state of high electrical conductivity.

The essential properties of the delocalised π-electron system, which differentiates a typical conjugated polymer from a conventional polymer consisting of sigma-bonds include, (i) a relatively small bandgap, (ii) polymer molecules that can easily be oxidised and reduced through charge transfer with molecular dopant species, and (iii) carrier mobilities that are large enough to yield high electrical conductivities. While a band structure can be established for conjugated polymers, unlike conventional semiconductors, however, the charge carrying species are not free electrons and holes but, as will be seen, quasi-particles which can, nevertheless, still move relatively freely through the material.

3.3.2 Doping of Conjugated Polymers: Solitons, Polarons, Bipolarons

Polymers such as those shown in figure 3.3 are usually electrically insulating in their neutral state. However, when exposed to suitable electron acceptors (oxidising agents)

or electron donors (reducing agents), transformation from an insulator to a conductor takes place. This involves redox type reactions of the backbone C-C structure of the polymer, whereby new (mobile) quasi-particles taking the form of electronic charges are introduced onto the polymer chain. (In PANI though, an internal redox reaction takes place, with no external charge transfer). In all doped polymers the new mobile charges are responsible for their enhanced electrical conductivity. The charge transfer agents are normally known as dopants by analogy with the doping process used to increase the electrical conductivity of inorganic materials. Most conducting polymers can be both oxidised and reduced, but p-type materials are generally much more stable than their n-type counterparts. However there are examples of new groups of materials which are stable in both their oxidised and reduced states (Ferraris *et al.*, 1994). Since most materials are p-type, the following discussion will highlight only the processes involved in the oxidation of polymeric materials, an example being polythiophene.

At first sight, oxidation of the polymer chain, by using chemical-doping agents (I_2, $FeCl_3$, AsF_5, and $CuCl_2$) or electrochemical-doping agents ($TBAPF_6$ or $TBABF_4$) in solution would be expected simply to remove electrons from the valence band thus giving rise to band-like conduction of free spins, in the form of unpaired electrons. In contrast to the case of conventional, inorganic materials such as silicon, this does not occur in conducting polymers. Using Electron Spin Resonance (ESR) measurements, Rachdi and co-workers, 1986, suggested that the concentration of free spins in conducting polymers having low doping levels increased with conductivity, but that as the doping level continued to increase, the concentration first saturates and then decreases dramatically. It became apparent that conduction in the high conductivity region occurred without the benefit of free, unpaired electrons.

The explanation for these effects is as follows. Polymer oxidation initially results in the removal of electrons from the π-system to the doping agent, which creates mobile, 'positive holes' in the polymer chain. These holes are stabilised by counter-ions derived from the dopant (A), or from the electrolyte solution in the case of electrochemically prepared polythiophene, as shown in fig 3.7. If this hole can overcome the binding energy between it and the counterion, it becomes mobile and can contribute to the flow of current within the polymer.

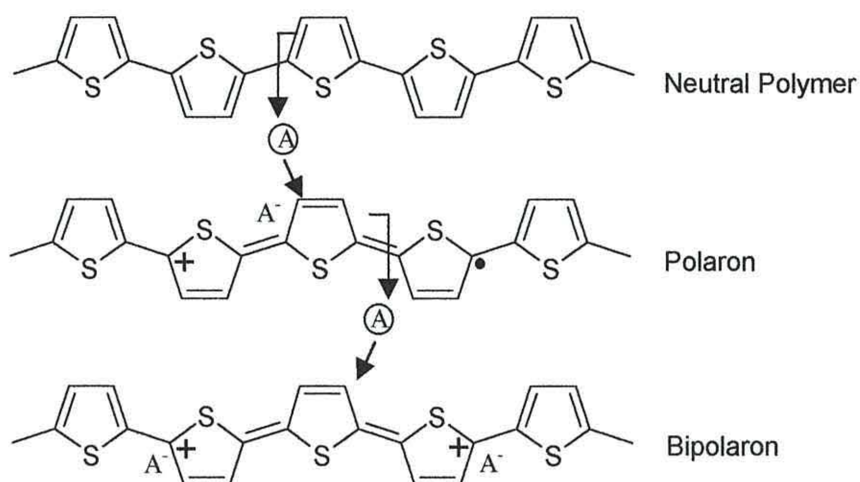

(a)

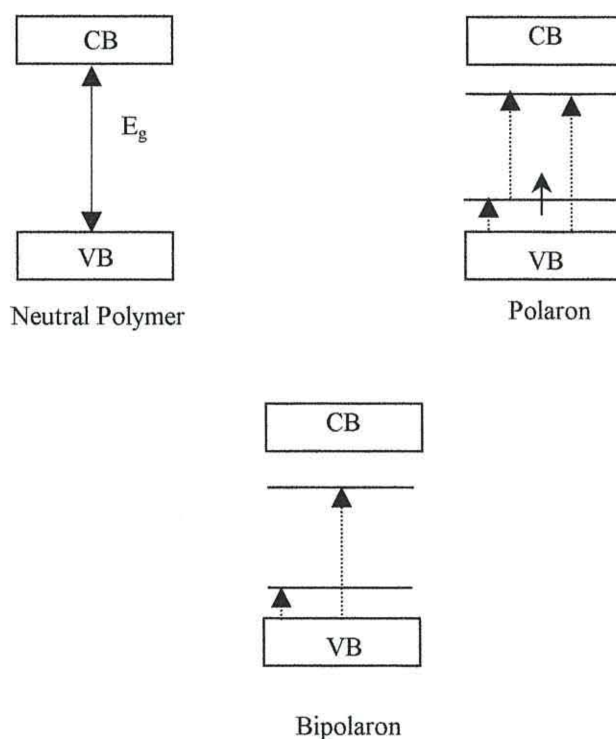

(b)

Figure 3.7 *(a) The formation of polarons and bipolarons (b) corresponding energy band diagrams. The dotted vertical arrows show the new interband transitions that arise from the presence of the polaronic/bipolaronic states.*

The polymer chain can accommodate this positive charge either by (i) delocalising it over the whole of the chain, which is equivalent to removing an electron from the valence band or (ii) localising the charge in a very small region of the chain. The latter is more energetically favourable, but involves a local rearrangement of the bonding

configuration in the vicinity of the charge (Ashwell, 1992). The combination of a charge and the resulting lattice distortion surrounding it, is known as a polaron (molecular cation) and creates a new polaronic state in the bandgap symmetrically located above the valence band and below the conduction band, as shown in figure 3.7. The occupation of these states varies with the doping concentration.

Further oxidation of the polymer, by increasing the doping concentrations to 1 or 2 % results in the removal of a further unpaired electron from the newly formed polaron. This in turn introduces a second positive charge onto the chain in the form of another polaron. The two new polarons can exist independently as two separate lattice distortions or can combine to form a spinless charge defect, a bipolaron (molecular dication). This latter process is more energetically favourable and accounts for the spinless conductivity observed in conducting polymers by Rachdi, 1986. At even higher doping concentrations (30 %) the bipolaron states overlap and form two bipolaron bands which eventually 'grow' and merge with the valence and conduction bands leading to a reduction of the band gap and greater metallic–like behaviour (Stubb *et al.*, 1993). The doping process, which leads to the presence of polarons/bipolarons on the chain, gives rise to a number of new optical transitions below the interband transition, which can lead to modifications in both the electrical and optical properties (Kaneto *et al.*, 1984) as shown in figure 3.7. The doping process also leads the chain to adopt a quinoid conformation, as shown in figure 3.7, in contrast to the aromatic conformation of the neutral state.

Polarons and bipolarons can be envisaged as charge carriers moving along the alternating double bonds in the polymer backbone. A number of different mechanisms exist for charge transport but most involve a type of charge hopping. The counterions (also called the dopant anions) which stabilise the charge on the polymers are relatively immobile and have been shown to play no direct role in electronic conduction (Stallinga *et al.*, 1998). However, the effects of so-called "mobile" dopants have also been observed, particularly in devices based on PPV and its derivatives (Burroughes *et al.*, 1990; Friend *et al.*, 1997; Halls *et al.*, 1995).

The evolution of the energy level diagram as a function of doping for polythiophenes (figure 3.8) depends on a number of factors, including the ease with which a particular

ring achieves the quinoidal arrangement and steric effects which can inhibit adjacent rings from adopting the required quinoidal arrangement and thus achieving coplanarity.

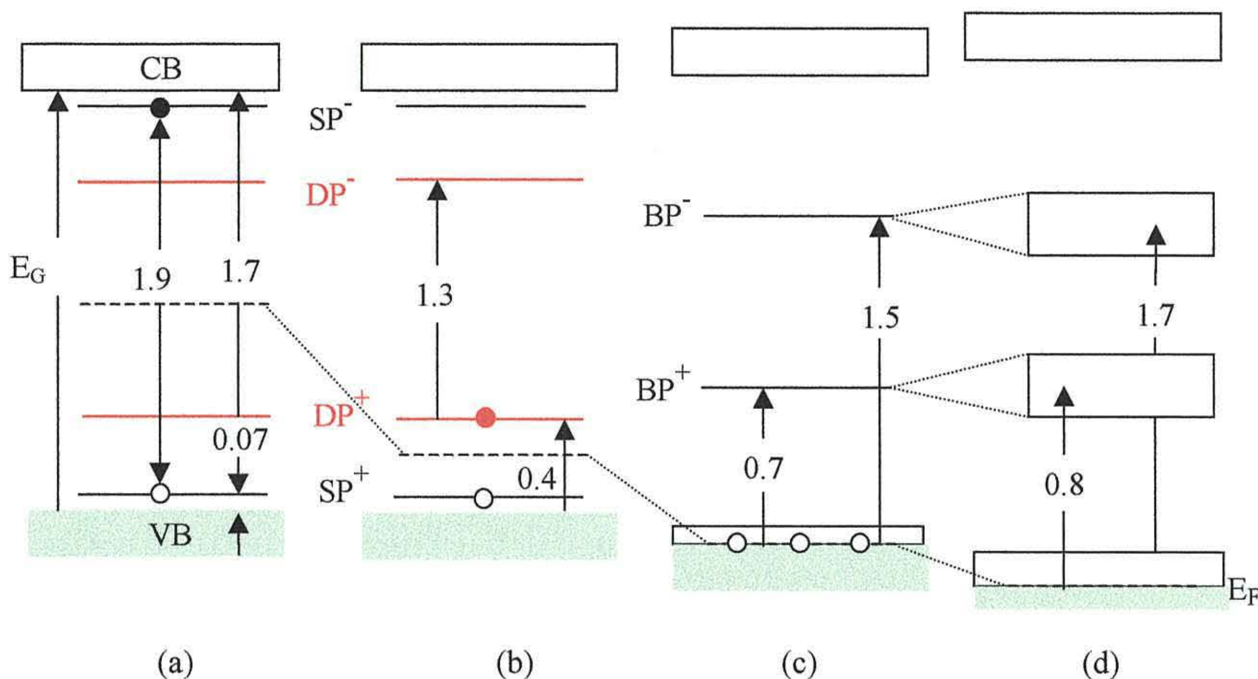

Figure 3.8 *Energy band diagram of polythiophene showing the evolution of gap states as a function of doping. (a) shallow polaron states (SP+ and SP-) and deep polaron states (DP+ and DP-) in a neutral film. (b), (c) and (d) show the evolution of states at a doping concentration of 0.4, 3 and 18 mol % respectively, BP+ and BP- are bipolaronic states. Solid and open circles represent an electron and hole respectively. Figures give the energy difference between the levels in eV. (courtesy of Kaneto et al., 1984).*

In non-degenerate ground state conducting polymers, such as polythiophene and PPV, the quasi-particles take the form of polaronic and bipolaronic species as discussed above, whereas in degenerate polymers, which possess structural symmetry, the quasi-particles take the form of solitons.

Solitons are associated with conjugational defects on symmetrical polymers, e.g. PA which give rise to an electronic state exactly at the midgap. Similar to a polaron, this state can be unoccupied or it can carry one or two electrons, depending on the charge at the defect: positive, neutral or negative, which in turn depends on the extent of the doping.

For a more detailed discussion of polarons, bipolarons and in particular solitons the reader is referred to a number of review articles (Handbook of Conducting Polymers - Skotheim *et al.*, 1998).

3.4 Electrical/Optical Properties of Thiophene Polymers and Oligomers

3.4.1 Introduction

Over the last year or two it has become increasingly apparent that a number of researchers are now working on the characterisation of a wide range of both new and old thiophene derivatives, in particular, thin films which have been electropolymerised onto a working substrate (Gomes, 1993; Yassar *et al.*, 1989).

New compounds such as poly(3,4-ethylenedioxythiophene) (PEDOT) show partial crystallinity with short inter-chain distances leading to highly anisotropic films. This gives PEDOT remarkable properties, in particular, very high mobility (Inganäs *et al.*, 1999).

Similar compounds have the potential for interesting optical applications including a range of low bandgap materials, such as PCDM (Ferraris and Lambert, 1991; Gunatunga *et al.*, 1997), discussed in greater detail in chapter 6.

Various oligothiophenes have been used to investigate the conductivity and mobility of films based on varying lengths of short chain molecules. This work has recently led to various applications including solar cells and high mobility FET structures (Videlot and Fichou, 1999).

In almost all 'plastic devices', the polymeric film acts as the electroactive semiconducting material sandwiched between metal contacts. Even though metal-semiconductor interfaces have been extensively studied in inorganic devices since the reported work of Schottky, further work is required for polymeric devices, in particular, the instances where polymeric devices deviate from the ideal behaviour usually characteristic of inorganic devices.

3.4.2 Electrical Properties

3.4.2.1 Schottky Barrier Diodes

One of the most successful means of probing the electrical characteristics of polymer films, is by using a simple Schottky barrier diode structure that has been adopted by a number of groups to study films which have been deposited using various techniques (as discussed in section 3.5).

Schottky barrier diodes usually comprise of two metal-semiconductor interfaces, as shown in figure 3.9.

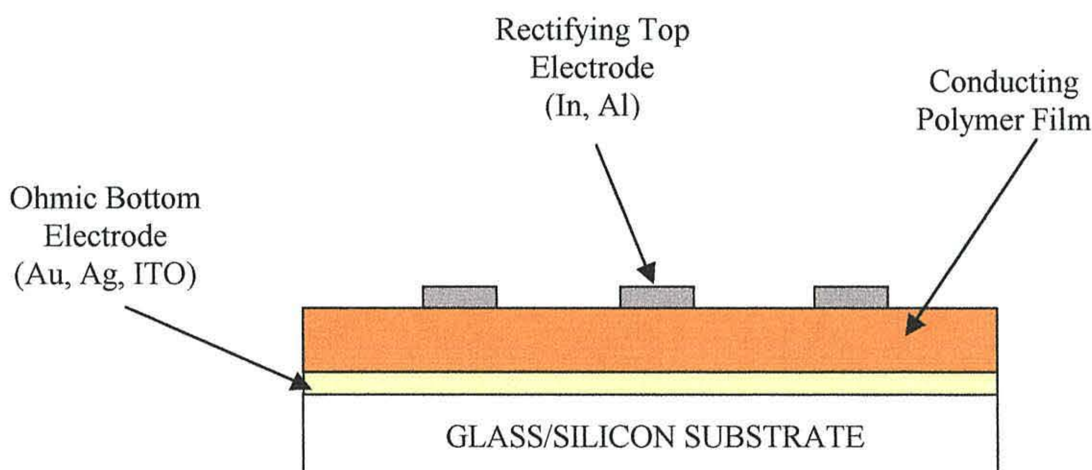

Figure 3.9 *A Schottky barrier diode structure.*

However in some cases, all polymer-structures have been prepared by using heavily doped conducting polymeric materials, instead of various metals, to form the junction (Gustafsson *et al.*, 1992).

In the past ten years or so Schottky barrier diodes have been traditionally studied in structures based on polypyrrole, polyaniline and polyacetylene (Burroughes *et al.*, 1988; Grant *et al.*, 1981). One of the major problems with devices based on the above materials, in particular, polypyrrole and polyacetylene was their poor stability to

ambient conditions which meant that exposure to oxygen during and after processing had to be minimised.

As a result, the highly reactive nature of polymers such as polyacetylene usually requires the careful control of processing to yield devices with good performance (Burroughes *et al.*, 1988). Poly(p-phenylene) similarly attracted much attention, in particular, when it was discovered that the polymer could be both oxidised and reduced to give high electrical conductivities (Ivory *et al.*, 1979).

When Garnier and co-workers (Tourillon and Garnier, 1983) discovered in the late 1980's that most of the solution processible poly(3-alkylthiophene)s (P3ATs) were particularly stable to oxygen, water and temperature, these materials became the focus of much research. However some three years later the susceptibility of P3MeT to reversible doping by oxygen was reported (Taylor *et al.*, 1991).

Further work on P3MeT, by the same group, showed improved rectification and ideality factor in Schottky diodes that had been submitted to a post-metal annealing process. In fact, some of these devices showed among the highest ever reported values of rectification ratios (of the order of 10^4 at +/-2.5 V) for electropolymerised films and suggested the formation of high quality films. The highest recorded rectification ratio to date of all organic polymer materials, of 10^6 at +/- 1 V, was reported in spin coated films of a thiophene oligomer by de Leeuw and Lous (1994). However Kuo *et al.* (1993), have also reported similar values in poly(3-hexylthiophene) based Schottky diodes, but over a greater voltage range of +/- 2 V.

Further breakthroughs in this field came when Gustafsson reported results of an investigation into P3HT based devices (Gustafsson *et al.*, 1990). AC capacitance measurements on various structures led to the observation that the dopant distribution was not homogenous. In fact it was found that the dopants accumulated near the polymer/rectifying metal interface. This led to a thinning of the barrier and a resulting increase in the tunnelling current. Further studies demonstrated that the accumulation of the dopants at the interface could be modulated by an electric field across the structure. However recent admittance spectroscopy results by Stallinga and co-workers (1998), on

electropolymerised P3MeT devices have shown that dopants, in this type of polymer, do not move under the influence of a strong electric field at the interface.

The high ideality factor obtained for the devices studied by Gustafsson suggested a deviation from the classical thermionic emission model (Sze, 1981) used to describe the I-V characteristics of Schottky devices, but at the time compared well with similar reports by Tomozawa on In/P3HT diodes (Tomozawa *et al.*, 1989). The model adopted by Gustafsson and co-workers to explain these findings suggested the immediate relaxation of injected holes into polaron or bipolaron states and that the tunnelling process originated from these states (Gustafsson *et al.*, 1990).

Assadi and co-workers (Assadi *et al.*, 1992) showed that charge transport mechanism in poly(3-octylthiophene)/aluminium diodes was heavily dependent on temperature, being dominated by diffusion theory (Sze, 1981) at high temperatures (>300 K) and tunnelling at low temperatures (<300 K). However, the work of Tomozawa on the temperature dependence of the I-V characteristics in indium/P3HT/ITO diodes, showed forward currents increasing exponentially at low bias and high temperatures. The slope was found to be almost temperature independent, suggesting a tunnelling process instead of the expected thermionic behaviour. Similar results in a PPV-based diode also showed evidence consistent with a tunnelling model (Braun and Heeger, 1991). In some cases it is possible that the charge transfer through the barrier is enhanced by a multi-step trap assisted tunnelling in the depletion region. It has been shown that, by sufficiently increasing the temperature, the reverse and forward characteristics become increasingly ohmic (Ohmori *et al.*, 1990). In fact in some cases (Tomozawa *et al.*, 1989) the flattening of the I-V curves at high forward bias due to the effects of current limiting by the bulk conductivity have been observed. The most ideal polymeric Schottky diode characteristics with ideality factor n=1.2 have been observed in planar Al/poly(3-octylthiophene) contacts (Assadi *et al.*, 1992). The I-V curves showed agreement with diffusion theory (Sze, 1981) above room temperature and tunnelling at low temperature.

Further work by the Bangor group led to the belief that some of the anomalies in the dc characteristics of diode devices reported by many groups could be the result of deviations from the usual fabrication methods resulting in the formation of an interfacial layer at the rectifying interface. In many cases these anomalies resembled the

characteristics shown by minority carrier MIS structures in the early 1970s (Green *et al.*, 1974). These results along with the capacitance-voltage measurements suggesting the presence of both shallow and deep lying acceptor states in P3MeT were the main drive for the present study.

The degree of structure observed in device current-voltage characteristics, in particular, the deviation from ohmic to supralinear behaviour at higher voltages can be used in conjunction with Child's Law (Sze, 1981) to calculate the density of trapping levels and their energy. Characterisation of trapping levels is important in understanding the semiconducting properties of the films and more in assessing their potential for use in devices. A number of studies have suggested the presence of space charge limited currents (SCLC) in polymer films. For example studies by Musa and co-workers on thin films of a thiophene derivative, polybenzo[c]thiophene, led to the observation of extensive space charge limited conduction (Sze, 1981) which suggested the presence of three or even more trap levels (Musa *et al.*, 1997). Similarly a SCLC model has been used to explain the unique I-V characteristics observed in PPV based LEDs (Savvate'ev *et al.*, 1997).

3.4.2.2 Field Effect Transistors (FETs)

Metal-semiconductor junctions in the form of Schottky barrier diodes have generally been studied to further our understanding of their behaviour when used in more useful devices such as field effect transistors (FETs), where high quality blocking and ohmic contacts are used to achieve switching circuits.

Metal-semiconductor field effect transistors (MESFETs) and metal-insulator-semiconductor field effect transistors (MISFETs) are both commonly used structures in devices based on inorganic materials. However, in conjugated, polymeric materials, by far the most common structure is that of a MISFET (Burroughes *et al.*, 1988; Dodabalapur *et al.*, 1998; Sirringhaus *et al.*, 1998; Drury *et al.*, 1998; Ohmori *et al.*, 1991; Tsumura *et al.*, 1988; Tsumura *et al.*, 1991).

Regardless of the deposition technique used, all polymeric FET structures are generally based on the same principles, but in contrast to LEDs and Schottky barrier diodes, these

devices conduct laterally between the drain and source when modulated by a potential across the gate, as shown in figure 3.10. Most polymeric MISFETs operate in the accumulation mode, since the formation of an inversion layer when applying large positive potentials to the gate electrode is not expected to increase the channel conductivity (OFF state). As a result, no one has yet demonstrated the repeatable formation of an inversion layer in polymeric devices of this form. By applying a negative potential to the gate electrode, an accumulation layer is formed in the p-type polymer, which allows the flow of current when a negative drain voltage is applied compared to the source contact (ON state). The drain current can be reduced to zero by applying a positive voltage to the gate thus depleting the polymer. In the accumulation mode a parallel current flows through the bulk of the material. Hence to observe a strong field effect it is necessary to reduce the conductivity of the polymer or its thickness or both (Taylor *et al.*, 1991).

The most popular technique used for fabricating organic MISFETs is spin-coating of soluble polymers onto oxidised silicon already furnished with metal electrodes defining the drain and source contacts (Paloheimo et al., 1989 and 1991; Assadi *et al.*, 1988).

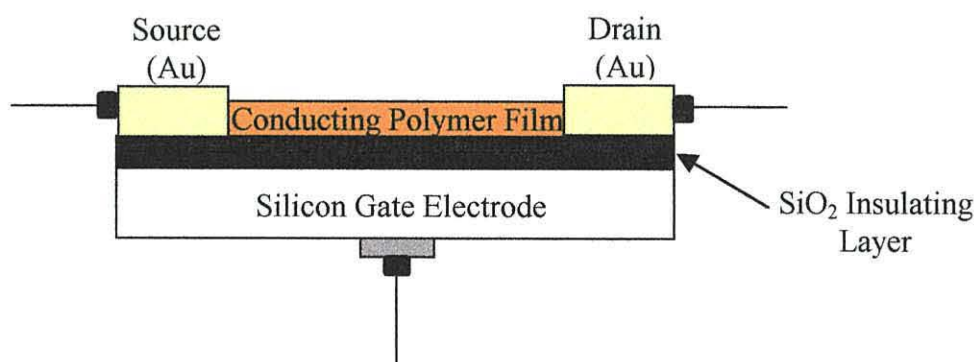

Figure 3.10 *A field effect transistor (FET) structure.*

A number of other deposition techniques have been successfully used, including electropolymerisation (Tsumura *et al.*, 1986 and 1988), a precursor route (Burroughes *et al.*, 1988 and 1989), LB deposition (Paloheimo *et al.*, 1990), or vacuum evaporation of oligomers (Paloheimo *et al.*, 1991; Akimichi *et al.*, 1991).

As a result of their excellent chemical properties, large proportions of MISFET devices reported so far have been based on PATs. However, one major drawback of many of these devices is the low carrier mobility, which results in poor performance.

In 1990 Paloheimo and co-workers reported carrier mobilities in the range of 10^{-7} $cm^2V^{-1}s^{-1}$. In many cases the low carrier mobility in devices based on P3ATs have been attributed to the poor structural order of the soluble alkyl side chain molecules. Assadi and co-workers, 1988, also reported relatively low values of field effect mobility suggesting a form of hopping transport, consistent with transport by self-localised polaron or bipolaron charge carriers. However, the observed variation of the mobility with film thickness indicated the possible influence of intramolecular transport on the macroscopic mobility. A possible explanation for the variations between thin and thick films may be the variation in packing of polymer molecules with different thickness.

By 1991 a Schottky gated FET (Sze, 1981) had been realised for the first time using free standing P3AT (Ohmori *et al.*, 1991). This FET, based on poly(3-butylthiophene), had a high carrier mobility approaching 3 x 10^{-3} $cm^2V^{-1}s^{-1}$ which compared well with the value reported at the time by Gomes, of 8.5 x 10^{-4} $cm^2V^{-1}s^{-1}$. The reasons for such a high mobility FET were believed to be that (i) as a result of being free standing the film was free from stress and (ii) the channel is formed along the Schottky barrier.

Also in 1991 Garnier and co-workers fabricated a similar device using short chain polythiophene oligomers, which had been deposited by vacuum evaporation. In this case a significant improvement was noticed in the carrier mobility, with typical values in the range 10^{-3} - 10^{-2} $cm^2V^{-1}s^{-1}$. However if these organic materials were to be a threat to the traditional inorganic semiconductor devices, mobility values needed to be much nearer the 1 $cm^2V^{-1}s^{-1}$ observed in amorphous silicon.

Taylor and co-workers (1991), furthermore reported that thermally induced changes in device conductance were clearly linked to the presence of oxygen in the polymer film. The low conductance state was readily attained by thermal annealing under vacuum while the high conductance state was recovered only by exposure to air or oxygen. It was concluded that oxygen could reversibly dope P3MeT films and was also most probably responsible for thermal instability in the film conductivity. Earlier work had

similarly shown that electropolymerised films of poly(3-methylthiophene) and solvent cast films of poly(3-hexylthiophene) and poly(3-decylthiophene), all underwent thermal dedoping when heated (Gustafsson *et al.*, 1988).

3.4.3 Optical Properties

3.4.3.1 Light Emitting Diodes (LEDs)

The most common LED device structure comprises a metallic base layer, usually indium tin oxide (ITO) coated glass substrates, a polymer film (~ 1000 Å thick), and an evaporated top metal electrode as shown in figure 3.2.

For high light output, it is essential to maximise the electron and hole injection currents in the device. Hence, the electron-injecting contact should match the conduction band of the polymer, i.e. it should have a low work function material; contrast the hole-injecting contact which should have a high work function. As a result the relative rates of hole and electron injection into the polymer governs the efficiency of light emitting diodes which is generally limited by the number of minority carriers.

In terms of LEDs the most commonly used hole injecting contact is indium tin oxide (ITO), with $\phi = 4.7$ eV (Handbook of Conducting Polymers, 1998), which, because of its low plasma frequency, is transparent to the visible and so ideal for luminescence applications. The use of transparent or semi-transparent top electrodes are also important in some structures where the light is coupled out of the bulk polymer through the top electrode, rather than through the bottom substrate electrode, as shown in figure 3.2.

Conjugated polymers used in LED applications are usually highly dedoped, so as to minimise the formation of barrier contacts and depletion regions and avoid non-radiative recombination, both of which can influence the effectiveness of the charge injection processes. However, conjugated polymers are never totally pristine in nature and commonly have a low level of residual-doping present. This doping level dictates the position of the Fermi energy in the semiconducting polymer, and usually small traces of p-type doping are common, which shift the Fermi energy downwards

compared to the pristine material. However, some oligothiophenes (for example sexithiophene) currently studied by a number of groups, that are prepared in ultra-high vacuum, have been shown to be almost pristine. In such cases, the energy diagram is very close to that of an intrinsic semiconductor, where the Fermi energy lies exactly at midgap.

Ever since the first report of electroluminescence in conjugated polymers and the formation of an OLED by Burroughes and co-workers, 1990, the main aims have been to improve the external quantum efficiency, turn-on voltages and device stability. To date organic LEDs have emissions that span most of the visible range (see Proceedings of ICSM '96 and ICSM '98), operate below 5 V, have lifetimes in excess of 1200 hrs (Cambridge Display Technology), have good mechanical flexibility (Gustafsson *et al.*, 1992) and have quantum efficiencies up to 4 %.

The efficiencies, brightness and device lifetimes reported above are rapidly approaching commercially useful targets for lighting and displays. It is soon envisaged that the further use of copolymers and heterostructures along with new designs and materials will lead to devices yielding quantum efficiencies that approach 5 % (Bradley, 1993).

The operating voltage and device efficiencies of MEH-PPV LEDs have been shown to be highly sensitive to the height of the internal energy barriers, with changes of a few tenths of an electron volt having major effects on the device characteristics (Parker, 1994). In general the I-V characteristic of a diode is controlled by the current density of the majority carriers, which are governed by the smaller of the two barriers, whereas the efficiency is controlled by the current density of the minority carriers which are governed by the greatest barrier. This sensitivity to the height of the interface barriers explains the wide range in operating voltages for polymer LEDs. Perfectly matched electrodes can lead to turn-on voltages as low as the magnitude of the material bandgap, and can be further lowered at the expense of efficiency (Parker, 1994). Slight shifts in HOMO or LUMO levels between the various polymers will give slightly changed barrier heights and corresponding changes in device characteristics.

In organic LED structures, polymers (PPV, P3ATs) are usually deposited onto the hole injecting contacts (Au or ITO coated glass substrates) by spin coating (Burroughes *et*

al., 1990; Barta *et al.*, 1998; Berggren *et al.*, 1995), followed by thermal evaporation under high vacuum of the electron injecting top electrode, which is usually aluminium or calcium (Bröms *et al.*, 1995). For use as LEDs the active organic material is generally dedoped and pristine so as to minimise the possibility of Schottky barrier formation (unlike the case for an ideal Schottky barrier diode) which could block the charge carriers from the active material.

Self-organisation in polymer blends were reported to give rise to voltage controlled multiple colour LEDs in structures based on various thiophene derivatives (Berggren *et al.*, 1994). However a major problem in these devices was degradation. Burrows and co-workers (Burrows *et al.*, 1996) successfully demonstrated a simple encapsulation technique, which increased the lifetime of their LED structures by a factor of 100. Their research demonstrated that degradation was primarily due to the formation of non-emissive regions in the polymer films. These so-called "hot spots" in the devices, were believed to arise from high local fields in areas of electrode non-uniformity caused either by defects introduced during fabrication or recrystallisation of the top electrode. The hot spots are generally characterised by an increase in the drive voltage and a decrease in efficiency.

Bröms and co-workers have shown that the use of magnesium top electrodes on clean (oxygen free) polymer surfaces can improve device efficiency (Bröms *et al.*, 1997). In a similar study calcium on 'dirty' (i.e. in the presence of a partial pressure of about 10^{-6} mbar of O_2) polymer surfaces led to devices having enhanced lifetimes (Bröms *et al.*, 1995).

A possible new market for organic based LEDs could be generated if, using gap engineering techniques, low optical gap materials could be achieved for NIR diodes. A diode, which shows an electroluminescent emission peak at 740 nm using a cyano substituted PPV material has already been demonstrated (Baigent *et al.*, 1996). The majority of the electroluminescent emission was shown to occur in the NIR and the efficiency of the device can be subsequently improved by using a hole-transporting layer.

As described earlier P3AT based devices have proven very successful, in particular, for colour tuning. However studies have shown rather unique properties of the top electrode in poly(3-octylthiophene) (P3OT) LEDs (Garten *et al.*, 1996). The top electrode was found to have a dominant effect on the shape of the I-V characteristics and on the electroluminescent efficiency. Light output was observed for both current directions with an Al top electrode, whilst no light at all was observed when using an Au electrode. In fact the ITO/P3OT/Al devices, operating in reverse bias demonstrated electroluminescence at a much higher drive voltage, suggesting the increased presence of a field-controlled injection mechanism i.e. direct carrier tunnelling into the transport bands.

3.4.3.2 Solar Cells

The solar cell is usually considered as an extension to the simple principle of the Schottky barrier diode, which uses the photovoltaic effect to convert solar energy into electrical energy.

Devices based on inorganic semiconductors including Si and CdS (cadmium sulphide), are the only commercially available devices, even though, GaAs, which has a higher E_G, yields higher voltages and efficiencies (Bar-Lev, 1984). However, the high price and difficult technology of GaAs makes such cells still uneconomic today.

In general, the process of converting optical energy into electrical energy in a p-n junction (but which also applies to metal semiconductor contacts) involves the following basic steps:

- absorption of photons to form electron hole pairs in both the p and n sides of the junction
- diffusion into the space charge region, of electrons and holes generated sufficiently close to the junction
- separation of electron-hole pairs by the strong electric field in the junction
- if the p-n diode (device) is open-circuited, this accumulation of electrons and holes on the two sides of the junction give rise to an open circuit voltage. However, if a load is connected to the diode, a current will flow through the circuit. The

maximum current is realised when an electrical short is placed across the diode terminals, in which case the short-circuit current flows.

Schottky barrier diode structures based on polymers could become a common, low cost replacement for p-n junction solar cells. Any cost reduction would be primarily due to the simplicity of fabrication, where a thin, semi transparent top electrode is used in conjunction with an anti-reflection coating to minimise surface reflection.

However, device performances in solid state photovoltaic cells based upon conjugated polymers or oligomers are relatively poor compared to their inorganic counterparts. This is due to the complex nature of the processes involved in the generation and separation of charges within organic materials as compared to crystalline semiconductors. Traditionally organic devices have been built with the organic material sandwiched between two electrodes of different work functions that provides the internal field. Device characteristics can be vastly improved by constructing multi-layer cells of polymers which jointly acts as light absorbers and hole transporting media. The use of blends and composites to improve properties have been widely reported, including polythiophene/C60 (Roman *et al.*, 1997) , thiophene/CdS (Spearman *et al.*, 1997), and PPV/C60. Recent studies by Videlot and co-workers (Videlot and Fichou, 1999) have shown the importance of molecular orientation of thiophene oligomers on the light efficiency of photovoltaic cells based on such materials. A discussion of the effect of polymer film thickness on the performance of PPV derivative based organic photovoltaic devices was addressed by Petritsch and Friend, 1999.

3.4.3.3 Lasers

The use of lasers has become widespread in applications such as compact disc players, optical fibre based telecommunications, and laser surgery. Until recently most lasing materials only allowed for red or infrared lasers, so the search for a new lasing medium to extend the wavelength range has attracted much attention over the last few decades. Recently reports of continuous operation blue lasers based on inorganic materials such as indium gallium nitride emerged from researchers at Nichia Chemical Industries in Japan (Nakamura, 1998).

When the first reports of electroluminescence in conjugated polymers appeared in 1990, researchers were able to foresee the possibility of fabricating lasers based on the same technology. The recent discovery of collective stimulated emission processes in conjugated polymers has proved that conducting polymers are potential candidates for laser applications (Hide *et al.*, 1996; Tessler *et al.*, 1996; Frolov *et al.*, 1997). Advantages such as high quantum efficiencies, ease of fabrication, the possibility of depositing large-area devices onto flexible substrates and the prospect of achieving a wide range of operational wavelengths from the near infra-red to the blue, have led to applications that have not been available to the more traditional inorganic semiconducting materials.

Lasing can only occur if the following conditions are fully met (i) the active material exhibits strong stimulated emission (SE) and (ii) an optical feedback path is present in the lasing structure. Stimulated emission has by now been reported in PPV (Yan *et al.*, 1994) and other conducting polymers (Pauck *et al.*, 1995; Graupner *et al.*, 1996). By improving synthetic methods and structure designs, significant enhancements have recently been reported in SE and optical gain (Denton *et al.*, 1997; Schwartz *et al.*, 1997).

The observation of amplified spontaneous emission (ASE) by a number of groups (Hide *et al.*, 1996; Frolov *et al.*, 1997; Brouwer *et al.*, 1996; Gelinck *et al.*, 1997) proved that lasers based on organic polymers could exhibit optical gain that was comparable to that achieved by lasers based on inorganic semiconductors. Using a suitable resonator geometry (Tessler *et al.*, 1996; Berggren *et al.*, 1997) allows the second requirement for an optical feedback path to be satisfied. The most popular method of obtaining resonance is to use a structured substrate to provide distributed feedback (DFB) in the lateral direction, which has the advantage of allowing the use of spin-coating techniques for depositing large-area emissive layers.

Kallinger and co-workers, 1998 reported the fabrication of a low-cost flexible conjugated polymer based DFB laser. Spin-coating was used to deposit ladder type poly(p-phenylene) (LPPP), which is known to exhibit strong SE under optical pumping (Pauck *et al.*, 1995; Graupner *et al.*, 1996) to a thickness of approximately 400 nm, onto a specially structured plastic substrate, poly(ethylene terephthalate), (PET). Optically

induced vertical single-mode laser emission was reported in the blue-green wavelength range. A schematic of the laser device is shown in figure 3.11. The periodic height modulation of the substrate causes diffraction of the waveguide modes. The first order diffracted light (1) is coupled perpendicularly out of the material, whilst the second order (2) light is fed into the counterpropagating wave and gives rise to the required optical feedback path.

In some cases conjugated polymer based microcavities could well be used as a new class of compact laser sources, where the active volume is extremely small (Tessler *et al.*, 1996). A typical structure of a microcavity LED as used by the Cambridge group is shown in figure 3.12.

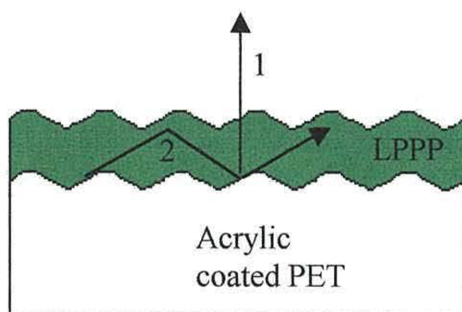

Figure 3.11 *A schematic of the flexible distributed feedback laser device (as used by Kallinger et al., 1998).*

Since lasing is an extension of the operational properties of LEDs, a modified LED structure is normally used. By placing a sandwiched organic polymer film in between two mirrors as shown in figure 3.12 the structure acts as a microcavity resonator when the film thickness is of the order of the wavelength of the emitted light. In this and other cases, a planar microcavity is used as a means of introducing feedback into an optically pumped polymer film. This feedback principle can greatly enhance the stimulated emission process within the material. This structure has been used to control and achieve narrow emission line widths and good directionality lasing action under intense optical excitation or 'pumping'.

The structure shown in figure 3.12 consists of a 160 nm thick layer of PPV sandwiched between an ITO electrode and either an aluminium or silver electrode. The microcavity is formed between the distributed Bragg reflector and the upper aluminium or silver electrodes which behave as a semi-transparent mirror. Microcavity devices based on such a design have been shown to achieve very narrow linewidths in the range of 5 - 7 nm for Ag and Al electrodes respectively.

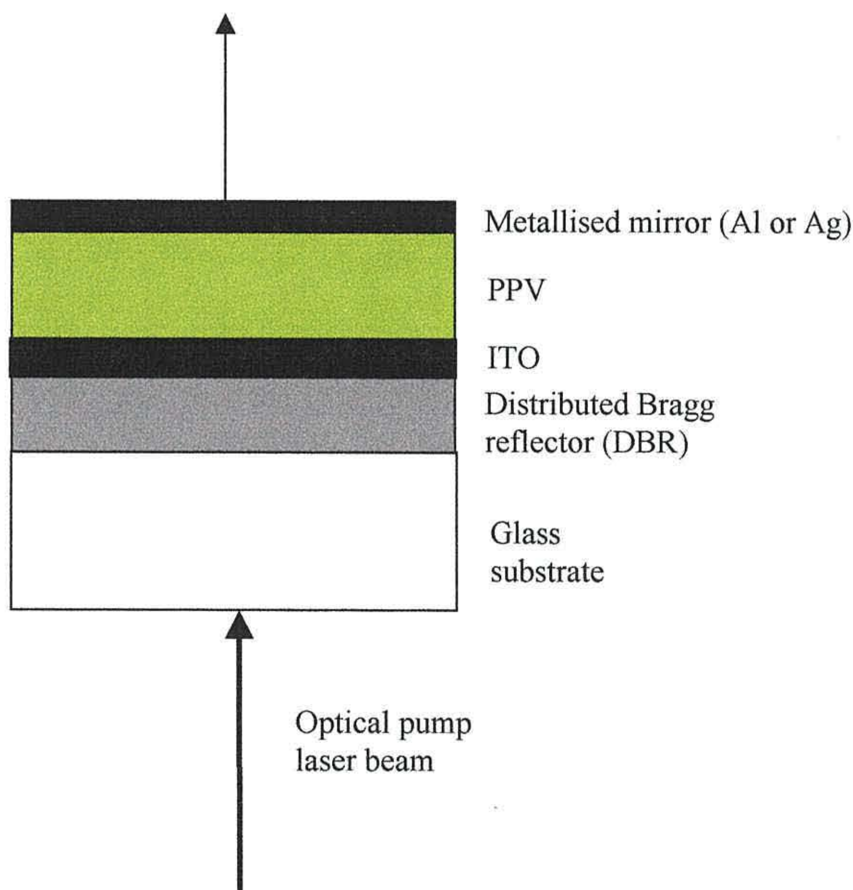

Figure 3.12 *A schematic of the structure of a microcavity laser.*

Another technique that has been widely used for achieving tunable lasers has been organic dye solutions for which lasing has already been observed in dilute solutions of conjugated polymers (Moses, 1992; Brouwer *et al.*, 1995). However, it is only recently that similar effects have been observed in solids, since the general consensus of opinion was that strongly competing induced absorptions would kill the net gain (Yan *et al.*, 1994).

In many of the cases of reported lasing, researchers are currently investigating whether or not what they are observing is indeed lasing action, and not superradiance or superfluorescence phenomena. The greatest drive at the moment would be to induce lasing action by electrical pumping rather than optical pumping, but practical devices of this type look a long way off at the moment.

3.4.3.4 Photoexcitation and Optical Characterisation

Photoexcitation of charge carriers has been a commonly used alternative method of investigating localised states in conjugated polymers. Improving our knowledge of how efficiently light generates charge carriers in semiconducting materials (and vice-versa), or how fast they move upon applying an electric field is a necessary requirement both for establishing a theoretical description and for designing photoelectronic devices (Burroughes *et al.*, 1988).

Both photocurrent and photoconductivity measurements have been used to study a number of conjugated polymer structures including PPV (Takiguchi *et al.*, 1987), PA (Friend *et al.*, 1987) and P3ATs (Binh *et al.*, 1992 and 1993). In addition photoluminescence and photo-induced absorption measurements have led to a better understanding of the photoexcitation processes occurring in conjugated polymers (Bradley *et al.*, 1989). Complex features in photocurrent action spectra have been successfully related to film quality and in particular, the extents of disorder (Binh *et al.*, 1993).

Devices based on conjugated polymers such as PPV have shown large open-circuit voltages, ideal for photovoltaic device applications. Marks and co-workers (Marks *et al.*, 1993) discovered that the open-circuit voltage of a Schottky device based on PPV generally scaled with the work function of the top electrode, which suggested that the polymer material was relatively trap-free. However, devices based on an Al top electrode, demonstrated high open-circuit voltages suggesting a degree of modification to the polymer interface during deposition of the electrode.

Kaneto and co-workers (Kaneto *et al.*, 1984) successfully studied the effects of photoexcitation and electrochemical doping on the optical properties of polythiophene

by observing changes in the absorption spectra. A model for the evolution of gap states in polythiophene was developed from the results of this work, a representation of which is shown in figure 3.8.

Recent studies have demonstrated the viability of applying new spectroscopic techniques such as Raman spectroscopy and UV-vis absorption measurements to probe and characterise the effects of doping on the optical properties of thiophene based materials (Kaneto *et al.*, 1984; Favre *et al.*, 1997; Casado *et al.*, 1998).

3.5 Preparation Methods

3.5.1 Introduction

By the early 1990's polythiophene and its derivatives were under increasing investigation, but most of the work based on the morphology of conducting polymers had been performed on polyacetylene (PA) films. Electron micrographs of *trans*-PA showed that the individual polymer chains aligned to form fibrilar structures. At the same time results from X-ray measurements indicated an underlying crystalline order to the fibrils. Similar alignment of polymer chains were also observed in polythiophene (PT) and other conducting polymers, but the degree of crystallinity varied quite significantly. In fact for electrochemically prepared polythiophene it has been shown that the material is almost totally amorphous, whereas 80-90% crystallinity is observed in some carefully prepared PA films. The addition of large amounts of dopants can lead to the disruption of any inherent crystalline order in neutral films. Doping can also give rise to inhomogeneous doping profiles especially in thick films.

Film conductivity is considered to be a good reflection of the structure of the material. Doped, highly ordered, crystalline materials tend to exhibit the highest conductivities. By deliberately adding conjugation-breaking agents to *trans*-PA films the conductivity was reported to decrease by three orders of magnitude, which suggests that polymer chain ends hinder the charge carrier motion (Schafer-Siebert *et al.*, 1987).

Although structural order is obviously of paramount importance and is increasingly emphasised, the importance of chain alignment cannot be ignored. A large variation in

the anisotropic properties of stretch-oriented samples has been observed, for example, a factor of 10-50 increase in conductivity in the stretch direction. The correlation between high conductivity and high mechanical strength in oriented fibres, which has been experimentally verified for polymer blends including PANI and thiophene derivatives has further fuelled interest.

Structural order is often determined by the film preparation method used. Several deposition techniques exist for thin film applications, including plasma polymerisation, electropolymerisation, spin coating, Langmuir-Blodgett, self-assembly and vacuum evaporation. In terms of the deposition of semiconducting organic films, the three most commonly applied techniques are electropolymerisation, spin coating and Langmuir-Blodgett deposition.

All deposition techniques, with the exception of electropolymerisation, result in the formation of neutral or dedoped films. Electrochemically prepared films are formed in their oxidised state and need to be reduced in order to attain their semiconductive properties, a process which is of particular importance when investigating the non-linear optical properties of conducting polymers (Masuda *et al.*, 1989). This reduction step has been shown to radically change the polymer morphology (Yassar *et al.*, 1989) which leads to potential problems in the formation of devices by this method of polymerisation. However one of the main advantages of electropolymerisation is the control that is possible over the thickness and doping of the thin films.

If a non-electrochemical deposition technique is used, a range of common oxidising agents, such as I_2, $FeCl_3$ (PPy), AsF_5 (PA), $CuCl_2$ (PA), and $NOPF_6$ (P3HT) may be used to initiate the polymerisation process and subsequently dope the film. The main disadvantage of this technique, is the lack of control over the doping concentration.

Chemical doping normally entails firstly synthesising the polymer followed by dissolving the material in a solution of one of the above oxidising agents. The concentration of the oxidant in the solution will determine the density of the dopant in the final polymer film. Casting the polymeric material onto a suitable substrate using a technique such as spin coating, as discussed in section 3.5.3 can then form thin films.

3.5.2 Electropolymerisation

3.5.2.1 Introduction

In 1979, Diaz and co-workers (Kanazawa *et al., 1979*) obtained homogenous films of polypyrrole having a high conductivity, by electropolymerisation of pyrrole. Subsequently electrochemical polymerisation was found to be suitable for other aromatic compounds such as, thiophene (Tourillon and Garnier, 1982), P3ATs (Gomes, 1993; Yassar *et al.*, 1989; Roncali and Garnier, 1986) and polyaniline.

Electrochemical polymerisation was seen as a means of exercising some degree of control over the film growing process and in particular to the doping procedure. The electrical, optical and morphological characteristics of electropolymerised films, and any subsequent devices, are defined during this polymer growth period and many workers have reported studies of growth mechanisms for various polymers (Handbook of Conducting Polymers, 1998).

In this section the discussion will concentrate on the electrochemical growth of P3MeT films. In many respects the technique is analogous to that of metal electroplating, but here the electrolytic solution consists of a suitable solvent, a supporting salt, which is the doping material and the monomer.

3.5.2.2 Polymerisation

Electrochemical polymerisation is normally conducted in a three-electrode cell, which is inserted in the electrolytic solution, similar to that shown in figure 3.13. The three electrodes are (i) silver wire, which is used as a reference electrode (ii) platinum metal foil, the counter electrode (cathode) and (iii) the metallised (Ag, Au or ITO) glass slide or platinum used as the working electrode (anode), onto which the polymer film is grown. The three electrodes are connected to an external control circuit as shown in figure 3.13, which can be a potentiostat or galvanostat. The three-electrode potentiostat (galvanostat) controls the potential of (current through) the working electrode vs. the reference electrode, while compensating for as much of the cell resistance as possible. Both anodic and cathodic polymerisation reactions have been reported, but due to its

simplicity anodic polymerisation has proved the most popular and will be the one described here.

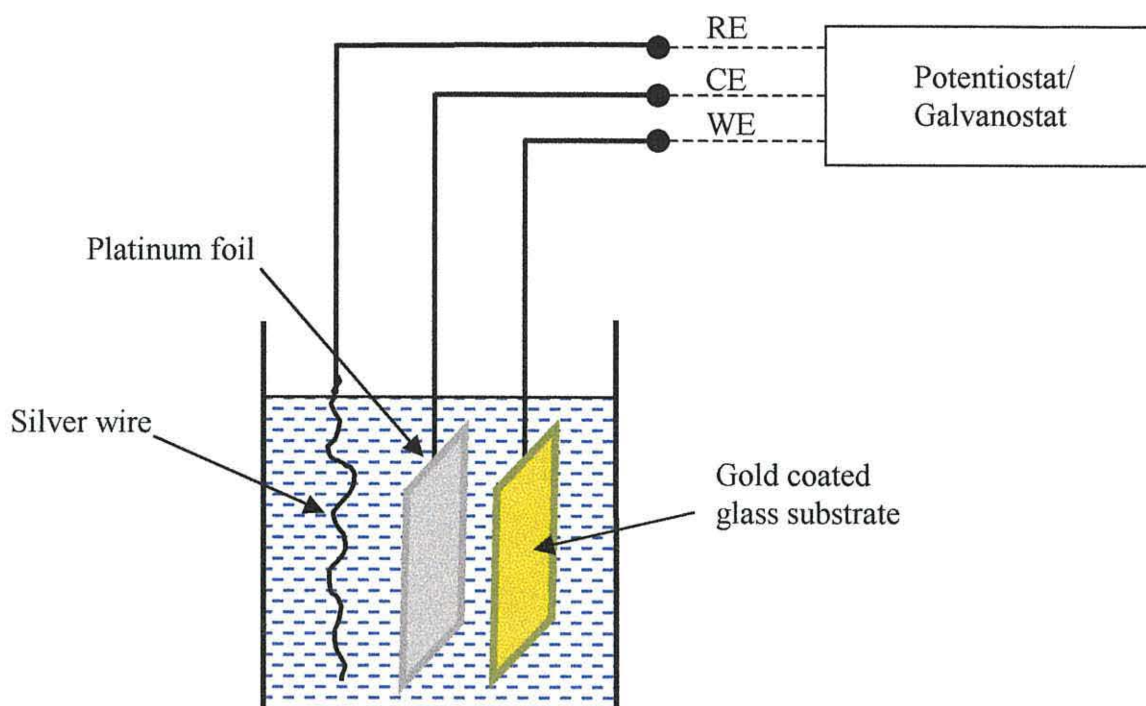

***Figure 3.13** Schematic diagram of the three electrode cell.*

Electropolymerisation proceeds by applying a suitable potential to the working electrode compared to the counter electrode (with reference to the silver wire), which oxidises the soluble, hetrocyclic monomer into an insoluble polymer, as shown in figure 3.14. However, more detailed investigations have revealed that many more steps are involved (John and Wallace, 1991) a detailed representation of which is shown in figure 3.15

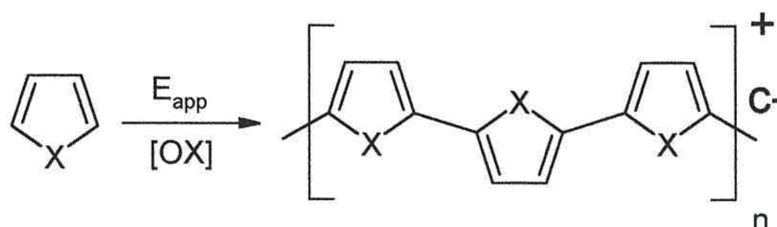

***Figure 3.14** Schematic diagram of a generalised and simplified mechanism of electropolymerisation.*

The process involves transport of the monomer to the electrode surface, electron transfer with simultaneous incorporation of counterions (the doping process), radical-radical coupling, oxidation of oligomer (short polymer chain) and further coupling prior to deposition onto the electrode surface. The rate of the above reactions will determine whether or not a polymer is deposited, as well as the chemical and the physical properties of the polymer.

The monomer material in solution is firstly oxidised at the anode surface by applying a potential E_1 between the working and the counter electrodes with reference to the silver wire. The removal of the electron results in a radical cationic species. Reaction kinetics allows for a high concentration of radicals at the anode electrode at all times which allow radical cations to form dimer dicationic species, which subsequently form a dimer (dithiophene molecule) after the loss of two protons. Further oxidation of this molecule at a reduced potential E_2 leads to further coupling with radical monomeric molecules and the formation of longer chains. When the chain is sufficiently long the polymer becomes insoluble and forms a thin film on the working electrode. It is believed that this polymerisation process proceeds by the initial formation of oligomers in solution followed by their deposition on the electrode surface (Lang *et al.*, 1987).

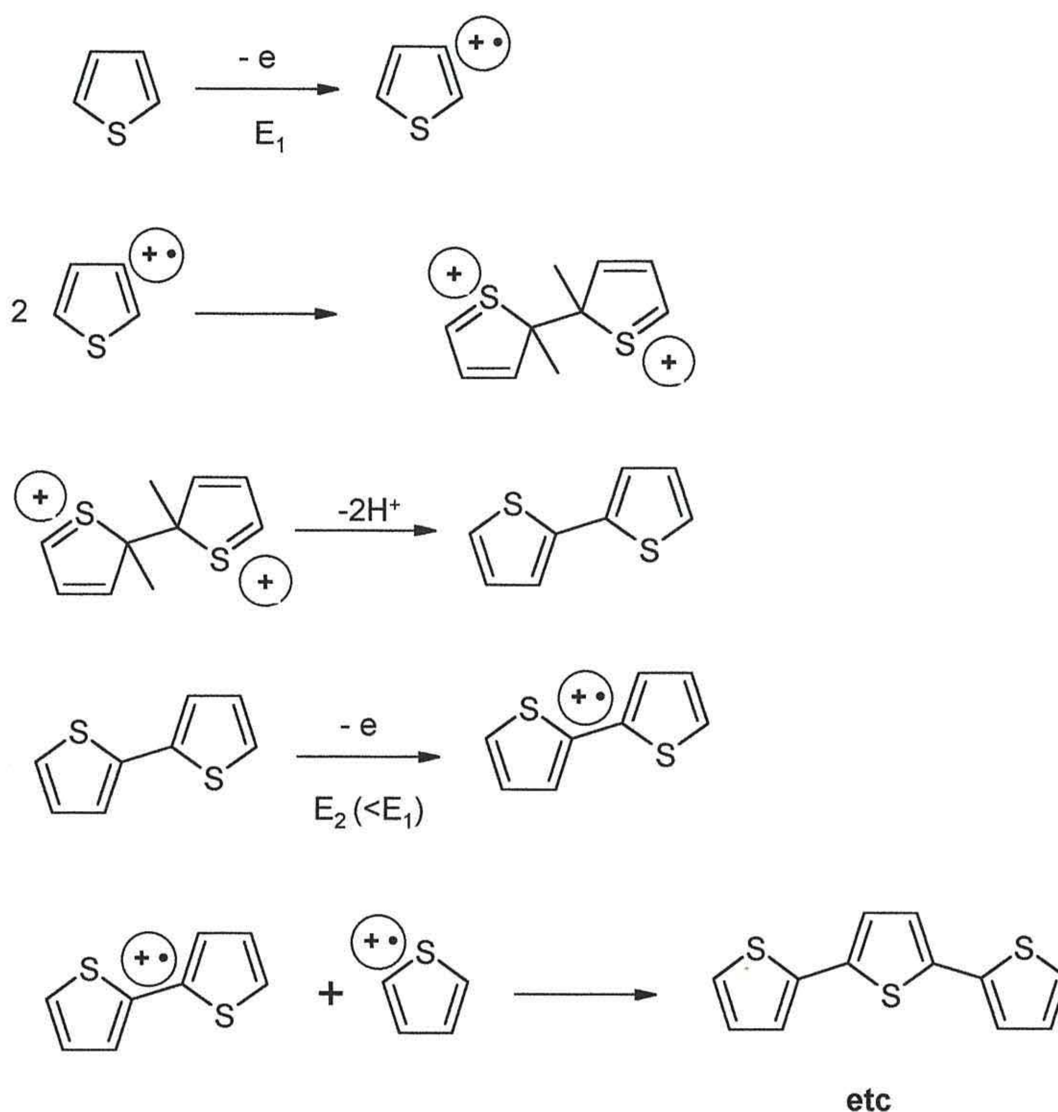

Figure 3.15 Schematic of the detailed polymerisation mechanism.

A number of parameters are known to influence the quality of the thin films, including solvent, concentration of reagents, temperature, cell geometry, nature and shape of electrodes, and applied electrical conditions, all of which have been the subject of many studies (Gomes, 1993; Roncali and Garnier, 1986; Sato *et al.*, 1985; Hotta, 1988; Casalbore-Miceli *et al.*, 1998). These parameters can greatly influence the quality, structure and both optical and electrical properties of the polymer films.

The electrochemical reaction at the electrode surface is sensitive to the extent of nucleophilicity and to maintain this the most commonly used solvents include acetonitrile, propylene carbonate and chloroform which are aprotic solvents. The electrolytic salt should be highly soluble and possess a high degree of dissociation and

nucleophilicity. With these requirements in mind, the most commonly used electrolytic salts are those based on the tetraalkylammonium cation, for example tetrabutylammonium tetrafluoroborate or tetrabutylammonium hexafluorophosphate. Observations by Favre *et al.* (1997), have concentrated on the role that the anion has on ageing of electropolymerised P3MeT films.

Thin films of polythiophene have been prepared using galvanostatic (Hotta, 1988) and potentiostatic (Tourillon and Garnier, 1983) methods, with the most homogenous films being galvanostatically prepared (Roncali and Garnier 1986; Yassar *et al.*, 1989). The technique used by Gomes, which will be adopted for use in this study, followed reports by Roncali of overoxidation leading to a high concentration of nucleation sites and a resulting compact film (Roncali *et al.*, 1989). The work of Krische and Zagroska suggested that overoxidation could prove deleterious to P3MeT films (Krische and Zagroska, 1989) and is the reason why the electroactivity of a film should be checked after deposition using a technique known as cyclic voltammogram. Cyclic voltammetry is a dynamic electrochemical method for measuring redox events. It can be used to study the electrochemical behaviour of species diffusing to an electrode, interfacial phenomena at an electrode surface and bulk properties of materials in or on electrodes. Cyclic voltammetry is one of a family of dynamic electrochemical methods in which the potential applied to an electrochemical cell is scanned. The resulting cell current is plotted as a function of potential. The potential scan is programmed to begin at an initial potential where no electrolysis occurs. The scan continues at the desired linear scan rate to the switching potential then reverses direction and returns to the initial potential (Bard, 1966)

Totally reversible reactions would show symmetrical peaks of equal magnitude, with little or no separation between oxidation and reduction peaks. In practice, fully symmetrical CVs for films are rarely obtained. Peak shapes and potentials of cathodic and anodic peaks are strongly influenced by interactions between electroactive species within the film (Murray, 1984).

The cyclic voltammogram produced from a typical P3MeT film in a monomer free supporting electrolyte is shown in figure 3.16. The polymer film oxidation peak at 0.8 V

can easily be identified along with a number of reduction peaks in the cathodic region of the scan which suggests some degree of reversibility of the redox reaction.

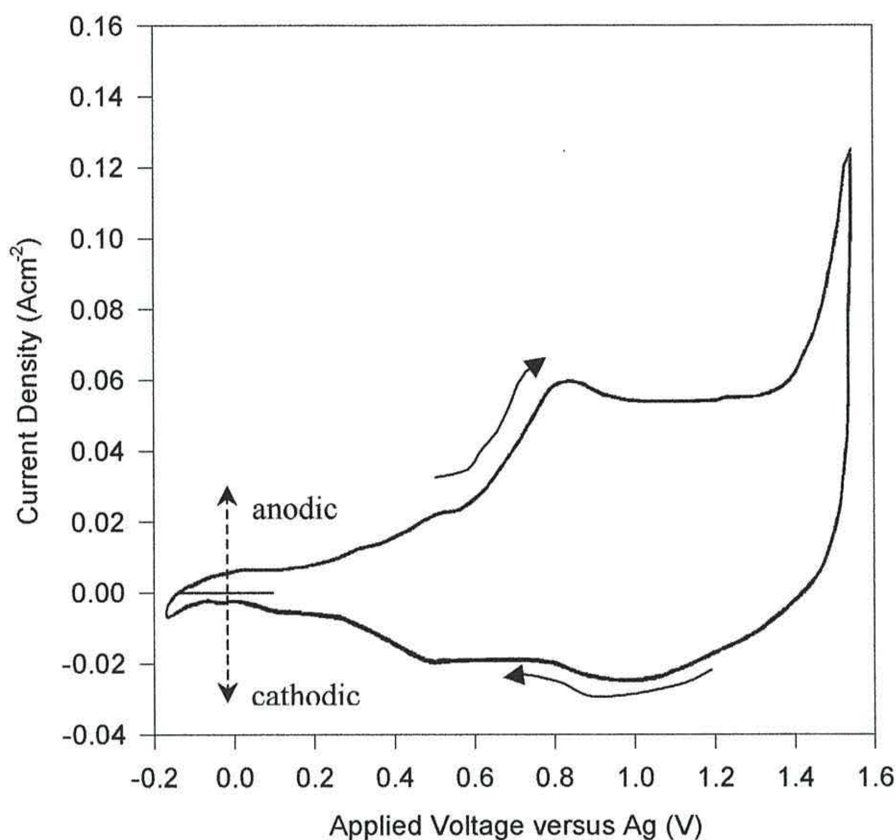

Figure 3.16 *A cyclic voltammogram for a typical P3MeT film grown using the overoxidation technique.*

The oxidation and reduction peaks observed in figure 3.16 arise from the controlled diffusion of anions into and out of the electrolytic solution respectively. This electroactive process constitutes the doping / dedoping process. This process also demonstrates that the film can be reversibly cycled between the oxidised (doped) state and the reduced (dedoped) state.

Electropolymerised polymers are oxidised (doped) as they are formed on the electrode. The oxidation leads to the incorporation of charge-compensating anions (from the electrolyte solution) into the oxidised film. In this case anions are incorporated into the film by applying, a positive oxidation potential. The oxidised state is usually

characterised by the dark blue colour of the deposited film. The resulting films may be electrochemically dedoped (reduced) by removing the anions from the film. This is usually achieved by slowly decreasing the applied potential to a pre-selected value. In P3MeT this reduction potential can take a value between +0.2 V and – 0.2 V versus Ag depending on the required extent of dedoping. Film reduction is characterised by a colour change from dark blue to red / brown. The dedoping process is not only a function of the reduction potential but also of the reduction time, which for a particular potential is dependent on the polymer film thickness.

Electropolymerisation has the advantage over other deposition techniques of being, at least in principle, simple and easy to use and is a technique which can yield high quality, smooth films with controlled doping and thickness. However, in reality, great care must be taken to repeatedly achieve films of this nature.

In this study the growing procedures developed by Gomes (1993) have been used to grow thin films of poly(3-methylthiophene), experimental details of which will be given in Chapter 4.

3.5.3 Spin Coating

Spin coating is a technique that is widely used for the fabrication of thiophene based LED and Schottky diode structures (Barta *et al.*, 1998; Romero *et al.*, 1995, Ohmori *et al.*, 1990; Gustafsson *et al.*, 1991; Trznadel *et al.*, 1996; Louarn *et al.*, 1996). In some cases, this technique can overcome the complications associated with successfully growing, doping and dedoping high quality, electropolymerised films. However, in general, polythiophene and poly3-methylthiophene and other films based on monomers having short side chains, cannot be prepared by spin coating, since the polymeric material is insoluble. This can be a disadvantage since films prepared from short side–chained monomers have a greater mobility.

The polymeric material is chemically synthesised and dissolved in a suitable solvent, such as chloroform or xylene. Small volumes of the required polymer in solution are then cast over the whole surface of the required substrate, for example silica, ITO or gold coated glass. The substrate is supported on an assembly, which is then spun at a

pre-determined speed until the surface is coated in a smooth even film. The polymer concentration in the solution, the substrate spinning speed and time of spinning are all parameters that can be used to control film thickness and quality.

This technique is particularly suited to depositing thin films, which are generally less than a micrometer thick and is a convenient and quick way of depositing uniform conducting polymer films over large areas.

3.5.4 Precursor Polymerisation

A natural progression from the spin coating technique is precursor polymerisation. This technique involves the preparation of a solution-processable precursor polymer by a suitable chemical polymerisation process. The precursor polymer is subsequently re-dissolved in a common solvent and spin coated onto a suitable substrate as before. Thermal conversion (normally temperatures in excess of 250°C, in vacuum, for a number of hours) of the precursor film yields a dense, uniform and homogenous film of the required conducting polymer.

This technique has been used extensively to prepare films of polyacetylene and more recently of PPV (Burroughes *et al.*, 1990). The method used to prepare films of PA was commonly known as the "Durham" route following, the work of Feast and co-workers at Durham University (Edwards and Feast, 1980). This simple technique is widely used for depositing organic, electroluminescent layers for use in large area matrix displays (Cambridge Display Technology).

A particular problem associated with this technique has been observed when converting PPV on ITO substrates for LED applications. The hydrogen chloride gas liberated during the precursor polymerisation reaction that yields PPV (Burroughes *et al.*, 1990) has been shown to react with the ITO layer of the substrate. This reaction forms indium chloride ($InCl_3$) which subsequently doped the polymer material (Friend *et al.*, 1997). In LED applications, doping of the polymer is undesirable and leads to a lowering of the quantum efficiency of devices. This has since led to the use of new, 'inert' substrates.

3.5.5 Langmuir-Blodgett Technique

It was in 1917 that Langmuir published a paper in which he reported the development of both experimental and theoretical concepts, which became the foundations for understanding molecules in insoluble monolayers (Langmuir, 1915). Later he developed a simple technique for transferring the films from the water subphase onto a solid substrate by repeated dipping. It was this technique that was further refined by Langmuir and Blodgett to allow thick multilayers to be built. As a result of this both monolayer and multi-layer structures are commonly known as Langmuir-Blodgett (LB) films.

The LB deposition technique is considered to be a means for obtaining ultra-thin, ordered films of uniform thickness showing a high degree of molecular anisotropy. It is an important and widely used technique in the field of molecular electronics for it provides a controlled method of assembling molecular systems. It is one of only a few techniques that can be used for making separate electrical connections to the two ends of a single molecule.

The technique involves spreading a monolayer of an amphipathic molecule on the surface of water in a suitable trough, known as the Langmuir trough. The monolayer is subsequently compressed using a movable barrier/barriers and can then be deposited onto a clean substrate by dipping or by surface contact. It is possible to build up multilayer structures by repeated dipping into the water subphase. But there are several factors, which influence the type of deposition obtained. These include:

- nature and type of substrate
- dipping rate
- surface pressure
- subphase conditions.

It should be noted though that for the successful deposition of a multilayer structure, the film material must have some affinity for the substrate so as to reduce the probability of the first layer peeling off.

Molecular engineering allows the tailoring of material properties for specific applications, which by now include chemical/biological sensing, non-linear optical devices, photodiodes, conducting films for electrode materials and thermochromic devices (Ashwell, 1992).

Current research involving the deposition of conducting polymers using the LB technique include, deposition of poly(3-hexylthiophene) films for device characterisation (Österbacka *et al.*, 1998 – and references within).

3.5.6 Self Assembly Technique

The self-assembly technique entails the alternate dipping of a solid substrate into dilute solutions containing polyanions and polycations, with one or both of the polyions being a conjugated polymer (Ferreira *et al.*, 1994). By changing from a positively (negatively) charged solution to a negatively (positively) charged solution it is possible to make a complex, multilayer structure using two different materials, where each layer is only 5-20 Å thick. As the substrate is dipped in the first solution a thin layer attaches itself electrostatically to the substrate surface. By dipping alternately into the two solutions subsequent layers also attach themselves electrostatically building up a multilayer. This process of film formation is shown below in figure 3.17.

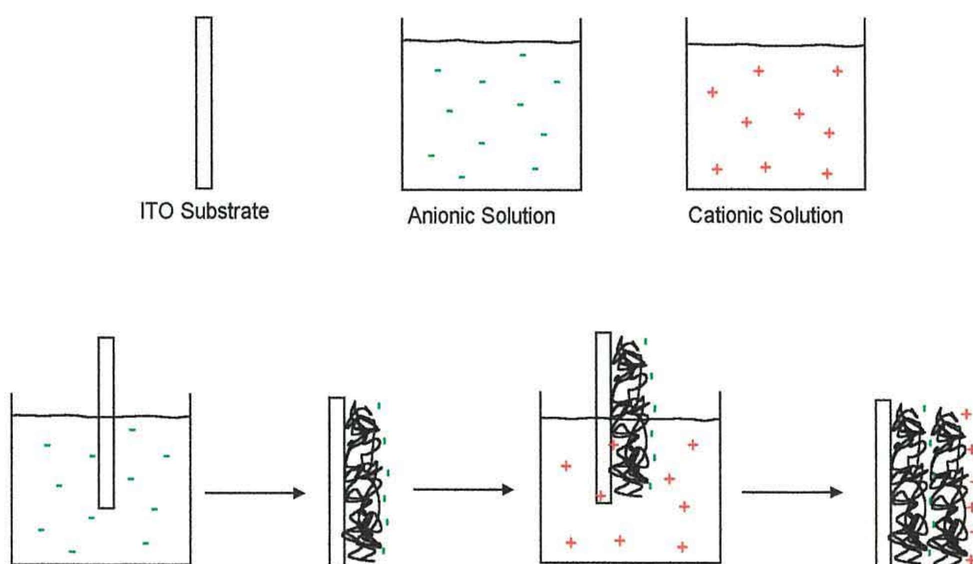

Figure 3.17 *A schematic of the steps required for the deposition of self-assembled thin films.*

Since this technique is a molecular level deposition process, it is possible to build heterostructure thin films with complex molecular architectures and thicknesses that can be controlled at the molecular level. Since this technique is easily applied to many different materials, is low cost, and yields high surface uniformity, it has attracted considerable interest for the formation of conducting polymers. Since optical and electrical properties in conducting polymers are determined by conformational changes and various redox states, the self-assembly technique has been widely employed in polymeric devices (Cheung *et al.*, 1994).

Normally, monolayers of electrically conductive polymers are spontaneously adsorbed onto a substrate from dilute solutions and subsequently built up into multilayer thin films by alternate deposition with a soluble polyanion. This technique has been applied successfully to the deposition of thin films of polypyrrole, polyaniline, and poly(3-hexylthiophene) (Cheung *et al.*, 1994). In these cases conductivities as high as 40 S cm^{-1} have been reported in films containing as few as four layers.

3.5.7 Plasma Polymerisation

Plasma polymerisation is one method that allows neutral polymer films to be deposited and has already been investigated in the preparation of polythiophene and its derivatives (Tanaka *et al.*, 1990; Haaland *et al.*, 1992). This technique allows for the controlled growth of dense films having a thickness ranging from a few hundred angstroms to a few microns.

Plasma polymerisation is a technique in which highly energetic meta-stable argon atoms collide with monomer molecules in a controlled environment. The collisions result in the formation of monomer ions, which combine on a substrate to form the polymer. A simple representation of the experimental set-up is shown in figure 3.18.

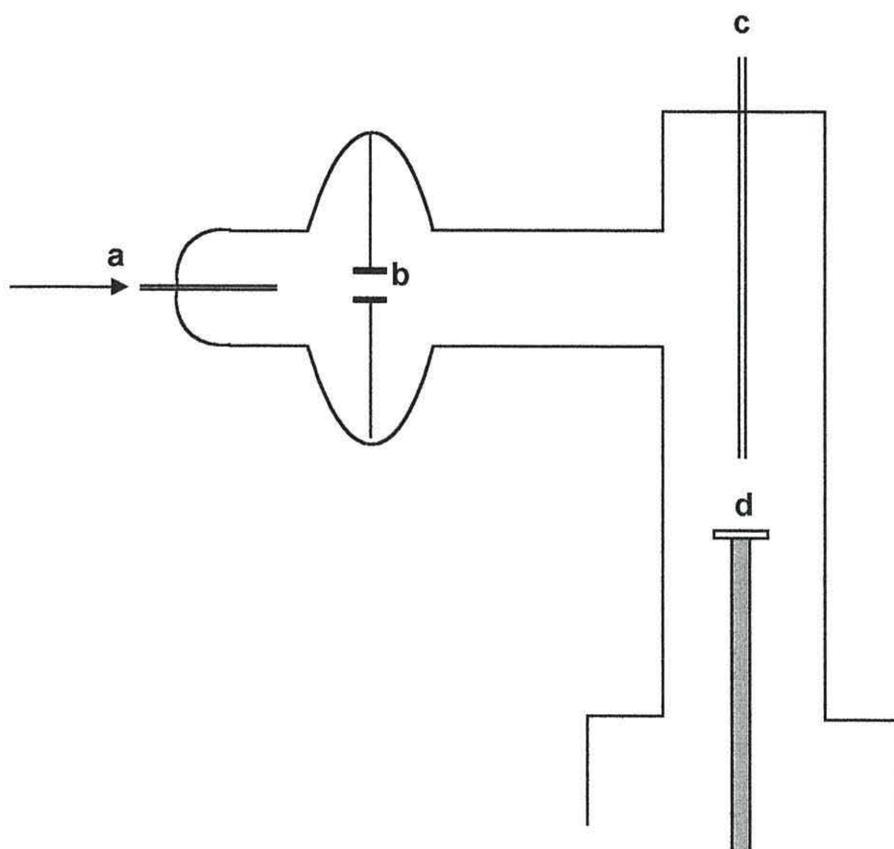

Figure 3.18 *A simple representation of the experimental set-up for plasma polymerisation.*

The main chamber is evacuated and kept at a pressure of approximately 0.5 Torr. The argon plasma is produced using RF excitation of the controlled gas flow (a). By applying a DC bias of approximately 200 V between the plasma producing electrodes (b), energetic, meta-stable argon atom production can be increased. (Electrons and ions formed in the plasma recombine within a few microseconds and so a few milliseconds downstream of the excitation point, at the point of monomer injection (c), it can be assumed that only meta-stable argon atoms exist).

The monomer material is contained in an independently controlled vacuum line (c) having a pressure of 20 – 30 Torr. From this line a known amount of monomer/argon gas mixture can be passed into the main reaction chamber in the form of a jet. At the injection point the monomer collides with the argon meta-stables, and ionisation of the monomer will occur as follows:

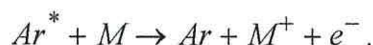

$$Ar^* + M \rightarrow Ar + M^+ + e^- .$$

In the case of thiophene, it has been shown that ionisation occurs in approximately one in every thousand collisions (Haaland *et al.*, 1992). The ionised monomer arrives at the substrate surface (d) with, in the case of thiophene, about 1-2 eV of kinetic energy. This allows the monomer to be incorporated in a highly reactive state in the substrate surface. As further monomer molecules bombard the surface, chemical bonding occurs and an extended polymer chain forms.

The monomer ions produced in the reaction chamber will be highly energetic and so it is probable that all the above reactions will take place at the polymer film surface. As a result, the film structure will be complex and, with short conjugation lengths owing to cross-linking of the polymer chains,

The film growth rate can be controlled by a number of factors, including the plasma RF input and the monomer concentration. A number of suitable substrates can be used including silicon, silicon oxide, and quartz.

A group working at the Wright-Patterson Air Force Base in Dayton, Ohio reported in 1992 a plasma polymerisation method for poly(3-hexylthiophene) (P3HeT) which provided a thin film of controllable thickness and morphology (Harrison, 1992). This work compared chemically polymerised P3HeT with its plasma-polymerised equivalent. It was observed that plasma polymerisation gave films of smooth morphology even down to the molecular level whereas chemically prepared spin coated material gave films with very rough morphology. Degradation of the chemically prepared polymer was observed especially in environments containing oxygen and water, but no degradation of the plasma polymerised polymer film was observed.

This technique is expensive to implement in terms of apparatus, and since the material has to be chemically modified in advance is somewhat inconvenient. But it is worth considering in the future, especially if further evidence is gathered to support the belief that good quality, smooth morphology films are essential for good electrical

characteristics in polymer based electronic devices (Roncali and Garnier, 1986; Sato *et al.*, 1985; Hotta, 1988).

3.5.8 Vacuum Evaporation

Vacuum evaporation of conducting oligomers (short-chain polymers) has recently emerged as a promising organic thin film deposition technique (Horowitz *et al.*, 1991; Burrows *et al.*, 1996), but has yet to be widely adopted.

The oligomer, normally in powder form, is typically heated in a resistive crucible or boat, under high vacuum conditions. For oligothiophenes, for example, evaporation temperatures of around 200 °C are usually used. The crystallinity of the deposited films can be improved by substrate heating.

This technique has the advantage of allowing co-evaporation of different oligomers onto a single substrate. The technique is similar to that used for metal electrode evaporation of contacts in device fabrication. The main disadvantage is the requirement for expensive, high vacuum systems.

3.6 Concluding Remarks

The aim of this chapter has been to introduce the main concepts leading to a better appreciation of conducting polymers in terms of their chemical structure, electrical characteristics and preparation techniques. Conducting polymers have been compared to conventional, inorganic semiconductors and the main features in which they differ have been elaborated. Discussions have concentrated on the unique properties of conducting polymers, which can lead to a better understanding of the properties of devices.

The chapter has also introduced a number of thin film deposition techniques. In some cases, for example, electropolymerisation, spin coating and precursor polymerisation, the techniques are widely used and have unique advantages and disadvantages. Currently, the most popular widely investigated conducting polymer materials are based

on either, PPV and its derivatives, which are either precursor polymerised or spin coated, or P3ATs, which are generally electropolymerised or spin coated.

In general the choice of materials, in this case PPV and P3ATs is based on a number of issues and properties which include ease of fabrication and handling, stability, cost, material conductivity, quantum efficiency, device lifetime etc.

Electropolymerisation is now receiving considerable interest for the formation of high quality, smooth films, which have good electrical and optical properties. Polythiophene, and in particular the poly(3-alkylthiophenes) have recently shown how versatile and appropriate they can be as test materials in simple device structures, in order to provide means of probing material properties.

However, this review serves to justify two key points for this study i.e. why it was undertaken and why any future work should continue. The major issue arising from previous work, which needs to be addressed, is to improve the overall understanding of the chemical, optical and electrical properties of conducting polymer materials and devices.

Consequently P3MeT will be used in this study to form Schottky barrier diode structures. The aim is to further characterise the Au/P3MeT and P3MeT/Al interfaces so that the properties of polymer based devices can be fully modelled. Extensive work has already been reported in this field as discussed earlier, however, topics including properties of trapping centres, the effect of material doping and details of charge transport mechanisms are still not fully understood.

The effects of trapping centres (or acceptor states) in the bandgap of conducting polymers have consistently proved problematic to model and their influence on device characteristics both undesirable and unpredictable. DLTS was envisaged as a suitable choice for analysing acceptor states in polymeric materials, particularly since it is a successful technique commonly used for characterising devices based on inorganic materials (Auret and Nel, 1986 – and references within).

New optical characterisation techniques such as in-situ Raman spectroscopy was considered as a novel way of identifying, characterising and monitoring the effects of

doping on polymer films. Since film doping can give rise to many of the acceptor states observed in polymer films and can control so many of the optical and electrical characteristics of devices, such a technique was considered invaluable.

Analysis of device photocurrent measurements was identified as a means of further characterising the processes occurring in and around the interface of polymeric devices which could explain some anomalies already reported in dc measurements in particular.

It was also foreseen that a combination of the above techniques could address the important issue of whether or not some of the observed ac characteristics in P3MeT Schottky barrier diodes originated from the effects of dopants drifting in an electric field, as suggested for other polymers such as PA and PPV (Burroughes *et al.*, 1988).

Further measurements addressing other important and outstanding issues include the effects of ageing, chemical preparation and handling techniques, breakdown phenomena and the relationship between device performance and film morphology.

Chapter 4 will address the fabrication details of P3MeT films and then describe in depth the experimental set-up and procedures used in obtaining the results, discussed in chapter 5.

4. Experimental

4.1 Introduction

This chapter will describe all the experimental procedures used in this work. Initially the procedures used to prepare thin film samples of P3MeT and the formation of Schottky barrier diodes will be described. Subsequently a detailed description is given of the experimental arrangements and methodology used for the electrical, optical, spectral and morphological studies of the films and devices made.

4.2 Sample Preparation

4.2.1 Substrate Cleaning Procedures

All samples were prepared on one of three base substrates, gold-coated float glass, indium-tin oxide (ITO) coated float glass, or gold-coated silicon substrates. In all cases rigorous procedures were adopted to ensure the cleanliness of the substrates prior to further processing. To ensure a high level of cleanliness, all sample preparation steps were conducted in a class 10,000 clean room (< 10,000 particles per cubic foot of 0.5 μm diameter or greater), which is air-conditioned to maintain a constant temperature of 293 ± 3 K.

Float glass substrates, supplied by White Hart Scientific Lens Co Ltd (Newcastle), were already pre-cut to microscope slide dimensions (75 x 25 x 0.8 – 1 mm). However, silicon substrates (n-type, phosphorus doped, with a 500 Å oxide layer) supplied by S.E.H Ltd (UK), were cut to the required dimensions from wafers. All ITO substrates were supplied as 300 x 300 mm^2 sheets, by Merck-Balzers AG (Balzers) and were subsequently cut to microscope slide dimensions for cleaning and preparation purposes. The ITO layer was 100 nm thick and had a sheet resistance < 20 Ω / □.

Additional scoring of the substrates to individual sample dimensions (usually half microscope slide 37.5 x 25 mm) was also performed prior to final cleaning.

After cutting and scoring of substrates the cleaning procedure outlined below was adopted:

- a pre-wash in acetone to remove traces of grease
- rinsing in a strong flow of ultrapure water (supplied from a Millipore System Q)
- thorough washing in a solution of hot, ultrapure water (80 °C) and Decon 90 cleaning agent
- wash in cleaning agent solution whilst placed in an ultrasonic bath for approximately 20 minutes
- repeated rinsing in hot, ultrapure water
- repeated rinsing in a strong flow of ultra pure water
- thorough drying in a hot flow of air

To reduce contamination of substrates during this procedure, care was taken to minimise the handling of substrates, by using specially designed holders.

4.2.2 Thin Film Evaporation

After cleaning, the substrates were placed in a Balzers type TSH 170 turbo pump system, the chamber of which was evacuated to a pressure less than 10^{-6} Torr prior to deposition of any layers. In order to improve adhesion of the gold layer to both the silicon and glass substrates, a thin layer of chromium, usually 10 nm thick was thermally evaporated on the surface prior to evaporation of a 100 nm thick gold layer.

In some cases microelectrode arrays were fabricated on the surface of glass slides, using photolithographic techniques. A mask was used to define the microelectrode structure, which consisted of four pairs of 12 mm long electrodes, each having a 25 mm^2 contact pad, for making electrical contact. Each electrode was 20 μm wide and approximately 0.5 μm thick. The spacing between individual pairs of electrodes ranged from 6 – 12 μm.

In order to minimise oxidation and contamination, once the metal layers had been deposited, substrates were removed from the turbo pump chamber and stored under

vacuum, prior to use. In general, however, attempts were made to use the coated substrates on the day of preparation.

In the case of ITO substrates, electropolymerisation of thin polymer films was performed directly onto the as-cleaned substrates.

4.2.3 Electropolymerisation

All chemicals were supplied by Aldrich Chemical Company, unless otherwise stated.

The electropolymerisation reaction was performed in a three-electrode cell as shown in figure 4.1. All electrical conditions were controlled by a EG&G PAR Model 273 A Potentiostat / Galvanostat.

The cleaned substrates form the working electrode onto which the thin film grows during the electropolymerisation reaction, as discussed in chapter 3. To ensure good electrical contact between the holder and the electrode a piece of platinum foil was usually placed between the two. The platinum plate which formed the counter electrode had an active area (i.e. area in solution) comparable to that of the working electrode. A cleaned length of silver wire was used as the reference electrode.

The electrolyte solution consisted of 0.5 M 3-methylthiophene monomer, in a 0.1 M solution of tetra-butylammonium tetra-fluoroborate salt (TBATFB) in propylene carbonate. The TBATFB not only doped the thin film but also maintained charge neutrality during the polymerisation process, as described earlier. The same procedure was adopted for preparing the dedoping solution except that in this case no monomer material was added. All solutions were usually prepared at least 24 hours in advance and always stored in a dark fridge. Following preparation, all solutions were degassed by bubbling with nitrogen gas through them for approximately 20 minutes. In addition, all reaction solutions were similarly degassed prior to electropolymerisation. During the reaction, care was taken to ensure that the electrodes remained isolated from each other.

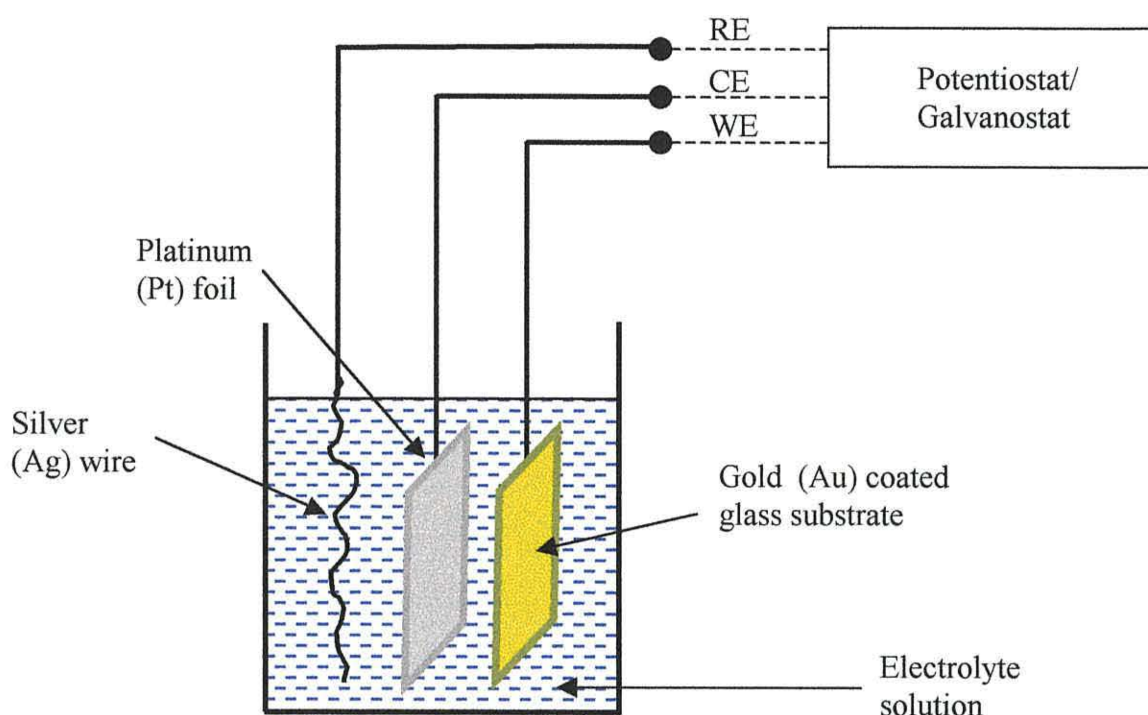

Figure 4.1 *Experimental set-up of three-electrode cell for electropolymerisation of 3-methylthiophene.*

Growing conditions adopted for film preparation in this study follow previously described procedures (Taylor *et al.*, 1991; Gomes, 1993). All potentials were applied between the working electrode and the counter electrode, and were measured relative to a silver wire reference electrode. A schematic of the potential applied to the working electrode as a function of time, during film growth is shown in figure 4.2. Initially an over potential (E_1), in the range 2 V – 2.5 V, was usually applied for a short period of time, approximately 5 s ($t_2 - t_1$) (Gomes, 1993). This induced the growth of nucleation sites on the surface of the substrate which encouraged the growth of a smooth, homogenous film. However, care was taken not to over-oxidise the solution to such an extent that chemical deterioration of the material occurred.

Following this initial step, the potential was reduced at a constant rate, usually 100 mVs^{-1} between t_2 and t_3 to the oxidation potential E_2 =1.8 V vs. Ag of P3MeT. The bulk of the film was grown at this potential during the period t_3 to t_4 , the time being determined by the thickness of the film required, which was usually 300 nm.

Subsequently, the potential was further reduced at a rate of 100 mVs^{-1} to E_3 (=1.6 V vs. Ag in most cases) and allowed to stabilise for approximately 2 mins before the cell was isolated and disconnected from the potentiostat.

The electrodes were immediately removed from the growing solution and placed in a cell containing the monomer free solution before the electrical connections were restored. The potential E_3 was then re-applied for a time period $t_8 - t_7$, usually two minutes, as shown in figure 4.3 and subsequently reduced at 100 mVs^{-1} to the required dedoping potential, E_4, which was maintained for the period t_9 to t_{10}. The extent of film dedoping was controlled by the magnitude and polarity of E_4 and the period for which the potential was applied. In general, the more positive the value of E_4 and the shorter the dedoping time, the less the dedoping. The process was also dependent on film thickness, with thicker films proving more difficult to dedope.

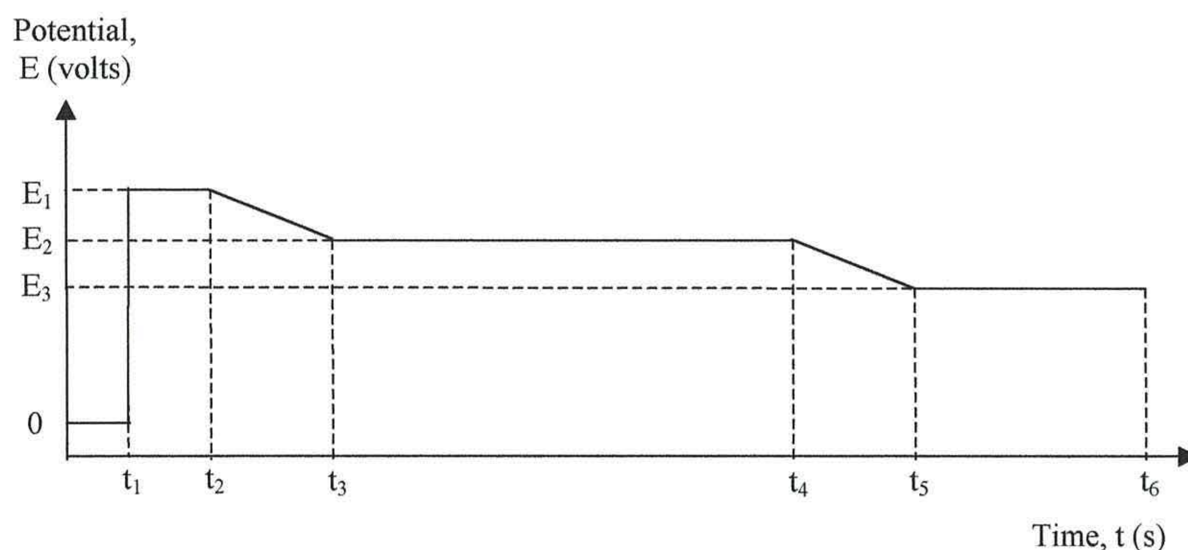

Figure 4.2 *Schematic of the variation of cell potential with time during the growing process.*

For this study potentials in the range 0 – 0.2 V were generally used and were applied for periods of time in the range of 30 s to 5 mins, depending on the required doping concentration. To simplify the dedoping procedure one rule of thumb adopted was to monitor the current crossing the electrolytic cell. In general the dedoping time required for the majority of samples, at a particular potential, was the time required for the current to fall to between 12 and 18 μA.

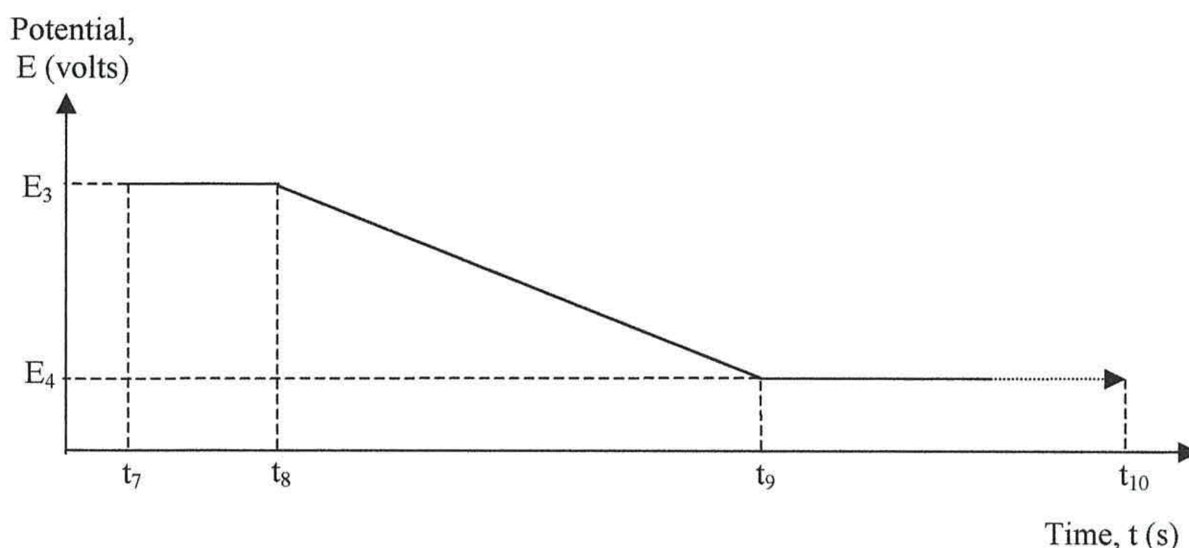

Figure 4.3 *Schematic of the variation of cell potential with time during the dedoping process.*

4.2.4 Device Formation

After dedoping, the sample was removed from solution and thoroughly rinsed in acetone, to remove traces of electrolyte solution and in particular any remaining deposits of salt. The film was then carefully dried in a gentle stream of nitrogen gas.

Samples were then returned to the turbo evaporator system, evacuated to at least 10^{-6} Torr, and a number of aluminium dots usually between 200 and 300 Å thick and 1 mm^2 in area, evaporated through a simple mask to form the Schottky diodes.

Electrical contacts to the sample were made using silver, conducting paste (Goodfellow) to attach very fine (0.025mm) gold wires (Goodfellow) to the underlying gold contact (ohmic) and the upper aluminium dot (rectifying), as shown in figure 4.4. In this set-up each aluminium dot forms a separate Schottky diode having a common ohmic contact.

Since extensive work had already been performed to study the effects of post-metal annealing of films (Gomes, 1993), it was decided that this effect would not be directly pursued in this study. Previous experience had demonstrated that variations to device

characteristics, as a result of device annealing were usually small and mostly observed as voltage offsets or anomalies in the dc characteristics.

Therefore in this study, post-metal annealing of films was not performed, however, the findings and conclusions of Gomes and co-workers (Taylor and Gomes, 1995; Gomes, 1993; Taylor *et al.*, 1991) were kept in mind, particularly, since films were being indirectly annealed when temperature scans were performed.

Applying a positive (negative) potential to the gold contact with respect to the aluminium contact places the diode in its forward (reverse) biased, conducting (non-conducting) state.

4.3 Electrical Measurements

Unless otherwise stated, the electrical characterisation of the devices was performed in the dark at 298 K in a temperature controlled sample holder located in an earthed, steel chamber. The chamber was evacuated to a vacuum of better than 10^{-5} Torr, for at least 24 hours prior to making any measurements. A combination of resistive heaters, a Peltier cooler, a cold finger, and a model 91E Eurotherm controller with a thermocouple feedback loop allowed the sample temperature under vacuum to be varied and controlled to within +/- 0.2 °C, in the range 253 K to 373 K . An optical window allowed the coupling of light to the device from an external source.

All measuring instruments were interfaced to a personal computer, which controlled and automated the measurement and data gathering procedures.

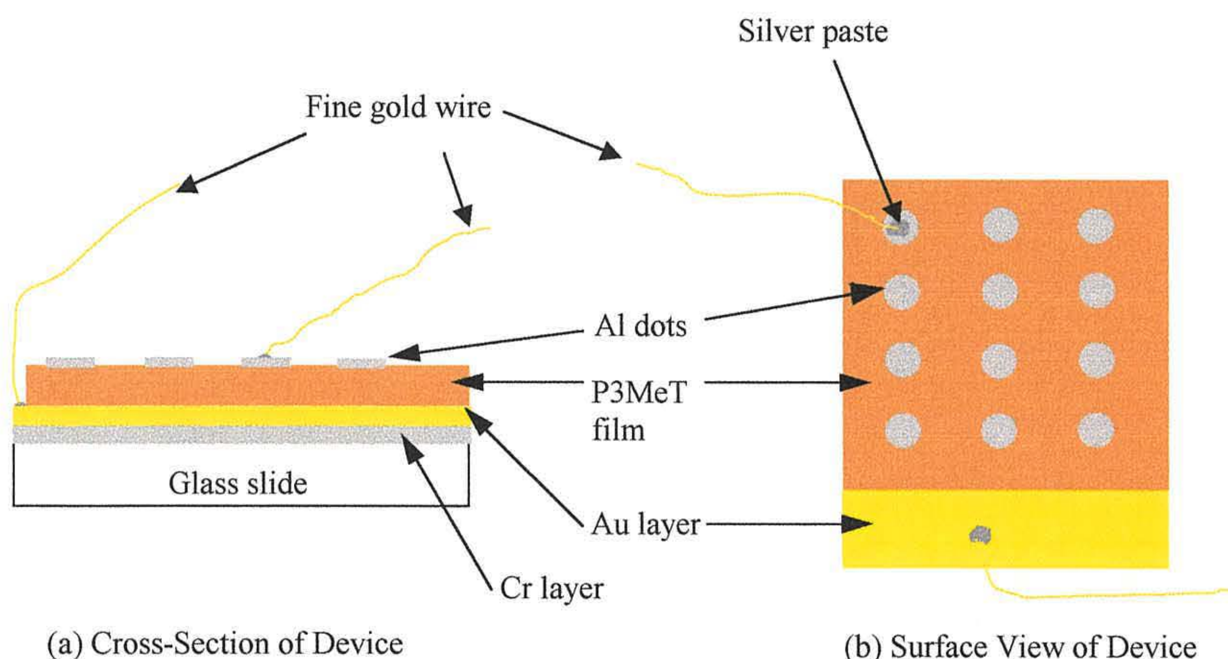

Figure 4.4 *A schematic representation of (a) the cross-section and (b) the surface view of a typical P3MeT sample.*

4.3.1 DC Measurements

Current-voltage characteristics were obtained using a Hewlett-Packard 4140B pA meter / voltage source. The typical scanned voltage range was from –2 V (reverse bias) to +2 V (forward bias). In all cases the bias was scanned from the most negative potential to the most positive, in accordance with procedures developed by Taylor and Gomes (Taylor *et al.*, 1991; Taylor and Gomes, 1995; Gomes, 1993). In some cases a back-scan from the final positive potential back to the initial most negative potential was performed immediately after the forward scan, to investigate the effects of hysteresis in the devices. The bias was usually increased in steps of 0.1 V, however in some cases 0.05 V steps were used in order to achieve greater resolution. To allow slow states to reach equilibrium, currents were allowed to stabilise for 2 minutes following each bias change (Taylor and Gomes, 1995).

Using the procedure described above, the I-V characteristics of some devices were obtained at different temperatures in the range 253 K to 373 K and the effects of optical excitation investigated using a 1 mW, 670 nm laser source. When samples were

illuminated by the laser source particular care was taken to minimise localised heating effects using various means including an IR filter.

4.3.2 AC Measurements

A Hewlett-Packard 4284A LCR bridge was used to make all ac measurements. Both the capacitance and conductance measurements of devices were measured over the frequency range 20 Hz to 1 MHz. Some measurements were also performed using a Solatron 1250 Frequency Response Analyser (FRA) to extend the low frequency range to 10^{-1} Hz. Both instruments applied a 50 mV ac test signal to the device.

C-V measurements were also performed using the HP 4284A bridge which has a built-in dc power supply for applying a bias to the device whilst measuring the resulting capacitance. The typical range of bias applied to the device was from –2 V to + 2V, with voltage steps of 0.1 V. A delay of 45 seconds was introduced at each bias to allow the device to reach a state of equilibrium prior to making any measurement. In all cases the bias was scanned from the most negative potential to the most positive, as before.

4.3.3 Deep Level Transient Spectroscopy (DLTS) and Capacitance Transients

The HP 4284A LCR bridge was also used for the DLTS measurement which involved recording the change in device capacitance consequent upon pulsing the bias voltage. The transients were usually obtained by initially reverse biasing the device to –2 V for 1 minute to provide a steady state condition at the start of the experiment. Then a pulse was applied to the device sufficient to bias it at a predetermined value in the range –1 to +2 V for a period of time ranging from 10-100 s, prior to returning the device to the initial reverse bias setting.

The recording of device capacitance commenced prior to the restoration of the initial reverse bias and continued every 500 ms for approximately 500 s or until the capacitance reached a constant value.

Individual capacitance transients were recorded every 10 K in the temperature range 298 K to 358 K. However, in some cases measurements were taken every 5 K, for

improved resolution. During each transient measurement the temperature was maintained to +/- 0.2 K of the target temperature using an Eurotherm controller.

4.4 Spectral Characterisation

4.4.1 Raman Spectroscopy

The Raman spectra of P3MeT were obtained using a Renishaw System 1000 Raman Microscope operating over the range 0 - 4000 cm^{-1}. Samples were placed onto the table immediately under the objective lens of the microscope used to focus the laser light onto selected areas of the sample.

Inelastically scattered photons reflected from the sample were collected by the same objective lens and coupled to the spectrometer and CCD detector. To avoid spurious Raman signatures from the substrate the P3MeT films investigated were grown on gold-coated silicon. (The single, narrow silicon band at 521 cm^{-1} is commonly used for calibration).

All measurements were made in an air ambient, normally using the red He-Ne laser (633 nm). Some measurements were made with a green Ar ion laser (488 nm). To minimise film damage, the laser power was kept low. Periodically samples were imaged optically using the microscope and attached CCD detector to observe any modifications to the polymer surface.

4.4.2 In-situ Raman Measurements

To investigate the spectral changes arising from dedoping, P3MeT films were electrochemically grown onto gold-coated silicon substrates using a conventional 3-electrode cell and initially dedoped at 0V for 5 minutes, as described previously. Prepared films were horizontally mounted in a specially constructed glass cell beneath a platinum foil counter electrode, as shown in figure 4.5. The distance between the film and the secondary electrode was approximately 0.5 cm. Solutions of three doping salts, sodium tetrafluoroborate ($NABF_4$), tetrabutylammonium hexafluorophosphate ($TBAPF_6$) and sodium perchlorate ($NaClO_4$) were prepared in degassed methanol to a

concentration of 0.07 M. The cell was filled with doping solution such that the working and the counter electrodes were fully immersed and the full assembly placed under the Renishaw System 1000 Raman microscope

The spectra of the films were obtained using the Helium Neon laser by focusing the light source onto the sample through a small hole in the platinum counter electrode. The potential across the cell was varied relative to a cleaned Ag wire using an EG&G PAR Model 273 potentiostat. All films were initially dedoped at 0 V, before being re-doped at successively higher doping potentials. At each potential a Raman spectrum was obtained.

To investigate the doping behaviour of films as a function of film thickness, three films were specially grown with thicknesses of 70 nm, 190 nm, and 380 nm, and their Raman spectra taken at various potentials in $NaBF_4$ solution. Subsequent studies investigated the effect of using various doping solutions as described above.

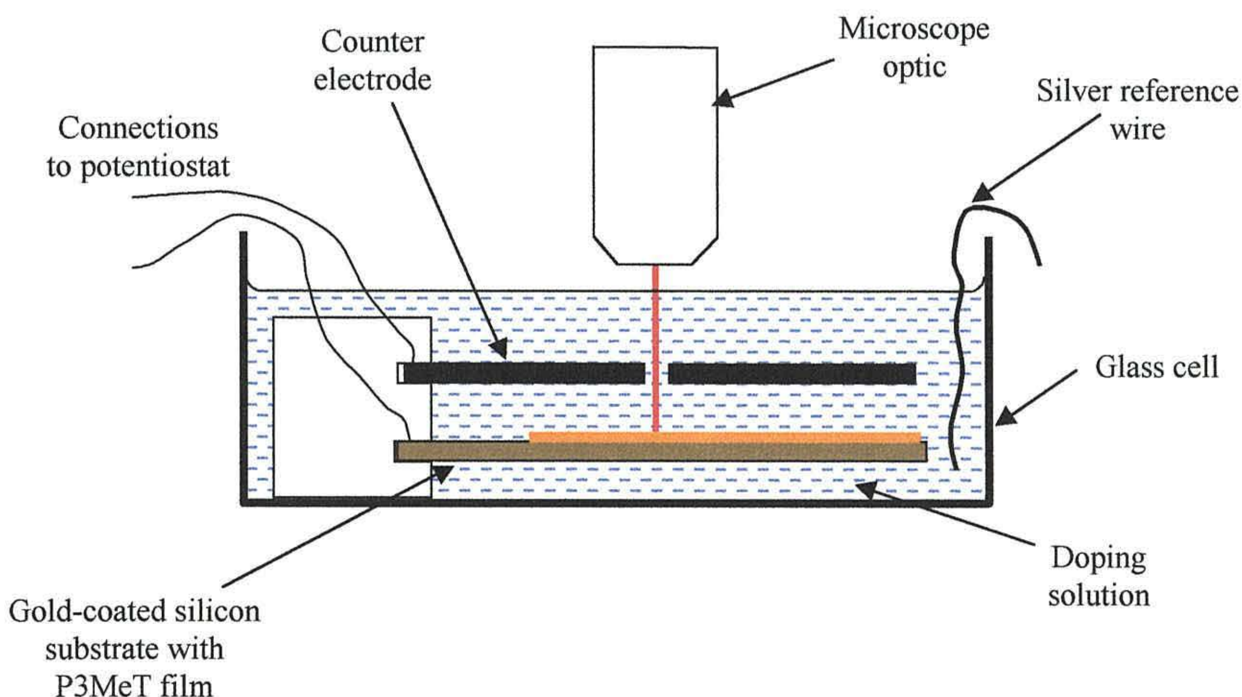

Figure 4.5 *A schematic of the cell arrangement used for making in-situ Raman measurements.*

4.5 Morphology

4.5.1 Scanning Probe Microscopy (SPM) and the Atomic Force Microscope (AFM)

The surface morphology of the films prepared in this study was investigated with a Digital Instruments Nanoscope IIIA STM/AFM with an extender box facility to enable Electric Force Microscopy (EFM) measurements to be carried out. For fuller details see the following references: **AFM Imaging Modes,** TopoMetrix Corporation, (1993), **Digital Instruments,** Support Notes, No. 231, Rev.A, **Digital Instruments,** Support Notes, No.207 and **Dimension 3000,** Instruction Manual. Initial studies using contact mode AFM, even with relatively low applied forces between probe and sample, led to extensive film damage. Since most films that were investigated were thin and easily damaged, the instrument was normally used in tapping / phase shift detection mode, which minimised damage to the film surface.

In this technique the silicon fabricated probe/cantilever assembly was oscillated above the film surface at its resonant frequency (usually in the range 300 – 450 kHz) by using a drive voltage amplitude in the range 100 – 500 mV. The set-point value, which determines the effective force of the probe on the sample, was in the range +0.5 to +2.5 V. The amplitude of parameters such as resonant drive voltage and set-point, generally varied from sample to sample and depended on the tolerance of film characteristics such as roughness and thickness. Scan areas were typically 25 μm x 25 μm down to 500 nm x 500 nm.

Film thickness was readily measured by scoring the surface with a sharp blade and using the "section" facility of the instrument. When using the instrument to analyse film thickness, an additional "look ahead gain" of approximately 0.6 was usually applied.

4.5.2 Electric Force Microscopy (EFM)

Two types of electric force microscopy are available using the Nanoscope IIIA instrument with extender box used in this study, 1) electric field gradient imaging; and 2) surface potential imaging. Each of the electric field measurement techniques are based on a two-pass lift-mode measurement. Lift mode allows the imaging of relatively

weak but long-range electrostatic interactions while minimising the influence of topography. Measurements are taken in two passes (each consisting of one trace and one retrace) across each scanline. First, topographical data is taken in tapping mode (as described in section 4.5.1) on one trace and retrace. The tip is then raised to the required lift height, and a second trace and retrace performed while maintaining a constant separation between the tip and local surface topography. The tips used in electric force microscopy are metal-coated silicon cantilevers, which can also be used for tapping mode imaging. These are usually placed in special holders, which allow a potential to be applied to the tip via the metal coating, and usually have a resonant frequency of approximately 70 kHz.

4.5.2.1 Electric Field Gradient Imaging

Electric field gradient measurements were carried out to investigate the feasibility of imaging the depletion region at the Al/P3MeT interface. Since it was not practical to perform measurements on the cross-section of a normal sandwich type device, the initial investigation was confined to lateral devices in which the polymer was grown onto the interdigitated electrodes as decribed in section 4.2.2. The connections to all the electrodes on a particular sample were shorted and electropolymerisation of P3MeT onto the electrodes made in the usual way, as described in section 4.2.3, with only minor modifications to the growing conditions to accommodate for changes in growing current density with decreasing effective electrode area.

Measurements were carried out using a lift height of 100 nm on both uncoated and film coated electrodes, with potentials of ± 2 V applied across the electrodes. Similarly, a dc bias could also be applied, via the cantilever, to the tip and was varied in the range –2 to +2 V as shown in figure 4.6. Phase detection methods similar to those used in tapping mode AFM are used to quantify the electric field gradient.

4.5.2.2 Surface Potential Imaging

Surface potential imaging data was obtained using the same set-up as that described for electric field gradient measurements described in section 4.5.2.1. However, in this case a potential nulling technique involving a combination of the sample potential, the tip

potential and the ac tip drive potential is used to build up the resulting image of the surface potential. These measurements were conducted to investigate the suitability of applying this technique to accurately measure the potential at various points.

4.5.4 Scanning Electron Microscopy (SEM)

In addition to SPM, films were also investigated using an ISI–400 scanning electron microscope.

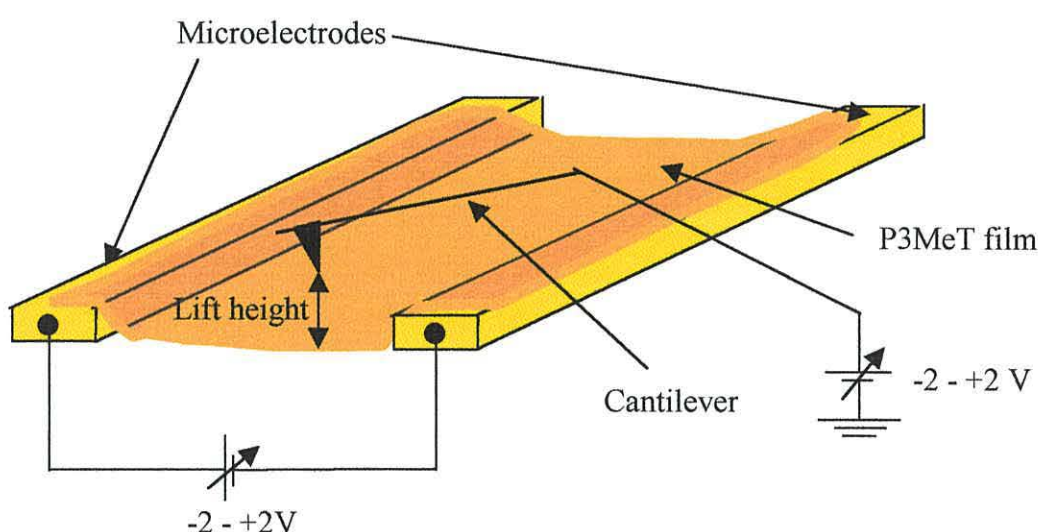

Figure 4.6 *EFM studies of P3MeT coated microelectrode arrays.*

4.6 Optical Characterisation

4.6.1 UV-Visible Spectroscopy

The UV-visible spectra of various P3MeT samples grown onto ITO substrates, having different doping concentrations, were investigated using a Hitatchi U-2000 Spectrophotometer. The effect of prolonged exposure to oxygen in the air and electrochemical dedoping techniques were studied. Particularly thin films of P3MeT were grown onto ITO substrates to ensure some degree of transmittance of the light beam through the film. In order to reduce substrate-based signatures, reference baseline scans were performed prior to each measurement, using ITO glass alone. The scanned

wavelength range was 190 nm to 1100 nm, with film absorbance values plotted against wavelength in each case. Lamp changes always occurred at 370 nm.

In each case two P3MeT films were grown onto a pre-scored ITO slide. This allowed the oxidised film to be grown over the whole surface with uniform thickness. The slide was then removed from the growing solution and cut in half, one half had a coating of oxidised film whilst the remaining segment was placed in monomer free solution and dedoped in the usual way to its fully reduced form. In this way the spectra of both highly oxidised and highly reduced films were obtained.

In each case a signal of 2 V (+/- 10 %) at the output terminal of the detector was equivalent to an absorbance of 1.

4.6.2 In-situ UV-Vis

A Lot Oriel MS-125 1/8 in-situ UV-Vis spectrograph was used to obtain spectra for various P3MeT samples grown onto ITO glass. The film was electrochemically grown in a glass cell containing monomer solution, as discussed in section 4.2. However no attempt was made at this stage to dedope the film. The doped film was then placed in a specially constructed, sealed cell (figure 4.7) containing monomer free solution of TBATBF salt, as described previously in section 4.2.3 .

The doping potential applied to the cell was gradually increased from 0 V to +1.4 V using a EG&G Model 273A potentiostat as before, and a uv-vis spectral scan from 220nm to 1150 nm performed at each bias.

4.6.3 Photocurrent Measurements

To investigate their electro-optical behaviour, films were fabricated with thin, semitransparent aluminium electrodes typically < 150 Å thick. This ensured that incident light was transmitted into the depletion region of the device.

Photocurrent measurements were performed on a fully computer controlled system, incorporating a SPEX 270 M monochromator, a Keithley 617 programmable

electrometer, Stanford Research Systems SR530 lock-in amplifier, 15Hz chopper, magnetron xenon lamp, and an Ealing 250 W universal arc lamp supply.

Device photocurrent was measured as a function of bias over the wavelength range 200 – 800 nm. All measurements were conducted at room temperature in a vacuum chamber, which was evacuated to less than 10 $^{-5}$ Torr.

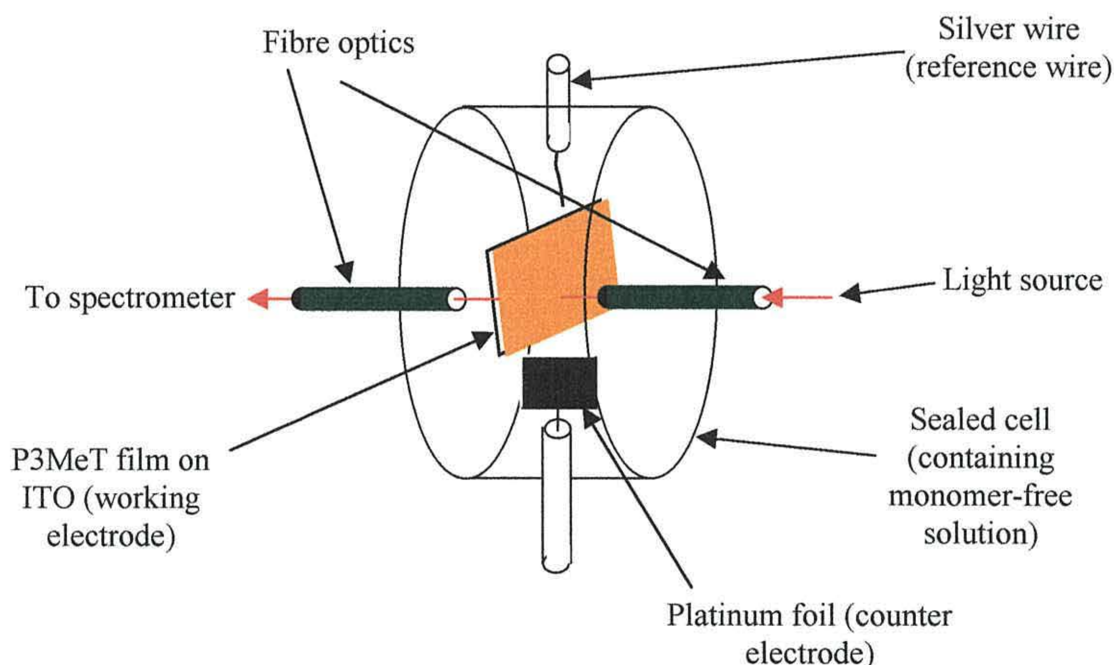

Figure 4.7 *A schematic of the experimental set-up used for making in-situ uv-vis measurements of P3MeT films.*

4.6.4 Photocapacitance Measurements

Optically induced capacitance transients were measured using the same arrangement as that for the DLTS measurements. The only difference was that the device was stimulated with a 1mW, 670 nm laser source (Oriel Merlot) at constant bias voltage. Particular care was taken at all times to minimise localised heating effects using an IR filter.

4.7 Concluding Summary

This chapter gives an outline of all the experimental procedures and techniques used in this study. It describes in detail the exact film and device preparation procedures, some of which have been adopted from previously reported work and others which were identified during the course of this study.

Further discussion concentrated on the nature of the measurements undertaken, with particular reference to the experimental conditions, apparatus and set-up. Greater emphasis has been placed on new, novel techniques such as DLTS, in-situ Raman and EFM measurements applied, in some cases, for the first time to conducting polymers.

The following chapter will include in detail the important findings of applying the above techniques to P3MeT based Schottky barrier diodes, with relevant discussions and comments.

5. *Results and Discussion*

5.1 Introduction

This chapter will present and discuss, in detail, the main findings of the present study. Topics will include morphology and dedoping, electrical characteristics of devices, DLTS and photocapacitance measurements, and a brief section on EFM and Kelvin Probe Microscopy results.

The extensive work carried out on P3MeT devices by Gomes (1993), identified and discussed a number of characteristics inherent to polymeric devices of this nature. However, in many cases, the techniques developed by Gomes failed to yield either high quality devices or reproducible results. The present study intends to further our knowledge and understanding of the primary factors that influence device characteristics.

By using analytical techniques such as SEM, AFM, UV and Raman spectroscopy, a link between sample morphology and the degree of sample dedoping has been identified. This relationship will be used to characterise and introduce a degree of control to the dedoping process, a particularly important requirement in determining the electrical and optical properties of resulting devices based on electropolymerised polymer films.

The doping process, which occurs during the formation of electropolymerised films, introduces polaronic states into the bandgap which can have detrimental effects on the electrical and optical properties of devices (Taylor and Gomes, 1995). The ac characteristics of P3MeT Schottky diodes have been used in this study in an attempt to characterise the acceptor states which form during doping. Specific techniques such as DLTS, successfully applied to inorganic devices, and applied here for the first time to conducting polymers, along with more commonly used Mott-Schottky plots have formed the main characterisation tools. In order to distinguish between the effects, if any, of electrical and optical excitation processes, photocapacitance measurements have also been performed on these devices.

In the first section, reference will be made to typical samples (A to E). These samples were used to investigate the parameters that require to be controlled to achieve devices

displaying good electrical characteristics. In subsequent sections, samples were usually prepared so as to be typically represented by sample C, D or E.

5.2 Morphology and Dedoping

5.2.1 SEM and AFM

In this study approximately 75 film samples were prepared using a range of growing conditions, the first of which were based on those exact parameters and conditions reported by Gomes (1993). Samples A to E studied in this section were typical and results for these samples will be given in this study. Devices prepared from these films displayed poor electrical characteristics with between 80 % and 90 % of all devices displaying short circuits. Electropolymerisation film growth is proportional to the current density at the working electrode, which, due to edge effects, is higher at the electrode edges and gives rise to thicker, non-uniform films around these areas. As a result it was usual to characterise devices which were situated near the centre of each sample, where the film is most uniform.

These first films, usually in excess of 1 μm thick, showed a decrease in relative roughness with increasing thickness, similar to the relationship reported by Gomes. Using the SEM, a thin (usually < 200 nm), smooth looking base layer was observed which was coated in a rough, granular and open–type structure, as shown in figures 5.1 and 5.2. The combination of pin-holes in the base layer (not shown) and the open structure, explains why resulting devices displayed a high percentage of electrical shorts. However, even though the same procedure and conditions were used, this type of structure does not compare well with that observed in samples studied by Gomes (1993).

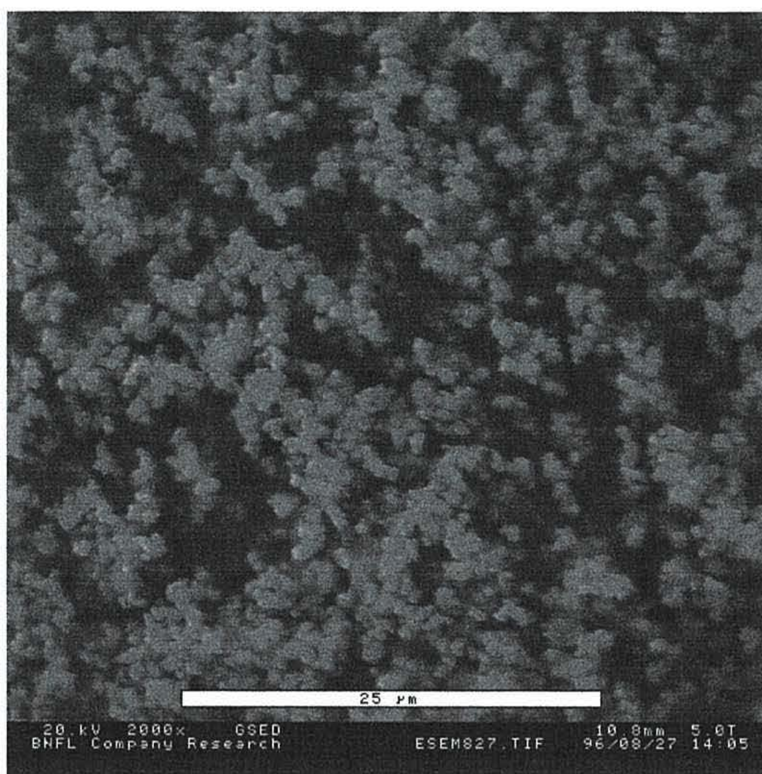

Figure 5.1 *A typical SEM image of an as-grown P3MeT film (2000 x magnification).*

In order to overcome the limitations and poor electrical characteristics displayed in devices prepared from thicker films, an investigation of the growing conditions required for thinner films, the dependency of thickness on the growing time, and of the roughness on film thickness was undertaken.

In general, thinner samples were obtained by reducing the growing time ($t_4 - t_3$) accordingly. Figure 5.3 shows the linear relationship between the sample thickness and time of growth, all other parameters remaining constant. This confirms the degree of thickness control achievable with electropolymerised films. From this data it can be seen that P3MeT films grow onto gold-coated substrates, at a rate of approximately 7 nm / sec, under the conditions described in section 4.2.3.

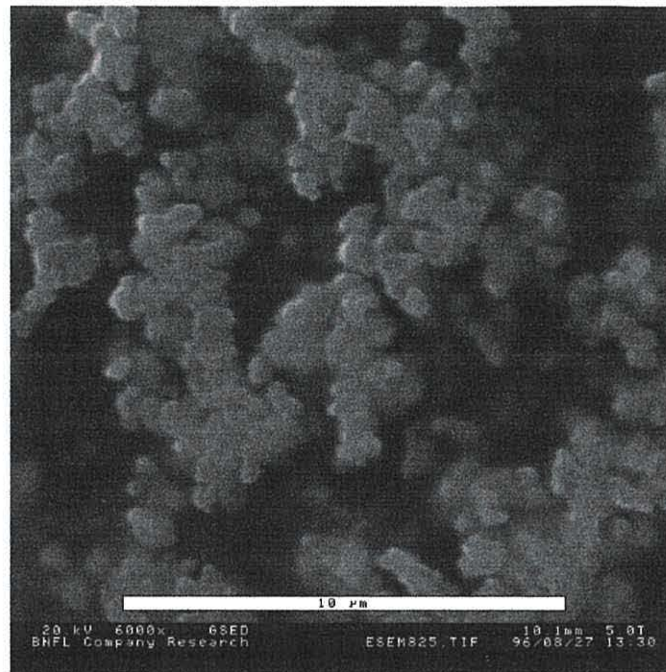

Figure 5.2 *A typical SEM image of an as-grown P3MeT film (6000 x magnification).*

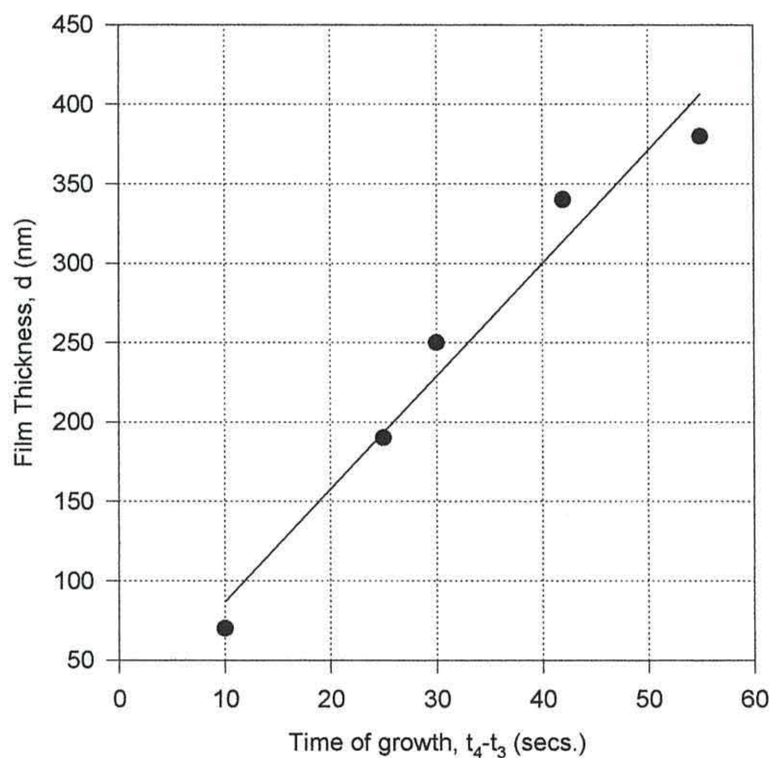

Figure 5.3 *The relationship between time of film growth and measured thickness for P3MeT films electropolymerised onto gold-coated substrates.*

However, in order to improve both the structural characteristics of the film and the electrical characteristics of subsequent devices, further modifications were made to the

initial growing conditions, in particular, a reduction in the value of E_1 to potentials nearer 2 V and reducing the duration of this applied potential ($t_2 - t_1$) to approximately 3 s, a combination of which effectively decreased the concentration of nucleation sites.

It was observed that the best electrical behaviour was generally observed in samples having a thickness in the range 300 –350 nm or a growing time of approximately 45 s. Films thinner than 300 nm usually displayed an increased probability of large areas of poor coverage, leading to "punch-through" of aluminium dots and electrical shorts. A combination of these modifications to the growing parameters led to a more tightly packed structure, even down to the micron level. A set of AFM images showing the structure at various scan areas, for a typical sample (in this case sample E - see table 5.1) is shown in figure 5.4 along with an image obtained using the sectioning technique for measuring film thickness (section 4.5.1). The scan areas were usually varied in the range 25 μm x 25 μm down to 500 nm x 500 nm, even though detail at the 500 nm x 500 nm level was extremely limited. All samples displayed characteristics similar to those typically depicted in figure 5.4.

Table 5.1 shows the relationship between the roughness and thickness of five P3MeT films grown under the new conditions, but with different growing time to achieve the required thickness (figure 5.5).

	Film Thickness (nm)	RMS Roughness (nm)	Relative Roughness
A	70	10	0.143
B	190	15	0.079
C	250	18	0.072
D	340	24	0.071
E	380	25	0.066

Table 5.1 *The relationship between film thickness and surface roughness for typical P3MeT films.*

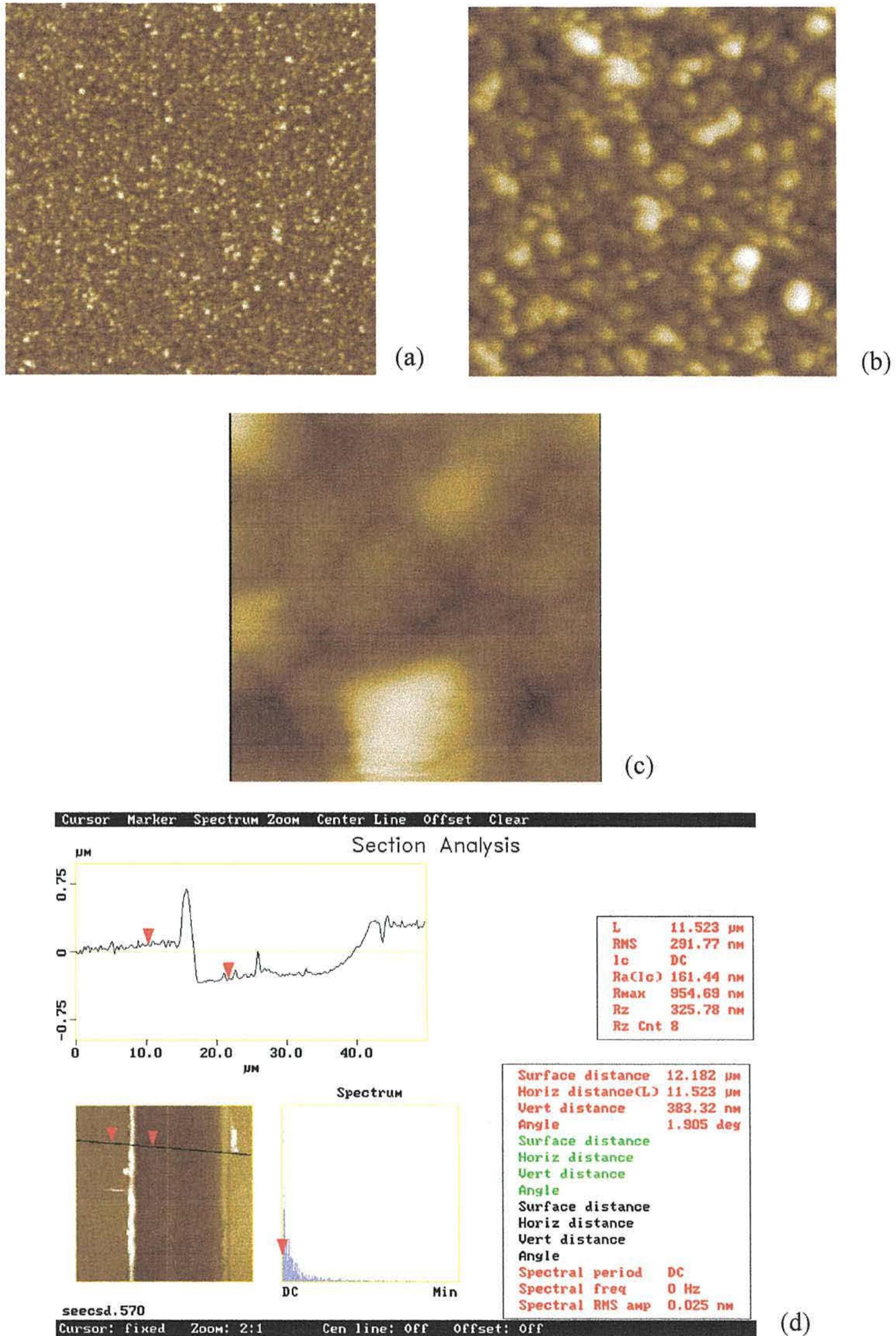

Figure 5.4 *AFM images of sample E at (a) 20 μm x 20 μm, (b) 5 μm x 5 μm and (c) 1 μm x 1 μm scan areas. A section image displaying the technique used to measure film thickness using the AFM is shown in (d).*

The relative roughness decreases with increasing thickness, for these thinner films (Table 5.1), similar to the observations made by Gomes for thicker films of approximately 1 μm.

In most samples tested the rms roughness was constant for all scan areas from approximately 400 to 1 μm^2, as shown in table 5.2, for sample E, confirming the uniformity of the surface morphology.

Scan Area (μm^2)	RMS Roughness (nm)
400	25.8
20	26.2
1	24.9

Table 5.2 *The relationship between AFM scan area and surface roughness for sample E*

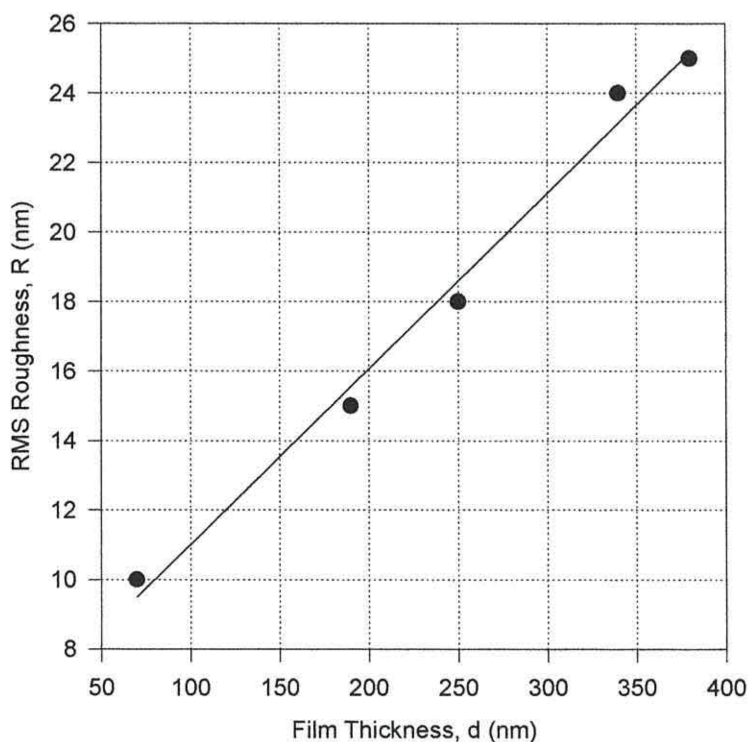

Figure 5.5 *The relationship between film thickness and RMS roughness for P3MeT films electropolymerised onto gold-coated substrates.*

5.2.2 UV-Vis and Raman Spectroscopy

5.2.2.1 UV-Visible Spectroscopy

The effects of exposure to ambient air and electrochemical dedoping were investigated by collecting spectra for two P3MeT films with different doping densities, grown onto ITO substrates.

In each case the doped (oxidised) film on ITO was dark blue in colour, whilst the dedoped (reduced) film on ITO was brown/red in colour. The spectra of the (a) oxidised and (b) reduced films for the range 190 – 1100 nm, and obtained within half an hour of preparation are shown in figure 5.6. In all cases an automatic lamp change within the instrumentation occurs at approximately 370 nm, but yields no response in any spectra. The sharp cut-off observed in each case at approximately 300 nm, is most probably due to the ITO coating of the glass substrate, and the 'peak' at approximately 329 nm due to intra-molecular excitation of the monomer material.

The dominant absorption peak observed at approximately 489 nm or 2.54 eV in reduced (in this case effectively neutral, since the film was de-doped for longer than usual) poly(3-methylthiophene) is ascribed to the $\pi - \pi^*$ transition across the band gap (E_G) of 2.2 eV (Gomes, 1993). This is slightly lower than the 2.54 eV quoted earlier, since the figure of 2.2 eV was deduced from the onset of absorption whereas the 2.54 eV value is taken from the maximum of the absorption curve. However, in the doped case, two broad peaks appear in the band gap, at the expense of the interband transition at 480 nm. The two new states are a consequence of the formation of non-degenerate polarons on the polymer backbone. The first polaron band occurs at 753 nm or 1.65 eV and the second (which is beyond the scope of this instrumentation) in excess of 1100 nm or < 1.1 eV.

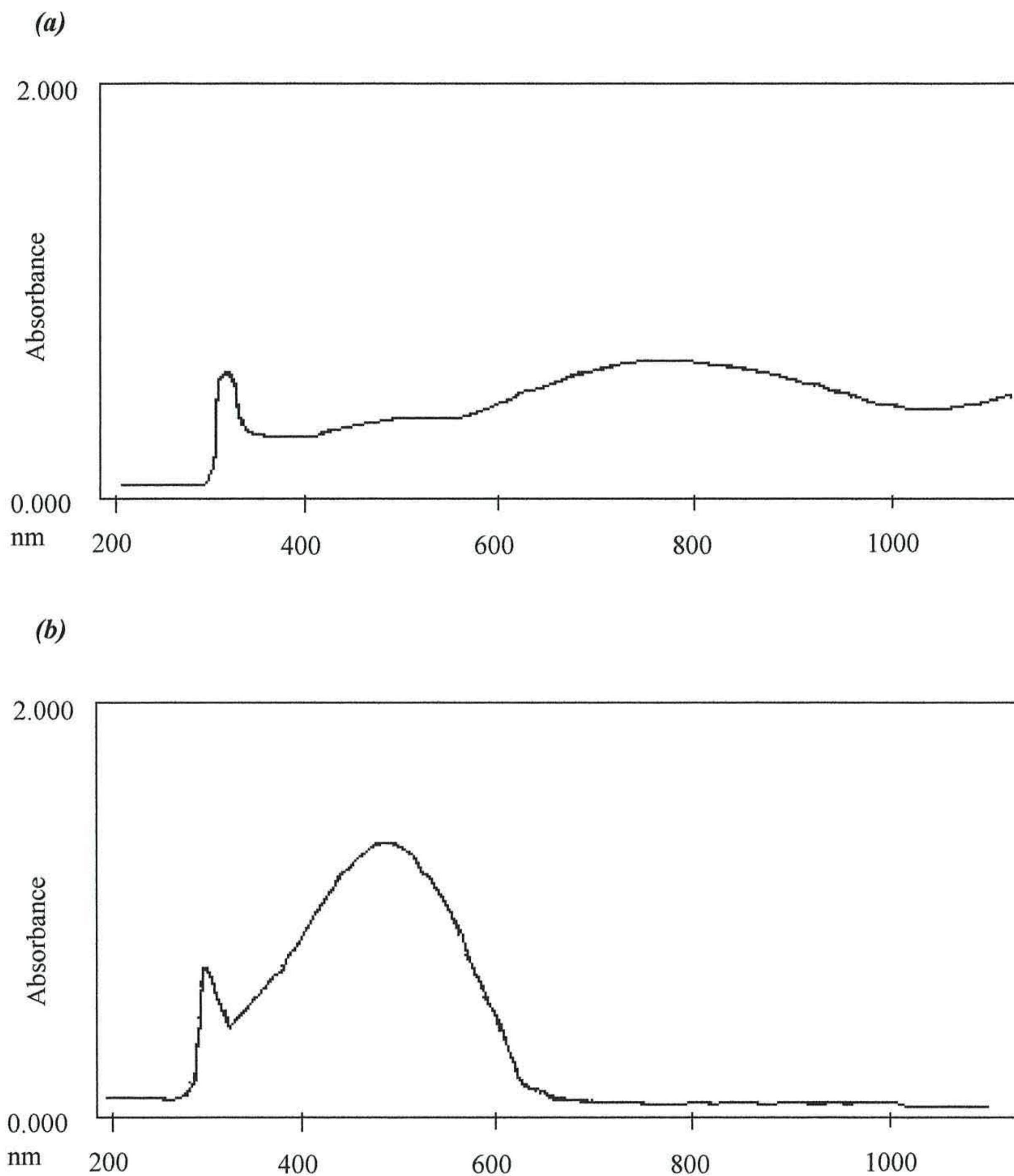

Figure 5.6 *UV-Vis absorption measurements for (a) an oxidised and (b) a reduced P3MeT film.*

Both samples were subsequently stored at room temperature at atmospheric pressure, with no attempt made to exclude light or air. After four days a further set of absorption measurements were made and are shown in figure 5.7. As shown the spectrum for the dedoped film is almost unchanged but the spectrum for the doped film shows the

presence of a more prominent peak at 488 nm. This suggests a partial dedoping of the doped film upon exposure to air and light with a consequent reduction in the polaronic peaks. This is in contrast to previous reports (Taylor *et al.*, 1991) of oxygen doping of P3MeT based FETs giving rise to improved conductivity. A possible explanation is that moisture in the air interacts with the dopants in the doped film and modify the observed absorption. Due to time constraints, this effect was considered beyond the scope of this work, thus an alternative technique for characterising the doping concentration in P3MeT films was pursued.

However, one interesting investigation was the possible use of chemical dedoping as an improved means of controlling doping levels. A doped (dark blue) film having an initial absorption spectrum similar to that shown in figure 5.6 (b) was immersed in methanol for 24 hours. In this period no attempt was made to restrict exposure to light or air. When recovered, the film had noticeably changed colour to red, similar to that of an initially dedoped film. The spectrum for this chemically modified film shown in figure 5.8, compares well with that shown in figure 5.6 (a), for the dedoped film. The peak centred at 481 nm corresponds to an interband transition of 2.57 eV and the absence of polaronic peaks reinforces the fact that all dopants have been removed, and that the film has been successfully de-doped chemically.

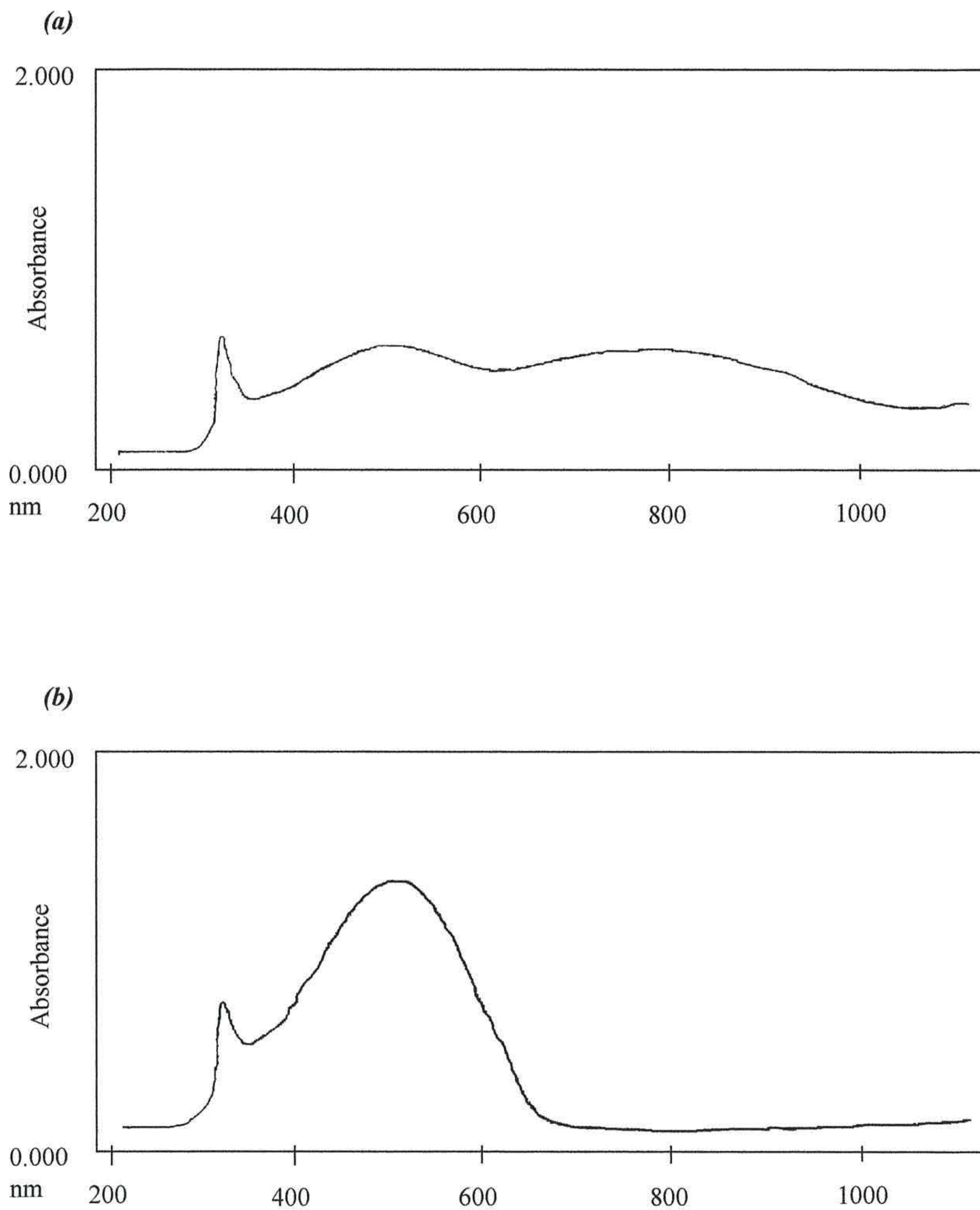

Figure 5.7 *UV-Vis absorption measurements for (a) an oxidised and (b) a reduced P3MeT film after four days storage in ambient air.*

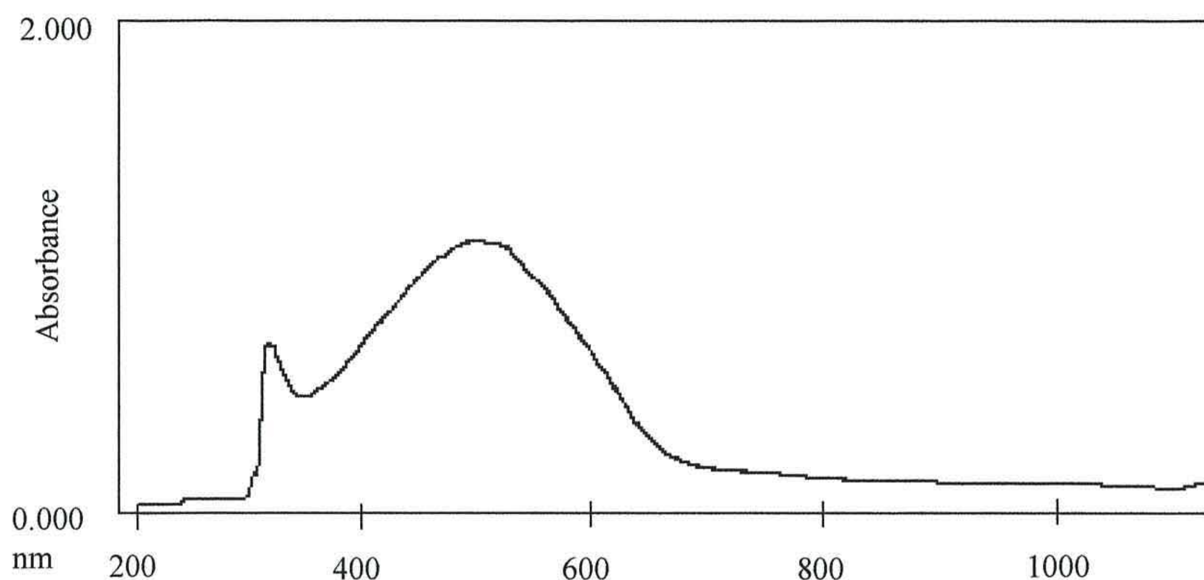

Figure 5.8 *UV-Vis absorption spectrum for a chemically de-doped P3MeT film.*

5.2.2.2 In-situ UV-Vis

The properties investigated using ex-situ UV-Vis techniques were further studied using an in-situ technique, with the advantage that only one sample was used and that the cell was completely isolated and required no intervention after set-up.

At 0 V bias the film used for making these measurements was in the dedoped state and was brown / red in colour. As the potential was increased the film darkened as it gradually became doped. When the potential reached approximately 1.4 V, in terms of colour change the film had reached its fully doped state and was dark blue in colour. This process was fully reversible, and the potential could be scanned in either direction inducing a change in doping concentration and a corresponding change in the colour of the film.

With this set-up, the available grating allowed for a window of approximately 330 nm, and as the window was moved to higher wavelengths the spectra became non-continuous at the changeover wavelengths and is the reason why the results are displayed as two separate windows. The spectra in the range 230 nm to 560 nm are

shown in figure 5.9. For the dedoped case there exists a very broad peak centred at 475 nm which corresponds to the π-π^* transition giving rise to a bandgap value of approximately 2.61 eV, which compares well to values obtained using the ex-situ techniques and to previously reported values (Kaneto *et al.*, 1984). As the potential is increased this peak diminishes in magnitude, at the expense of the formation of inter-gap (polaronic) states, as before.

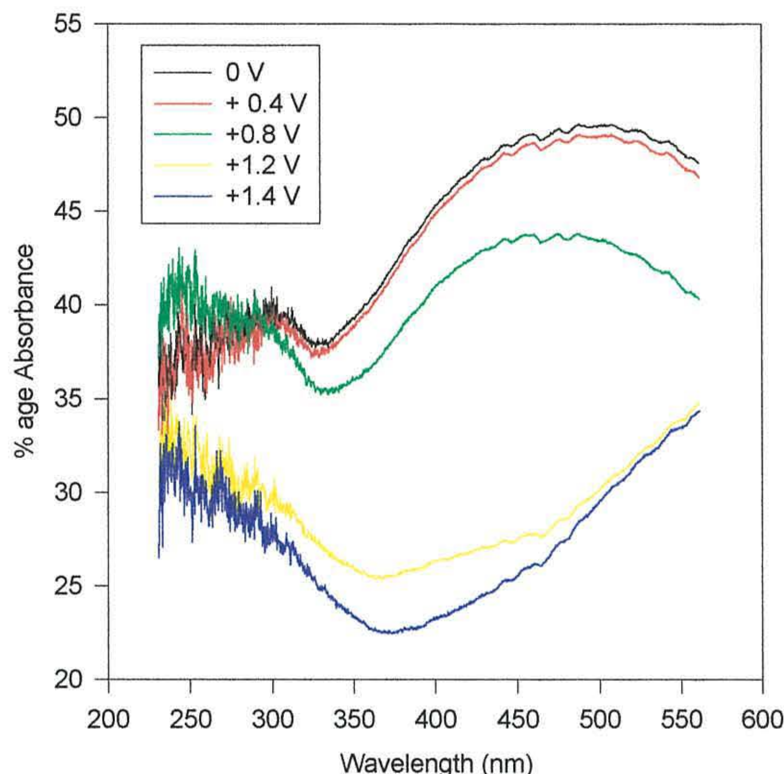

Figure 5.9 *In-situ UV-Vis spectra for an initially doped (blue) film on ITO substrate in the wavelength range 230 nm – 560 nm.*

Corresponding spectra in the range 840 nm – 1140 nm for the same film are shown in figure 5.10. In this higher wavelength window, the inverse is true. At high doping potentials, the existence of polaronic states in the band-gap gives rise to high absorbance at corresponding high wavelengths. In this case a flat, high absorbance signal exists across the whole window, which suggests the presence of a degenerate polaronic band rather than a single state. However, from this result it is again very difficult to make an assessment of the exact position of the state in the gap.

At lower doping potentials (~ 0.8 V), greater structure is observed in the absorbance measurements, suggesting the possible presence of more than one peak and hence more than one polaronic state. At even lower doping potentials the absorbance in this window is significantly reduced as the concentration of polaron states is further reduced.

The spectra between 560 nm and 840 nm was observed to be non-continuous, possibly as a result of inconsistencies in the baseline measurements as the window was moved. Another possibility was that the time between measurements was insufficient to consistently allow the system to reach equilibrium.

The problem of non-continuous spectra, in this case between 560 nm and 840 nm once again makes this technique, with the present set-up, unsuitable for determining the exact optical characteristics of a sample as a function of doping potentials.

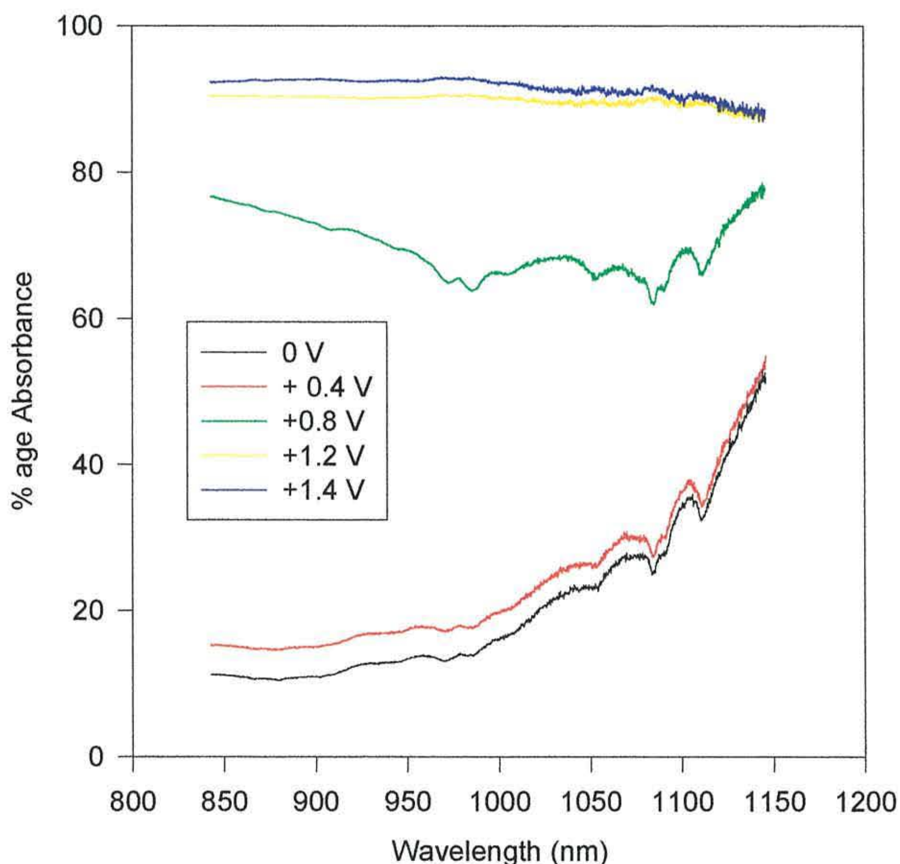

Figure 5.10 *In-situ UV-Vis spectra for an initially doped (blue) film on ITO substrate in the wavelength range 840 nm – 1140 nm.*

5.2.2.3 Raman Microscopy

Raman spectrometry was initially used to identify the main peaks characteristic of P3MeT films. A typical spectrum obtained for a dedoped P3MeT film is shown in figure 5.11. A typical spectrum for a doped film would display a major reduction in the background fluorescent intensity observed in figure 5.11. The major peaks identified in the spectrum compare well with published results for similar P3MeT films (Favre *et al.*, 1997) and to preliminary assignments made using semi-empirical quantum mechanical calculations performed on tetra-3-methylthiophene (see table 5.3) (Hughes *et al.*, 1998).

In 1989, Brédas reported the change in aromaticity (or the effective conjugation) of thiophene rings from predominantly benzenoid to predominantly quinoid as a function of increased doping (Brédas *et al.*, 1989). The fact that doping also induces states in the form of polarons and bipolarons on the backbone, as discussed earlier, implies therefore that the vibrational frequency of the bonds that constitute the polymer backbone are modified.

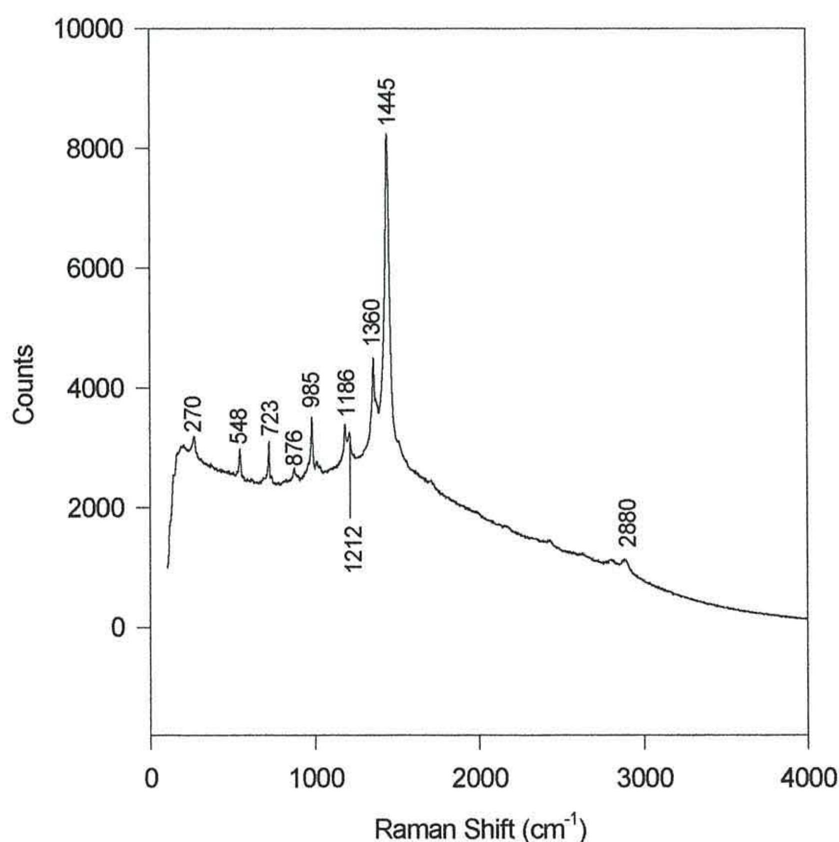

Figure 5.11 *Raman spectrum for dedoped P3MeT film on a gold coated silicon substrate.*

Wavenumbers (cm^{-1})	Assignments
1445	C=C stretch
1360	C-H deformation / C-H bend
1210	-
1186	-
984	Ring deformation
871	C-S stretch
740	C-S stretch
720	Ring-ring stretch
548	Ring-ring stretch
270	Ring deformation

Table 5.3 *A table of the relevant vibrational assignments in tetra-3-methylthiophene.*

A combination of preliminary experimental results such as that shown in figure 5.11 and the results of the quantum mechanical calculations, identified two strong peaks. One at 1360 cm^{-1} associated with the C-H deformation of the CH_3 group (not in the backbone) and one at 1445 cm^{-1} associated with the C=C stretches in the backbone (table 5.3). The magnitude of the 1445 cm^{-1} line is largely influenced by changes in the conjugation length along the polymer backbone, which in turn is related to the extent of doping. Similarly the line at 1360 cm^{-1} is influenced by changes in the spatial arrangement of the thiophene rings. The effect of doping on the magnitude of the 1360 cm^{-1} band is much less pronounced than that on the 1445 cm^{-1} line as expected, since doping affects conjugation in the ring and not the aliphatic CH_3 group.

5.2.2.4 In-situ Raman Investigation of P3MeT

Following the relative success and ease of obtaining and identifying the doping peaks associated with polarons and bipolarons using both ex-situ and in-situ UV-Vis absorption measurements, as described in section 5.22, it was decided to pursue and develop an in-situ Raman technique as an alternative means of characterising the doping concentration and profile in P3MeT samples. This technique was used to obtain a number of spectra for samples with various doping concentrations.

An interesting observation made during this investigation was the apparent increase in fluorescence from P3MeT films as the doping concentration is reduced, i.e. polymer doping gives rise to fluorescence quenching. Similar observations have been previously reported for other conducting polymers, for example, PPV and its derivatives (Baigent *et al.*, 1988). However, no reference could be found to any comparable results for polythiophene and its derivatives, and in particular to any reference of using Raman spectroscopy techniques to monitor the effect.

During these measurements the CCD camera of the Raman microscope was used to closely monitor the relatively fast (less than 0.5 s) switching speed from the doped to de-doped state (and vice-versa) and its corresponding colour change. Excessive state switching, usually more than twice the number required to successfully complete this investigation, gave rise to relatively minor film damage mostly observed as the loss of film from the substrate surface.

The samples were allowed to stabilise at each doping potential for in excess of 30 seconds, which compares well with the average dedoping time used throughout this study.

The Raman spectra of a typical film as a function of the doping potential between 0 V and 140 mV, in a solution of methanol and sodium tetrafluoro-borate, is shown in figure 5.12, even though the overall study included measurements in the range 0 V to ~ 500 mV (see later). There are two evident effects. (i) The background photoluminescence of the film decreases with increasing potential (i.e. the concentration of dopant increases) and (ii) close inspection reveals that changes occur in the relative intensities of several of the peaks.

From preliminary experimental studies and semi-empirical calculations, the peaks at 1445 and 1360 cm^{-1} displayed the most dramatic change in amplitude as a function of bias applied to the film. The ratio of the intensity of the 1445 cm^{-1} amplitude mode peak relative to the 1360 cm^{-1} peak was taken in this study as a measure of the average doping concentration of the film.

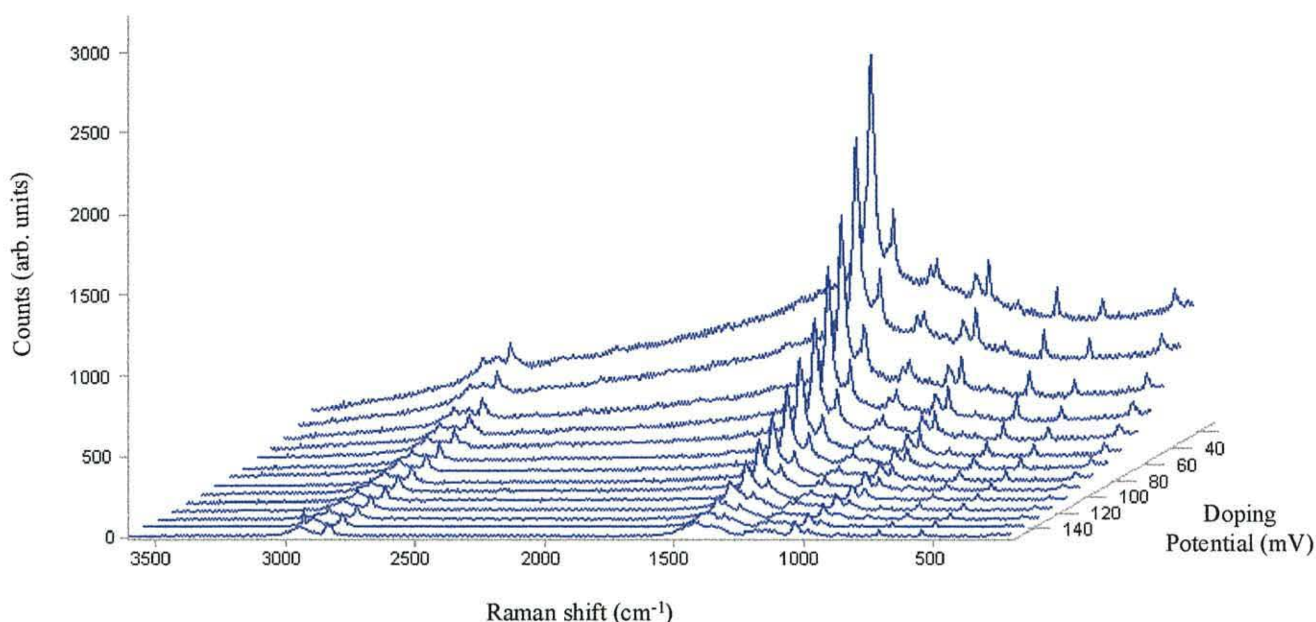

Figure 5.12 *The effect of doping potential on the Raman spectrum of a typical P3MeT film on gold coated silicon substrate.*

The peak intensity ratios for the three separate films of different thickness as a function of applied potential are shown in figure 5.13. As can be seen, the thicker film is far more easily doped (i.e. lower potentials are required to achieve a given doping concentration) than thinner films. This trend was also confirmed by analysing the background fluorescent intensity against doping potential (not shown here). Assuming that all other parameters are constant and since all potentials are measured relative to the Ag electrode, the approximately + 475 mV vs. Ag required to reduce the photoluminescence intensity to zero in the thinner film is almost twice the + 250 mV vs. Ag required for the thicker film. In addition, since the laser source will penetrate the whole of the sample, rather than being surface sensitive, then the possibility of a significantly lower signal originating from the structural effects alone of a thicker, more porous sample, is unlikely.

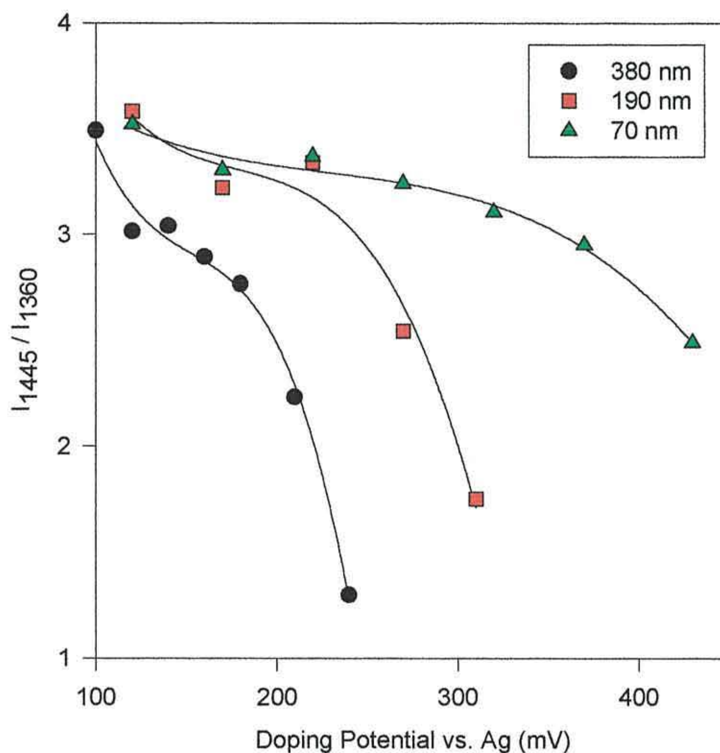

Figure 5.13 *Peak intensity ratios for three separate P3MeT films as a function of thickness and doping potential.*

This argument is counterintuitive though, since it would be expected that a larger voltage drop would exist across a thick film than a thin film and hence a larger applied potential would be required to achieve any given doping concentration, unless again that the thicker films are extremely porous.

Using AFM images and analysing in particular, the roughness of the three samples, a possible explanation for this effect was obtained. A number of reports have been filed relating the degree of disorder of P3MeT films with thickness (Gomes, 1993). As in this case the disorder in the films increase with thickness, whilst the relative roughness decreases, as discussed previously in section 5.2, and as shown in table 5.1.

These findings suggest that the lower doping potential required for the thicker films could reflect the fact that the dopant ions can penetrate the rougher, more disordered structure more easily than a denser, smoother film.

As part of the same study, the role of the dopant anion was further investigated. In particular, the doping effectiveness of the solutions containing the three anions (PF_6^-, ClO_4^-, BF_4^-) was studied in the 1300 – 1500 cm^{-1} range. In this case one film, 200 nm thick was used and cut into three sections, one of which was investigated in each of the three doping solutions. The resulting variation in the peak intensity ratios is shown in figure 5.14.

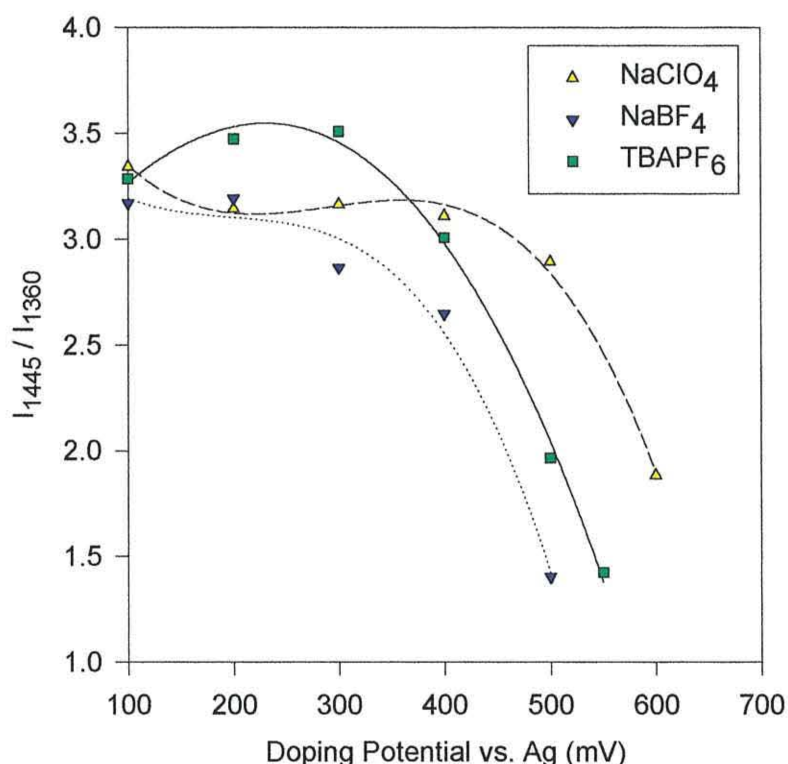

Figure 5.14 *A comparison of the doping efficiency of different dopants..*

The most mobile dopant appears to be the BF_4 anion, whilst the highest potentials for a given doping level are required of the ClO_4 anion with the behaviour of the PF_6 anion intermediate between these two extremes. A similar trend was also observed in the intensity of the background photoluminescence. However the exact reason for this effect is unclear since PF_6 has the largest radius (see table 5.4). Most probably it reflects a combination of the ease of charge transfer between the P3MeT and the dopant molecules and of the ease of penetration of the dopants into the film, which in turn is related to the size of the species.

The spectra of the doped films of each of the three anions were identical, suggesting that the final structure of the polymer film is not influenced greatly by the type of anion used in the doping process. This also confirms that the difference in the ratio of the doping peaks are solely attributable to changes occurring in the polymer.

Anion	**Radius of anion, r (nm)**
PF_6^-	0.301
ClO_4^-	0.290
BF_4^-	0.284

Table 5.4 *The radius of the three doping anions Note: All three anions are spherical (from Peulon et al., 1996).*

5.3 DC Behaviour

As discussed in section 5.2, film quality was a major hurdle to the successful formation of devices having good electrical characteristics. Following modifications to the growing parameters (as described in section 4.2), the range of characteristics displayed by devices became narrower and more predictable in nature. In general though, minor refinements to the procedures, including greater care of handling and improved cleaning of the base substrates also yielded better quality devices.

This section identifies and discusses the typical characteristics displayed by the majority of tested devices, and aims to identify the major differences between experimental and ideal devices.

5.3.1 Typical Device Characteristics

Figure 5.15 shows the dc characteristics of three typical P3MeT Schottky barrier diodes based on three different samples. The growing parameters for each sample are given in table 5.5. Almost all devices that were tested, which were not short-circuit in nature, displayed a characteristic closely resembling one of the the plots given in figure 5.15. The largest current density was consistently observed when the device was forward biased, with a positive potential applied to the gold, ohmic contact and lower current density values observed when the device was in the reverse biased, blocking state, with a negative potential applied to the gold, ohmic contact.

Almost all devices displayed rectification of some form, the ratio of the forward to the reverse current at the quoted potentials, usually in the range 500 to 10,000 and over a voltage range –2 V to + 2V. However, with improved control of the doping and de-doping processes, devices with rectification ratios of approximately 100,000, over a reduced voltage range of -1 V to + 2 V, were occasionally fabricated towards the end of the study (sample H, figure 5.15). These compared well with some of the highest ever reported values to date in conducting polymers (de Leeuw *et al.*, 1994; Kuo *et al.*, 1993). By studying figure 5.15 and table 5.5, it is evident that the device based on sample H displays the greatest rectification consistent with a greater degree of dedoping during preparation. However, an important finding of this study was that this greater

degree of dedoping rarely gave rise to devices with adequate ac characteristics for probing acceptor states.

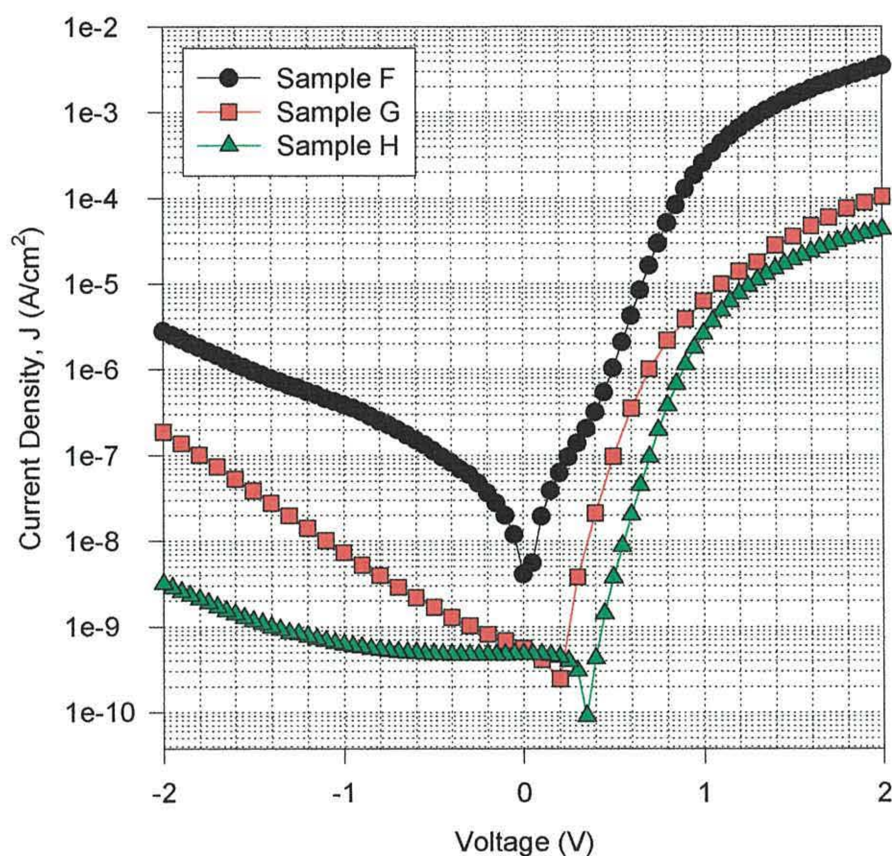

Figure 5.15 *The typical range of DC characteristics displayed by three P3MeT Schottky barrier diodes.*

	F	G	H
E1 (V)	2.2	2.0	2.4
D1 (s) ($t_2 - t_1$)	4	5	5
S1 (mV/s)	50	50	50
E2 (V)	1.8	1.8	1.8
D2 (s) ($t_4 - t_3$)	50	60	60
S2 (mV/s)	50	50	50
E3 (V)	0.1	0.1	0.1
Dedoping Time (s) ($t_{10} - t_9$)	540	900	1200

Table 5.5 *Growing parameters for sample F, G, and H.*

The reverse current in almost all devices fails to saturate in the manner predicted by the thermionic and diffusion theories given in equations 2.8 and 2.10 respectively. In the cases described in figure 5.15, the device based on sample H is the only one that displays any saturation, which occurs only over a small voltage range from + 0.25 V to – 1 V, whilst samples F and G show no saturation of the reverse current. However, from the slope of the linear portion of each plot, the diode ideality factor was: sample F = 2.60, sample G = 1.95, and sample H = 2.38, which demonstrates the relatively good forward diode behaviour exhibited by all three samples.

As discussed in section 2.5.2, the inclusion of image force effects allows for the current to grow by reducing the barrier height. Equation 2.15 describes the effect of the decreased barrier height, which allows for the reverse current to increase with potential following an approximately $V^{1/4}$ law. A plot of log J_R vs. $(V_{SO}-V)^{1/4}$ for the devices studied in figure 5.15, is given in figure 5.16, where J_R is the reverse current density. In this case V_{SO} has been assumed to be 0.3 V, a typical value displayed by many devices (reverse bias measurements: Taylor and Gomes, 1995), and the voltage offset in the devices of samples G and H have been accounted for.

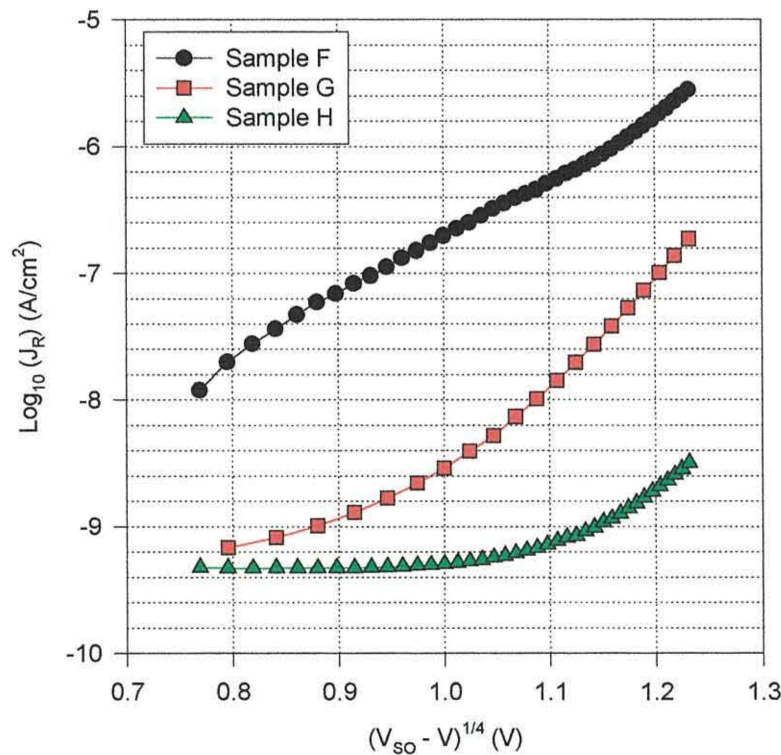

***Figure 5.16** A plot of log J_R vs. $(V_{SO}-V)^{1/4}$ for three typical devices.*

The approximately linear relationship observed for the device based on sample F suggests that an image force lowering process could be responsible for the lack of saturation expected for the current in reverse bias. Both other samples deviate from this linear behaviour to varying degrees, even though there is some evidence for image force lowering effects for sample G.

In addition, a number of devices displayed an anomaly similar to that observed at ~ 0.3 V for sample F in figure 5.15. In all these cases no offset voltage is observed, but a pronounced plateau appears in forward bias. A similar effect was observed for silicon MIS devices having a thin insulating layer between the semiconductor and the metal (Green *et al.*, 1974). In this case the plateau was believed to signify a transition at the silicon surface from inversion to depletion to accumulation, with increasing forward bias. The type of behaviour now observed in organic devices has similarly been attributed to the presence of an interfacial layer at the metal / polymer electrode (Taylor and Gomes, 1995).

Bulk polymer limiting of the forward current is commonly observed in many devices at voltages approaching + 2 V, and demonstrates the importance of the electrochemical doping and dedoping processes in determining the electrical characteristics of resulting devices. Extensive dedoping results in higher bulk polymer resistance and the earlier onset of current limiting effects, as shown in the heavily dedoped samples G and H in figure 5.15 and table 5.6.

The current density values observed here (10^{-2} – 10^{-10} A cm^{-2}) are typical of those observed and reflect the "operating range" of many devices characterised within this study.

5.3.2 Effect of Light

In this investigation the effect of shining a 670 nm, 1mW laser source at the top electrode of a typical device was investigated. Extreme care was taken to minimise the effect of sample heating from the light source by using suitable infra-red filters.

Measurements were conducted in the manner described in section 4.3.1. The current-voltage characteristics for the device were initially measured with the light source off, after which the sample was allowed to return to equilibrium and stabilised for one to two hours prior to repeating the measurement with the light source on.

A log – lin plot of the characteristics obtained are shown in figure 5.17. As expected, with the light source off the magnitude of the current in both forward and reverse bias is generally lower than the current observed for the device with the light source on. This is believed to be due to the formation of charge carriers in the depletion region of the Schottky barrier diode.

The initial characteristic, with the light source off, is similar to that displayed by device F, in figure 5.15. However, with the light source on, a dc offset, to forward bias, of approximately 0.3 V is observed, at which the current reverses.

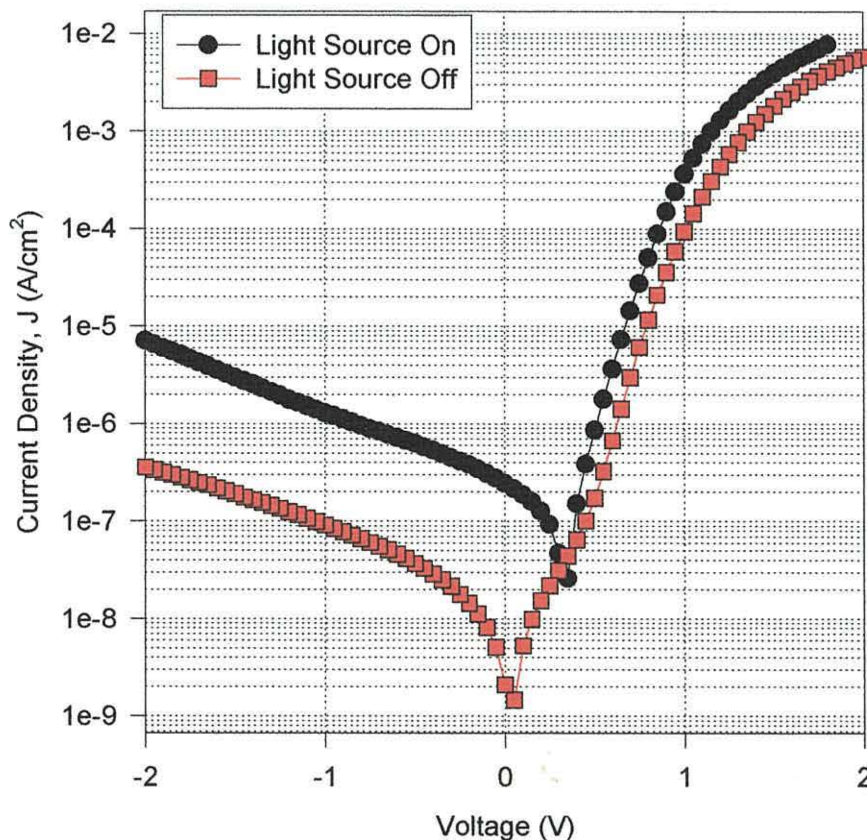

Figure 5.17 *The effect of photoexcitation on the dc characteristics of a typical Schottky barrier diode*

By considering the diode structure as a solar cell arrangement, this dc offset would correspond to the open-circuit potential (V_{oc}), of a solar cell diode. The combination of the increase in the magnitude of the current and the open circuit voltage would constitute the fill factor, usually characterised for solar cells (Sze, 1981). However, in this case where the device is in the form of a Schottky barrier diode, V_{oc}, would correspond to the junction built-in potential (V_{SO}) and in fact compares well to previously reported values of V_{SO} in P3MeT diodes, deduced from reverse bias plots only and not from Mott-Schottky plots (Taylor and Gomes, 1995). In turn, by using equation 2.15, the built-in potential determines the magnitude by which the barrier height (ϕ_b) is reduced. The values of V_{SO} determined by the above optical studies could well account for the increase in current observed in reverse bias when the light source is switched on. The resulting image force lowering of the barrier can also account for the $V^{1/4}$ behaviour observed earlier in this device.

5.4 AC Behaviour

5.4.1 Capacitance and Loss Curves

A set of typical ac characteristics for a P3MeT Schottky barrier diode are shown in figure 5.18. Curves such as these are commonly used to describe the depletion region, from the variation of capacitance with frequency, and the extent of doping from the maxima of the loss curve with frequency.

In most cases, frequency dependent measurements of capacitance and loss were measured in the range 20 Hz to 1 MHz. However, to investigate whether or not the capacitance and loss curves remained constant at low frequency, the lower range was extended to 0.1 Hz as shown in figure 5.19.

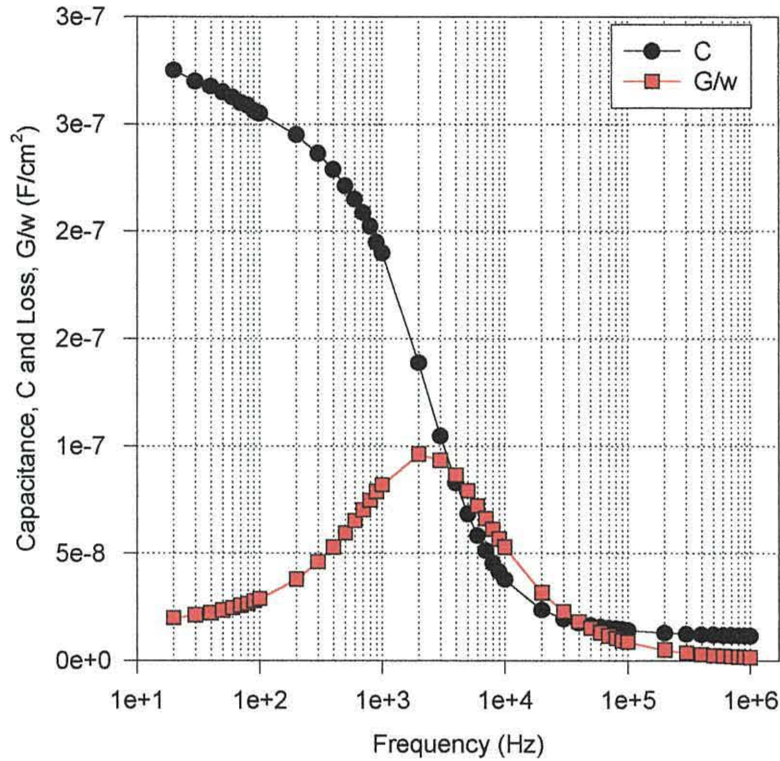

Figure 5.18 *AC characteristic of a typical P3MeT Schottky barrier diode.*

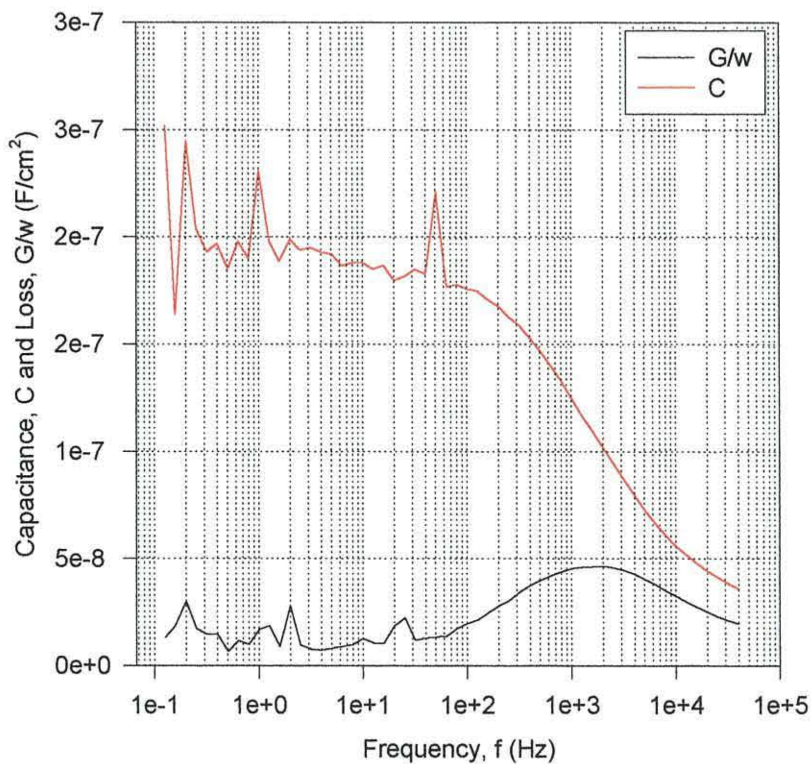

Figure 5.19 *AC characteristic of a typical P3MeT Schottky barrier diode from 0.1 Hz to 1 MHz.*

5.4.2 Mott-Schottky (Capacitance - Voltage) Plots

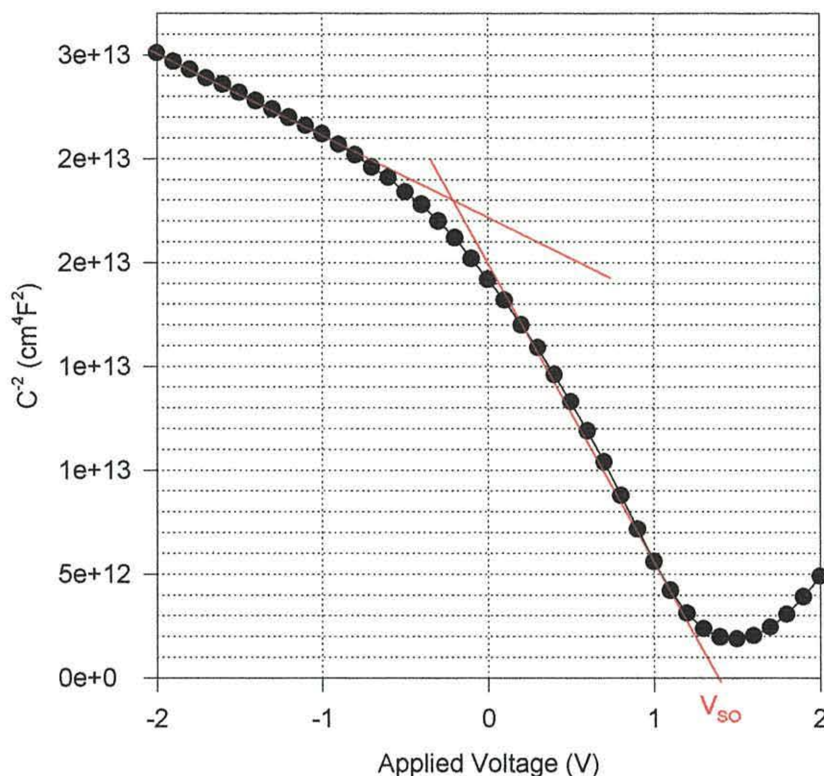

Figure 5.20 *Mott-Schottky plot of a typical P3MeT Schottky barrier diode at a frequency of 1kHz.*

Figure 5.20 shows a typical Mott-Schottky plot for a P3MeT Schottky barrier diode. As described in section 2.7, the gradient of the curves are proportional to the polymer doping density. In this sample, as in many others, two distinct doping densities exist which suggests a non-uniform doping density and the x-axis intercept gives the value of V_{SO}. However, the two separate gradients displayed in Mott-Schottky plots of P3MeT diodes have also been used to suggest the presence of both shallow and deep lying states (Taylor and Gomes, 1995).

Typical values for V_{SO} were in the range 0.5 - 1.5 V, and in the above case the value is approximately 1.3 V. A major discrepancy exists between the values of V_{SO} deduced from reverse current measurements and Mott-Schottky plots. Taylor and Gomes suggested that the forward diode currents were limited by an additional series resistance which was much greater than the bulk resistance of the polymer. Therefore not all of the applied bias appeared across the depletion region leading to higher values of V_{SO}

from Mott-Schottky plots. As a result, values of V_{SO} at the lower end of the above range have been assumed to be correct and used in the discussions of section 5.3.1, 5.3.2 and 5.6.1.

5.5 Capacitance Transients and DLTS

5.5.1 Majority Carrier Transients

Figure 5.21 shows typical capacitance transients for a Schottky barrier device formed on P3MeT. The transients presented here are in the temperature range 298 K to 358 K. The device was initially subjected to a reverse bias of 2V for 1.5 minutes, then a 0V pulse of 10 s duration, followed by return to a reverse bias of – 2 V.

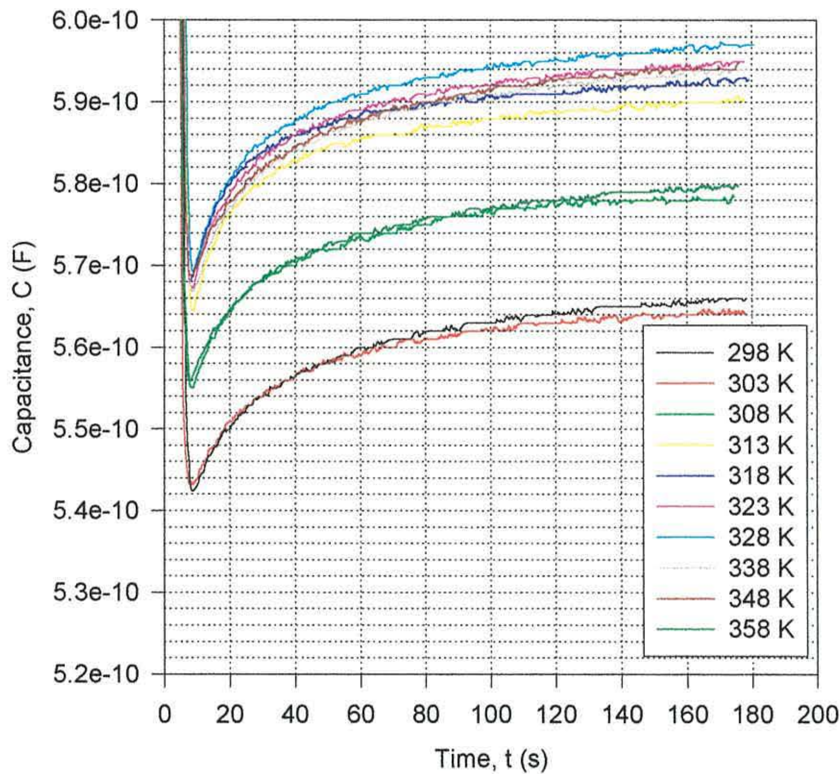

Figure 5.21 *Capacitance transients for a typical Schottky diode. Pulse magnitude = 0 V, duration = 10 s.*

The transients shown in figure 5.22, 5.23 and 5.24 are similarly for the temperature range 298 K to 358 K, with the same initial and final conditions as above but the magnitude of the pulse was 0 V for 100 s duration in 5.22, 1 V for 10 s duration in 5.23 and 1 V for 100 s in 5.24.

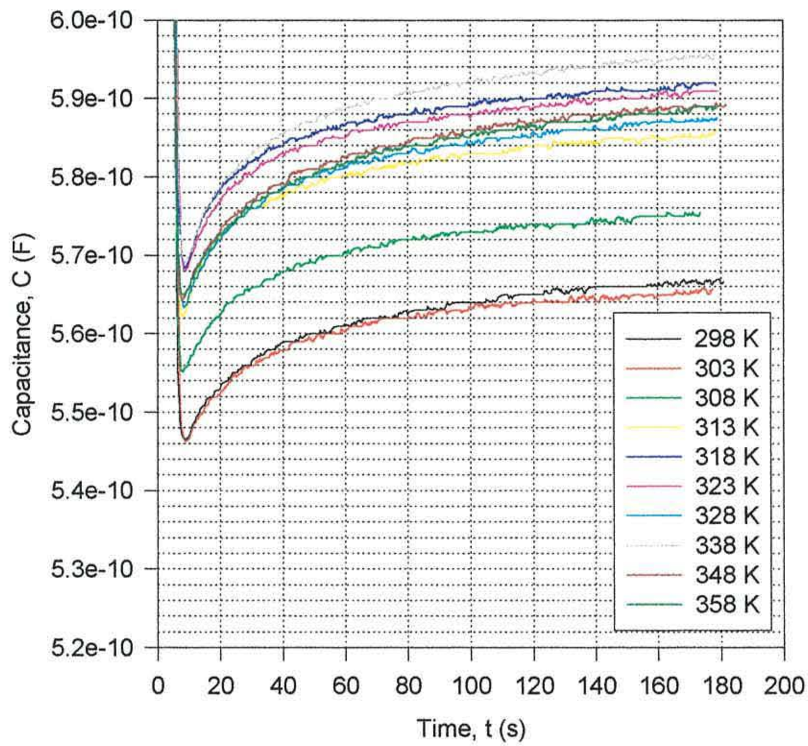

Figure 5.22 *Capacitance transients for a typical Schottky diode. Pulse magnitude = 0 V, duration = 100 s.*

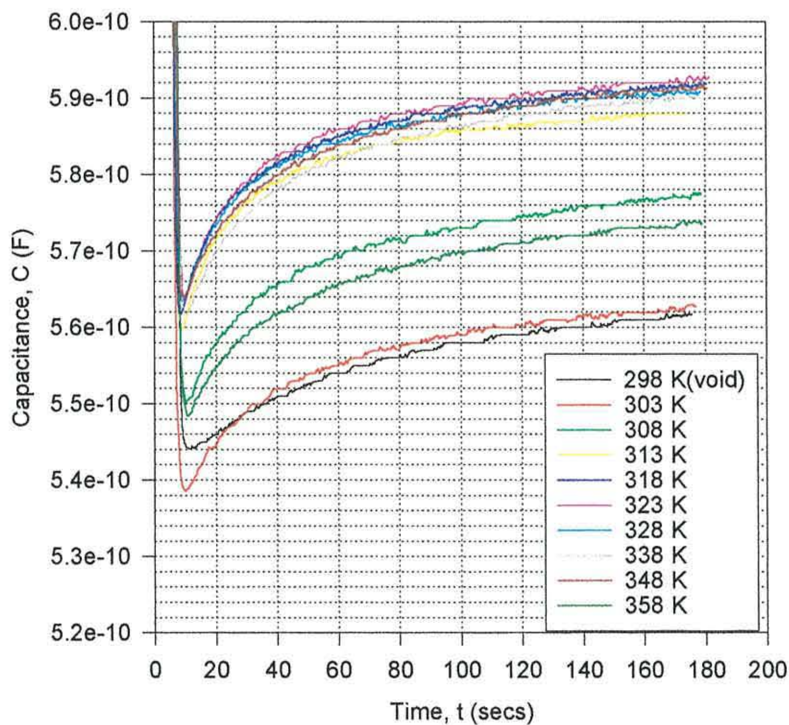

Figure 5.23 *Capacitance transients for a typical Schottky diode. Pulse magnitude = 1 V, duration = 10 s.*

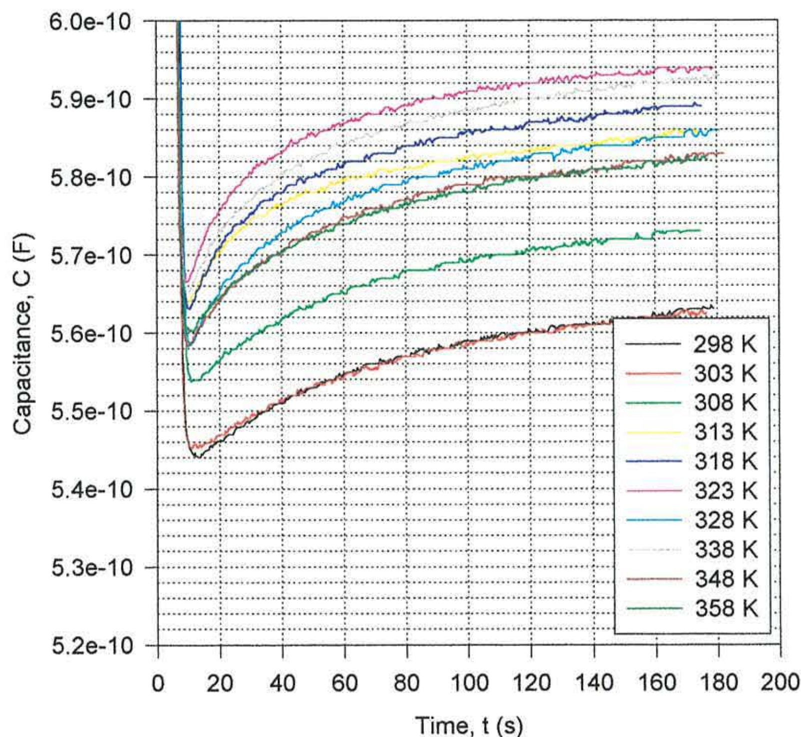

Figure 5.24 *Capacitance transients for a typical Schottky diode. Pulse magnitude = 1 V, duration = 100 s.*

All the transients shown in the above figures show the same general characteristics of device capacitance increasing exponentially with time. These results show an increase in the steady state depletion region capacitance with increasing temperature, as expected, owing to an increase in the degree of ionisation of acceptor states in the polymer. However, at temperatures in excess of approximately 325 K, the capacitance decreases with increasing temperature for some unknown reason.

All transients comprise two components, one fast and one slow. The fast component is not easily resolved and generally has a time constant (τ_1) in the range 15 to 30 s. The slower component has a time constant (τ_2) in the range 90 to 120 s and has a modified exponential nature, possibly suggesting that it may be influenced by high fields in the space charge region.

In general, the fast component of the transients display a shorter time constant when probed with the majority carrier pulse of 0 V magnitude, compared to the injection 1 V pulse. However, transients obtained using the 100 s pulses show no significant

dependence on the pulse magnitude. One noticeable effect, particularly when using an injection pulse at low temperatures, is an increase in the effective capacitance measured in the time range 10 to 20 s. This effect results from a decrease in the depletion region width which can be considered as an increase in confined charge due to interfacial trapping states and is suggestive of minority carrier behaviour.

A number of attempts were made using the above transients to obtain a DLTS type spectrum. However, each attempt resulted in a scatter of points which yielded no definitive interpretation of the concentration or depth of any trapping states, as shown in figure 5.25. Low pass filtering of the transient signals failed to sufficiently reduce the noise superimposed onto the transient signals and similarly proved inconclusive.

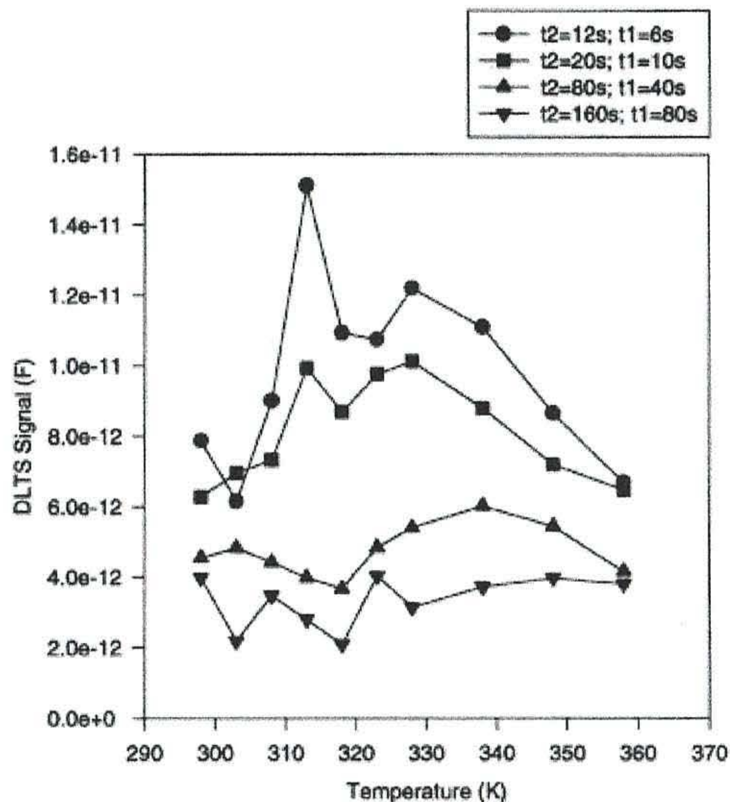

Figure 5.25 *DLTS spectra obtained from transients shown in figure 5.21. t_1 and t_2 are time intervals for which the differential capacitance (DLTS Signal) is measured for successive temperatures.*

By re-arranging equation 2.43 the following expression can be obtained

$$\tau = \tau_0 \exp\left(\frac{E_A}{kT}\right),$$

where τ is th time constant of the transient, τ_0 a constant and E_A the trap activation energy. By measuring the time constant of the transient and assuming a typical value of 10^{-12} s for τ_0 (from section 2.8), an approximate value for the trap activation energy can be obtained.

The time constants of both the fast and slow components of the transients displayed in figures 5.21 to 5.24 at a temperature of 298 K and 358 K are given in table 5.6, along with the corresponding, calculated value of E_A.

Pulse Properties	T (K)	τ_1 (s)	τ_2 (s)	E_{A1} (eV)	E_{A2} (eV)
0 V, 10 s	298	15	100	0.778	0.826
0 V, 100 s	298	20	120	0.785	0.831
1 V, 10 s	298	15	100	0.778	0.826
1 V, 100 s	298	60	120	0.813	0.831
0 V, 10 s	358	12	90	0.927	0.989
0 V, 100 s	358	20	90	0.943	0.989
1 V, 10 s	358	30	100	0.955	0.992
1 V, 100 s	358	60	120	0.977	0.998

***Table 5.6** A table showing the time constants and activation energies associated with the two components of the transients at 298 K and 358 K.*

The occurrence of two time constants in each capacitance transient suggests the presence of two acceptor states. By first principles, the activation energy of the shallow lying state has been calculated to be in the range 0.778 to 0.977 eV, whilst the deep lying state has an activation energy in the range 0.826 to 0.998 eV. The fact that the activation energies associated with both states are similar could well give credence to the observations made in attempted DLTS spectra of this study, where it is possible that

a number of overlapping or discrete states could well give rise to a complex distribution of peaks, characterised by a scatter of points (figure 5.25). The results summarised in table 5.6 also suggest that the temperature resolution used during these measurements were not sufficiently high and that the 60 K temperature range used was a major limiting factor. In previous studies on inorganic devices the temperature range was of the order of 300 K (Lang, 1974).

5.5.2 Minority Carrier Effects

As part of the study to characterise the transients, further measurements were conducted at room temperature, 313 K and 323 K and repeated 3 hours later (figures 5.26 and 5.27). As before the device was initially subjected to a reverse bias of 2V for 1.5 minutes, then a 1V pulse of 10 s duration, followed by return to a reverse bias of – 2 V.

In this case at temperatures in excess of 313 K transients became exponentially decreasing in nature suggesting the possibility that the device had switched from majority carrier behaviour to minority carrier behaviour. Therefore, a trap filling pulse of 0 V can be used to probe majority carrier traps, whilst an injection pulse (which momentarily forward biases the device and injects electrons) allows minority carrier traps to be studied.

This type of behaviour is consistent with observations made in MEH-PPV devices based on silicon (Gomes *et al.*, 1999). In this case Gomes and co-workers noted that large forward bias injecting pulses led to a complete collapse of the depletion region which significantly changed the occupation of surface states. These extra states masked the dynamics and characteristics of the bulk trap transients being studied.

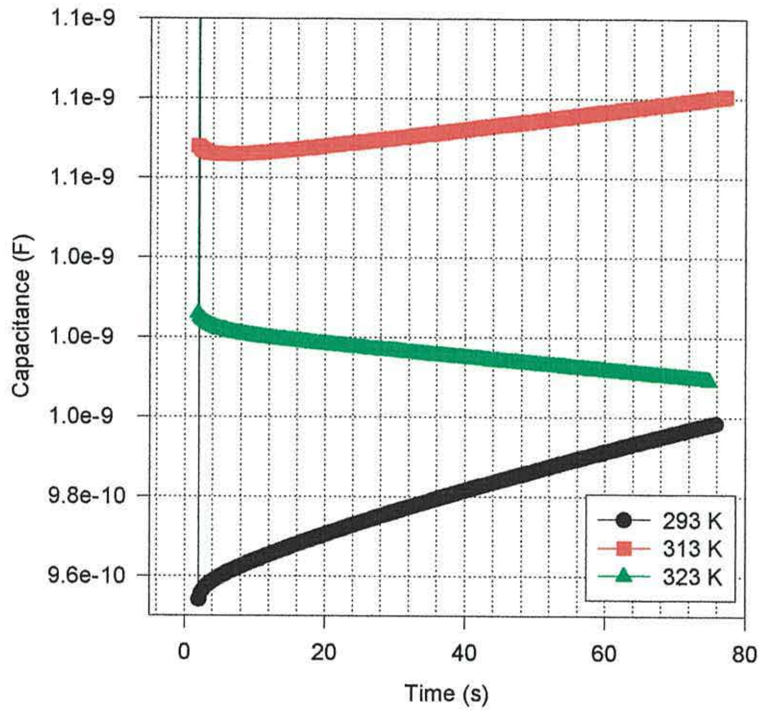

Figure 5.26 *Temperature dependence of capacitance transients for a typical device.*

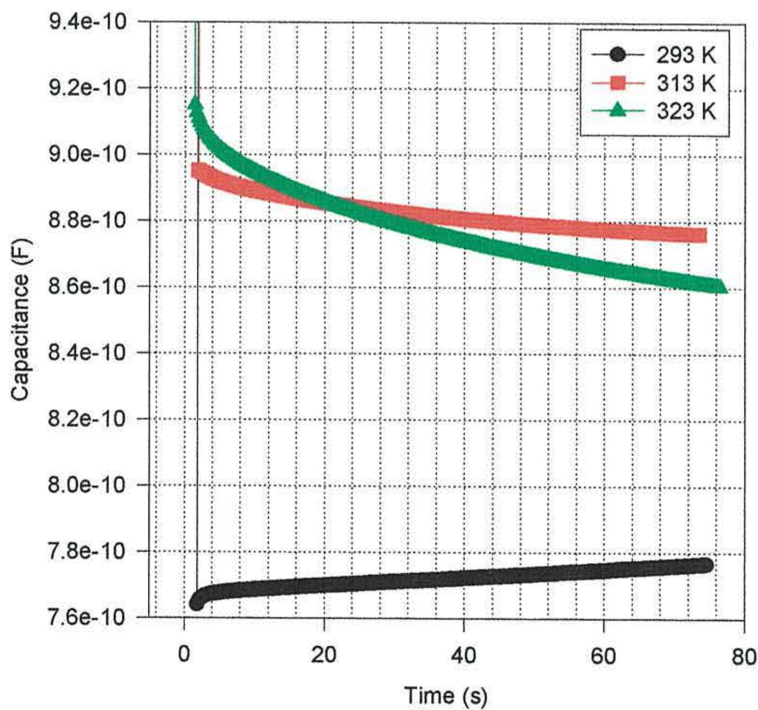

Figure 5.27 *Temperature dependence of capacitance transients for a typical device (repeated measurement 3 h later).*

5.6 Photoconduction and Photocapacitance Measurements.

5.6.1 Photoconduction

The photocurrent spectra as a function of the voltage applied to the gold electrode of a P3MeT Schottky diode is shown in figure 5.28. The curves are seen to decrease in magnitude as the applied bias is changed from – 1.4 V (reverse bias) to + 1.0 V (forward bias). The photocurrent action spectrum peaks at ~ 488 nm, however small shoulders are clearly visible at ~ 550 nm and ~ 420 nm. A second bias-dependent feature, though less prominent, is seen to peak at ~ 770 nm.

Similarly the maximum in the absorption spectra also peaks at ~ 480 nm, but additionally displays a small shoulder on the short wavelength edge and a broad feature extending into the infrared.

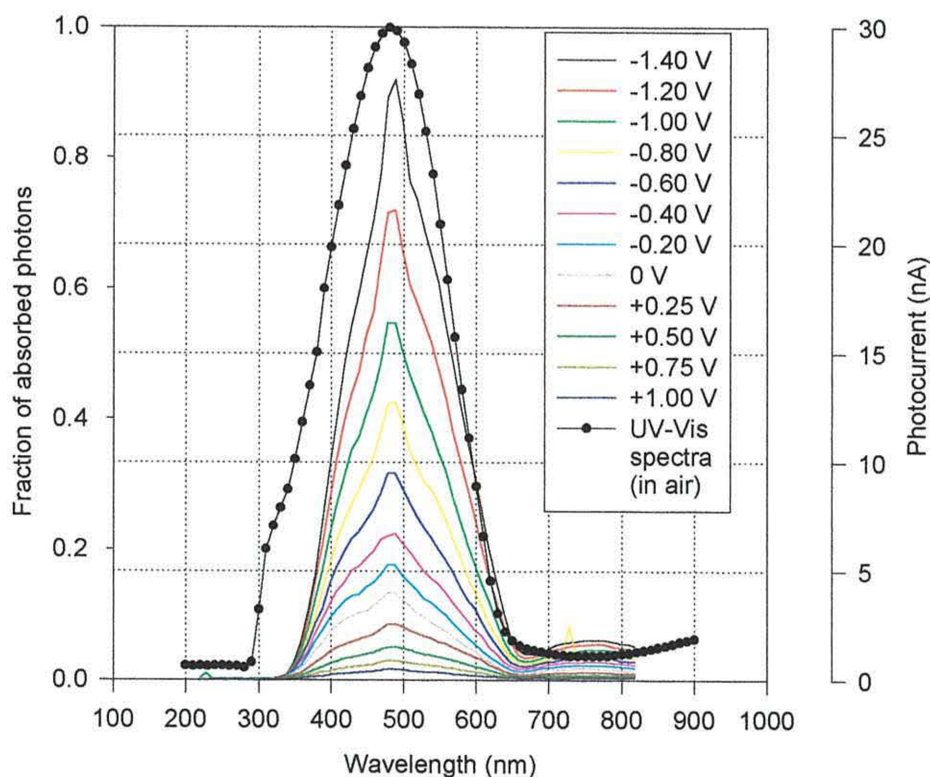

Figure 5.28 *Photocurrent action spectra and UV-vis absorption spectra for a typical P3MeT device.*

Binh and co-workers reported similar absorption spectra for solvent cast poly(3-dodecylthiophene), PDT, at room temperature, which showed a maximum at the same wavelength but with additional features on both the low and high energy edges in good agreement to that showed in figure 5.28 (Binh *et al.*, 1992) .

They further showed that the features evident at the low energy edge had all the features of a Wannier-like excited state of a conjugated chain. It was additionally demonstrated in PDT that this band decreased in strength with increasing temperature (as a result of possible increased disorder) whilst the intensity of the high energy band increases.

By comparing the findings of Binh and co-workers, 1992, with the present work, it can be appreciated that the absence of a shoulder at low energy coupled to the presence of one at high energy (figure 5.28) is likely to be related to the poor quality of the films grown onto ITO glass. Films of significantly better quality were grown on gold substrates for photoconduction measurements.

The two distinct slopes observed in Mott-Schottky plots for P3MeT diodes and the derivation of the built-in potential, V_{SO}, for such devices has already been discussed in chapter 2 and section 5.4.2. In general, the V_{SO} of diodes based on conducting polymers, and in particular, polythiophene derivatives, has been shown to be in the range 0.5 – 1.5 V.

By assuming that the incident radiation uniformly induces charge carriers throughout the depletion region, then the photocurrent is expected to be proportional to the width, w, of the depletion region. It is expected that for a conventional, uniformly doped semiconductor

$$w \propto V_t^{1/2}$$

where V_t ($=V_{SO} - V_{app}$)is the total potential across the depletion region and V_{app} the applied voltage.

In this case since no capacitance-voltage measurements were performed on these particular devices, figure 5.29 is a double log plot of peak photocurrent versus V_t for three assumed values of V_{SO}.

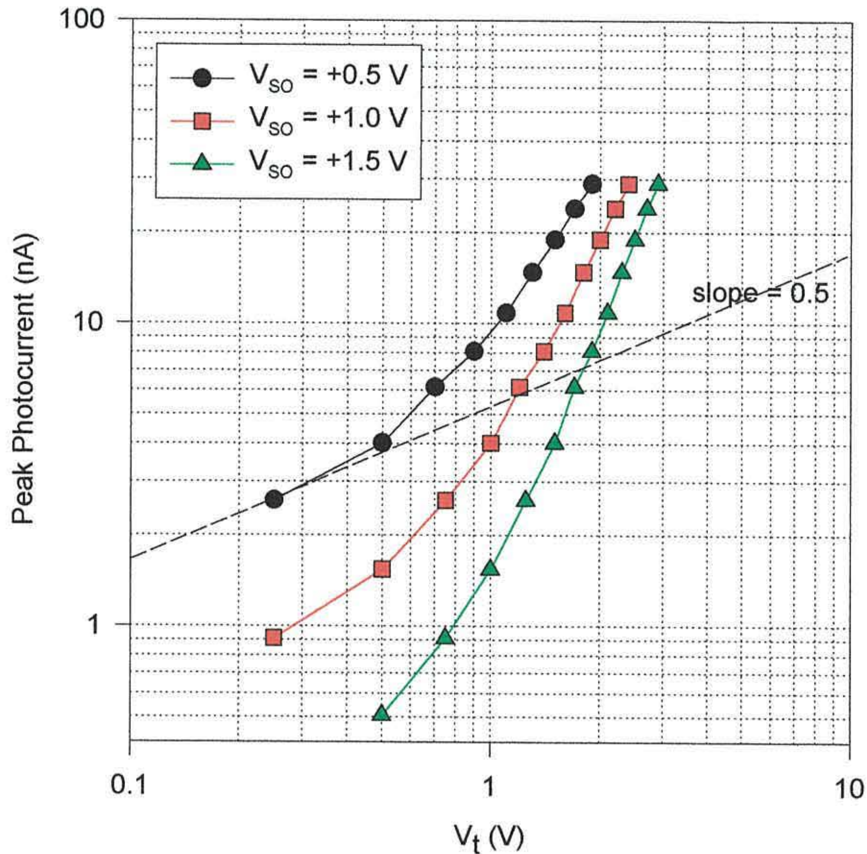

Figure 5.29 *Log-log plot of peak photocurrent versus total voltage for various built-in potentials.*

From these measurements it is evident that at high reverse bias (high values of V_t), the peak photocurrent varies superlinearly with potential in the range $V_t^{1.5}$ to $V_t^{2.5}$. This is in contrast with the behaviour at low V_t where the curves asymptote to the expected $V_t^{1/2}$ dependence.

The superlinear dependence observed at higher potentials is believed to arise from either the presence of field-dependent charge generation process in the depletion region or more realistically from an internal photoemission process occurring at the rectifying aluminium contact, similar to that reported by Rikken and co-workers (Rikken *et al.*, 1994).

5.6.2 Photocapacitance

A 670 nm, 1 mW laser source was used to investigate optically induced capacitance transients. A typical transient obtained for a 70 second pulse is shown in figure 5.30. The exponential like relationship after switch on and switch off of the light source is worth noting. These preliminary results display noise-free characteristics when compared to transients obtained using electrical pulsing. The presence of noise in the electrically pulsed transients was believed to be a source of scatter in the resulting DLTS spectra.

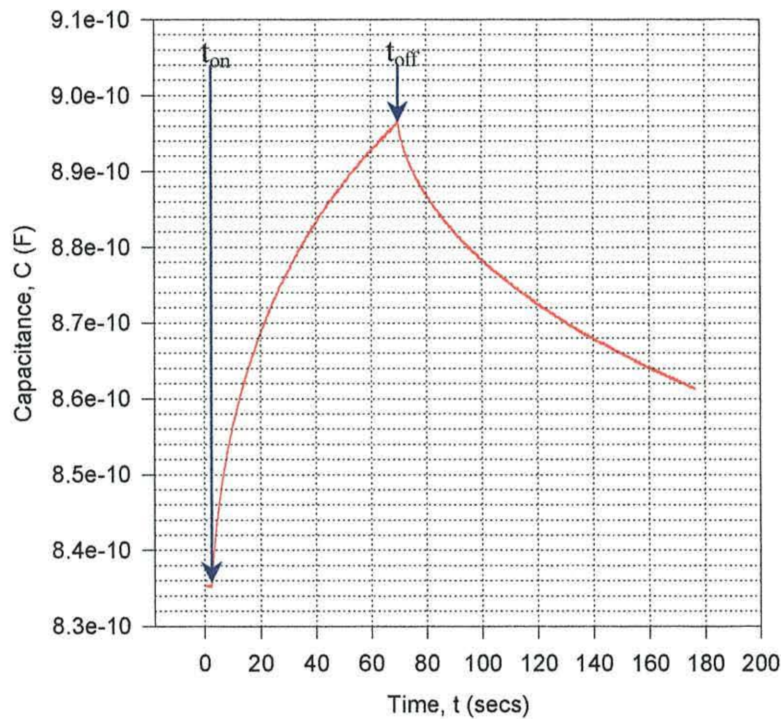

Figure 5.30 *Optically induced capacitance transient for a typical P3MeT based Schottky barrier diode.*

The optically induced transients have time constants of the same order as both the fast and slow transients obtained using electrical excitation, confirming that the charge carrying species are the same in both cases. However, the optical transients consist of only one time constant, having a value in the range 30 to 50 s. Using the same analysis as before these values correspond to acceptor state activation energies in the range 0.795 to 0.808 eV.

5.7 Electric Force Microscopy (EFM) and Kelvin Probe Microscopy (KPM)

Preliminary studies on the possibility of using EFM and KPM techniques (see **Dimension 3000,** Instruction Manual; **Digital Instruments**, Support Notes, No. 231, Rev. A.). for probing the depletion region and the interfacial layer of a Schottky barrier diode were performed, and gave promising results. In the first case a thin film of P3MeT was electropolymerised over a set of gold electrodes with various inter-electrode spacings. Figure 5.31 shows a topographical image (left) and surface potential measurement image (right), with a potential of + 5 V applied to the left most electrode with respect to the right electrode which was earthed. In this case the inter-electrode spacing was 10 μm.

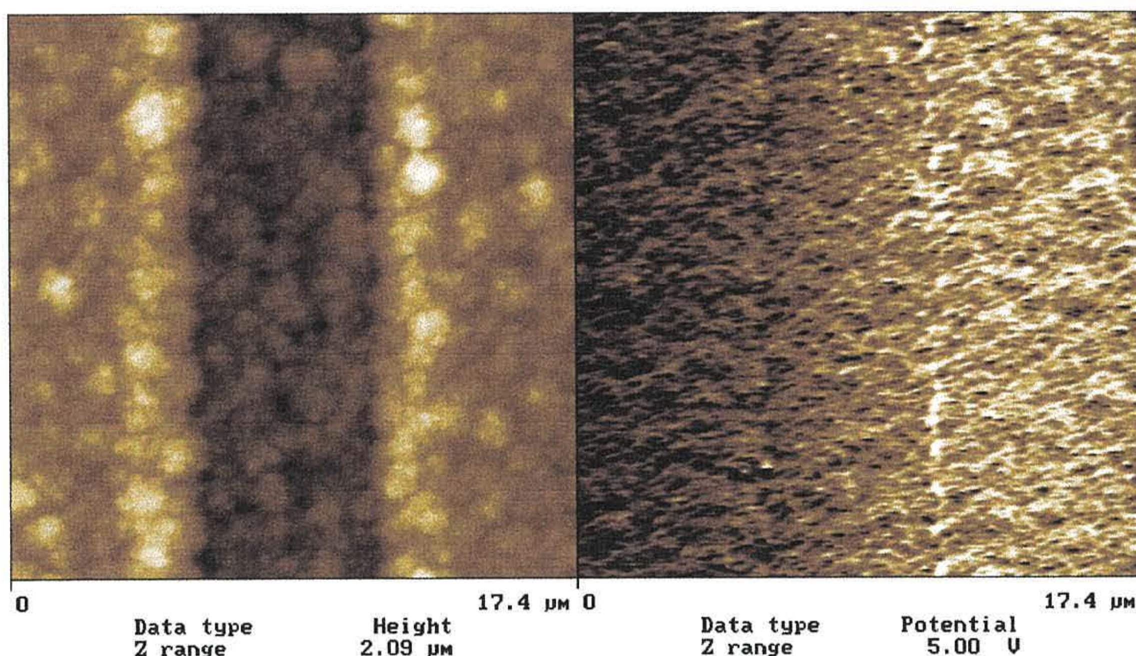

Figure 5.31 *KPM images of P3MeT coated gold electrodes.*

Figure 5.32 shows a topographical image (left) and an electric field gradient measurement (right) with + 5 V applied to the left most electrode as before.

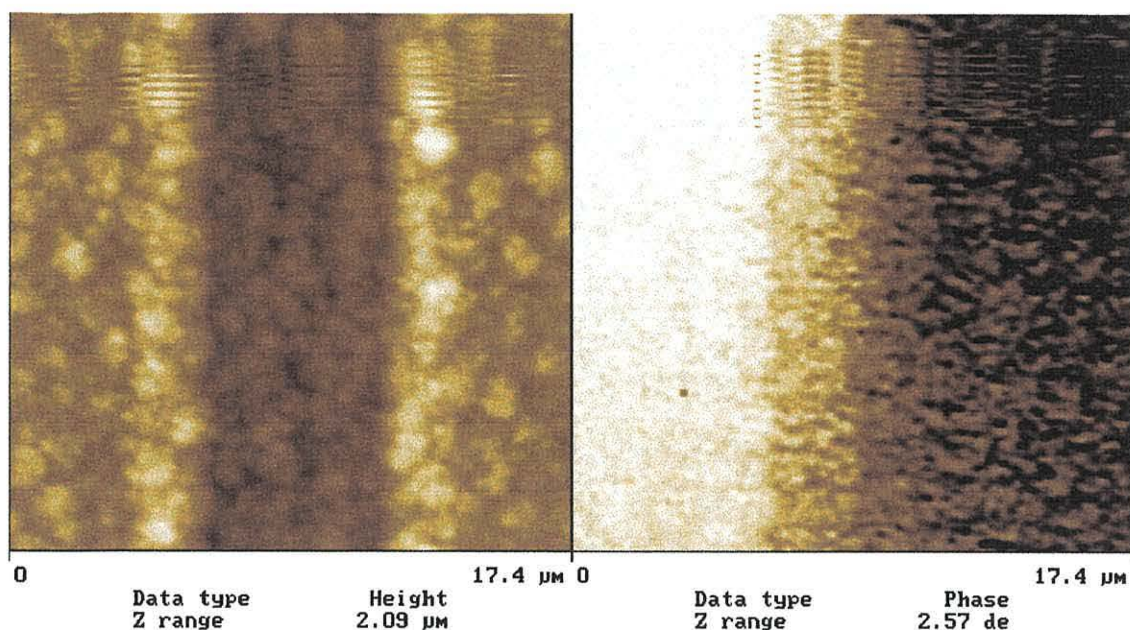

Figure 5.32 *EFM images of P3MeT coated gold electrodes.*

The following figures present Electric Force Microscopy (EFM) measurements made as a function of varying tip sample potentials. In this case the sample is again a microstructure gold fingers evaporated onto a glass substrate. However, in this case the polymer film has not been allowed to grow in the gap between consecutive electrodes.

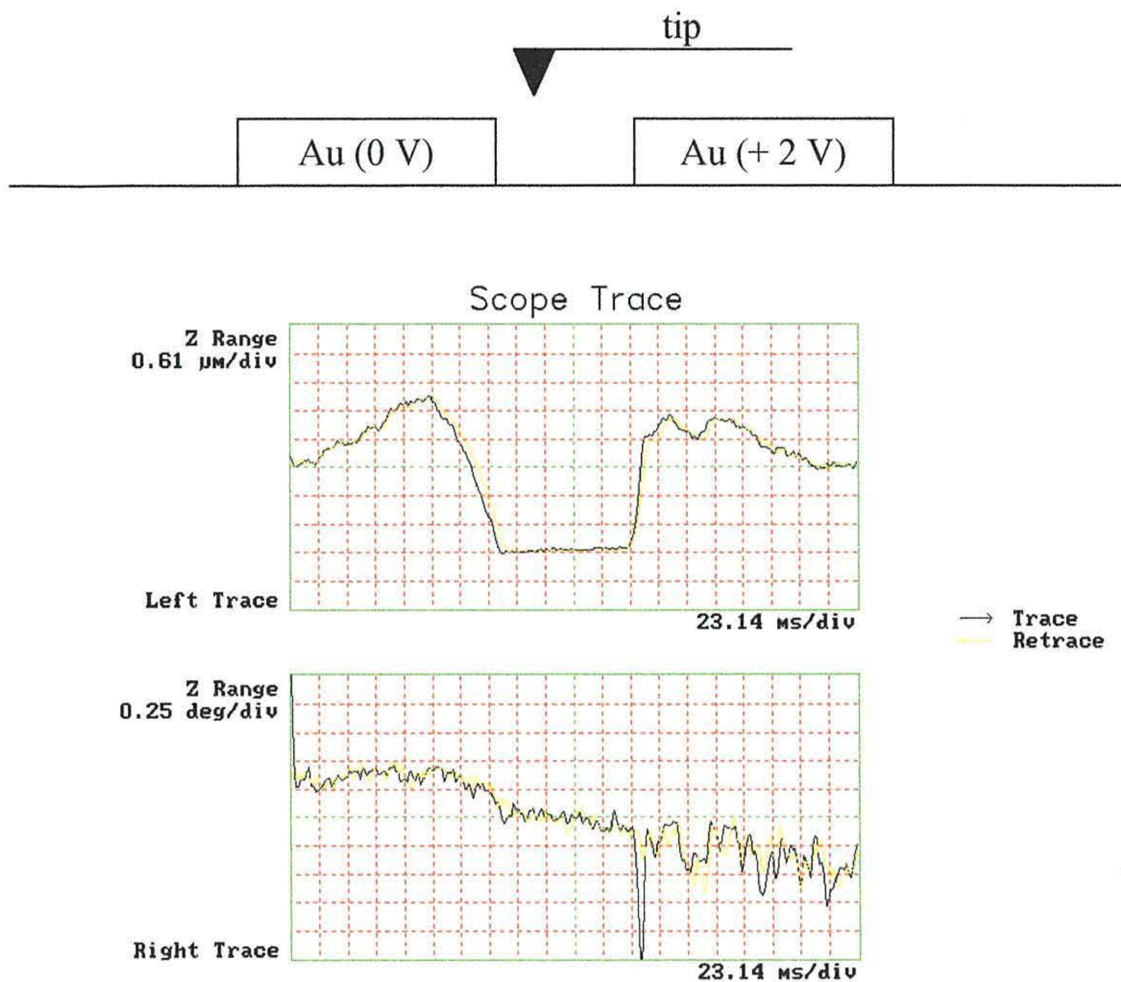

Figure 5.33 *AFM scans across a pair of gold electrodes coated in P3MeT. (a) Topography and (b) electic field gradient, E_Z (0 V tip bias).*

In each of the cases presented here the electrodes formed by photolithographical techniques should have an almost vertical edge, but as observed in the topographical data there is some tip convolution occurring where the image is dominated by the shape of the tip, and hence the edges are imaged as if they were at an angle. The true edge can be identified by a spike in the electric field measurements, in particular for the right-most electrode. In each case the left-most electrode is maintained at ground potential and the right-most electrode held at a constant potential of + 2 V. Each figure has two traces, the upper trace gives an indication of the sample topography, illustrating the two gold electrodes separated, in this case, by 8 μm, and the lower trace which gives the force gradient data measured in terms of a phase shift. Figure 5.33 shows the

information gathered with the tip biased at 0 V, figure 5.34 with the tip biased at +2 V and figure 5.35 with the tip biased at – 2 V.

Figure 5.34 *AFM scans across a pair of gold electrodes coated in P3MeT. (a) Topography and (b) electic field gradient, E_Z (+ 2 V tip bias).*

The electrical field gradient traces of figures 5.33, 5.34 and 5.35 can prove difficult to interpret since the images have a dc offset or planefit superimposed upon them, which effectively offsets the image about the 0 degrees phase shift. In order to establish the true field measurement, the potential difference between the tip and the sample needs to be considered. In addition, it must be identified whether or not the resulting field gives rise to an attractive gradient, in which case the resonant frequency would decrease, resulting in a smaller phase offset, or a repulsive gradient, which would give rise to an increase in the resonant frequency and a corresponding increase in the phase offset. By using both pieces of information, a representation of the field gradient measurement may be obtained as shown in figure 5.36. In this case the tip was biased at – 2 V, resulting in the field gradient being greatest at the right hand electrode, i.e. a potential difference of – 4 V. In this particular set-up it is the darker contrast that represents the greatest field gradient.

Figure 5.35 *AFM scans across a pair of gold electrodes coated in P3MeT. (a) Topography and (b) electic field gradient, E_Z (- 2 V tip bias).*

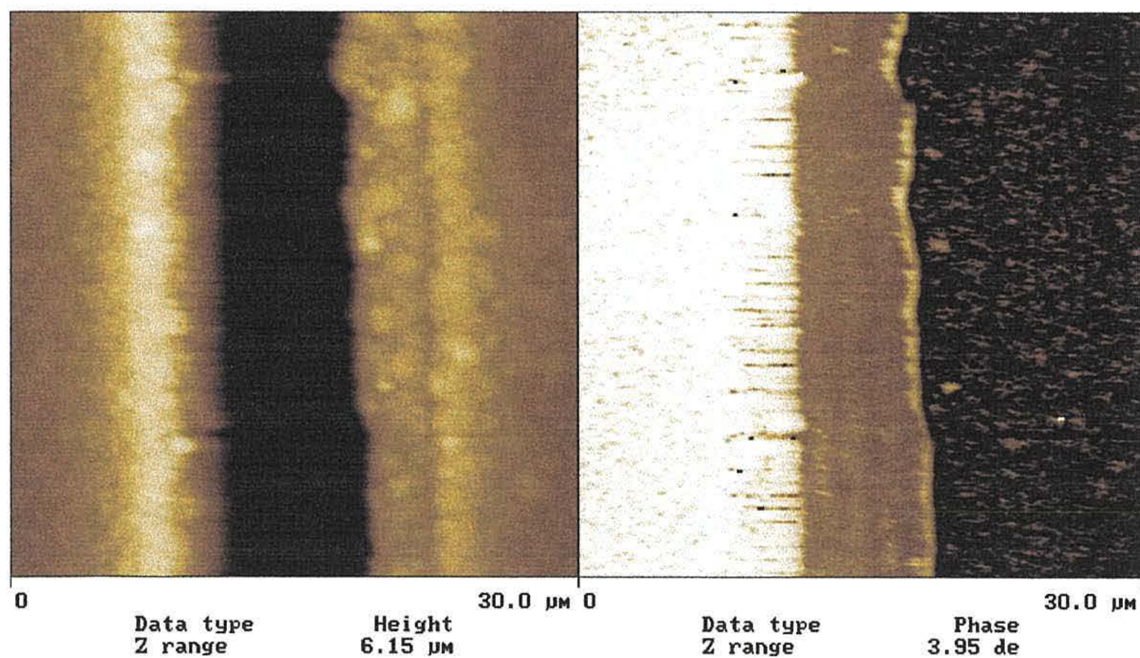

Figure 5.36 Topography (left image)and Electric Force Gradient (right image). Left electrode (0 V), right electrode (+ 2 V), tip bias – 2 V.

6. Low Bandgap Polymers

6.1 Introduction

Two low band-gap polymers (E_G ~1 eV) based on carbon-bridged dithienyl monomers synthesised by Dr P.J. Murphy, School of Chemistry, UWB, have been prepared by using an electropolymerisation technique similar to that described in section 3.52 and 4.23. These samples were subsequently used as the basis for preparing Schottky barrier diode structures using the technique described in section 4.2.4. Preliminary investigations of the dc and ac characteristics of these devices have been studied and compared to those of P3MeT based devices.

The theoretical absorption spectra of the monomers, dimers and trimers of the two polymers were determined by Professor Bernardo Laks, University of Campinas, Brazil, from semi-empirical chemical structure calculations. In general the theoretical spectra displayed similar features to the experimental spectra of both polymers. A combination of the theoretical calculations and experiment indicate a red-shift in corresponding features as the length of the molecule increases.

Semiconducting polymers with band-gaps in the range 0.5 - 3.0 eV have a number of potential advantages over their inorganic counterparts, such as ease of processing, cost of manufacture and greater variety. An emerging area of application for semiconducting polymers is in light emitting diodes (LEDs), first reported in 1990 by the Cambridge group (Burroughes *et al.*, 1990), since which a range of multicoloured LED structures have been developed. While considerable effort has been expended in developing efficient, high luminosity LEDs operating in the visible, there would be considerable interest also in organic devices operating in the near infrared, for example in sensor applications.

To decrease the bandgap (E_G) of a polymer system, the monomer structure must be tailored in such a way as to increase the quinoid character of the extended π-conjugated system, thus decreasing its aromaticity (Brédas, 1985). One suitable method of achieving this involves the introduction of electron-withdrawing groups at the sp^2

carbon bridging the 4, 4-positions of a bithienyl precursor. Such an approach was adopted by Ferraris and Lambert (Lambert *et al.*, 1991; Ferraris *et al.*, 1991) to produce, by electropolymerisation, the polymer poly(4-dicyanomethylene-4H-cyclopenta[2,1-b:3,4b']dithiophene) (PCDM). The band-gap of the resulting film was reported to be less than 1 eV (Ferraris *et al.*, 1991). In this study the same approach has been used to fabricate Schottky barrier diodes of PCDM (Gunatunga *et al.*, 1997).

Beginning with the same starting material as used to prepare the monomer 4-dicyanomethylene-4H-cyclopenta[2,1-b:3,4b']dithiophene (CDM) (Lambert *et al.*, 1991; Ferraris *et al.*, 1991) and following a previously reported synthetic route (Kozaki *et al.*, 1994), we have synthesised 1,3-benzodithiole-4H-cyclopenta[2,1-b:3,4-b']dithiophene (BDT) which was subsequently electropolymerised to form the polymer PBDT. All PBDT samples were used to study the optical properties of the films and due to difficulty in obtaining sufficient quantities of the monomer material, PBDT based Schottky barrier diodes were not prepared during the course of this study. The monomer structures of both materials are shown in figure 6.1.

Figure 6.1 *Monomer structures of (a) 4-dicyanomethylene-4H-cyclopenta[2,1-b:3,4b']dithiophene (CDM) and (b) 1,3-benzodithiole-4H-cyclopenta[2,1-b:3,4-b']dithiophene.*

6.2. Experimental

All polymer films were grown potentiostatically in a 3-electrode cell containing a 0.01 mol dm^{-3} solution of the monomer (CDM or BDT, for structure see figure 6.1) in nitrobenzene and 0.1 M tetrabutylammonium tetrafluroborate (TBATFB), as the supporting salt. ITO-coated glass formed the working electrode with platinum foil and

a clean silver wire used as the counter and reference electrodes respectively. The growing conditions followed the methodology discussed in sections 3.5.2 and 4.2.3 as successfully used by others (Taylor *et al.*, 1991; Roncali *et al.*, 1989; Chao *et al.*, 1993) for producing good quality films of poly(3-methylthiophene).

For the monomers investigated here, films were grown at a lower oxidation potential (1.2 V vs Ag), prior to electrochemical reduction at 0 V (vs Ag). Following electropolymerisation, the polymer-coated ITO substrate was removed from solution, thoroughly rinsed in acetone to remove any excess electrolyte, and dried in a stream of nitrogen gas. Films were stored overnight under rotary pump vacuum prior to carrying out any measurements. Electrical characterisation of the Schottky diodes was performed using the techniques described in section 4.3.

Experimental UV-visible absorption spectra of the grafted polymer films were obtained over the range 190 – 1100 nm using a Hitatchi U-2000 Spectrophotometer as described in section 4.6.1. To reduce substrate-based signatures, reference runs were always performed in advance on the ITO substrates alone.

The semi-empirical calculations at the AM1 (Dewar *et al.*, 1985) and PM3 (Dewar *et al.*, 1977) levels were performed for the two molecules shown in figure 6.1 so that a fully optimised geometry could be deduced. The parameters used in the calculations by Laks and co-workers were the defaults within the MOPAC package (Mopac), except for the convergence criterion, where a maximum step size of 0.05 was used instead. All other parameters were as used in the original references (Dewar *et al.*, 1985; Dewar *et al.*, 1977; Stewart, 1989). For both structures, a planar configuration was assumed as the starting point for the geometry optimisation calculations.

Absorption spectrum calculations were made using the ZINDO package (Ridley *et al.*, 1973) with geometry being fully optimised by PM3. All calculations were made at the INDO/CI (Intermediate Neglect of Differential Overlap/Configuration Interaction) level. This method was parameterised so as to give the best description of the UV-visible optical transitions, particularly in organic materials. Approximately 200

configurations were investigated for each molecule including singlet and doublet states (Salaneck *et al.*, 1996).

6.3. Results and Discussion

6.3.1 Sample Characterisation

The best quality films were electropolymerised galvanostatically, i.e. in constant current mode, onto gold coated glass substrates. This is in contrast to the highly successful potentiostatic technique used for preparing P3MeT samples.

Films used for studying the electrical properties of Schottky devices were usually grown onto gold-coated substrates and had an average thickness of approximately 300 nm and a structure similar to that observed for P3MeT films. An AFM scan showing the surface morphology of a typical PCDM sample is shown in figure 6.2. PBDT films also displayed a similar structure.

As discussed in section 4.6.1, all films prepared specifically for studying optical properties were grown onto ITO glass, and to a thickness of approximately 200 nm.

Initial problems were encountered in obtaining high quality, uniform films free from pin-holes. This was generally overcome by careful cleaning and preparation of the ITO coated substrate, in advance of polymer deposition.

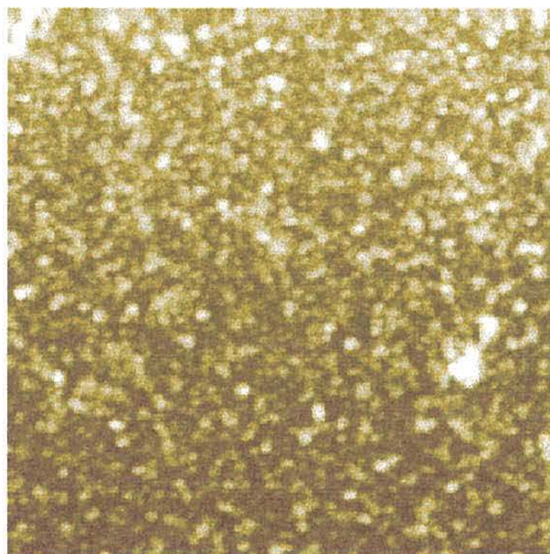

Figure 6.2 *A 20 μm x 20 μm AFM scan of a typical PCDM film sample.*

6.3.2 Electrical Characterisation

6.3.2.1 DC Characteristics

In most cases the I-V characteristic for Schottky diodes formed on CDM were non-linear yet displayed no, or very little, rectification, as shown in figure 6.3. This device like many others, including P3MeT devices, does however show a displacement of the characteristic along the voltage axis. In figure 6.3 the offset is ~ 0.1 V to forward bias. However, in some cases this voltage shift was as great as 0.25 V. Many authors have reported such an observation, but as yet no consensus has been reached as to its origin. This most likely cause is the presence of internal fields arising from a permanent polarisation within an interfacial layer formed between the polymer and the electrodes.

It was expected that devices based on low band-gap polymers would exhibit very large rectification ratios, with high currents flowing at high positive bias. However, the dc characteristics for the samples prepared in this study shows that this is not the case. This could be as a result of the high resistance of the bulk polymer, which is sufficiently high to limit the current through the device. For the device studied in figure 6.3, the bulk resistance, R_b is of the order of 1 MΩ.

However, some devices did show a small amount of rectification, but with the reverse current greater in magnitude than the forward current. In general, as the study progressed more and more devices were displaying this type of characteristic. As was the case for early P3MeT devices the reverse current fails to saturate as predicted by the thermionic theory, which suggests the presence of image force effects.

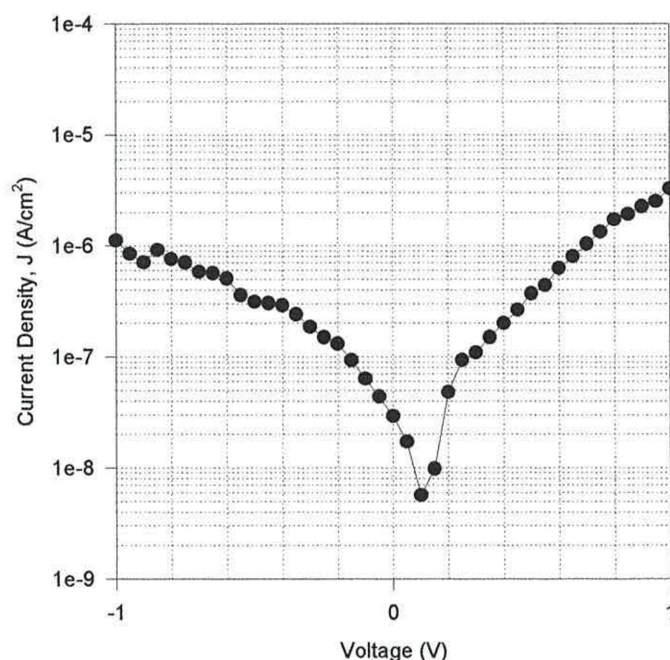

Figure 6.3 *DC characteristic of a typical PCDM Schottky barrier diode displaying a voltage offset, and no rectification.*

6.3.2.2 AC Characteristics

In general the ac characteristics support the theory that the devices are being limited by the high resistance of the bulk polymer. The capacitance and loss curves as a function of frequency for sample A, shown in figure 6.4, are expected to follow a Debye-like relaxation process as discussed in section 2.7.1 and equation 2.38, where the loss curve passes through a maximum at a relaxation frequency f_R.

If we assume that the current for the device given in figure 6.3 is being limited by the bulk polymer, which has a resistance, R_b of ~ 1 MΩ and f_R is to be less than 20 - 30 Hz

then using equation 2.38, C_d must be greater than ~ 500 nF/cm^2 which compares favourably with the data given in figure 6.4.

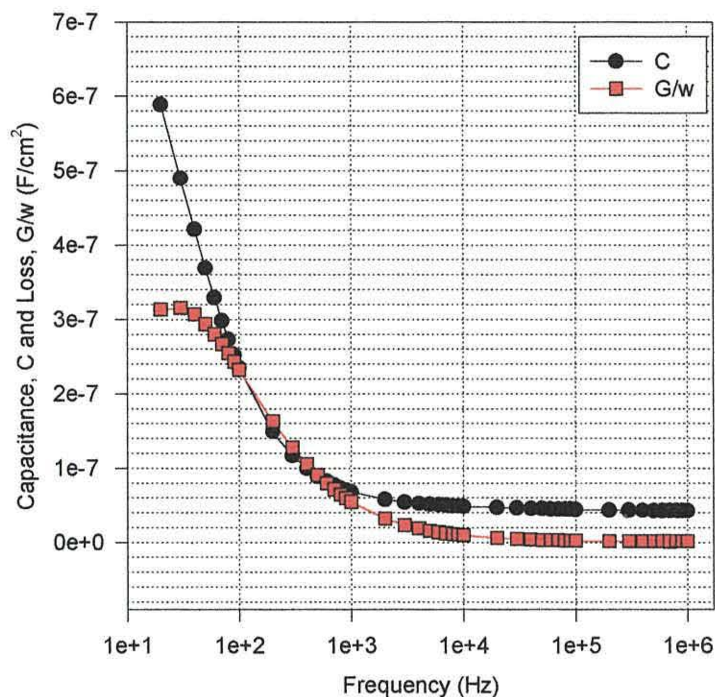

Figure 6.4 *AC characteristic of a PCDM Schottky barrier diode.*

In order to improve device performance, and to achieve the type of characteristics that are now reproducible with P3MeT, better control must be achieved for the dedoping process of CDM samples, so that devices with relaxation frequencies in the kHz to MHz range may be obtained. AC characteristics of this form generally display relatively constant values of capacitance at frequencies below the relaxation frequency. This is particularly useful when performing DLTS type measurements for analysing localised states in polymer films. It is also an important requirement for high-speed device applications.

6.3.3 Theoretical Modelling

The experimental UV-visible absorption spectra of the polymers of both CDM and BDT are shown in figure 6.5. Both polymers show a broad, long wavelength absorption consistent with a $\pi-\pi^*$ transition centred at 968 nm or 1.28 eV (PCDM) and 716 nm or

1.73 eV (PBDT). The red shift compared with previously reported values (950 nm (Ferraris *et al.*, 1991) and 626 nm (Kozaki *et al.*, 1994) respectively) can be explained by the presence of greater conjugation in the present films.

(a)

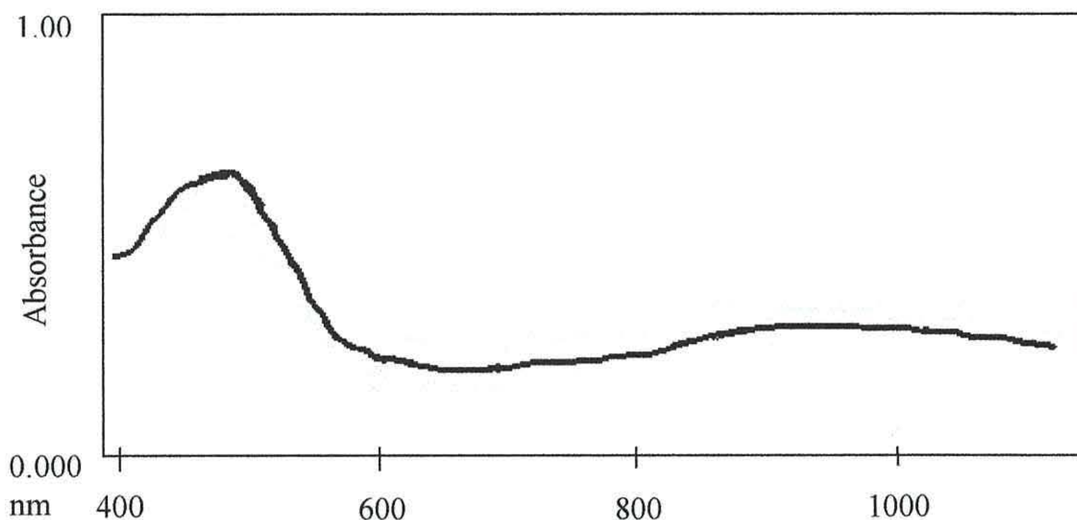

(b)

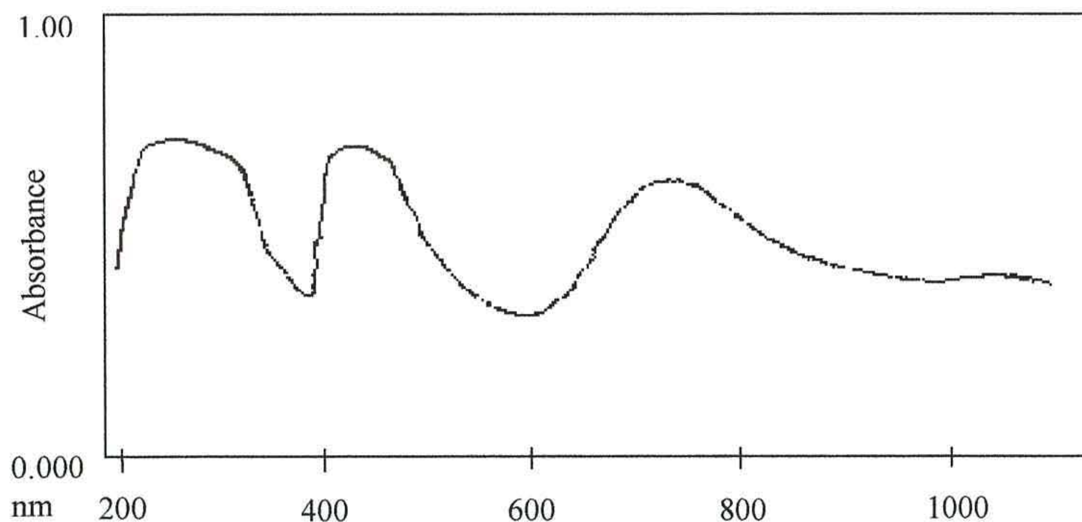

Figure 6.5 *Experimental UV-Vis absorption spectra for (a) PCDM and (b) PBDT.*

Table 6.1 shows the dipole moments and heats of formation for the monomer (m), dimer (d) and trimer (t) of CDM and BDT, calculated using semi-empirical techniques. The most probable geometrical structures for the dimer and trimer of each molecule, which were optimised using semi-empirical calculations at the PM3 level, were found

to be essentially planar, and having the configurations denoted by a, b or c in figures 6.6 and 6.7. The dipole moments of the parallel arrangements in both the dimer and trimer are almost equal to an integer multiple of the monomer dipole moment, as would be expected from a simple summation of non-interacting monomer moments.

Molecular Geometry (AM1)	Dipole Moment (Debye)	Heat of Formation, ΔF (Kcal)
CDM (m)	6.351	164 $\pm$ 1
CDM (d)[a]	11.405	332
CDM (d)[b]	0.007	330
CDM (t)[a]	4.79	496
CDM (t)[b]	16.03	500
CDM (t)[c]	6.16	496
BDT (m)	0.650	133
BDT (d)[a]	1.722	267
BDT (d)[b]	0.009	267
BDT (t)[a]	1.982	401
BDT (t)[b]	2.698	402
BDT (t)[c]	0.675	401

Table 6.1. *Dipole moment, and heat of formation, for AM1 calculated geometries of CDM and BDT in the ground state. (m, d, and t denotes monomer, dimer and trimer respectively; whilst a, b and c denote the possible geometrical structures for the dimer and trimer as shown in figures 6.6 and 6.7).*

When one of the monomers adopts an antiparallel configuration, as expected, a significant reduction in the molecular moment occurs. However, the fact that the moment remains significantly above zero indicates strong intermonomer interactions in this configuration.

(i)

(ii)

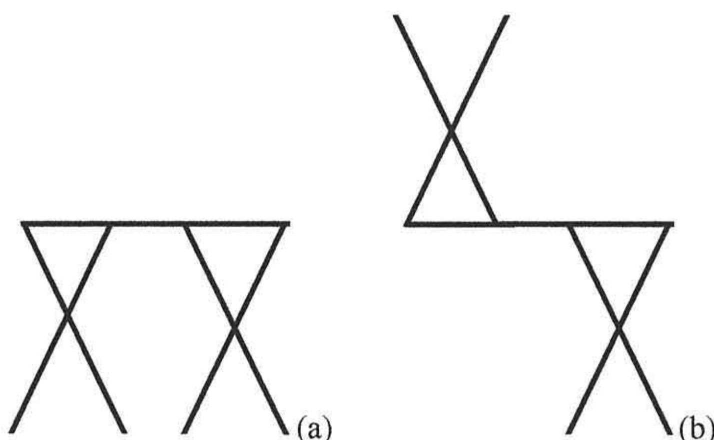

Figure 6.6 *Diagram depicting (i) a hypothetical monomer molecule and (ii) two (a and b) possible configurations of the dimer.*

In two isomers of the trimer (figure 6.7), distinct configurations (a) and (c) were found to have the same heat of formation values. Both CDM and BDT have a twisted angle configuration with (i) 30° (CDM) and (ii) 50° (BDT) between the rings as depicted in figure 6.7 (a) and (iii) 0° between the rings, as shown in figure 6.7 (b).

Of greater importance is that, for each compound, the heats of formation of the various configurations of the dimeric and trimeric isomers are similar, indicating equal probabilities of formation.

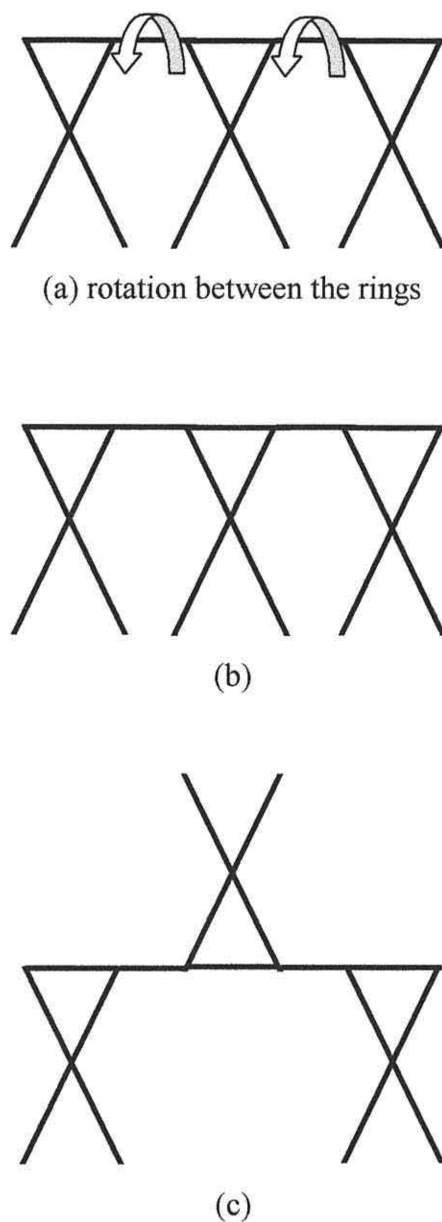

(a) rotation between the rings

(b)

(c)

Figure 6.7 *Diagram depicting three possible configurations of the trimer.*

Based on the above structures, the principle transitions contributing to the optical spectra were identified. These are listed in Table 6.2. The (H-1) » L transitions in the monomers of CDM and BDT are of similar strengths and are likely, therefore, to be related to the common central structure of the molecules. In BDT, the H » (L+2) transition appears to be a dominant feature in both the monomer and the dimer.

Molecular Geometry	Neutral Oscillator Strength	Principal Contributions to CI State Transitions
CDM (m)	0.906	H-2 » L+1
		H-3 » L+2
	0.816	H-1 » L
		H » L+4
CDM (d)	1.011	H » L
		H-1 » L+1
	0.9425	H-3 » L
		H-2 » L
BDT (m)	0.7053	H-1 » L
		H » L+2
	0.6070	H » L+2
		H –3 » L
BDT (d)	1.2859	H » L+3
		H-3 » L
	1.1546	H » L+2
		H-1 » L+1

Table 6.2 *Principal electronic transitions as determined from INDO/CI calculations based on optimised ground-state geometry. (H and L represent HOMO and LUMO respectively).*

Further AM1 calculations of the geometries were performed for the ground state to obtain the absorption spectra. As the experimental system was neutral, the geometry for the ground state was used to obtain theoretical absorption spectra by INDO/CI calculations. The final spectra, presented in figure 6.8, were obtained from normalised Gaussian functions weighted by the oscillator strengths. Full details of the calculations

can be found elsewhere (Ridley *et al.,* 1973). Thus, theoretical spectra may be generated which are in good agreement with experiment, as shown in figures 6.5 and 6.8. The theoretical spectra of the dimers are red-shifted with respect to their monomers (figure 6.8), a trend which continues with the increased chain length in the polymer (figure 6.5). The mixture of dimers which exist for the BDT system, as represented by figure 6.6 ii (a) and (b), along with solvent action is believed to give rise to the red-shifted spectra. However, for CDM the same structures are observed in the absorption spectra for both dimers (theoretical model).

This trend is also seen clearly in table 6.3 which shows the energies of the $\pi-\pi^*$ transitions (corresponding to the long wavelength transitions) in the monomer, dimer and polymer. The data also confirms that by bridging two thiophene moieties with electron-withdrawing groups a significant reduction in the bandgap of the resulting polymer may be achieved compared with polymers based on the 3-alkylthiophenes (E_G ~ 2.2 eV).

Material	**Monomer Calc. , (eV)**	**Dimer Calc. , (eV)**	**Polymer Experimental, (eV)**
CDM	1.70	1.44	1.28
BDT	2.38	1.95	1.73

Table 6.3 *Theoretically calculated energies of the $\pi-\pi^*$ transitions in monomers and dimers of CDM and BDT compared with those estimated from experimental UV-visible absorption spectra.*

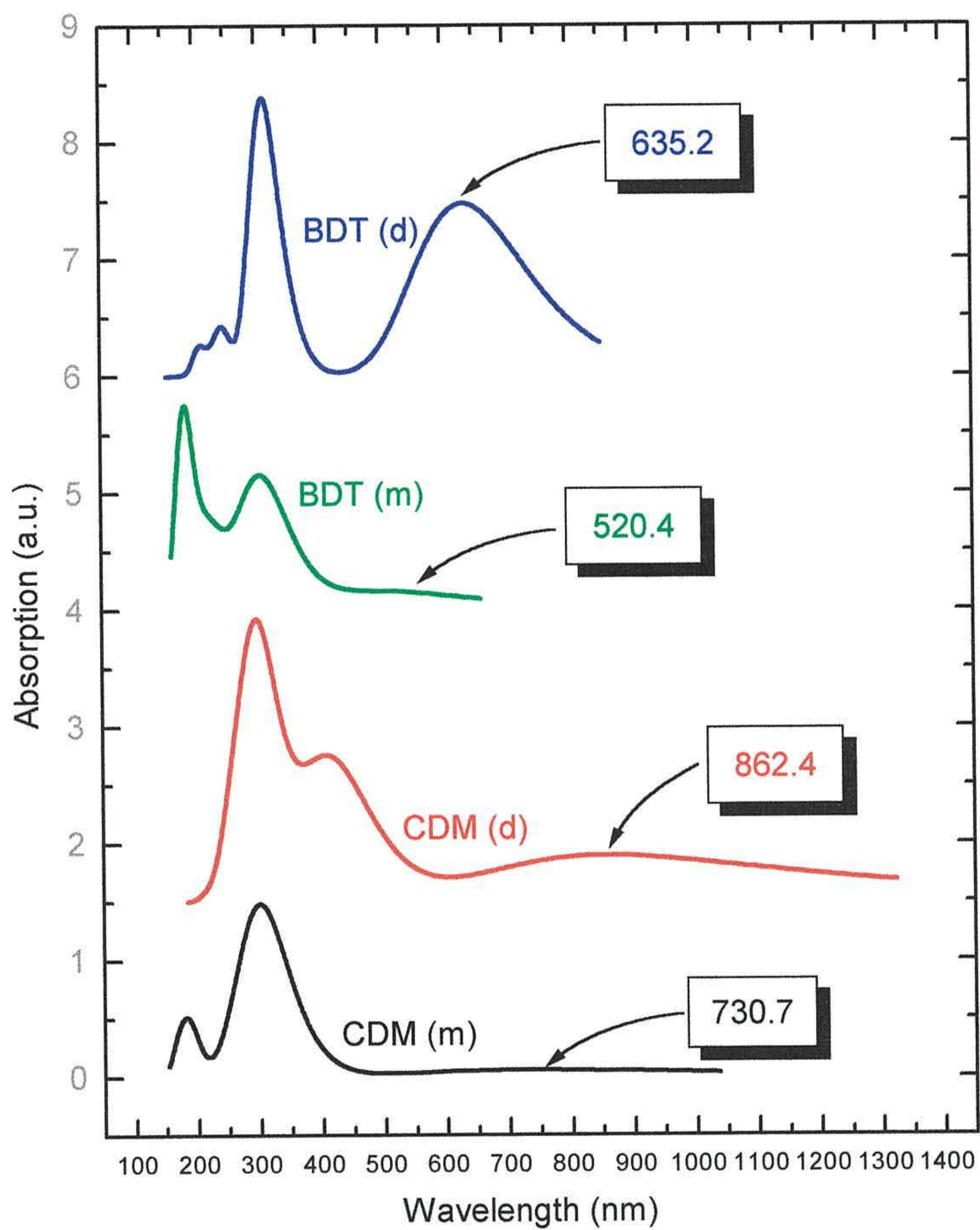

Figure 6.8 *Theoretical UV-visible ground-state absorption spectra for monomers and dimers of CDM and BDT.*

6.4 Conclusion

Two low band gap polymers PCDM and PBDT have been prepared by electropolymerisation of their respective monomers which are based on the carbon-bridged dithienyl structure.

The electrical characterisation of Schottky barrier diodes based on PCDM has demonstrated the need for better control of the doping and de-doping techniques in order to achieve devices with better rectification and frequency response properties. Some of the techniques and procedures developed for growing high quality P3MeT films with good electrical properties now need to be systematically applied to thiophene based, low band-gap polymers such as PCDM and PBDT.

The long wavelength features in the absorption spectra of the polymers which we relate to the $\pi-\pi^*$ transitions are red-shifted compared to previously reported values suggesting more extensive conjugation in the present sample. Taking the maximum absorption as the energy gap, the corresponding band gaps are 1.28 and 1.73 eV for PCDM and PBDT respectively.

The semiempirical AM1 and PM3 calculations indicate that dimers and trimers adopt a planar configuration with individual monomers adopting either a parallel or antiparallel configuration with equal probability.

7. Conclusions and Further Work

The aims of this research project were to investigate how the inherent properties of semiconducting conjugated polymers and their preparation techniques influenced the overall electrical and optical properties of devices based on this relatively new class of semiconducting material.

In the late eighties and early nineties, Gomes, Taylor and co-workers within the Bangor group made significant contributions to this field by successfully fabricating Schottky barrier diodes and field-effect transistors based on poly(3-methylthtiophene) (P3MeT). Extensive electrical measurements within the group led to an improved understanding of the characteristics that influenced the observed properties of electrochemical polymer based devices.

In the current work, the knowledge already gathered by previous members of the group was used along with both established and new analytical techniques to further improve our knowledge of semiconducting polymeric devices.

Particular emphasis has been placed on investigating the nature and origin of deep lying acceptor states, the nature of the metal / polymer interface, characterisation of the doping / undoping process and a general appreciation of the electrical and optical properties.

7.1 Contributions of this Work

The main findings of this work were as follows:

- A procedure for repeatedly growing thin, high quality films, which display good electrical properties, has been developed. This technique has been used to introduce some degree of control to the film doping / undoping procedure, which can strongly influence the electrical properties of resulting devices. In this study of Schottky barrier diode structures the relaxation frequency was varied from 1 kHz to in excess of 1 MHz and rectification ratios as high as 100,000 were observed.

- Raman spectrometry is a relatively new technique in the field of polymer science. In addition, using a Ramascope system with the flexibility of making measurements in air, and in solution, meant that these investigations were again among the first to be used on conducting polymeric materials.
    - Initial studies performed in air were used in an attempt to characterise and identify the more pronounced peaks observed in the spectra of P3MeT films. These results compared well with theoretical semi-empirical calculations based on thiophene oligomers.
    - The Raman peaks, in particular at 1360 and 1445 cm^{-1}, were identified as being related to the doping density of the film, in terms of induced structural changes to the backbone chain of the polymer during doping.
    - In-situ Raman measurements were used to improve our appreciation of the spectral changes occurring in P3MeT during doping. Various experimental conditions were applied, but in particular, it was observed that doping became easier as the film thickness increased, and that the BF_4^- anion was more efficient as a dopant than the ClO_4^- anion, with the PF_6^- anion intermediate between the two.
- Sample characterisation techniques such as AFM and SEM were successfully used to relate structural changes of the film surface to observed electrical anomalies. For example, the high percentage (~ 80 %) of device failures encountered at the onset of this project were related to pin holes observed in thick films. AFM images showed clearly how the film roughness (which increases with thickness) contributed to this effect.
    - Preliminary studies of using the AFM in SPM and EFM modes attempted to identify the feasibility of making similar measurements on the depletion region of Schottky barrier diodes. Large scale measurements (compared to the dimensions of a typical depletion region) on P3MeT coated electrode structures proved successful and yielded interesting results concerning the field profile near electrodes.
- The application of the Deep Level Transient Spectroscopy technique has enabled acceptor states in polymer based Schottky barrier diodes to be probed. Capacitance transients representing the dynamics of trapping states studied as a function of temperature were observed to consist of two components, a fast component with a

short time constant, usually less than 20 s and a slow component with a long time constant, usually in excess of 120 s. Devices were probed with two types of pulse mechanisms (i) zero bias and (ii) forward bias electron injection. The characteristics of measured transients were found to depend on the magnitude, duration and type of pulse and the sample temperature. The most interesting finding was that zero bias pulses probed majority carrier traps, whereas injection, forward bias pulses probed minority carrier traps. This result once again gave firm evidence for the existence of minority carrier behaviour in predominantly p-type polymer material.

- Successful measurements showing the photoconducting properties of P3MeT devices show a strong dependence on the applied voltage. The superlinear dependence at high potentials was believed to arise from either a field-dependent carrier generation in the depletion region or a photoemission process at the rectifying metal electrode.
- Films of two low band-gap polymers PCDM and PBDT were prepared by electropolymerisation of their respective monomers. The long wavelength features in the absorption spectra of the polymers have been related to the $\pi-\pi^*$ transitions but are red-shifted compared to previously reported values suggesting more extensive conjugation in the present samples. Taking the maximum absorption as the energy gap, the corresponding band gaps of these materials are 1.28 and 1.73 eV for PCDM and PBDT respectively. A study of the electrical characteristics of Schottky barrier diodes based on these materials has revealed extremely low rectification ratios, and poor control of doping, compared to P3MeT. The semiempirical AM1 and PM3 calculations performed on these materials suggest that dimers and trimers adopt a planar configuration with individual monomers adopting either a parallel or antiparallel configuration with equal probability.

7.2 Questions Arising from this Work

Are there any long-term implications that the doping and undoping processes have upon the lifetime, electrical and optical characteristics of devices and if so what are the effects and how can they be minimised?

This work has introduced some interesting concepts regarding the doping and undoping processes, especially in terms of new techniques that can be used to monitor the extent of doping and some of the inherent changes in the film properties. However there is still no consensus of opinion about the true, underlying effects that these processes have on the quality and properties of the film, in both the short-term and long-term. It would be advantageous to determine relationship between quantitative doping measurements and device characteristics, which could be used to predict the extent of film deterioration. Whether or not film deterioration could be minimised or controlled in such a manner that overall behaviour could still be accurately predicted is still unknown.

Which property(ies) of the electrochemical growing process determines the film quality?

The presence of water, even in small amounts, during the growing process has been studied by many workers (Downward and Pletcher, 1986; Delabouglise *et al.*, 1988), however, no study has successfully predicted the effect of these changes on the electrical and spectral properties of films or devices.

A number of other parameters can be foreseen to induce similar changes, the presence of air, temperature and humidity to name only a few. However, in this study, initial observations suggest that the age of the doping and undoping solutions contributed towards determining the ease with which film growth could be established and how efficient the degree of undoping. A quantitative analysis relating these observations might identify the requirement and extent (or otherwise) of a contaminant free environment for film formation and processing, and could lead to an improved understanding of film and device stability and lifetimes.

What factor induces the n-type minority carrier behaviour in p-type P3MeT Schottky barrier diodes and can it be minimised or controlled?

The observation, in this study, of minority carrier behaviour in undoped P3MeT based Schottky barrier diodes, is an important discovery. However, additional work is now required to determine and quantify the exact factor(s), which gives rise to this effect.

In applications such as LEDs, this observation need not specifically be undesirable since both minority and majority carrier behaviour is simultaneously required. In reality this could lead to tuneable LEDs emitting in the non-visible region which have a range of potential applications such as short range communications and security.

How are the doping variations observed using in-situ Raman spectroscopy related to structural and chemical changes in the film and is the doping density profile uniform over the film surface?

The use of in-situ Raman techniques as described for the first time in this study is seen as a simple, easy to use technique which can link together the mechanisms in which doping induces variations in the chemical and structural properties of the film / material. This technique could additionally be used to predict the type of structure adopted by the film as a function of doping density.

In addition, device behaviour and the chemical composition of the film could be related to doping, by mapping the density of dopants over the whole surface of the film and determine the degree of uniformity.

7.3 Further Work

During the course of this work a number of issues arose, which were observed to influence device properties, but were considered beyond the scope of the original aims of the project and were not further investigated in depth. However, some preliminary investigations were carried out. Some of these investigations are briefly outlined below.

- **Film and Device Preparation Techniques**

As discussed by many workers, the properties of conducting polymeric devices can prove extremely sensitive to the type of processing techniques used during preparation. Issues such as solution ageing, the environment in which films are prepared and stored prior and during measurements are considered highly relevant and important.

A study addressing in particular how the chemical solutions are prepared and stored prior to usage would be advantageous especially since observations in this study suggested that films could not be grown successfully in freshly prepared solutions. In most cases the solutions needed to be stored in a dark, cool environment for 24 – 48 hours prior to successful usage in obtaining high quality, uniform films.

- **In-situ Raman Measurements**

A link to the dedoping time used in the preparation stages could be obtained by making time – dependent Raman measurements at constant doping potentials and monitoring the resulting changes in the peak intensity ratio, as discussed in section 5.2.2.4.

By using the same film and fully extracting the various dopants in-between each measurement, would have removed any possibility of structural effects when comparing the doping efficiency of the different dopants (section 5.2.2.4).

- **DLTS Measurements**

Further analysis of measured capacitance transients for P3MeT could yield important data, which would allow characterisation of the various bulk trapping states. Gomes and co-workers (Gomes *et al.*, 1999) have already studied the time constants of the transients as a function of temperature in MEH-PPV samples and obtained activation energies for the traps. In P3MeT samples, extending the range of temperature measurements would be advantageous, as discussed earlier. In view of the inherent changes to polymer properties that occur at elevated temperatures reduction of the temperature from ambient levels would be of particular interest.

- **SPM and EFM Measurements**

As suggested earlier, preliminary studies showed that using the AFM for making SPM and EFM mode measurements of potential and electric fields in the vicinity of large electrode structures both coated and uncoated in polymer films was feasible.

However, in order to investigate the properties of the depletion region near the metal / semiconductor interface, new film and device preparation techniques would need to be developed, in order to allow devices to be prepared laterally on extra smooth substrates, as shown in figure 7.1.

- **Low Bandgap Polymers and Hetereojunctions**

The electrical and spectral properties of two low bandgap polymers, in particular, were extensively studied. However, unlike the improvement observed in rectification ratios and relaxation frequencies of devices prepared using P3MeT, no real progress was achieved in realising high quality devices with good electrical properties.

The degree of control available during the doping / undoping processes was much reduced compared to that of P3MeT, which resulted in devices having very low rectification ratios and extremely low or extremely high relaxation frequencies resulting in either highly conducting or highly insulating films.

However, by forming bi-layered heterostructures, combinations of a low bandgap polymer with P3MeT have recently displayed improved device characteristics, further investigations of which are currently progressing.

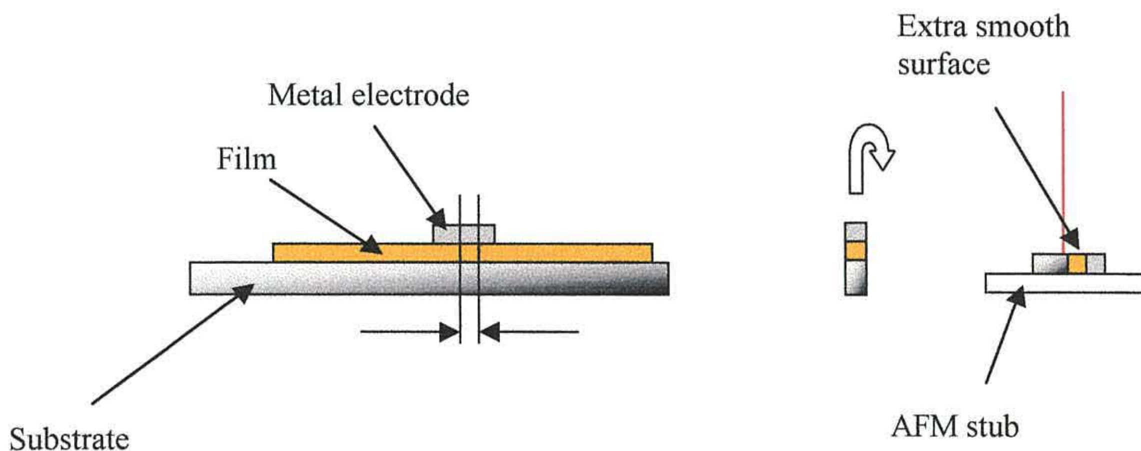

Figure 7.1 *A schematic representation of the mounting procedure required for probing the depletion region at the metal / semiconductor interface of a Schottky barrier diode.*

- **Optically Induced DC Characteristics**

The dc characteristics of some devices were investigated under illumination by a 1 mW, 670 nm laser source, as described in section 4.31. However, the comments made in section 2.6.2, might suggest that the energy of a photon from this laser source would not be sufficient to maximise the observed photocurrent and the underlying structure of the action spectra.

Similarly the photocurrent action spectra measurements discussed in section 5.5.1 also displayed a reduction in photocurrent magnitude when the source wavelength exceeded ~ 600 nm.

Future studies should focus on the variations in device I-V characteristics as a function of source wavelength and how these could be attributed to anomalies already observed in P3MeT diodes.

- **Photocapacitance Transients**

During the course of this work, a number of simple photocapacitance based measurements have been conducted on P3MeT based Schottky barrier diodes, to investigate whether or not optical excitation techniques resulted in behaviour similar to that observed under electrical excitation.

A detailed study addressing the mechanisms by which device properties change in response to the type of excitation, electrical or optical, could identify the suitability of polymer based devices to sensing-type applications.

Prospects

The progress achieved in this thesis has been highly satisfactory and no doubt some of the results and discussion here will be of great value to future research investigating the viability of conducting polymer devices.

In the context of this work it is unfortunate that the outcome of the DLTS work failed to yield the expected amount of information about the acceptor states present in partially doped organic materials such as P3MeT. However, the information gathered during the course of making DLTS measurements has proved extremely useful and can now be used to develop new techniques to probe these states.

P3MeT has proved a popular material used as a benchmark for investigating the general properties of conducting polymers. By understanding how to accurately control the doping process, and minimising its effect on device properties is of paramount importance in making sure that P3MeT and similar polymers can be successfully applied, at least to specialised markets, within the ever growing polymer optoelectronics industry.

The emphasis on investigating the surface structure of polymer films (before and after device formation) and the effects of the chemical preparation methods cannot be disregarded, since an adequate explanation of the role of the metal / polymer interface has still to be identified.

References

Akimichi, H., Waragai, K., Hotta, S., Kano, H. and Sakaki, H. (1991). *Appl. Phys. Lett.*, **58**, 1500.

Anderson, J.C., Leaver, K.D., Rawlings, R.D. and Alexander, J.M. (1990 4th Edition). *Materials Science.* Chapman Hall.

Andersson, M.R., Berggren, M., Gustafsson, G., Hjertberg, T., Inganäs, O. and Wennerström, O. (1995). *Synthetic Metals*, **71**, 2183.

Andre, J.J., Simon, J., Guillaud, G., Boudjema, B. and Maitrot, M. (1985). Mol. Cryst. Liq. Cryst., **121(1-4)**, 277.

Ashwell, G.J. (1992). *Molecular Electronic Materials.* Taunton Research Studies Press. New York: Wiley.

Assadi, A., Svensson, C., Willander, M. and Inganäs, O. (1988). *Appl. Phys. Lett.*, **53 (3)**, 195.

Assadi, A., Svensson, C., Willander, M. and Inganäs, O. (1992). *J. Appl. Phys.*, **72 (7)**, 2900.

Auret, F.D. and Nel, M. (1986). *Appl. Phys. Lett.* **48(2)**, 130.

Baigent, D.R., Holmes, A.B., Moratti, S.C. and Friend, R.H. (1996). *Synthetic Metals,* **80(2)**, 1119.

Bao, Z., Feng, Y., Dodabalapur, A., Raju, V.R. and Lovinger, A.J. (1997). *Chem. Mater.*, **9**, 1299.

Bantikassegn, W. and Inganäs, O. (1997). *Synthetic Metals,* **87**, 5.

Bard, A.J. (1966). *Electrochemical Methods*, Wiley.

Bar Lev, A. (1984, 2nd Edition). *Semiconductors and Electronice Devices*. Prentice Hall.

Barta, P., Sanetra, J., Grybos, P., Niziol, S. and Trznadel, M. (1998). *Synthetic Metals*, **94**, 115.

Barta, P., Sanetra, J. and Zagórska, M. (1998). *Synthetic Metals*, **94**, 119.

Baughman, R. H., Bredas, J.L., Chance, R.R., Elsenbaumer, R.L. and Shacklette, L.W. (1982). *Chem. Rev.*, **82**, 209

Berggren, M., Inganäs, O., Gustafsson, G., Rasmusson, J., Andersson, M.R., Hjertberg, T. and Wennerström, O. (1994). *Nature*, **372**, 444.

Berggren, M., Dodabalapur, A., Slusher, R.E. and Bao, Z. (1997). *Nature*, **389(6650)**, 466.

Berggren, M., Inganäs, O., Gustafsson, G., Andersson, M.R., Hjertberg, T. and Wennerström, O. (1995). *Synthetic Metals*, **71**, 2185.

Bethe, H.A. (1942). *MIT Radiation Laboratory Report*, **43-12**.

Beyer, R., Kalaji, M., Kingscote-Burton, G., Murphy, P.J., Pereira, V.M.S.C., Taylor, D.M. and Williams, G.O. (1998). *Synthetic Metals*, **92**, 25.

Bharathan, J. and Yang, Y. (1998). *Appl. Phys. Lett.*, **72(21)**, 2660.

Bharathan, J. and Yang, Y. (1998). *J. Appl. Phys.*, **84(6)**, *1998.*

Billingham, N.C., Calvert, P.D., Foot, P.J.S. and Mohammad, F. (1987). *Polymer Degradation Stability*, **19**, 323.

Binh, N.T., Gailberger, M. and Bässler, H. (1992). *Synthetic Metals*, **47**, 77.

Binh, N.T., Minh, L.Q. and Bässler, H. (1993). *Synthetic Metals*, **58**, 39.

Blood, P. and Orton, J.W. (1992). *The Electrical Characterization of Semiconductors: Majority Carriers and Electron States*. Oxford: Academic Press.

Bloor, D. and Movaghar, B. (1983). *IEE Proceedings*, **130 Pt 1 (5)**, 225.

Bradley, D.D.C. (1993). *Synthetic Metals*, **54(1-3)**, 401.

Bradley, D.D.C. (1996). *Nature*, **382**, 671.

Bradley, D.D.C., Colaneri, N.F. and Friend, R.H. (1989). *Synthetic Metals*, **29**, E121.

Braun, D. and Heeger, A.J. (1991). *Appl. Phys. Lett.*, **58**, 1982.

Braun, F. (1874). *Ann. Phys. Chem*, **153**, 556

Brédas, J.L. (1985). *J. Chem. Phys*, **82(8)**, 3808.

Brédas J.L., Silbey, R., Boudreaux, D.S. and Chance, R.R. (1983). *J. Am. Chem. Soc.*, **105**, 6555.

Brédas, J.L., Dory, M., Themans, B.,Delhalle, J. and Andre, J.M. (1989). *Synthetic Metals*, **28(3)**, D533.

Brédas, J.L. (1995). *Advanced Materials*, **7(3)**, 263.

Bröms, P., Birgersson, J., Johansson, N., Lögdlund, M. and Salaneck W.R. (1995). *Synthetic Metals*, **74**, 179.

Bröms, P., Birgerson, J. and Salaneck, W.R. (1997). *Synthetic Metals*, **88**, 255.

Brouwer, H.J., Krasnikov, V.V., Hilberer, A. and Hadziioannou, G. (1996). *Advanced Materials*, **8**, 935.

Brown, A.D., Bradley, D.D.C., Burroughes, J.H., Friend, R.H., Greenham, N.C., Burns, P.L., Holmes, A.B. and Kraft, A. (1992). *Appl. Phys. Lett.*, **61**, 2793.

Bryce, M.R., Chissel, A.D., Smith, N.R.M., Parker, D. and Kathirgamanathan, P. (1988). *Synthetic Metals*, **26**, 153.

Burroughes, J.H., Jones, C.A. and Friend R.H. (1988). *Nature*, **355**, 137.

Burroughes, J.H., Friend, R.H. and Allen, P.C. (1989). *J. Phys. D: Appl. Phys.*, **22**, 956.

Burroughes, J.H., Bradley, D.D.C., Brown, A.R., Marks, R.N., Mackay, K., Friend, R.H., Burns, P.L. and Holmes A.B. (1990). *Nature*, **347**, 539.

Burrows, P.E., Shen, Z., Bulovic, V., McCarty, D.M., Forrest, S.R., Cronin, J.A. and Thompson, M.E. (1996). *J. Appl. Phys.*, **79(10)**, 7991.

Cambridge Display Technology – see World Wide Web site for examples (www.cdtltd.co.uk)

Campbell, A.J., Bradley, D.D.C., Lidzey, D.G. (1997). *J. Appl. Phys*, **82(12)**, 6326.

Campbell, I.H., Davids, P.S., Smith, D.L., Barashkov, N.N. and Ferraris, J.P. (1998). *Appl Phys. Lett.*, **72(15)**, 1863.

Campos, M. and Bello Jr, B. (1993). *J. Phys. D: Appl. Phys.*, **26**, 1274.

Cao, Y., Yu, G. and Heeger, A.J. (1998). *Advanced Materials*, **10(12)**, 917.

Cao, Y., Smith, P., and Heeger, A.J. (1992). *Synthetic Metals*, **48 (1)**, 91.

Casado, J., Bengoechea, M., Lopez-Navarrette, J. T. and Otero, T. F. (1998). *Synthetic Metals,* **95,** 93.

Casalbore-Miceli, G., Camaioni, N., Catellani, M. and Gallazzi, M.C. (1998). *Synthetic Metals,* **95**, 211.

Chao, F., Costa, M. and Tian, C. (1993). *Synthetic Metals,* **53**, 127.

Cheung, J.H., Fou, A.F. and Rubner, M.F. (1994). *Thin Solid Films*, **244(1-2)**, 985

Chiang, C.K., Fincher, C.R., Park, Y.W., Heeger, A.J., Shirakawa, H., Louis, E.J., Gao, S.C. and MacDiarmid, A.G. (1977). *Phys. Rev. Lett.*, **39**, 1098.

Conwell, E.M. and Mizes, H.A. (1993). *Synthetic Metals*, **57(2-3)**, 4284.

Crowell, C.R. and Sze, S.M. (1966). *Solid State Electronics,* **9**, 1035.

Dannetun, P., Lögdlund, M., Fahlman, M., Fauquet, C., Beljonne, D., Brédas, J.L., Bässler, H. and Salaneck, W.R. (1994). *Synthetic Metals,* **67**, 81.

Danno, T., Kastner, J. and Kuzmany, H. (1993). *Synthetic Metals,* **58**, 257.

Delabouglise, D., Garreau, R., Lemaire, M. and Roncali, J. (1988). *New Journal of Chemistry*, **12(2-3)**, 155.

De Leeuw, D.M., and Lous, E.J. (1994). *Synthetic Metals*, **65**, 45.

Denton, G.J., Tessler, N., Harrison, N.T. and Friend, R.H. (1997). *Phys. Rev. Lett.*, **78**, 733.

Dewar, M.J.S. and Thiel, W. (1977). *J. Am. Chem. Soc.*, **99**, 4899.

Dewar, M.J.S., Zoebisch, E.G., Healy, E.F. and Stewart, J.P. (1985). *J. Am. Chem. Soc,* **107**, 3902.

Diaz, A.F. (1981). *Chem. Scr.* **17**, 142.

Dodabalapur, A., Bao, Z., Makhija, A., Laquindanum, J.G., Raju, V.R., Feng, Y., Katz, H.E. and Rogers, J. (1998). *Appl. Phys. Lett.*, **73(2)**, 142.

Downard, A.J. and Pletcher, D. (1986). *Journal of Electroanalytical Chemistry*, **206(1-2)**, 147.

Drury, C.J., Mutsaers, C.M.J., Hart, C.M., Matters, M. and de Leeuw, D.M. (1998). *Appl. Phys. Lett.*, **73(1)**, 108.

Duke, C.B. (1987). *Synthetic Metals*, **21**, 5.

Edwards, J.H. and Feast, W.J. (1980). *Polymer Commun.* **21**, 595.

Etemad, S., Mitani, T., Ossaki, M., Chung, T.C., Heeger, A.J. and MacDiarmid, A.G. (1981). *Solid State Communications*, **40**, 75.

Ettedgui, E., Razafitrimo. H., Gao, Y., Hsieh, B.R. and Ruckman, M.W. (1996). *Synthetic Metals*, **78**, 247.

Favre, C., Abello, L. and Delabouglise, D. (1997). *Advanced Materials*, **9(9)**, 722.

Ferraris, J.P. and Lambert, T.L. (1991). *J. Chem. Soc., Chem. Commun.*, **18**, 1268.

Ferreira, M., Cheung, J.H. and Rubner, M.F. (1994). *Thin Solid Films*, **244(1-2)**, 806.

Frankevich, E.L., Lymarev, A.A., Sokolik, I., Karasz, F.E., Blumstengel, S., Baughman, R.H. and Horhold, H.H. (1992). *Phys. Rev. B*, **46**, 9320.

Friend, R.H. and Jerome, D. (1979). *J. Phys. C.*, **12(8)**, 1441.

Friend, R.H., Bradley, D.D.C. and Townsend, P.D. (1987). *J. Phys. D: Appl. Phys.*, **20**, 1367.

Friend, R.H., Denton, G.J., Halls, J.J.M., Harrison, N.T., Holmes, A.B., Köhler, A., Lux, A., Moratti, S.C., Pichler, K., Tessler, N. and Towns, K. (1997). *Synthetic Metals,* **84**, 463.

Frolov, S.V., Gellermann, W., Ozaki, M., Yoshino, K. and Vardeny, Z.V. (1997). *Phys. Rev. Lett.*, **78**, 729.

Garnier, F., Horowitz, G., Peng, X.-Z. and Fichou, D. (1990). *Advanced Materials*, **2**, 592.

Garten, F., Vrijmoeth, J., Schlatmann, A.R., Gill, R.E., Klapwijk, T.M. and Hadziioannou, G. (1996). *Synthetic Metals,* **76**, 85.

Gelinck, G.H., Warman, J.M., Remmers, M., Neher, D. (1997). *Chem. Phys. Lett.*, **265**, 320.

Glenis, S., Horowitz, G., Tourillon, G. and Garnier, F. (1984). *Thin Solid Films,* **111**, 93.

Gomes H.L. (1993). *Fabrication and Characterisation of Electronic Devices Based on Poly(3-methylthiophene)*. PhD Thesis, University of Wales, Bangor.

Gomes, H.L., Taylor, D.M. and Underhill, A.E. (1993). *Synthetic Metals*, **55-57**, 4076.

Gomes, H.L. and Taylor, D.M. (1993). *Mol. Cryst. Liq. Cryst.*, **236**, 151.

Gomes, H.L. and Taylor, D.M. (1997). *IEE Proc.-Circuits Devices Syst.*, **144(2)**, 117.

Gomes, H.L., Jones, G.W. and Taylor, D.M. (1997). *Synthetic Metals*, **85(1-3)**, 1351.

Gomes, H.L., Stallinga, P., Rost, H., Holmes A.B., Harrison, M.G. and Friend, R.H. (1999). *Appl. Phys. Lett.*, **74(8)**, 1144.

Gomes da Costa, P. and Conwell, E.M. (1993). *Phys. Rev. B.*, **48**, 1993.

Grant, P.M, Tani, T., Gill, W.D., Krounbi, M. and Clarke, T.C. (1981). *J. Appl. Phys.*, **52(2)**, 869.

Graupner, W., Leising, G., Lanzani, G., Nisoli, M., De Silvestri, S. and Scherf, U. (1996). *Phys. Rev. Lett.*, **76**, 847.

Green, M.A., King, F.D. and Shewchun, J. (1974). *Solid State Electronics*, **17**, 551.

Greenham, N.C., Moratti, S.C., Bradley, D.D.C, Friend, R.H. and Holmes, A.B. (1993). *Nature*, **365**, 628.

Gunatunga, S.R., Jones, G.W., Kalaji, M., Murphy, P.J., Taylor, D.M. and Williams, G.O. (1997). *Synthetic Metals*, **84(1-3)**, 973.

Gustafsson, G., Inganäs, O., Nilsson, J.O. and Lideberg, B. (1988). *Synthetic Metals*, **26**, 297.

Gustafsson, G., Inganäs, O. and Nilsson, J.O. (1989). *Synthetic Metals*, **28(1-2)**, C427.

Gustafsson, G., Sundberg, M., Inganäs, O. and Svennson, C. (1990). *Journal of Molecular Electronics*, **6**, 105.

Gustafsson, G., Inganäs, O., Sundberg, M. and Svennson, C. (1991). *Synthetic Metals*, **41-43**, 499.

Gustafsson, G., Cao, Y., Treacy, G. M., Klavetter, F., Colaneri, N. and Heeger, A. J. (1992). *Nature,* **357**, 477.

Haaland, P. and Targove, J. (1992). *Appl. Phys. Lett.*, **61(1)**, 34.

Halls, J.J.M., Walsh, C.A., Greenham, N.C., Marseglia, E.A., Friend, R.H., Moratti, S.C. and Holmes, A.B. (1995). *Nature,* **376**, 498.

Hamaguchi, M., Fujii, A., Omhori, Y. and Yoshino, K. (1997). *Synthetic Metals,* **84(1-3)**, 557.

Harrison, R.M. (1992). *Private Communication.*

Henisch, H.K. (1984). *Semiconductor Contacts.* Clarendon, Oxford.

Hide, F., Diaz-Garcia, M.A., Schwartz, B.J., Andersson, M.R., Qibing, P. and Heeger, A.J. (1996). *Science*, **273**, 1833.

Horowitz, G., Peng, X.Z., Fichou, D. and Garnier, F. (1991). *J. Mol. Electron.*, **7(2)**, 85.

Hotta, S. (1988). *Synthetic Metals,* **22(2)**, 103.

Hughes, A.V., Jones, G.W., Mills, C.A. and Taylor, D.M. (1998). *Private Communication.*

Ioannidis, A., Forsythe, E., Gao, Y., Wu, M.W. and Conwell, E.M. (1998). *Appl. Phys. Lett*, **72(23)**, 3038.

Inganäs, O., Berggren, M., Andersson, M.R., Gustafsson, G., Hjertberg, T., Wennerstrom, O., Dyreklev, P. and Granstrom, M. (1995). *Synthetic Metals*, **71(1-3)**, 2121.

Inganäs, O. (1999). *Private Communication.*

Ito, T., Shirikawa, H. and Ikeda, S. (1974). *J. Polym. Sci. Polym. Chem. Ed.*, **12**, 11.

Ivory, D.M., Miller, G.G., Sowa, J.M., Shacklett, L.W., Chance, R.R. and Baughman, R.H., (1979). *J. Chem. Phys.*, **17**, 1506.

John, R. and Wallace, G.G. (1991). *J Electroanal. Chem.*, **306**, 157.

John, R. and Wallace, G.G. (1992). *Polymer International*, **27**, 255.

Jones, G.W., Taylor, D.M. and Gomes, H.L. (1997). *Synthetic Metals*, **85(1-3)**, 1341.

Jones, G.W., Taylor, D.M. and Gomes, H.L. (1999). *Synthetic Metals,* **101(1-3)**, 431.

Kalaji, M., Murphy, P.J. and Williams, G.O. (1999). *Synthetic Metals*, **101**, 123.

Kallinger, C., Hilmer, M., Haugeneder, A., Perner, M., Spirkl, W., Lemmer, U., Feldmann, J., Scherf, U., Müllen, K., Gombert, A. and Wittwer, V. (1998). *Advanced Materials*, **10(12)**, 920.

Kanazawa, K.K., Diaz, A.F., Gill, W.D., Grant, P.M., Street, G.B., Gardini, G.P. and Kwak, J.F. (1979/1980). *Synthetic Metals*, **1**, 329.

Kaneto, K. (1983). *Jpn. Jn. App. Phys.* **22**, L412.

Kaneto, K., Kohno, Y. and Yoshino, K. (1984). *Solid State Communications,* **51(5)**, 267.

Kaneto, K., Asano, T. and Takashima, W. (1991). *Japanese Journal of Applied Physics,* **30(2A)**, L215.

Kaneto, K., Asano, T. and Takashima, W. (1991). *Jpn. Jn. Appl. Phys.,* **30 (2A)**, L215.

Karasz, F.E., Capistran, J.D., Gagnon, D.R. and Lenz, R.W. (1985). *Mol. Cryst. Liq. Cryst.*, **118(1-4)**, 327.

Karg, S., Meier, M. and Riess, W. (1997). *J. Appl. Phys.*, **82(4)**, 1951.

Koezuka, H., and Tsumura, A. (1989). *Synthetic Metals*, **28**, C753.

Kozaki, M., Tanaka, S. and Yamashita, Y. (1994). *J. Org. Chem*, **59**, 442.

Krische, B. and Zagorska, M. (1989). *Synthetic Metals*, **28**, C263.

Kuo, C.S., Wakim, F.G., Sengupta, S.K., Tripathy, S.K. (1993). *J. Appl. Phys.*, **74(4)**, 2957.

Lambert, T.L. and Ferraris, J.P. (1991). *J. Chem. Soc., Chem. Commun*, **11**, 752.

Lang, D.V, (1974). *J. Appl. Phys.*, **45**, 3023.

Lang, P., Chao, F., Costa, M. and Garnier, F. (1987). *Polymer*, **28**, 668.

Langmuir, I. (1915). Jn. Am. Chem. Soc., **37**, 1139.

Louarn, G., Trznadel, M., Buisson, J.P., Laska, J., Pron, A., Lapkowski, M. and Lefrant, S. (1996). *J. Phys. Chem.*, **100(30)**, 12532.

MacDiarmid, A.G. and Heeger, A.J. (1980). *Synthetic Metals*, **179(1)**, 101.

Marks, R.N, Bradley, D.D.C, Jackson, R.W, Burn, P.L and Holmes, A.B. (1993). *Synthetic Metals*, **55-57**, 4128.

Masuda, H., Tanaka, S. and Kaeriyama, K. (1989). *Synthetic Metals*, **31**, 29.

Mazumdar, S., Guo, D.D. and Dixit, S.N. (1993). *Synthetic Metals*, **57(1)**, 3881.

McCullough, R.D. and Williams, S.P. (1993). *J. Am. Chem. Soc.*, **115**, 11608.

Meier, M., Karg, S. and Riess, W. (1997). *J. Appl. Phys.*, **82(4)**, 1961.

Meyer, H., Haarar, D., Naarmann, H., Horhold, H.H. (1995). *Phys. Rev. B.*, **52**, 2587.

MOPAC, *Program Version 6* (QCEP 455).

Moses, D. (1992). *Appl. Phys. Lett.*, **60**, 3215.

Munn, R.W. (1984). *Chemistry in Britain,* 518.

Murase, I., Ohnishi, T., Noguchi, T. and Hirooka, M. (1984). *Pol. Commun.,* **25(11)**, 327.

Murray, R.W. (1984). *Electroanalytical Chem., **13**, 191.*

Musa, I., Higgins, S.J. and Eccleston, W. (1997). *J. Appl. Phys.,* **81(5)**, 2288.

Musa, I., Eccleston, W. and Higgins, S.J. (1998). *J. Appl. Phys.,* **83(10)**, 5558.

Nakamura, S. (1998). *Physics World,* **11(2)**, 31.

Naarmann, H. and Theophilou, N. (1987). *Synthetic Metals*, **22**, 1.

Nigrey, P.J., Macinnes, D., Nairns, D.P., MacDiarmid, A.G., and Heiger, A.J. (1981). *J Electrochem. Soc.,* **128(8)**, 1651.

Ohmori, Y., Takahashi, H., Kawai, T. and Yoshino, K. (1990). *Japanese Journal of Applied Physics*, **29(10)**, L1849.

Ohmori, Y., Takahashi, H., Muro, K., Uchida, M., Kawai, T. and Yoshino, K. (1990). *Japanese Journal of Applied Physics Part 2 - Letters*, **30(7B)**, L1247.

Ohmori, Y., Takahashi, H., Muro, K., Uchida, M., Kawai, T. and Yoshino, K. (1991). *Japanese Journal of Applied Physics Part 2 - Letters*, **30(4A)**, L610.

Ohtani, A., Abe, M., Ezoe, M., Doi, T., Miyata, T. and Miayke, A. (1992). Proceedings of ICSM '92, Gothenburg, Sweden.

Österbacka, R., Juska, G., Arlauskas, K., Pal, A.J., Källman, K-M. and Stubb, H. (1998). *J Appl. Phys.*, **84(6)**, 3360.

Paloheimo, J., Punkka, E., Kuivalainen, P., Stubb, H. and Lahti, P.Y. (1989). *Acta Polytechnica Scandinavica, Elect. Eng. Ser.*, **64**, 178.

Paloheimo, J., Kuivalainen, P., Stubb, H., Vuorimaa, E. and Lahti, P.Y. (1990). *Appl. Phys. Lett.*, **56(12)**, 1157.

Paloheimo, J., Stubb, H., Yli-Lahti, P. and Kuivalainen, P. (1991). *Synthetic Metals*, **41-43**, 563.

Parker, I.D. (1994). *J. Appl. Phys.*, **75(3)**, 1656.

Pauck, T., Henning, R., Perner, M., Lemmer, U., Siegner, U., Mahrt, R.F., Scherf. U., Müllen, K., Bässler, H. and Göbel, E.O. (1995). *Chem. Phys. Lett.*, **244**, 171.

Peierls, R.E. (1955). *Quantum Theory of Solids*, Clarendon Press, Oxford.

Petritsch, K. and Friend, R.H. (1999). *Synthetic Metals*, **102(1-3)**, 976.

Peulon, V., Barbey, G., Malandain, J-J. (1996). *Synthetic Metals*, **82**, 111.

Pfluger, P., Krounbi, M., Street, G.B. and Weiser, G. (1983). *J. Chem. Phys.*, **78**, 3212.

Pochan, J.M. (1986). In Handbook of Conducting Polymers Vol 2. Ed. T.A. Skotheim (Marcel Dekker, New York).

Rachdi, F. and Bernier, P. (1986). *Phys. Rev. B.*, **33**, 11.

Rhoderick, E.H. (1970). *J. Phys. D: Appl Phys.*, **3**, 1153.

Rhoderick, E.H. (1978). *Metal Semiconductor Contacts.* Clarendon Press, Oxford.

Rice, M.J. (1979). *Phys Rev A.*, **71**, 152.

Ridley, J. and Zerner, M.C. (1973). *Theoret. Chim. Acta.*, **32**, 111.

Rikken, G.L.J.A., Kessener, Y.A.R.R., Braun, D., Staring, E.G.J. and Demandt, R. (1994). *Synthetic Metals*, **67**, 115.

Roberts, G.I. and Crowell, C.R. (1970). *J. Appl. Phys.*, **41**, 1767.

Roberts, G.I. and Crowell, C.R. (1973). *Solid State Electronics*, **16**, 29.

Roman, L.S., Andersson, M.R., Yohannes, T. and Inganäs, O. (1997). *Advanced Materials*, **9(15)**, 1164.

Romero, D.B., Schaer, M., Zuppiroli, L., Cesar, B. and François, B. (1995). *Appl. Phys. Lett.*, **67(12)**, 1659.

Roncali, J. and Garnier, F. (1986). *New J. Chem.*, **4-5**, 237.

Roncali, J., Yassar, A. and Garnier, F. (1989). *J. Chem. Phys.*, **86**, 85.

Roncali, J., Yassar, A. and Garnier, F. (1989). *Synthetic Metals*, **28**, C275.

Salaneck, W.R. and Brédas, J.L. (1994). *Solid State Communications*, **92(1-2)**, 31.

Salaneck, W.R., Staffström, S. and Brédas, J-L. (1996). *Conjugated Polymer Surfaces and Interfaces.* Cambridge University Press.

Sato, M., Tanaka, S. and Kaeriyama, K. (1985). *J. Chem. Soc. Chem. Commun.*, 713.

Savvate'ev, V.N., Tarabia, M., Chayet, H., Farragi, E.-Z., Cohen, G.-B., Kirstein, S., Davidov, D., Avny, Y. and Neumann, R. (1997). *Synthetic Metals*, **85(1-3)**, 1269.

Schäfer-Siebert, D., Roth, S., Budrowski, C. and Kuzmany, H. (1987). *Synthetic Metals*, **37**, 145.

Schoch, K.F. and Saunders, H.E. (1992). *IEEE Spectrum*, **29(6)**, 52.

Schwartz, B.J., Hide, F., Andersson, M.R. and Heeger, A.J. (1997). *Chem. Phys. Lett.*, **265**, 327.

Shirakawa, H., Louis, E.G., MacDiarmid, A.G., Chiang, C.K. and Heeger, A.J. (1977). *J. Chem. Soc.Chem. Commun.*, 578.

Shurmer, H.V., Corcoran, P. and Gardner, J.W. (1991). *Sensors and Actuators B - Chemical*, **4(1-2)**, 29.

Sirringhaus, H., Tessler, N. and Friend, R.H. (1998). *Science*, **280**, 1741.

Skotheim, T.A., Elsenbaumer, R.L. and Reynolds J.R. (ed.) (1998). *Handbook of Conducting Polymers*. Marcel Dekker, New York.

Smith, R.W. and Rose, A. (1955). *Phys. Rev.*, **97**, 1531.

Spearman, P. (1997). *Private Communication.*

Stallinga, P., Gomes, H.L., Jones, G.W. and Taylor, D.M. (1998). *Acta Physica Polonica A*, **94(3)**, 545.

Stewart, J.J.P. (1989). *J. Comp. Chem.*, **10**, 209.

Stubb, H., Punkka, E. and Paloheimo, J. (1993). *Material Science and Engineering*, **10**, 85.

Su, W.P., Schrieffer, J.R. and Heeger, A.J. (1979). *Phys. Rev. Lett.*, **42**, 1698.

Sze, S.M. (1981). *Physics of Semiconductor Devices*. New York: Wiley.

Takiguchi, T., Park, D.H., Ueno, H., Yoshino, K. and Sugimoto, R. (1987). *Synthetic Metals*, **17**, 657.

Tanaka, K., Yoshizawa, K., Takeuchi, T. and Yamabe, T. (1990). *Synthetic Metals*, **107**, 38.

Tani, T., Grant, P.M., Gill, W.D., Street, G.B and Clarke T.C. (1980). *Solid State Communications*, **33**, 499.

Taylor, D.M., Gomes, H.L., Underhill, A.E., Edge, S. and Clemenson, P.I. (1991). *J.Phys. D: Appl. Phys*, **24**, 2032.

Taylor, D.M. and Gomes, H.L. (1995). *J. Phys. D: Appl. Phys.*, **28**, 2554.

Tessler, N., Denton, G.J. and Friend, R.H. (1996). *Nature*, **382(6593)**, 695.

Tomozawa. H, Braun, D., Phillips, S., Heeger, A.J. and Kroemer, H. (1987). *Synthetic Metals*, **22**, 63.

Tomozawa. H, Braun, D., Phillips, S.D., Worland, R., Heeger, A.J. and Kroemer, H. (1989). *Synthetic Metals*, **28(1-2)**, C687.

Tourillon, G. and Garnier, F. (1982). *J. Electroanal. Chem.*, **135**, 173.

Tourillon, G. and Garnier, F. (1983). *J. Electrochem. Soc.: Electrochemical Science and Technology*, 2042.

Trznadel, M., Zagorska, M., Lapkowski, M., Louarn, G., Lefrant, S. and Pron, A. (1996). *J. Chem. Soc. Fara. Trans.* **92(8)**, 1387.

Tsumura, A., Koezuka, H. and Ando, T. (1986). *Appl. Phys. Lett.*, **49(18)**, 1210.

Tsumura, A., Koezuka, H. and Ando, T. (1988). *Synthetic Metals*, **25**, 11.

Tsumura, A., Fuchigami, H. and Koezuka, H. (1991). *Synthetic Metals*, **41(3)**, 1181.

Vandersluijs, M.J., Underhill, A.E. and Zaba, B.N. (1987). *J. Phys. D: Appl Phys.*, **20(11)**, 1411.

Vannikov, A.V. and Novikov, S.V. (1994). *Russ. Chem. Rev.*, **63**, 103.

Videlot, C. and Fichou, D. (1999). *Synthetic Metals*, **102**, 885.

Wagner, C. (1931). *Phys. Z.*, **32**, 641.

Wegner, G. and Ruhe, J. (1989). *Faraday Discussions Chem. Soc.*, **88**, 333.

Wudl, F., Khemani, K.C., Harlev, E., Ni, Z. and Srdanov, G. (1991). *Abstracts of Papers to the American Chemical Society*, **201(2)**, 118.

Yassar, A., Roncali, J. and Garnier, F. (1989). *Macromolecules*, **22,** 804.

Yan, M., Rothberg, L.J., Papadimitrakopoulos, F., Galvin, M.E. and Miller T.M. (1994). *Phys. Rev. Lett.*, **72**, 1104.

Yu, A.Y.C. and Snow, E.H. (1968). *Solid State Electronics*, **12**, 155.

Additional References

AFM Imaging Modes, *TopoMetrix Corporation, (1993).*

Digital Instruments, *Support Notes, No. 231, Rev.A.*

Digital Instruments, *Support Notes, No.207.*

Dimension 3000, *Instruction Manual.*

Publications based on the work reported in this thesis

Gomes, H.L., Jones, G.W. and Taylor, D.M. (1997). *Synthetic Metals,* **85(1-3)**, 1351.

Gunatunga, S.R., Jones, G.W., Kalaji, M., Murphy, P.J., Taylor, D.M. and Williams, G.O. (1997). *Synthetic Metals,* **84(1-3)**, 973.

Jones, G.W., Taylor, D.M. and Gomes, H.L. (1997). *Synthetic Metals,* **85(1-3)**, 1341.

Jones, G.W., Taylor, D.M. and Gomes, H.L. (1999). *Synthetic Metals,* **101(1-3)**, 431.

Mills, C.A., Taylor, D.M., Murphy, P.J., Dalton, C., Jones, G.W., Hall, L.M. and Hughes, A.V. (1999). *Synthetic Metals,* **102(1-3)**, 1000.

Stallinga, P., Gomes, H.L., Jones, G.W. and Taylor, D.M. (1998). *Acta Physica Polonica A,* **94(3)**, 545.

Stallinga, P., Gomes, H.L., Jones, G.W. and Taylor, D.M. (1999). *Synthetic Metals,* **101(1-3)**, 496.